

## Conceptual design of a concrete staircase based on topology optimization

A feasibility study on the development and application of topology optimization on a concrete staircase



BJØRNAR SANDVIK



EHSAN QARAEI



RAMESH KUMAR K C

### SUPERVISORS

Max Trommer, CEO Rebartek AS

Paul Ragnar Svennevig, Assistant professor University of Agder

**University of Agder, 2021**

Faculty of Engineering and Science

Department of Engineering sciences

## Summary

This master's thesis will investigate the possibility of applying topology optimization in the design of a concrete staircase. Topology optimization is a subcategory of structural optimization which aims to redistribute material usage in structures, to achieve designs where certain performances have been maximized. According to calculations based on the Eurocode 2, the work acknowledges that the reference concrete staircase design is not fully utilized, which indicates the potential for optimization.

Through this work, the authors will study the impacts of different topology optimization algorithms, namely the sensitivity-based and condition-based methods, mesh size and volume constraints on the final design's stiffness and deflection. In addition, the study will present other modern tools, such as parametric modeling and 3D printing, and will probe the feasibility of employing them together with topology optimization to obtain a better manufacturing line. Abaqus/CAE is chosen for the task of topology optimization and Finite Element Analysis, whereas the powerful plugin in Rhinoceros 3D, Grasshopper 3D, is employed for the purpose of parametric modeling in this thesis.

During this study, the authors discovered the significance of using CAD software and parametric modeling to increase precision and efficiency. After conducting multiple simulations with different variables, the study concludes that the reference staircase can be optimized up to 50% and still retain its original stiffness and deflection. Mesh dependency was more apparent for models with 30-40% volume of the original volume, particularly for the condition-based algorithm. To be able to manufacture such organic looking structures, the use of fused deposition modeling 3D printed formworks proved to be a promising option to overcome the geometric limitations of traditional timber formwork.

## Obligatory group declaration

Den enkelte student er selv ansvarlig for å sette seg inn i hva som er lovlige hjelpemidler, retningslinjer for bruk av disse og regler om kildebruk. Erklæringen skal bevisstgjøre studentene på deres ansvar og hvilke konsekvenser fusk kan medføre. Manglende erklæring fritar ikke studentene fra sitt ansvar.

1.	Jeg/vi erklærer herved at min/vår besvarelse er mitt/vårt eget arbeid, og at jeg/vi ikke har brukt andre kilder eller har mottatt annen hjelp enn det som er nevnt i besvarelsen.	<input checked="" type="checkbox"/>
2.	Jeg/vi erklærer videre at denne besvarelsen: <ul style="list-style-type: none"> <li>- ikke har vært brukt til annen eksamen ved annen avdeling/universitet/høgskole innenlands eller utenlands.</li> <li>- ikke refererer til andres arbeid uten at det er oppgitt.</li> <li>- ikke refererer til eget tidligere arbeid uten at det er oppgitt.</li> <li>- har alle referansene oppgitt i litteraturlisten.</li> <li>- ikke er en kopi, duplikat eller avskrift av andres arbeid eller besvarelse.</li> </ul>	<input checked="" type="checkbox"/>
3.	Jeg/vi er kjent med at brudd på ovennevnte er å betrakte som fusk og kan medføre annullering av eksamen og utestengelse fra universiteter og høgskoler i Norge, jf. Universitets- og høgskoleloven §§4-7 og 4-8 og Forskrift om eksamen §§ 31.	<input checked="" type="checkbox"/>
4.	Jeg/vi er kjent med at alle innleverte oppgaver kan bli plagiatkontrollert.	<input checked="" type="checkbox"/>
5.	Jeg/vi er kjent med at Universitetet i Agder vil behandle alle saker hvor det foreligger mistanke om fusk etter høgskolens retningslinjer for behandling av saker om fusk.	<input checked="" type="checkbox"/>
6.	Jeg/vi har satt oss inn i regler og retningslinjer i bruk av kilder og referanser på biblioteket sine nettsider.	<input checked="" type="checkbox"/>

## Publishing agreement

Fullmakt til elektronisk publisering av oppgaven

Forfatter(ne) har opphavsrett til oppgaven. Det betyr blant annet enerett til å gjøre verket tilgjengelig for allmennheten (Åndsverkloven. §2).

Alle oppgaver som fyller kriteriene vil bli registrert og publisert i Brage Aura og på UiA sine nettsider med forfatter(ne)s godkjenning.

Oppgaver som er unntatt offentlighet eller taushetsbelagt/konfidensiell vil ikke bli publisert.

Jeg/vi gir herved Universitetet i Agder en vederlagsfri rett til å gjøre oppgaven tilgjengelig for elektronisk publisering:

JA  NEI

Er oppgaven båndlagt (konfidensiell)?

JA  NEI

(Båndleggingsavtale må fylles ut)

- Hvis ja:

Kan oppgaven publiseres når båndleggingsperioden er over?

JA  NEI

Er oppgaven unntatt offentlighet?

JA  NEI

(inneholder taushetsbelagt informasjon. Jfr. Offl. §13/Fvl. §13)

## Preface

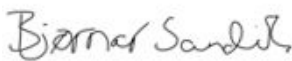
This master's thesis marks the end of a two-year master's degree in Civil and Structural Engineering. The report has been prepared at the University of Agder, Faculty of Engineering and Science in the spring of 2021, and has a weight of 30 credits. The master's thesis is a collaboration between three fellow students Bjørnar Sandvik, Ehsan Qaraee and Ramesh Kumar K C.

The master's thesis studies topology optimization of concrete staircases, with a main focus on the development and production aspects. The knowledge that underlines the individual authors is gained through a two-year course of study with a main focus on construction technology.

We would like to send a special gratitude to our internal supervisor Paul Ragnar Svennevig, Assistant Professor at the department for engineering and head of the department, for good guidance and constructive feedback throughout the report writing. We would also like to extend our special gratitude to our external supervisors Max Trommer, CEO of Rebartek AS and Serhii Zhubra, Structural Engineer at Rebartek AS, for generally good guidance and technical assistance. We would also like to send our special thanks to Andreas Bjune Kjølsest for his insightful advises which directed us in correct path. Lastly, we would like to thank other lecturers and staff at UiA who contributed with good input and feedback.

We are grateful to the Faculty of Engineering and Science, University of Agder (UiA) for providing us the privilege to pursue our master's degree in Civil and Structural Engineering. We are also thankful to all the department staffs, faculties, professors, and fellow students for creating good environment to learn.

We hope this master's thesis can be found useful for the individual reader, who has his or her field of application within construction technique.



Bjørnar Sandvik



Ehsan Qaraee



Ramesh Kumar K C

# Table of contents

<b>Summary</b>	<b>i</b>
<b>Obligatory group declaration</b>	<b>ii</b>
<b>Publishing agreement</b>	<b>iii</b>
<b>Preface</b>	<b>iv</b>
<b>Table of contents</b>	<b>v</b>
<b>List of figures</b>	<b>viii</b>
<b>List of tables</b>	<b>xi</b>
<b>Abbreviations</b>	<b>xii</b>
<b>1 Introduction</b>	<b>1</b>
<b>2 Social perspective</b>	<b>3</b>
<b>3 Theoretical background</b>	<b>5</b>
3.1 Finite element method	5
3.1.1 History	6
3.1.2 Mathematical interpretation	8
3.2 Topology optimization	12
3.2.1 History	13
3.2.2 Optimally criteria methods	14
3.2.3 Heuristic or Intuitive methods	15
3.2.4 Compliance and strain energy	16
3.2.5 Solid Isotropic Material with Penalization (SIMP)	18
3.2.6 Bi-directional evolutionary structural optimization (BESO)	21
3.3 Parametric modeling	30
3.3.1 Rhinoceros 3D and Grasshopper 3D	30
3.3.2 B-splines and NURBS	31
3.4 Abaqus	33
3.4.1 Part	33
3.4.2 Property	34
3.4.3 Assembly	34
3.4.4 Step	34
3.4.5 Load	34
3.4.6 Mesh	35
3.4.7 Optimization	36
3.5 Staircase	37
3.5.1 Staircase components	39

3.5.2	Staircase types . . . . .	40
3.5.3	Regulations based on TEK17 . . . . .	41
3.6	Basis for calculations . . . . .	42
3.6.1	Partial factors for materials . . . . .	42
3.6.2	Load and load factors . . . . .	42
3.6.3	Compressive strength . . . . .	43
3.6.4	Modulus of elasticity . . . . .	44
3.6.5	Durability . . . . .	44
3.6.6	Shear capacity . . . . .	44
3.6.7	Moment capacity . . . . .	45
3.6.8	Deflection . . . . .	46
3.7	3D printing . . . . .	46
3.8	Literature study . . . . .	49
3.8.1	3D-Printed Formwork for Bespoke Concrete Stairs - Andrei Jipa et al. . . . .	49
3.8.2	Topology optimized reinforced concrete walls constructed with 3D printed formwork - Triveni Mudaliar et al. . . . .	51
3.8.3	An application of structural topology optimization to create staircase - Isabel Moreira et al. . . . .	52
3.8.4	Topology-optimized design, construction and experimental evaluation of concrete beams - Jackson L. Jewett et al. . . . .	53
<b>4</b>	<b>Research question . . . . .</b>	<b>58</b>
4.1	Limitations . . . . .	58
<b>5</b>	<b>Case and materials . . . . .</b>	<b>59</b>
5.1	Background . . . . .	59
5.2	Conditions and drawing basis . . . . .	59
5.3	Material . . . . .	62
5.4	Boundary condition . . . . .	62
5.5	Load condition . . . . .	62
<b>6</b>	<b>Method . . . . .</b>	<b>64</b>
6.1	Literature review . . . . .	64
6.2	Parametric modeling with Grasshopper 3D . . . . .	64
6.3	Abaqus . . . . .	65
6.3.1	Part module . . . . .	65
6.3.2	Property module . . . . .	65
6.3.3	Assembly module . . . . .	65
6.3.4	Step module . . . . .	65
6.3.5	Load module . . . . .	66
6.3.6	Mesh module . . . . .	66
6.3.7	Optimization module . . . . .	67
6.4	3D printing . . . . .	67
6.5	Analysis of the reference staircase . . . . .	68

6.5.1	Design load . . . . .	68
6.5.2	Shear capacity . . . . .	68
6.5.3	Moment capacity . . . . .	68
6.5.4	Deflection . . . . .	68
6.6	Quality control and systematization . . . . .	69
<b>7</b>	<b>Results . . . . .</b>	<b>70</b>
7.1	Parametric model . . . . .	70
7.2	Structural analysis . . . . .	73
7.3	Topology optimization . . . . .	74
7.3.1	Reference model . . . . .	74
7.3.2	Deflection . . . . .	74
7.3.3	Strain energy . . . . .	80
7.4	3D printing . . . . .	86
<b>8</b>	<b>Discussion . . . . .</b>	<b>89</b>
8.1	Parametric modeling . . . . .	89
8.2	Structural analysis . . . . .	90
8.3	Deflection . . . . .	90
8.4	Strain energy and stiffness . . . . .	91
8.5	Manufacturing . . . . .	92
<b>9</b>	<b>Conclusion . . . . .</b>	<b>95</b>
<b>10</b>	<b>Recommendations . . . . .</b>	<b>96</b>
<b>11</b>	<b>References . . . . .</b>	<b>98</b>
<b>12</b>	<b>Appendix . . . . .</b>	<b>103</b>
<b>Appendix A</b>	<b>Drawings from Contiga AS . . . . .</b>	<b>104</b>
<b>Appendix B</b>	<b>Development of parametric staircase by the use of Rhinoceros 3D and Grasshopper 3D . . . . .</b>	<b>117</b>
<b>Appendix C</b>	<b>3D printing of formwork and staircase models . . . . .</b>	<b>132</b>
<b>Appendix D</b>	<b>Calculations of staircase according to Eurocode 2 . . . . .</b>	<b>144</b>



## List of figures

1.1	The Light Rider motorcycle, by Altair and APWorks with 30% weight reduction [1]. . . . .	1
1.2	Parametric concept bridge, courtesy of Michael Mitchell [2]. . . . .	1
2.1	The holistic view of sustainability [4]. . . . .	3
2.2	Steel fixers [11]. . . . .	4
2.3	Robotic fabrication method [12]. . . . .	4
3.1	Structural Analysis of a concrete beam by Finite Element Method [15]. . . . .	6
3.2	First appearance of the Finite Element Method in the paper, Stiffness and Deflection Analysis of Complex Structures, by Turner et al. in 1956 [16]. . . . .	7
3.3	History of Finite Element Method [13]. . . . .	8
3.4	Discretization of a 2D domain. (a) A typical domain. (b) Meshed representation of the domain. (c) A typical element. (d) Nodal representation of the domain [17]. . . . .	9
3.5	Three groups of structural optimization: a) Size optimization, b) Shape optimization and c) Topology optimization [21]. . . . .	13
3.6	An optimal Mitchell truss after 104 iterations [20]. . . . .	14
3.7	Application of several topology optimization algorithms in a cantilever beam [22]. . . . .	16
3.8	Algorithm of the SIMP [21]. . . . .	20
3.9	Evolution of a SIMP example with a) 2700; b) 4800 and c) 17200 elements [21]. . . . .	21
3.10	Evolution of the beam after a) 5 iterations; b) 10 iterations; c) 15 iterations; d) 25 iterations; e) 40 iterations; f) 53 iterations (final topology) [22]. . . . .	22
3.11	$\Omega_i$ which contains the nodes that are used in the filter scheme for the $i$ th element [22]. . . . .	24
3.12	A two-dimensional cantilever beam a) with no filter scheme (checkerboard pattern is visible); b) with filter scheme [28]. . . . .	25
3.13	Evolution of mean compliance: a) without stabilization scheme; b) with stabilization scheme [22]. . . . .	26
3.14	Flowchart of the BESO algorithm[22]. . . . .	29
3.15	Grasshopper 2D canvas [Appendix B]. . . . .	31
3.16	Bernstein polynomials [37]. . . . .	32
3.17	Control points and weights with the resulting curve geometry [36]. . . . .	32
3.18	Material properties tab from Abaqus/CAE. . . . .	34
3.19	Application of load in Abaqus/CAE. . . . .	35
3.20	Tetrahedron and hexahedron elements with both linear and quadratic geometric order [45]. . . . .	36
3.21	The Abaqus Topology Optimization Module work process [46]. . . . .	37
3.22	Stone staircase at the Tarxien temple, Malta (3600–2500 BC) [47]. . . . .	38
3.23	Northern staircase of the Louis XII wing, Blois, France (1501) [47]. . . . .	38
3.24	Palais d'Iena, the Conseil Economique et Social, Paris (1937-1943) [47]. . . . .	38
3.25	Modular Pre-stressed UHPC Staircase (2009) [49]. . . . .	38
3.26	Components of staircase [53]. . . . .	39

3.27	Different types of staircase. (a) and (b) Straight staircase (c) L-shaped staircase (d) U-shaped staircase (e) Spiral staircase (f) Curved staircase [55]. . . . .	41
3.28	The fabrication process of a FDM 3D printer illustrating the extrusion of a cantilever geometry with the belonging support structure marked in red [63]. . . . .	47
3.29	The 3D printer used in this thesis: Creality CR-6 SE 3D-Printer [Appendix C]. . . . .	48
3.30	Prototype A [52]. . . . .	50
3.31	Prototype B [52]. . . . .	50
3.32	3D printed formwork [52]. . . . .	50
3.33	Final staircase design [51]. . . . .	53
3.34	3D-printed model [51]. . . . .	53
3.35	The case design [67]. . . . .	54
3.36	Compliance design:	
	(a) Unrounded design	
	(b) as-built design	
	(c) constructed specimen [67]. . . . .	54
3.37	Low Tension design:	
	(a) Unrounded design	
	(b) as-built design	
	(c) constructed specimen [67]. . . . .	54
3.38	High Tension design: (a) Unrounded design (b) as-built design (c) constructed specimen [67].	55
3.39	Results obtained from the experiments: a) compliance plotted against volume, b) maximum load capacity [67]. . . . .	56
3.40	Maximum principal stress distributions: (a) unrounded Compliance design, (b) as-built Compliance design, (c) unrounded High Tension, (d) as-built High Tension, (e) unrounded Low Tension, and (f) as-built Low Tension [67]. . . . .	57
5.1	Bottom staircase drawing from Contiga AS [Appendix A]. . . . .	60
5.2	Top staircase drawing from Contiga AS [Appendix A]. . . . .	60
5.3	Reference staircase from Contiga AS [Appendix A]. . . . .	61
6.1	The imported and partitioned staircase geometry with the associated coordinate system. . .	65
6.2	Mesh size set to 40mm. . . . .	66
6.3	Mesh size set to 60mm. . . . .	66
6.4	Abaqus: Objective function. . . . .	67
6.5	Abaqus: Volume constraint. . . . .	67
7.1	The resulting parametric values, expressed by number sliders. . . . .	70
7.2	The resulting GH 2D canvas with the complete wired node-network. . . . .	72
7.3	U-shaped staircase modeled in GH with the properties given from Contiga [Appendix A]. . .	73
7.4	Reference model. . . . .	74
7.5	Deflection at reference point in sensitivity-based models with 40mm mesh size and a) 70%, b) 60%, c) 50%, d) 40% and e) 30% volume of the original volume. . . . .	75
7.6	Deflection at reference point in sensitivity-based models with 60mm mesh size and a) 70%, b) 60%, c) 50%, d) 40% and e) 30% volume of the original volume. . . . .	76
7.7	Deflection at reference point in condition-based models with 40mm mesh size and a) 70%, b) 60%, c) 50%, d) 40% and e) 30% volume of the original volume. . . . .	77

7.8	Deflection at reference point in condition-based models with 60mm mesh size and a) 70%, b) 60%, c) 50%, d) 40% and e) 30% volume of the original volume. . . . .	78
7.9	Maximum deflection in all models. . . . .	79
7.10	Maximum deflection in all models except 30% against the deflection in the reference model. . . . .	79
7.11	Evolution in strain energy of the sensitivity-based models with 40mm mesh size a) 70%, b) 60%, c) 50%, d) 40% and e) 30% volume of the original volume. . . . .	80
7.12	Evolution in strain energy of the sensitivity-based models with 60mm mesh size a) 70%, b) 60%, c) 50%, d) 40% and e) 30% volume of the original volume. . . . .	81
7.13	Evolution in strain energy of the condition-based models with 40mm mesh size a) 70%, b) 60%, c) 50%, d) 40% and e) 30% volume of the original volume. . . . .	82
7.14	Evolution in strain energy of the condition-based models with 60mm mesh size a) 70%, b) 60%, c) 50%, d) 40% and e) 30% volume of the original volume. . . . .	83
7.15	Strain energy in all models. . . . .	85
7.16	Strain energy in all models except 30% against the initial strain energy in the reference model. . . . .	85
7.17	3D printed topology optimized staircase with 30% volume of the original volume [Appendix C]. . . . .	86
7.18	Formwork parts [Appendix C]. . . . .	86
7.19	Assembled formwork [Appendix C]. . . . .	86
7.20	Visual presentation of a vertical cut of the formwork [Appendix C]. . . . .	87
7.21	3D printed formwork: Vertical cut [Appendix C]. . . . .	87
7.22	3D printed formwork: Vertical cut [Appendix C]. . . . .	87
10.1	Modeled reinforcement for nonlinear analysis. . . . .	96
10.2	Topology optimized design. . . . .	97
10.3	Topology optimized design. . . . .	97

## List of tables

3.1	Partial factor for concrete and steel [57]. . . . .	42
3.2	Load factors for permanent and variable actions [57]. . . . .	43
3.3	Span/effective depth ratio [57]. . . . .	46
3.4	Staircase loading according to Brazilian design code [51]. . . . .	52
5.1	Dimensions of bottom staircase [Appendix A]. . . . .	62
5.2	Properties of the B30 concrete [Appendix A]. . . . .	62
5.3	Type of loads applied to the staircase. . . . .	63
7.1	Thickness of reference staircase slabs [Appendix D]. . . . .	73
7.2	Shear capacity and design shear of the reference staircase [Appendix D]. . . . .	73
7.3	Moment capacity and design moment of the reference staircase [Appendix D]. . . . .	73
7.4	Calculated deflection of the reference model [Appendix D]. . . . .	74
7.5	Number of iterations, strain energy and achieved volume in each model. . . . .	84
7.6	Print time [Appendix C]. . . . .	88

## Abbreviations

- ATOM: Abaqus Topology Optimization Module
- BC: Boundary conditions
- BEM: Boundary Element Method
- BESO: Bidirectional Evolutionary Structural Optimization
- B-spline: Basis spline
- CAO: Computer-Aided Optimization
- CAD: Computer-Aided Design
- CNC: Computer Numerical Control
- CB: Condition-Based algorithm
- DOF: Degree of freedom
- Eurocode 1: NS-EN 1991-1-1:2002+NA:2019
- Eurocode 2: NS-EN 1992-1-2:2004+NA:2010
- ESO: Evolutionary Structural Optimization
- FDM: Fused Deposition Modeling
- FEA: Finite Element Analysis
- FEM: Finite Element Method
- FVM: Finite Volume Method
- ITD: Isolines/Isosurfaces Topology Design
- GH: Grasshopper 3D
- MSA: Matrix Structural Analysis
- NURBS: Non-uniform rational basis spline
- PDEs: Partial differential equations
- PLA: Polyactic Acid
- RC: Reinforced concrete
- SB: Sensitivity-Based algorithm
- SERA: Sequential Element Rejection and Admission
- SIMP: Solid Isotropic Material with Penalization

- SLS: Serviceability Limit State
- SO: Structural optimization
- TEK17: Regulations on technical requirements for construction works
- TO: Topology optimization / topologically optimized
- UHPC: Ultra High Performance Concrete
- ULS: Ultimate Limit State
- UN: United Nations

## 1 Introduction

Structural optimization (SO) has become a fundamental part of design process and has been widely used in different engineering fields, particularly aerospace and automotive industries. Nonetheless, SO's impact in structural engineering has been minimal thus far. It is commonly believed that compared to the other industries, the construction industry is usually reluctant to implement new technologies into practice. In form of shape and design, there is basically not much difference between now a days' bearing systems such as beams and columns than the ones in several centuries ago. It can be argued that lack of sophisticated numerical optimization algorithms and powerful computational software, that can produce an accurate representative of complex composite materials such as reinforced concrete, has been one of the main reasons for this issue.

Despite limited implementation, structural optimization has been a hot topic among structural engineers and researchers for the past hundred years. Fortunately, developments in mathematics and computer science have laid the foundation for many breakthroughs ever since. Topology optimization (TO), which is one of the main subcategories within structural optimization, is one of these grand discoveries in the field of design and engineering. TO is a mathematical approach which seeks to redistribute material usage in a given design with a set of load and boundary conditions where the goal is to obtain an optimized design with maximized certain performances. Notably, for the past three decades, and thanks to the development in computer technologies, many methods and algorithms have been introduced and implemented in several commercial software for the purpose of topology optimization. Abaqus, ANSYS and NASTRAN are some examples of these commercial software.



**Figure 1.1** – The Light Rider motorcycle, by Altair and APWorks with 30% weight reduction [1].



**Figure 1.2** – Parametric concept bridge, courtesy of Michael Mitchell [2].

In the past decade, many research and studies have been conducted to employ topology optimization in structural engineering, especially in concrete structures and the results offer huge potentials. Consequently, many innovative and modern construction and manufacturing companies throughout the world have started to put these findings into practice. One of these revolutionary companies in Norway is Rebartek which has already implemented robotic technology into the construction industry and now wants to explore the feasibility of topology optimization in precast concrete elements. This master thesis seeks to apply topology optimization algorithms in a concrete staircase and investigate the impact of material reduction on certain properties such

as deflection and stiffness. The benefits and potentials will be pointed out, and challenges and concerns will be discussed. Despite its extensivity, this report will only showcase the tip of the iceberg. Topology optimization is the future of engineering and manufacturing, and together with parametric modeling will enable mankind to turn many dreams into realities. Figure 1.1 and 1.2 illustrate the application of topology optimization in some industries.



## 2 Social perspective

Sustainable development is by definition the idea that human societies must live and meet their needs without compromising the ability of future generations to meet their own needs [3]. This definition is talking about the necessity of holistic approach regarding sustainability, by considering not only the environmental, but also the social and economic consequences of our behavior as indicated in figure 2.1 [4]. To work towards a greener and more sustainable future, the United Nations (UN) have provided a list of 17 sustainable development goals. Designing a sustainable structure means accounting for short term and long term environmental, social and economical consequences in the design. The UN aims to take climate action and to create both a more sustainable consumption and production [5].



**Figure 2.1** – The holistic view of sustainability [4].

The concrete production, mainly by the contribution of cement, accounts for 5-7% of the CO<sub>2</sub> emissions worldwide [6], and is currently the second most consumed material in the world, only surpassed by water [7]. CO<sub>2</sub> is one of the main contributors to the global climate change, and it is therefore of high priority to reduce this emission number. In other words, the concrete industry has a major responsibility regarding sustainable development. The demands and goals from the UN push the industry to develop new production methods and constantly look for new technologies to create greener manufacturing processes.

According to Agudo et al. [8] from the social point of view, the perception of the sustainability will be different, depending on the situation of the observer, both from a standpoint of social position, and depending on the general circumstances of the country. Thus, in a developing country, a new cement factory creates new jobs, but under the view of a developed country the same fact can be received as a negative for the environment.

One way of reducing the emission numbers is by reducing the consumption of material and amount of natural resources used by the construction industry. If the global concrete consumption was reduced by 25% it would correspond to approximately 600 million tons of CO<sub>2</sub> emission [9]. By applying topology optimization to the

workflow in construction, one is able to create structures with the same level of strength - but with less use of materials. Several studies have shown that it is possible to save up to 70% materials compared to current standardized solutions [9][10]. This shows the huge potential in TO in the construction industry.

TO is a relatively new addition to the industry, and has therefore still some drawbacks that needs to be dealt with before the method is cost efficient [9]. The main challenge is to produce the complicated designs that is developed by topology optimization. To deal with the complicated TO designs, robots are introduced in the production, which reduce the demand for human labor. Concrete labor is a profession that is physically very tough. There are a lot of heavy lifts, unfavorable working positions and abrasion on the neck, shoulders and back. By introducing robotic in the production process, the workers are spared for most of the toughest work. Figure 2.2 and 2.3 highlights the difference between manual labor and robotic fabrication.



**Figure 2.2** – Steel fixers [11].



**Figure 2.3** – Robotic fabrication method [12].

### 3 Theoretical background

#### 3.1 Finite element method

Generally, domains that need to be analyzed are not as simple as a simply supported beam with a conventional cross section. They usually have complex geometry, load and boundary conditions which complicate the analysis process. For these cases, it is generally easier to divide the base domain into smaller components or “elements” which have simpler conditions, geometries and behavior to work with. Hence, the complex continuous system with unknown and complicated geometry, load and boundary conditions will be turned into a discrete and simplified set of “finite” number of elements with already known behaviors and conditions. In the field of continuum mechanics this complex and continuous system is named as a continuum and the process of subdividing a continuum into discrete and simpler components is called discretization. People in different fields have different approaches for discretization of continuum problems, however, all these approaches employ approximation as the main technique. Some of these discretization methods listed below [13][14]:

- Finite Element Method (FEM)
- Boundary Element Method (BEM)
- Finite Difference Method (FDM)
- Finite Volume Method (FVM)
- Spectral Method
- Mesh-free Method

The goal of discretization in the field of engineering is to introduce a direct analogy between finite fragments of a continuum domain, with simple and discrete components in order to determine various properties such as displacements, stresses and strains under specific load and boundary conditions in a certain domain. This approach is called Finite Element Method (FEM). In other words, FEM is a numerical method for solving complex partial differential equations (PDEs) within the mathematical modeling which normally cannot be solved by using analytical methods. The numerical solution is in fact an approximation for the real solution of the PDEs. Such approximations can be estimated by utilizing the FEM. Hence, the purpose of the Finite Element Method is to solve PDEs for obtaining unknown and dependent variables of interest in a domain. These variables are called field variables [13][14]. A simple application of FEM in analyzing a concrete beam is displayed in figure 3.1.

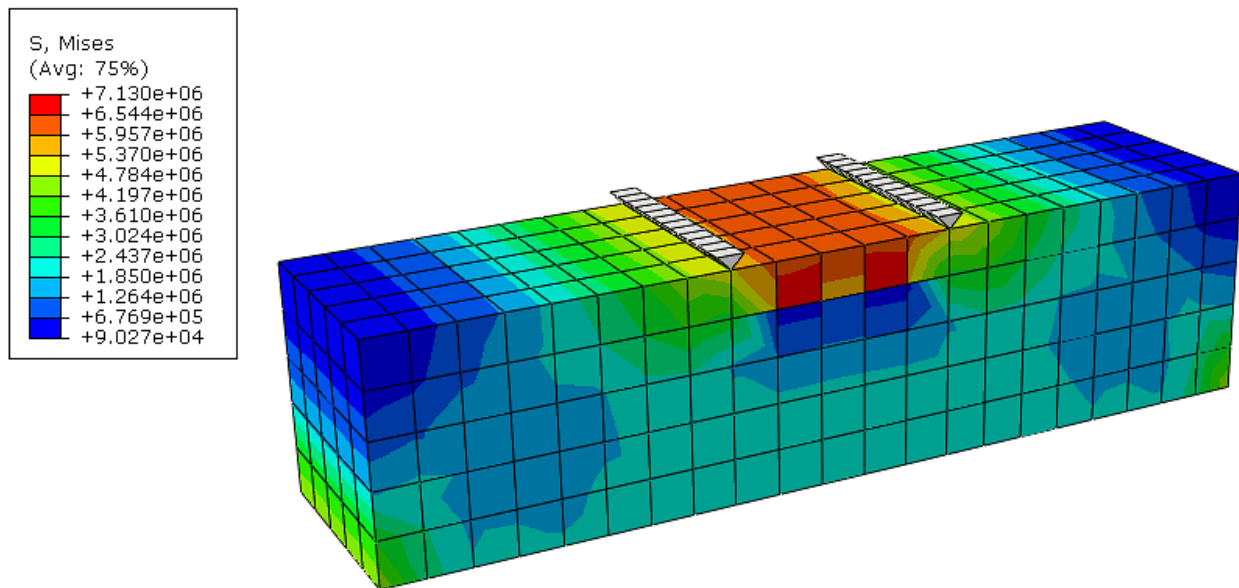


**Figure 3.1** – Structural Analysis of a concrete beam by Finite Element Method [15].

Three essential theories and inventions came together and gave birth to the idea of Finite Element Method listed as follows:

- Matrix Structural Analysis (MSA)
- Variational approximation theory
- Digital computing machines

The combination of these technologies evolved the Finite Element Method through the history and turned it to a strong and applicable tool that laid the foundation for many breakthroughs in the last 70 years. It has been used in various engineering fields such as structural, mechanical, electrical, marine and energy-environment engineering, and industries such as aerospace, oil and sport [13].

### 3.1.1 History

Although the American engineer, M. Jonathan Turner, and Ray Williams Clough, professor of structural engineering at the University of California, were among the first people who introduced the term “Finite Element” in scientific language in their paper, “*Stiffness and Deflection Analysis of Complex Structures*” in 1956 [figure 3.2], the method had its trace way back in the history. More than 2000 years ago, Archimedes used a basic approach of FEM for determining volume, area and length of objects with complex geometries by dividing them into smaller and simpler components and then calculating their contributions for the total geometry. In the 18th century, the Swiss mathematician and engineer, Leonhard Euler applied the Finite Element Method for introducing Euler-Lagrange differential equation of variational calculus [13][14].

In the early 30th, Arthur Roderick Collar and William Jolly Duncan presented the first matrix form solution for determining aeroelasticity. Furthermore, German American mathematician, Richard Courant implemented a

FEM-approach for determining the torsional stiffness of a hollow shaft in 1940s. He called his approach “generalized finite differences” which was inspired by earlier works and results of scholars such as John William Strutt, 3rd Baron Rayleigh, Walther Ritz and Boris Galerkin [13][14].

# JOURNAL OF THE AERONAUTICAL SCIENCES

VOLUME 23

SEPTEMBER, 1956

NUMBER 9

## Stiffness and Deflection Analysis of Complex Structures

M. J. TURNER,\* R. W. CLOUGH,† H. C. MARTIN,‡ AND L. J. TOPP\*\*

### ABSTRACT

A method is developed for calculating stiffness influence coefficients of complex shell-type structures. The object is to provide a method that will yield structural data of sufficient accuracy to be adequate for subsequent dynamic and aeroelastic analyses.

Stiffness of the complete structure is obtained by summing stiffnesses of individual units. Stiffnesses of typical structural components are derived in the paper. Basic conditions of continuity and equilibrium are established at selected points (nodes) in the structure. Increasing the number of nodes increases the accuracy of results. Any physically possible support conditions can be taken into account. Details in setting up the analysis can be performed by nonengineering trained personnel; calculations are conveniently carried out on automatic digital computing equipment.

Method is illustrated by application to a simple truss, a flat plate, and a box beam. Due to shear lag and spar web deflection, the box beam has a 25 per cent greater deflection than predicted from beam theory. It is shown that the proposed method cor-

rection on static air loads, and theoretical analysis of aeroelastic effects on stability and control. This is a problem of exceptional difficulty when thin wings and tail surfaces of low aspect ratio, either swept or unswept, are involved.

It is recognized that camber bending (or rib bending) is a significant feature of the vibration modes of the newer configurations, even of the low-order modes; in order to encompass these characteristics it seems likely that the load-deflection relations of a practical structure must be expressed in the form of either deflection or stiffness influence coefficients. One approach is to employ structural models and to determine the influence coefficients experimentally; it is anticipated that the experimental method will be employed extensively in the future, either in lieu of or as a final check on the results of analysis. However, elaborate

**Figure 3.2** – First appearance of the Finite Element Method in the paper, *Stiffness and Deflection Analysis of Complex Structures*, by Turner et al. in 1956 [16].

The first implementation of FEM in industry was in aerospace structural mechanics when the American company, Boeing, funded Turner in his work to generalize and perfect the Matrix Structural Analysis by introducing the direct stiffness method. So many scholars and engineers have contributed to development of Finite Element Method during the last several decades; pioneers such as Bruce Moncur Irons who invented several tools such as shape function, Robert J. Melosh who systematized the variational derivation of stiffness elements by employing the Rayleigh-Ritz’s variational methods, and Edward L. Wilson who developed the very first and highly regarded FEM-software, SAP, are just some of those contributors [14]. Figure 3.3 shows a chronological chart of the history and development of the FEM.

In the early 60th, Clough, Argyris and Martin, who had learnt the Finite Element Method under the supervision of Turner, implemented the FEM into other engineering fields, particularly civil and structural engineering for the first time. Subsequently, Clough urged Olek Zienkiewicz from the University of Wales, Swansea, to write the first textbook about the application of FEM in civil engineering [14].

Since 1980, due to several developments in software and mathematical abstraction fronts, there have been many breakthroughs and progresses in the Finite Element Method. These breakthroughs have paved the way for construction of many complex and sophisticated designs and structures.

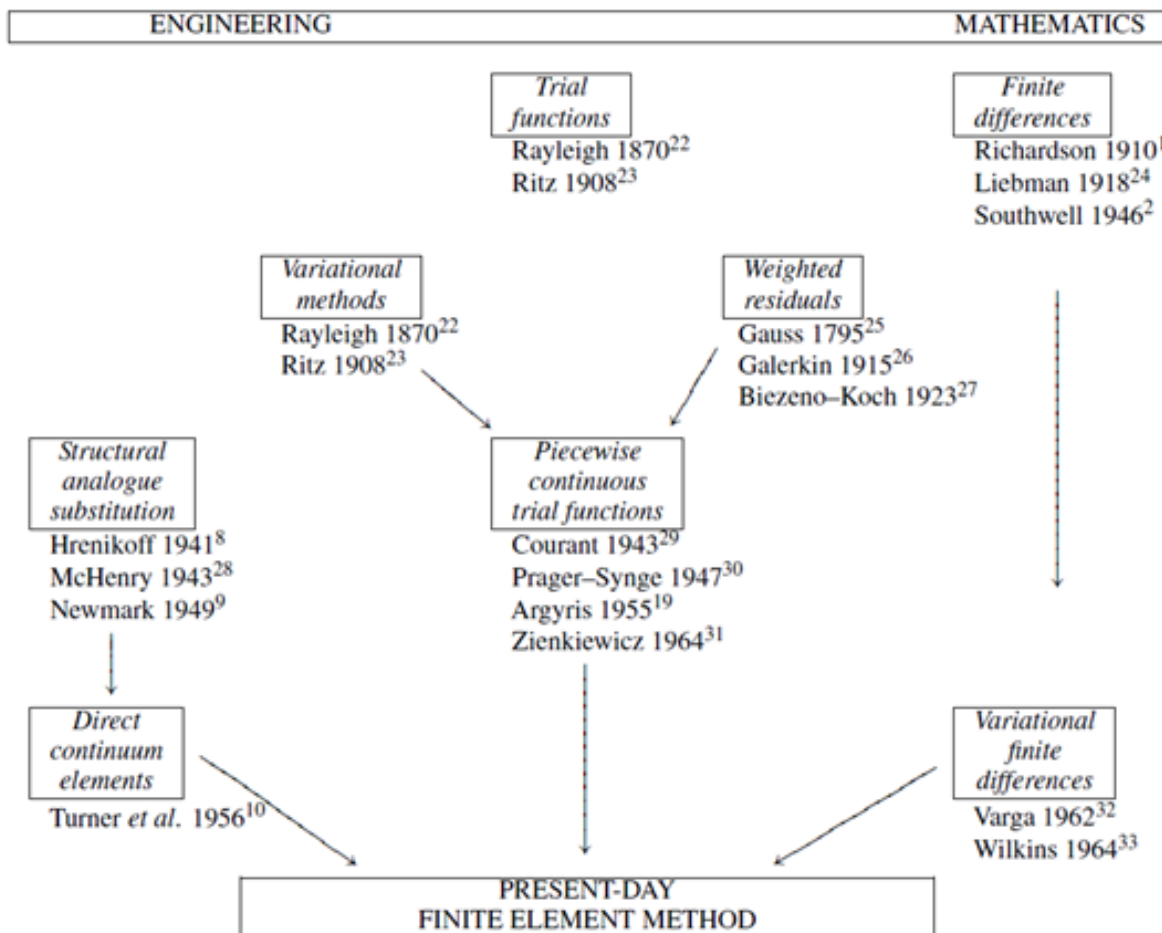


Figure 3.3 – History of Finite Element Method [13].

### 3.1.2 Mathematical interpretation

Introducing some basic terms are essential for better understanding the mathematical aspect of the Finite Element Method.

As described above, the Finite Element Method subdivides a domain,  $\Omega$ , into smaller components which are called finite elements or elements. The process of discretization of the domain is also called meshing. It is assumed that material properties are constant within each element. Elements can be visualized into different shapes based on the dimension of their domains. For instance, in a beam or a bar, which can be categorized as one-dimension objects, the representation of the elements is straight or curved lines while in two-dimension geometries such as plates, elements can be divided into squares, triangles or trapezoids. Illustration of elements in solids can be done by 3D shapes such as hexahedron or tetrahedron. [14][17].

Elements are only attached to each other via a set of joints or points which are called nodal points or nodes. Nodes are defined as specific points at the ambient of finite elements where the values of field variables can be explicitly calculated. Nodes can be categorized in two groups and each carries an important attribute of an element. These two groups and their distinctions are listed below:

- Geometric nodes, which determine geometry of an element through their positioning in the space
- Connection nodes, which decide the element's degrees of freedom (DOF) or in other words, number of primary field variables. In structural and solid mechanics, this term translates to the number of nodal displacements of all nodes in an element [14].

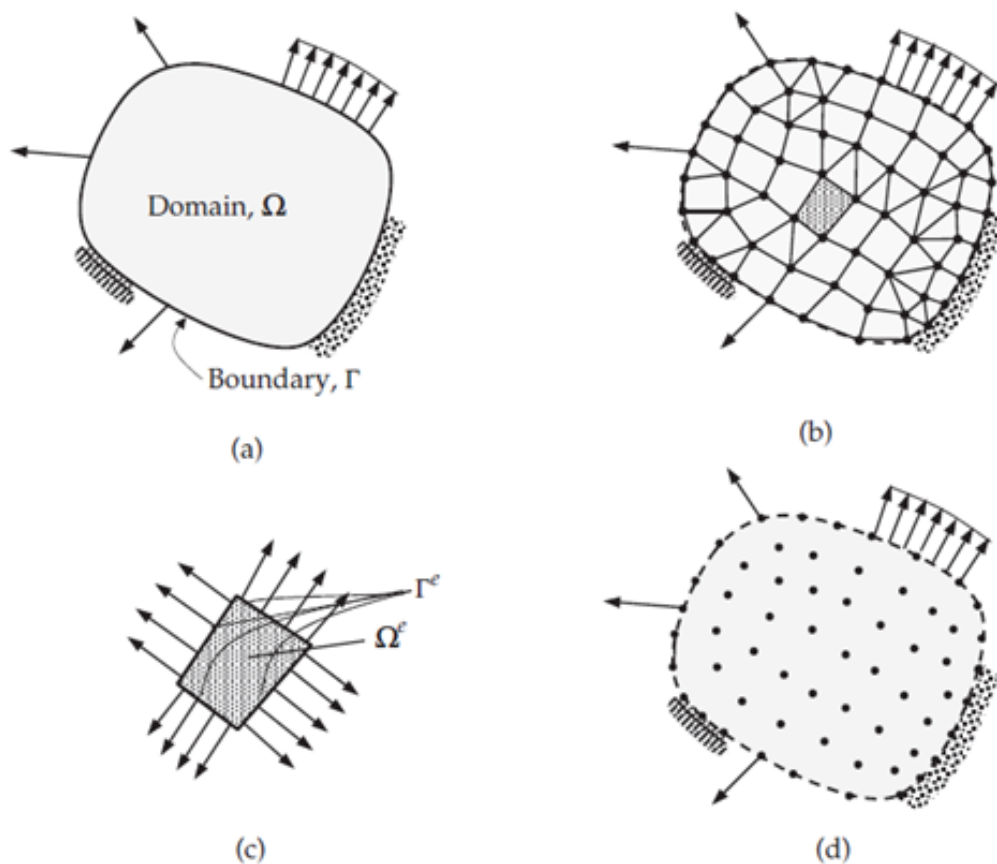


**Figure 3.4** – Discretization of a 2D domain. (a) A typical domain. (b) Meshed representation of the domain. (c) A typical element. (d) Nodal representation of the domain [17].

After introducing basic terms, steps below demonstrate the procedure of applying the Finite Element Method for a three-dimensional domain with hexahedron elements which contain 20 nodes [18]:

Consider  $\mathbf{q}$  as the vector of nodal displacements in a three-dimensional finite element. Let  $\mathbf{v}$  to be the displacement vector of an arbitrary point within this element with components  $v$ ,  $\nu$  and  $\omega$ . The point's coordinates in a local coordination system are  $\xi$ ,  $\eta$  and  $\zeta$ , and in a global coordination system are  $x$ ,  $y$  and  $z$ . Likewise, let  $v_i$ ,  $\nu_i$  and  $\omega_i$  to be displacements at node  $i$  which has local coordinates  $\xi_i$ ,  $\eta_i$  and  $\zeta_i$ , and global coordinates at  $x_i$ ,  $y_i$  and  $z_i$ .

$$\{\mathbf{q}\} = \{v_1 \nu_1 \omega_1 \ v_2 \nu_2 \omega_2 \ \dots \ v_i \nu_i \omega_i\} \quad (1)$$

$$\{\mathbf{v}\} = \{v \ \nu \ \omega\} \quad (2)$$

The next step is to determine the shape function, i.e.,  $\underline{\mathbf{N}}$ . Shape functions or interpolation functions are chosen to interpolate the field variables in each element. Usually, polynomials are employed as shape functions in the FEM where the number of nodes in each element will decide the degree of the polynomial. For a three-dimensional element, the shape function can be written in matrix form as shown below:

$$\underline{\mathbf{N}} = \begin{bmatrix} N_1 & 0 & 0 & N_2 & 0 & 0 & \dots & N_i & 0 & 0 \\ 0 & N_1 & 0 & 0 & N_2 & 0 & \dots & 0 & N_i & 0 \\ 0 & 0 & N_1 & 0 & 0 & N_2 & \dots & 0 & 0 & N_i \end{bmatrix} \quad (3)$$

Where:

$$N_i = \frac{1}{8}(1 + \xi_0)(1 + \eta_0)(1 + \zeta_0)(\xi_0 + \eta_0 + \zeta_0 - 2) \text{ at } i = 1, 3, 5, 7$$

$$N_i = \frac{1}{4}(1 - \xi^2)(1 + \eta_0)(1 + \zeta_0) \text{ at } i = 2, 6, 14, 18$$

$$N_i = \frac{1}{4}(1 - \eta^2)(1 + \xi_0)(1 + \zeta_0) \text{ at } i = 4, 8, 16, 20$$

$$N_i = \frac{1}{4}(1 - \zeta^2)(1 + \eta_0)(1 + \xi_0) \text{ at } i = 9, 10, 11, 12$$

And:

$$\xi_0 = \xi_0 \xi$$

$$\eta_0 = \eta_0 \eta$$

$$\zeta_0 = \zeta_0 \zeta$$

Based on geometrical equations, the following relation can be presented between nodal displacements and displacement of an arbitrary point in the element:

$$\{\mathbf{v}\} = \underline{\mathbf{N}}\{\mathbf{q}\} \quad (4)$$

Considering  $\epsilon$  to be the strain vector, following relation can also be defined between strains and displacements:

$$\{\epsilon\} = \underline{\mathbf{D}}\{\mathbf{v}\} \quad (5)$$

Where  $\underline{\mathbf{D}}$  is a mathematical operator and is called the differentiation matrix:

$$\underline{\mathbf{D}} = \begin{bmatrix} \partial/\partial x & 0 & 0 \\ 0 & \partial/\partial y & 0 \\ 0 & 0 & \partial/\partial z \\ \partial/\partial y & \partial/\partial x & 0 \\ 0 & \partial/\partial z & \partial/\partial y \\ \partial/\partial z & 0 & \partial/\partial x \end{bmatrix}$$



Note that the Hook's law also applies in elastic region between strains and stresses:

$$\{\boldsymbol{\sigma}\} = \underline{\mathbf{E}}\{\boldsymbol{\epsilon}\} \quad (6)$$

Where  $\boldsymbol{\sigma}$  is stress vector and  $\underline{\mathbf{E}}$  is elasticity matrix. They are respectively shown below:

$$\boldsymbol{\sigma} = \left\{ \sigma_x \quad \sigma_y \quad \sigma_z \quad \tau_{xy} \quad \tau_{yz} \quad \tau_{zx} \right\}$$

$$\underline{\mathbf{E}} = \begin{bmatrix} \lambda + 2\mu & \lambda & \lambda & 0 & 0 & 0 \\ \lambda & \lambda + 2\mu & \lambda & 0 & 0 & 0 \\ \lambda & \lambda & \lambda + 2\mu & 0 & 0 & 0 \\ 0 & 0 & 0 & \mu & 0 & 0 \\ 0 & 0 & 0 & 0 & \mu & 0 \\ 0 & 0 & 0 & 0 & 0 & \mu \end{bmatrix}$$

$$\lambda = \frac{\nu E}{(1 + \nu)(1 - 2\nu)}$$

$$\mu = \frac{E}{2(1 + \nu)}$$

- $E$ : elasticity modulus
- $\nu$ : Poisson's ratio

Following equations 4 and 5, the relation below can be acquired:

$$\{\boldsymbol{\epsilon}\} = \underline{\mathbf{B}}\{\mathbf{q}\} \quad (7)$$

Where  $\underline{\mathbf{B}}$  is called the displacement differentiation matrix and is equal to the product of differentiation operator matrix,  $\underline{\mathbf{D}}$  and the shape function,  $\underline{\mathbf{N}}$ :

$$\underline{\mathbf{B}} = \underline{\mathbf{D}}\underline{\mathbf{N}} = \left[ \underline{\mathbf{B}}_1 \quad \underline{\mathbf{B}}_2 \quad \underline{\mathbf{B}}_3 \quad \dots \quad \underline{\mathbf{B}}_i \right] \quad (8)$$

$$\underline{\mathbf{B}}_i = \begin{bmatrix} \partial N_i / \partial x & 0 & 0 \\ 0 & \partial N_i / \partial y & 0 \\ 0 & 0 & \partial N_i / \partial z \\ \partial N_i / \partial y & \partial N_i / \partial x & 0 \\ 0 & \partial N_i / \partial z & \partial N_i / \partial y \\ \partial N_i / \partial z & 0 & \partial N_i / \partial x \end{bmatrix} \quad (9)$$

Finally, by employing the theorem of virtual displacement, the following relation between nodal displacement and load vector can be attained:

$$\underline{\mathbf{K}}\{\mathbf{q}\} = \{\mathbf{f}\} \quad (10)$$

Where  $\{\mathbf{f}\}$  is the load vector which is applied to the element and  $\underline{\mathbf{K}}$  is called the element's stiffness matrix and can be calculated by the following equation:

$$\underline{\mathbf{K}} = \int \underline{\mathbf{B}}^T \underline{\mathbf{E}} \underline{\mathbf{B}} \, dv \quad (11)$$

### 3.2 Topology optimization

Due to reduction or exhaustion of material resources in the near future, and their extraction's impact on the environment, producing lightweight, low cost and high-performance structures are more demanded. Topology optimization is among methods which address these issues through optimizing material use in products and structures. In order to comprehend the notion of topology optimization, it is essential to define structural optimization. SO can be defined as a set of techniques which allows engineers to systematically design optimized components. The optimization can be based on different criteria, e.g. maximum stiffness, minimum self-load, etc. These criteria are called objective functions. In addition to objective functions which are the goal of simulation, one must also define some secondary objectives, called constraints. These are certain restrictions that are applied to the model when seeking to maximize or minimize an initially defined objective function. Amount of material used, type of material used, maximum allowed stress, etc., are some of the common constraints in structural optimization's problems. An optimization is successfully achieved when the objective function converges after a number of iterations, while simultaneously satisfying the criteria in predefined constraints. The main target of structural optimization consists of presenting the best possible way of material distribution within a given design space without exceeding the allowable stress due to applied loads to the element. SO seeks to increase efficiency of material usage in structural designs and introduce more economical solutions which satisfy specific objective functions due to some certain constraints. Developments in mathematics such as optimization theory and variational calculus, as well as computational methods such as Finite Element Method, and computer technology have facilitated a strong foundation for the SO [19]. Structural optimization can be divided in three main groups. These groups are listed below and their applications are demonstrated in figure 3.5 [20]:

- Size optimization, where the goal is to acquire an optimal design by changing size variables in a domain such as cross sections or thicknesses. This approach is the simplest and most primal method in the field of structural optimization.
- Shape optimization, that seeks to acquire the form or shape of some parts of the boundary in a domain. An unknown equation or a set of points with unknown positions can be applied to obtain the form of these parts.
- Topology optimization can be applied for both discrete and continuum structures. Finding optimal spatial order and connectivity of the bars are the goal of topology optimization in discrete structures such as trusses and frames. As for continuum structures, identifying the best geometries and positions of cavities in the domain is the way of obtaining the optimal design.

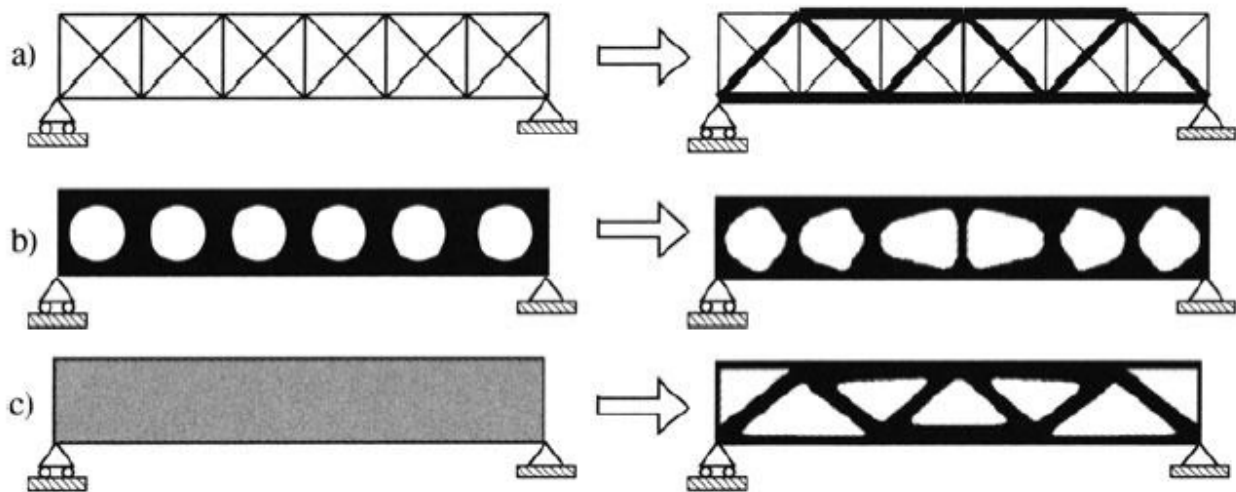


**Figure 3.5** – Three groups of structural optimization: a) Size optimization, b) Shape optimization and c) Topology optimization [21].

This study will only take topology optimization into account and therefore disregard the other two methods. The topology optimization is the most general, and at the same time the most sophisticated method of structural optimization. It is widely recognized that topology optimization has a great prospect in structural engineering design [20]. The range of its application knows no boundaries; although it is widely employed in structural engineering, it has also been applied in thermal, fluid, electrical and bio-mechanical cases. There are no scale- and size-related limitations on employment of topology optimization either; objects from large-scale structures such as buildings and bridges, to micro- or nano-size systems such as microstructures, can be optimally designed by utilizing the topology optimization [22]. Despite some complexities and challenges, topology optimization provides the most rewarding results with regards to economy and design's freedom compared to the two former approaches. The major difference between size and shape optimization with topology optimization lies in the degree of freedom of optimization. In the first two methods, elements of a structure can be optimized within their limits and constraints, however they cannot be omitted. In a different manner, topology optimization provides designers with two important and advantageous features [20]:

- Materials within the design domain can have various elastic properties meaning that the density of the material can vary.
- Materials can be completely omitted from the design domain.

### 3.2.1 History

It was first in 1854 that James Clerk Maxwell, the Scottish physicist and scientist who laid the foundation for topology optimization. In that year, he made a topological investigation of a truss where the goal was to minimize the weight under a certain load condition [23]. Subsequently, in 1904, Anthony Michell, the Australian mechanical engineer, published his theory which is commonly known as the Mitchell truss or Mitchell structure. His model, which is shown in figure 3.6, was based on volume reduction of 2D trusses with a single load condition and a stress constraint [24]. In his paper, Mitchell stated:

*“a frame (today called truss) (is optimal) attains the limit of economy of material possible in any frame-structure under the same applied forces, if the space occupied by it can be subjected to an appropriate small deformation, such that the strains in all the bars of the frame are increased by equal fractions of their lengths, not less than the fractional change of length of any element of the space [25].”*

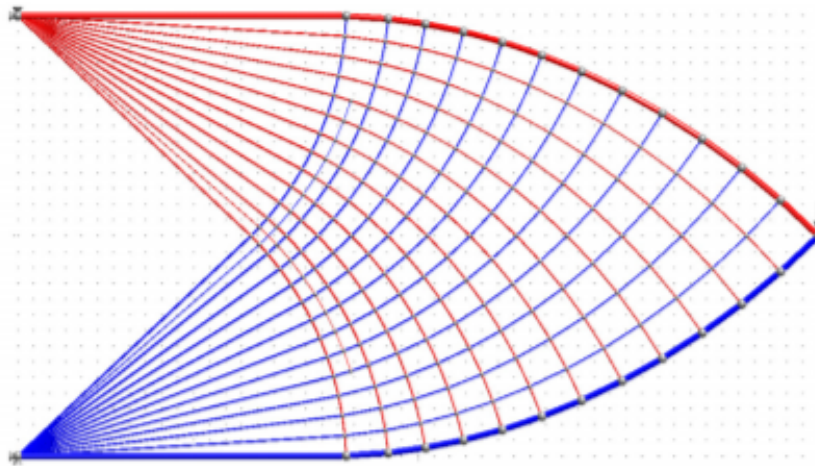


**Figure 3.6** – An optimal Mitchell truss after 104 iterations [20].

Mitchell's work was significant because he opened a new chapter in engineering science when mathematical knowledge was in early stage and computational tools were nonexistent. Despite his breakthrough, it took scientists and researchers more than half of a century to take the next important step in this field. In 1964, W. S. Dorn et al. proposed a new method which was called *Ground structure*. His proposal introduced a new approach for defining structural nodes, points of support and point of load application, and their connections through elements. Developments in computer science provided new opportunities for researchers to introduce and propose new theoretical and computational methods in the field of topology optimization and its application in different technologies and industries. During the 80th, several investigations were conducted with the help of newly developed software and application of Finite Element Method (FEM) and finite element meshes [26]. In 1988, Bendsøe and Kikuchi introduced a new approach for shape optimization which also took topology optimization into the next level [21].

Since then, many research and studies have been done in the field of topology optimization which have led to introducing and developments of several numerical methods to achieve the best topologically optimized structures. All these methods can be categorized in two main groups - optimally criteria and heuristic. The following sections will explain the characteristics and distinctions of these two groups.

### 3.2.2 Optimally criteria methods

The methods within this group can be applied for cases that must satisfy certain criteria which are related to the structure's behavior. Hence, there are some constraints that must be considered during optimization of the design. These methods are mostly applicable for cases that have a lot of design's variables and few constraints. The list below consists of the most notable optimally criteria methods:





- Homogenization
- Level set method
- Solid Isotropic Material with Penalization (SIMP)
- Growth Method for Truss Structures [20]

### 3.2.3 Heuristic or Intuitive methods

These methods are mainly inspired from the nature and biological systems. It is noteworthy to mention that although these methods do not necessarily lead to optimized designs, nonetheless, they can introduce new adequate solutions. The most applicable approaches of heuristic methods are listed below:

- Fully Stressed Design
- Computer-Aided Optimization (CAO)
- Soft Kill Option
- Evolutionary Structural Optimization (ESO)
- Bidirectional Evolutionary Structural Optimization (BESO)
- Sequential Element Rejection and Admission (SERA)
- Isolines/Isosurfaces Topology Design (ITD) [20]

Most of the mentioned methods above use iterative processes to identify elements which bear little load and then investigate the possibility of removing them. Despite their differences, all of them seek to achieve the same purpose. The goal of these methods in structural engineering is to identify an optimal domain,  $\Omega^{mat}$  within a larger domain,  $\Omega$ , which occupies less volume while still satisfies the requirements with regards to the objective functions and constraints. The reference domain,  $\Omega$ , which is also called ground structure or design space, is selected to allow for a definition of the applied loads and boundary conditions [21]. Figure 3.7 illustrates the optimal domains of different topology optimization algorithms.

	Optimization parameters	Total iteration	Solutions (for volume fraction of 50 %)		Error <sup>1</sup> (%)
Hard-kill BESO <sup>2</sup>	$ER = 2\%$ $AR_{\max} = 50\%$ $r_{\min} = 3.0 \text{ mm}$	52		$C = 181.79 \text{ Nmm}$	0.61
Soft-kill BESO	$ER = 2\%$ $p = 3.0$ $r_{\min} = 3.0 \text{ mm}$	46		$C = 181.71 \text{ Nmm}$	0.56
SIMP	$m = 0.02$ $p = 3.0$ $r_{\min} = 3.0 \text{ mm}$	44		$C = 201.70 \text{ Nmm}$	11.63
Continuation	$r_{\min}^{ini} = 3.0 \text{ mm}$ $\Delta r_{\min} = 0.1 \text{ mm}$ $r_{\min}^{evol} = 1.0 \text{ mm}$	267		$C = 180.69 \text{ Nmm}$	–

**Figure 3.7** – Application of several topology optimization algorithms in a cantilever beam [22].

This study will discuss two of these approaches, SIMP and BESO, in details in section 3.2.5 and 3.2.6, which are similar to the topology optimization algorithms that are employed in Abaqus Topology Optimization Module, also known as ATOM. However, in prior to discuss these two methods, it is essential to understand the concept of compliance and strain energy.

### 3.2.4 Compliance and strain energy

Compliance is a way of measuring overall flexibility or stiffness in structures and is equal to the sum of strain energy in the structure or the external work by the applied load. Mathematically in general form it can be derived from the equation 12 [22]:

$$C = \frac{1}{2} \mathbf{f}^T \mathbf{u} \quad (12)$$

- $\mathbf{f}^T$ : transposed load vector
- $\mathbf{u}$ : displacement vector

Knowing that the minimum displacement at the position of load application leads to minimum elastic energy stored in the structure, it can be concluded that minimizing the elastic energy in a structure results to a stiffer structure. This stored energy in a structure due to deformation is called strain energy and is equal to half of the mean compliance at equilibrium. Equations 13 and 14 are given to calculate strain energy of a three-dimensional continuum in general form and discretized finite element form respectively [19]:

$$\text{strain energy} = \int_V \frac{1}{2} \sigma \epsilon dV \quad (13)$$

$$\text{strain energy} = \frac{1}{2} \{u\}^T [K] \{u\} \quad (14)$$

Based on equation 15 it can be mathematically shown that an increase in the mean compliance due to removal of the element  $i$  is equal to the strain energy in the element  $i$  [22]:

$$\Delta C = \frac{1}{2} \mathbf{f}^T \Delta \mathbf{u} = \frac{1}{2} \mathbf{u}_i^T \mathbf{K}_i \mathbf{u}_i \quad (15)$$

- $\mathbf{u}_i$ : displacement of the  $i$ th element
- $\mathbf{K}_i$ : stiffness matrix of the  $i$ th element

A large number of the topology optimization's methods seeks to minimize the compliance in structures. This configuration is usually referred to as minimizing strain energy in most of the current commercial software. Compliance is inversely proportionated with stiffness and therefore minimum compliance leads to maximum stiffness. Considering an arbitrary design space, the optimal domain based on minimum compliance can be obtained as the optimal choice of stiffness tensor which is denoted as  $E_{ijkl}(x)$ . This tensor is a variable over the domain and can be obtained through equation 16 which shows the internal virtual work of an elastic body at the equilibrium  $v$  and for an arbitrary virtual displacement  $\nu$  [21]:

$$a(v, \nu) = \int_{\Omega} E_{ijkl}(x) \epsilon_{ij}(v) \epsilon_{kl}(\nu) d\Omega \quad (16)$$

Whereas  $\epsilon_{ij}(v)$  and  $\epsilon_{kl}(\nu)$  are linearized strains and can be calculated by the following formula [21]:

$$\epsilon_{ij}(v) = \frac{1}{2} \left( \frac{\partial v_i}{\partial x_j} + \frac{\partial v_j}{\partial x_i} \right)$$

Ultimately the minimum compliance can be shown in its weak, variational form in the equation 17 [21]:

$$\begin{aligned} & \min_{\epsilon \in U, E} l(v) \\ & \text{subject to: } a_E(v, \nu) = l(v), \text{ for all } v \in U \ \& \ E \in E_{ad} \end{aligned} \quad (17)$$

Where  $U$  represents the space of kinematically admissible displacement fields and  $l(v)$  is the load in its linear form and can be illustrated in the following formula [21]:

$$l(v) = \int_{\Omega} f v d\Omega + \int_{\Gamma_T} t v ds$$

- $f$ : body forces
- $t$ : boundary tractions on the traction part  $\Gamma_T \subset \Gamma \equiv \partial\Omega$  of the boundary

In equation 17,  $E_{ad}$  stands for the set of admissible stiffness tensors for the design domain. Hence, it contains all the stiffness tensors within the optimal design ( $\Omega^{mat}$ ) and is set to zero elsewhere [21].

Commercial software operate on the basis of discretization approach to solve optimization problems. Assuming that the same finite element mesh has been applied for displacement and stiffness tensor,  $E$ , and that discretized  $E$  remains constant in each finite element, the following discretized form of equation can be constructed in equation 18 [21]:

$$\begin{aligned} & \min_{\epsilon, E_e} \mathbf{f}^T \mathbf{v} \\ & \text{subject to: } \mathbf{K}(E_e) \mathbf{v} = \mathbf{f}, \text{ for } E_e \in E_{ad} \end{aligned} \quad (18)$$

- $f$ : load vector
- $v$ : displacement
- $K$ : stiffness matrix which can be obtained by the following formula [21]:

$$K = \sum_{e=1}^N K_e(E_e)$$

- $N$ : number of finite elements
- $E_e$ : stiffness in element  $e$
- $K_e$ : global element stiffness matrix

### 3.2.5 Solid Isotropic Material with Penalization (SIMP)

Introduced by Bendsøe in 1989 and then extensively developed by Rozvany and Zhou in 1991, Solid Isotropic Material (Microstructure) Penalization (SIMP) is the most implemented topology optimization method in commercial software. SIMP is based on the idea of discretization of the domain and utilizing one design variable per finite element. This design variable is in fact the relative density in an artificial isotropic material, which can vary continuously in the range of zero and one, where zero represents void (no material) and one means filled with material. It is noteworthy to mention that the elasticity tensor of this artificial isotropic material is considered to be a function of penalized density of the material [21]. Rozvany proposed five types of finite elements for the SIMP-method:

- Solid (S) where the element is filled entirely with one material.
- Empty (E) where it contains no material.
- Porous (P) if it contains one material and void (i.e., cavities or empty space).
- Composite (C) where element consists of more than one material but no void.
- Composite-Porous (CP) which consists of more than one material and void [27].

SIMP can be mathematically described in the equation set 19 [21]:

$$\begin{aligned}
 E_{ijkl}(x) &= \rho^p(x) E_{ijkl}^0 \quad \text{for } p > 1 \\
 \int_{\Omega} \rho(x) d\Omega &\leq V \quad \text{for } 0 \leq \rho(x) \leq 1 \quad \& \quad x \in \Omega
 \end{aligned}
 \tag{19}$$

In equation 19,  $p$  is called penalization factor. The reason that it has been set to be greater than one is to make intermediate densities unfavorable. Therefore, the acquired stiffness will be small in comparison to volume of the material which makes it uneconomical to include intermediate densities in the final optimal design. Moreover, experiments show that in problems where volume constraint is active, choosing a significantly large penalization factor ( $p \geq 3$ ) will lead to better and more realistic results [21][27].



That is, the minimum compliance problem which is shown in equation 17 can be rewritten as follow [21]:

$$\begin{aligned}
 & \min_{\epsilon \in U, \rho} l(v) \\
 & \text{subject to: } a_E(v, \nu) = l(v), \text{ for all } v \in U \text{ \& } \\
 & E_{ijkl}(x) = \rho^p(x) E_{ijkl}^0 \text{ for } p > 1 \\
 & \int_{\Omega} \rho(x) d\Omega \leq V; \text{ for } 0 < \rho_{min} \leq \rho(x) \leq 1 \text{ \& } x \in \Omega
 \end{aligned} \tag{20}$$

$\rho_{min}$  is called lower bound and has been introduced to prevent any possible singularity of the equilibrium problem. Its value is usually set as  $\rho_{min} = 0.001$  [21].

An iterative procedure is implemented in the SIMP-algorithm which employs a displacement-based finite element analysis and then optimally updates the density's criteria scheme. After making the initial model, the iterative process starts as followed [21]:

1. The first step is to run a finite element analysis in order to calculate displacements and strains which define distribution of density.
2. The next step is to compute the derivatives of the displacement with respect to the design variables which is called sensitivity analysis.
3. Prior to initiate the updating process of the densities, filtering techniques must be applied to ensure numerical stability. Minimum compliance criteria and a new finite element analysis are employed for this purpose. The mathematical approach is shown in the equation set 21:

$$\begin{aligned}
 & \min_{\rho_e} C(\rho_e) \\
 & \text{subject to: } \sum_{e=1}^N v_e(\rho_e) \text{ for } 0 < \rho_{min} \leq \rho_e \leq 1 \\
 & C(\rho_e) = \mathbf{f}^T \mathbf{u} \text{ and } \sum_{e=1}^N \rho_e^p \mathbf{K}_e \mathbf{u} = \mathbf{f}
 \end{aligned} \tag{21}$$

- $N$ : number of finite elements in the domain
- $v_e$ : volume of the element  $e$
- $\rho_e$ : artificial density of the element  $e$

The iterative procedure above will repeat until either of convergence or the stopping criteria is achieved. Figure 3.8 illustrates the steps of the SIMP-algorithm in a flowchart [21]. An analogous algorithm has been integrated in Abaqus Topology Optimization Module (ATOM) under the name of general or sensitivity-based method [28]. The Abaqus/CAE user's manual describes the algorithm with the following comment [29]:

*“General topology optimization uses an algorithm that adjusts the density and stiffness of the design variables while trying to satisfy the objective function and the constraints.”*

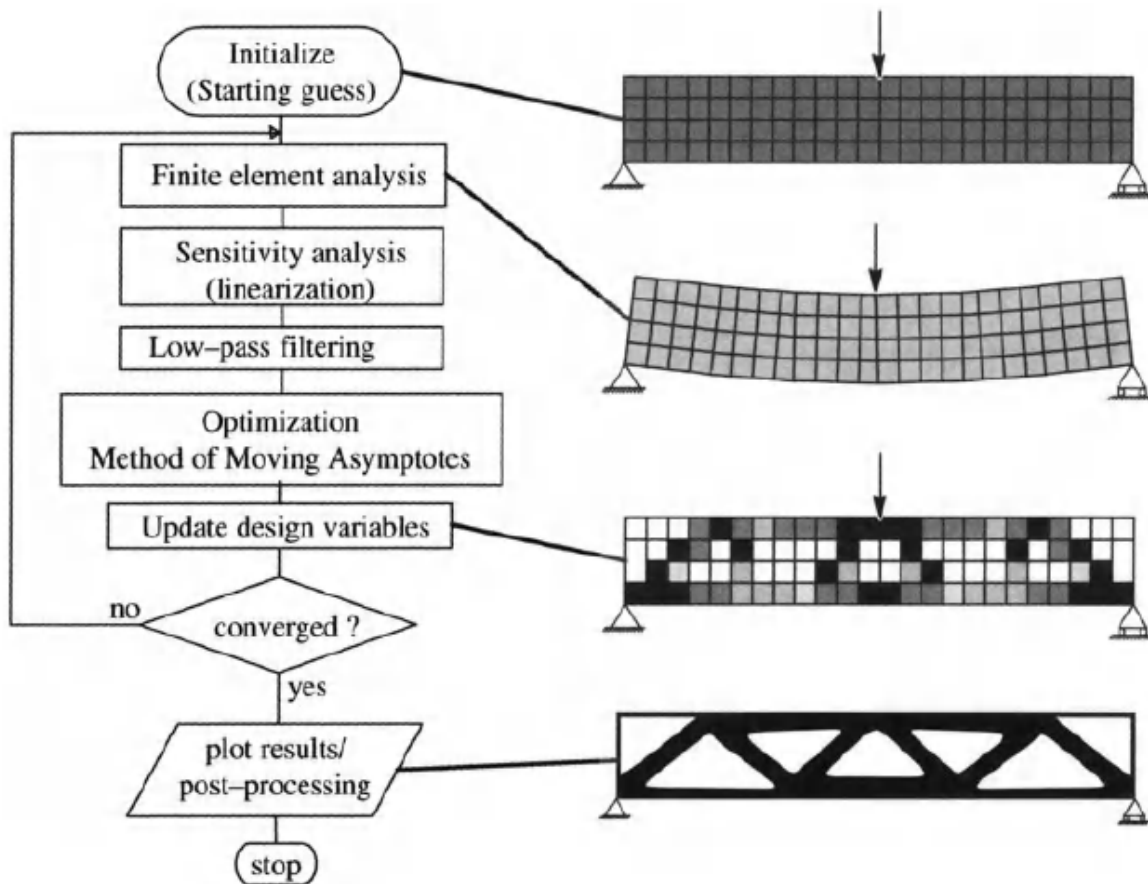


**Figure 3.8** – Algorithm of the SIMP [21].

Implementation of the SIMP-method provides some advantages and also have some limitations. Some of the most important pros and cons of the SIMP are listed below:

- Since SIMP solves for only one design variable per element the CPU usage and calculation time are considerably lower than other methods which increase the computational efficiency of the method.
- SIMP can be freely applied in any combination of design constraint which makes the method remarkably robust.
- Penalization can be chosen freely depending on the required precision of the results.
- SIMP does not require derivations involving higher mathematics and therefore bears conceptual simplicity.
- The microstructure in SIMP is not necessarily needed to be homogeneous.
- A disadvantage of the SIMP is that the solution is heavily dependent on the penalization factor and it does not always converge to the optimal design.
- SIMP is extremely mesh-dependent. By employing finer mesh, larger number of holes and voids will be created. Figure 3.9 illustrates mesh-dependency of the SIMP method.

- Density-based models such as SIMP are mostly applied for linear elastic analysis in view of their limited ability to solve non-linear problems with considerable deflection [27].

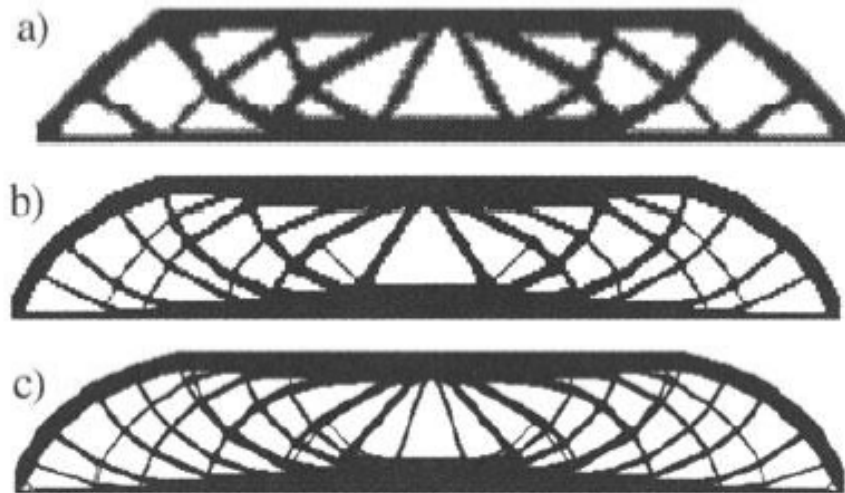


**Figure 3.9** – Evolution of a SIMP example with a) 2700; b) 4800 and c) 17200 elements [21].

### 3.2.6 Bi-directional evolutionary structural optimization (BESO)

BESO was first introduced in 1998 by Querin and Yang et al. [22][28]. BESO and SIMP are fairly similar as both of them employ outputs from Finite Element Analysis to determine efficiency and distribution of finite elements in a domain after consecutive iterations [28]. However, unlike SIMP which only removes material from the model, BESO allows materials to be simultaneously added to the initial domain too. Subsequently, relative density value in the SIMP can vary between  $\rho_{min}$  and 1, while elements in the BESO can be either be discretely present (1) or absent (0) [28]. Final design in the BESO is obtained when a given convergence or stopping criteria is reached. Since its first appearance, there have been several modifications and new approaches in BESO in order to address some problems. However, the two most notable versions are soft-kill method and hard-kill method. In soft-kill method, void elements attain an adequately low Young's modulus to reduce their influence in the design whereas, in hard-kill method, elements can be completely removed from the final design [28]. In his initial paper, Yang introduced sensitivity numbers for void elements which could be obtained through a linear extrapolation of the displacement field after the finite element analysis. Subsequently, solid elements which owned low sensitivity numbers would be removed from the initial domain, and void elements with high sensitivity numbers would be turned into solid elements. After each iteration, the number of added and removed elements were estimated through the rejection ratio (RR) and the inclusion ratio (IR) which are two independent parameters. Later on, Querin et al. proposed another approach for BESO where the sensitivity numbers were substituted with von Mises stresses. Consequently, void elements with high von Mises would become solid elements and solid elements with low von Mises stress would be removed [22].

However, these approaches have proved to be cumbersome in practice; the required accuracy in selecting the RR and IR values is evidently high in order to achieve a good optimal design. It is also confirmed that due to large number of required iterations, the computational efficiency is relatively low. Additionally, in some cases, the final optimized design must be chosen from a large number of generated topologies while the convergence

history of the targeted design is usually very disordered. In 2007, Huang and Xie presented a new BESO procedure for stiffness optimization which addresses the mentioned concerns above. Instead of displacement or von Mises stresses, their sensitivity numbers are based on elemental strain energy density. They introduced a mesh-independency filter in order to flatten these sensitivity numbers within the design domain. This approach greatly improves the convergence histories of the mean compliance and the structural topology [22]. Figure 3.10 displays the evolution of a simply supported beam with a point load at the bottom center with the help of the BESO method where symmetry is employed and therefore only half the domain is designed.

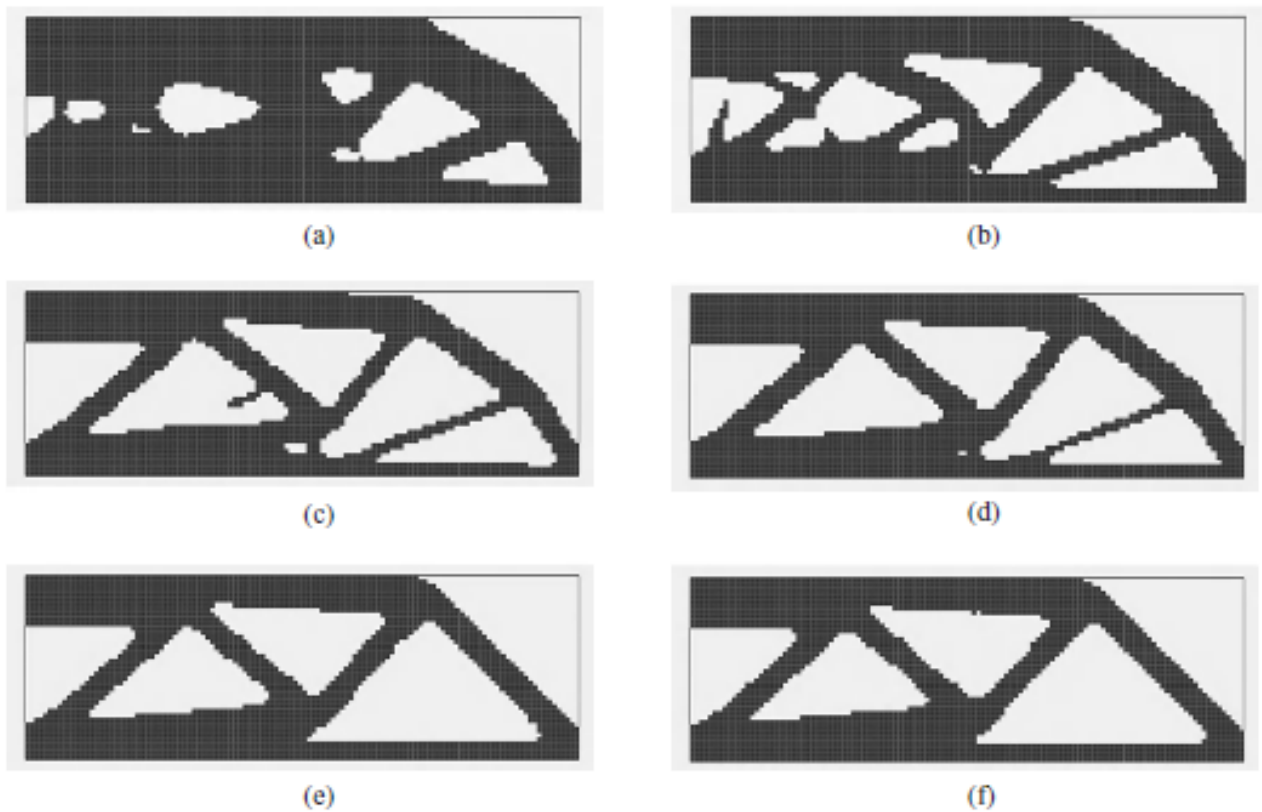


**Figure 3.10** – Evolution of the beam after a) 5 iterations; b) 10 iterations; c) 15 iterations; d) 25 iterations; e) 40 iterations; f) 53 iterations (final topology) [22].

Mathematically, the BESO-model can be described in equation 22 :

$$\begin{aligned}
 \min C &= \frac{1}{2} \mathbf{f}^T \mathbf{u} \\
 \text{subject to: } V^* - \sum_{e=1}^N V_e x_e & \text{ for } x_e = \begin{cases} 0 \\ 1 \end{cases}
 \end{aligned} \tag{22}$$

- $\mathbf{f}^T$ : transposed applied load vector
- $\mathbf{u}$ : displacement vector
- $C$ : mean compliance
- $V^*$ : volume constraint or total structural volume

- $V_i$ : volume of the element  $i$
- $N$ : total number of finite elements
- $x_i$ : binary design variable which is either 0 (absence of an element) or 1 (presence of an element) in the design domain

Subsequently, the elemental sensitivity number or as presented by Huang and Xie, the elemental strain energy, is equal to the change of the mean compliance and is expressed in equation 23:

$$\alpha_i^e = \Delta C = \frac{1}{2} \mathbf{u}_i^T \mathbf{K}_i \mathbf{u}_i \quad (23)$$

Where  $\mathbf{K}_i$  and  $\mathbf{u}_i$  are elemental stiffness matrix and nodal displacement vectors in  $i$ th element, respectively. In case of nonuniform mesh, the effect of the volume of each element must also be taken into consideration and therefore the equation above can be rewritten as stated in equation 24:

$$\alpha_i^e = \Delta C = \left( \frac{1}{2} \mathbf{u}_i^T \mathbf{K}_i \mathbf{u}_i \right) / V_i \quad (24)$$

One of the advantages that the BESO method has in comparison to the SIMP method, is mesh-independency. It is common knowledge that often different finite element meshes generate different topologies. In order to achieve mesh-independency, the BESO introduces the sensitivity filter scheme which is shown in equation set 25:

$$\begin{aligned} \omega_i &= \frac{1}{1 - M} \left( 1 - \frac{r_{ij}}{\sum_{i=1}^M r_{ij}} \right) \\ \alpha_j^n &= \sum_{i=1}^M \omega_i \alpha_i^e \\ \omega(r_{ij}) &= r_{min} - r_{ij} \quad j = 1, 2, \dots, K \\ \alpha_i &= \frac{\sum_{j=1}^K \omega(r_{ij}) \alpha_j^n}{\sum_{j=1}^K \omega(r_{ij})} \end{aligned} \quad (25)$$

In this equation set  $r_{ij}$  denotes the center distance between the  $i$ th element and the  $j$ th node.  $M$  stands for the total elements that are connected to the  $j$ th node.  $\omega_i$  represents the weight factor of the  $i$ th element where  $\sum_{i=1}^M \omega_i = 1$  and  $\alpha_j^n$  is called the average elemental sensitivity numbers.  $r_{min}$  is the length scale which creates a circular sub-domain,  $\Omega_i$ , as shown in figure 3.11. This sub-domain contains the nodes that influence the sensitivity of the  $i$ th element. The scale length is usually chosen big enough so that  $\Omega_i$  covers more than one element. The number of elements in the  $\Omega_i$  is shown by  $K$  and  $\omega(r_{ij})$  is the linear weight factor [22].

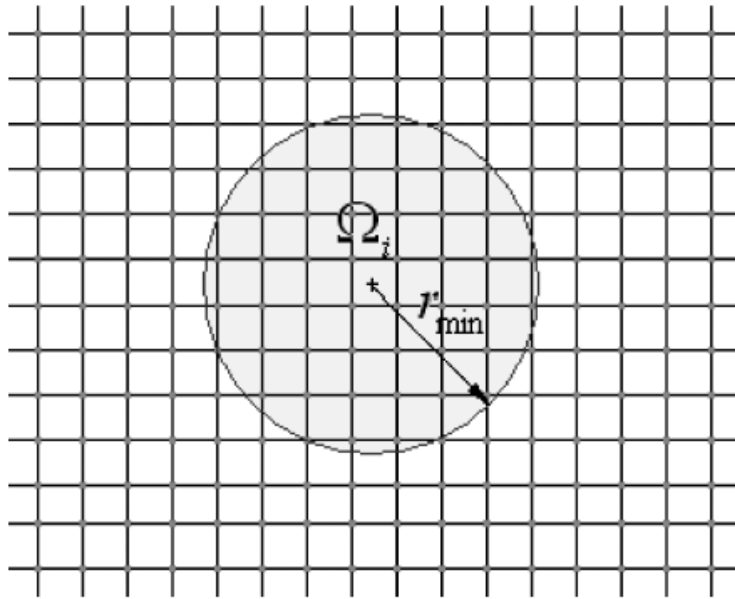
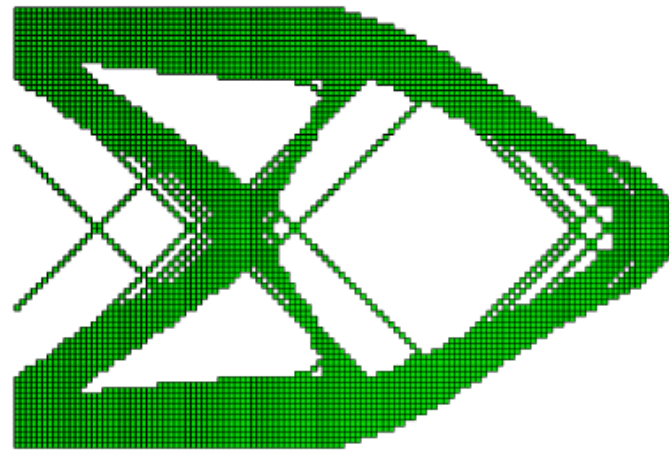
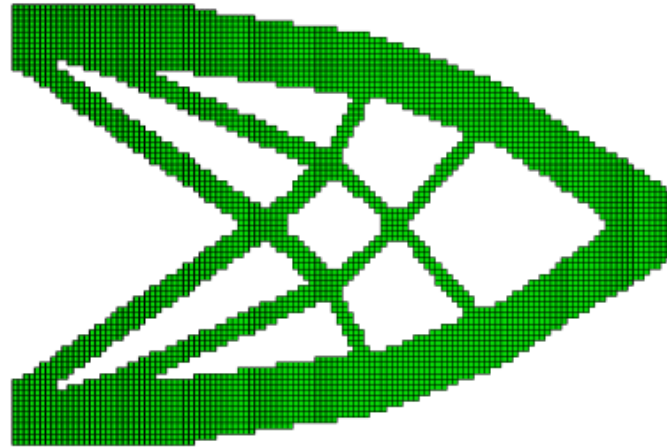


**Figure 3.11** –  $\Omega_i$  which contains the nodes that are used in the filter scheme for the  $i$ th element [22].

Implementation of this heuristic filter scheme in the BESO algorithm overcomes mesh-dependency and prevents checkerboard patterns in the final design topology such as the 2D beam in figure 3.12. Checkerboard pattern refers to regions where solid and void elements have an alternating behavior. This phenomenon also appears in the SIMP method as well [21][28]. Despite solving these issues, this filter scheme does not excessively increase the computational time and hence, it turns the BESO into a truly powerful tool with an enhanced accuracy [22].



(a) No Filter (checker-boarding)



(b) Filter

**Figure 3.12** – A two-dimensional cantilever beam a) with no filter scheme (checkerboard pattern is visible); b) with filter scheme [28].

Although this filter scheme will solve the mesh-dependency and checkerboard pattern, the objective function and its corresponding structural topology may still not converge. The dependency of the sensitivity numbers of the solid and void elements on design variables of present and absent elements causes this issue. Huang and Xie discovered that averaging the sensitivity number with its historical information can be beneficial to overcome this problem and obtain a convergent mean compliance and topology. By applying this approach, the whole history of the sensitivity numbers in previous iterations will be included in the new sensitivity number in the last iteration which increases the stability of both mean compliance and structural topology [22]. This approach is called stabilization scheme and its effect is illustrated in figure 3.13. Equation 26 presents the stabilization scheme in a mathematical form:

$$\alpha_i = \frac{\alpha_i^k + \alpha_i^{k-1}}{2} \quad (26)$$

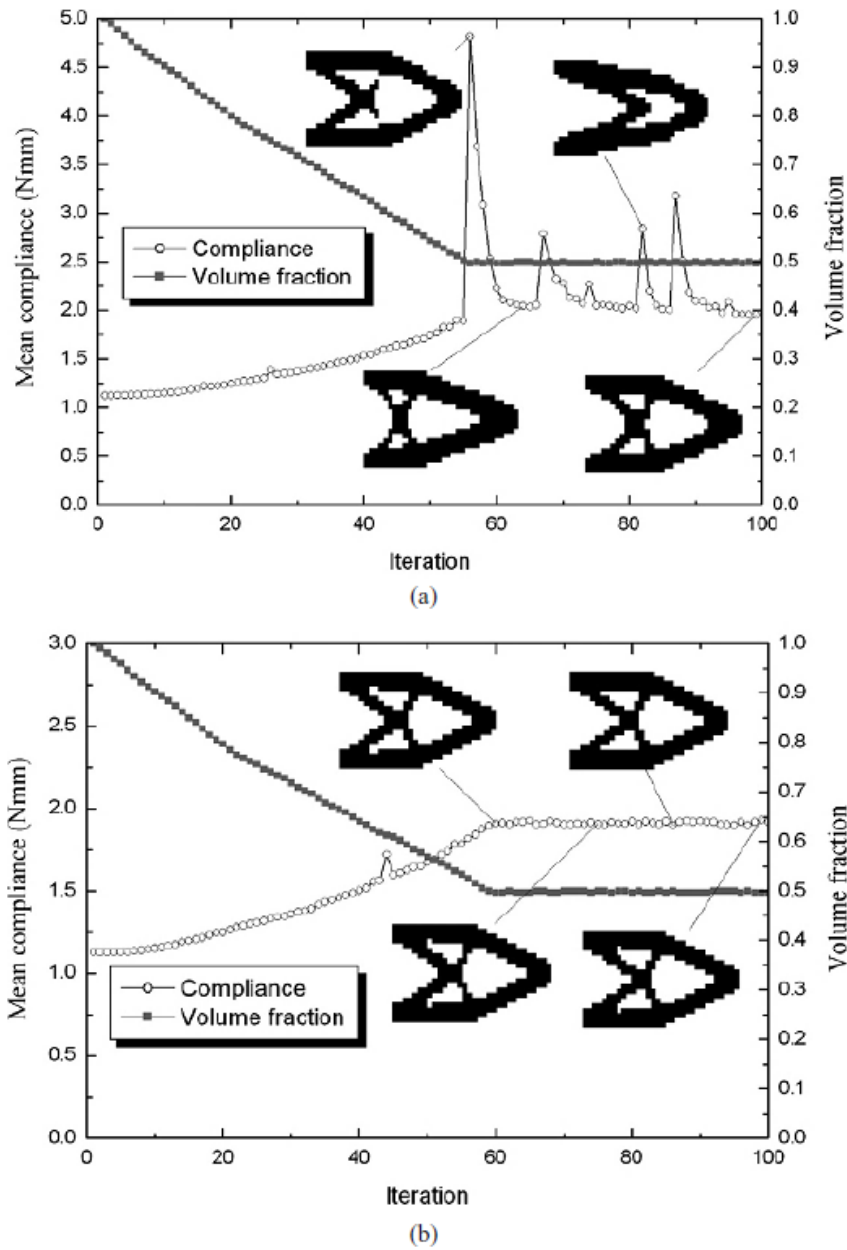


**Figure 3.13** – Evolution of mean compliance: a) without stabilization scheme; b) with stabilization scheme [22].

Note that in the BESO, the target volume may increase or decrease after each iteration until the constraint volume is reached. This process can be mathematically shown in equation 27:

$$V_{k+1} = V_k(1 \pm ER), \quad k = 1, 2, 3, \dots \quad (27)$$

Wherein  $V_{k+1}$  and  $V_k$  are the target volume after  $k + 1$  and  $k$  iterations respectively and  $ER$  is called evolutionary volume ratio. Once the criteria for the volume constraint is achieved, the volume of the structure for the remaining iterations will be treated as constant, as illustrated in equation 28:

$$V_{k+1} = V^* \quad (28)$$



Elements will be sorted from highest to lowest according to their sensitivity numbers which was calculated in equation 26. Then they will be compared to two threshold sensitivity numbers that decide which solid elements must be removed and which void elements must be switched into solid. If a solid element has a sensitivity number lower than the removing threshold ( $\alpha_i \leq \alpha_{del}^{th}$ ) it will be removed and if a void element has a sensitivity number higher than the adding threshold ( $\alpha_i \geq \alpha_{add}^{th}$ ) it will be turned into a solid element. Huang and Xie proposed the following steps to identify these thresholds [22]:

1. Assume  $\alpha_{add}^{th} = \alpha_{del}^{th} = \alpha_{th}$ . As the result,  $\alpha_{th}$  can be easily obtained from  $V_{k+1}$ . For example, consider a design domain with 1000 elements where  $\alpha_1 > \alpha_2 \cdots > \alpha_{1000}$ . If  $V_{k+1}$  corresponds to a design with 725 solid elements, then  $\alpha_{th} = \alpha_{725}$ .
2. The next step is to determine the volume addition ratio ( $AR$ ). This value can be calculated from dividing the number of added elements in the design domain by the total number of elements in the the design domain. If  $AR \leq AR_{max}$  where  $AR_{max}$  is a recommended value for maximum volume addition ratio, skip step 3. If not,  $\alpha_{del}^{th}$  and  $\alpha_{add}^{th}$  must be calculated again based on step 3.
3. The sensitivity number of void elements must be sorted. The number of elements that must be converted from void to solid can be calculated by multiplying  $AR_{max}$  to the total number of elements in the design domain. Hence, the sensitivity number of the element which its rank comes just before the last added element is equal to  $\alpha_{add}^{th}$ . Eventually,  $\alpha_{del}^{th}$  can be obtained, considering the fact that the removed volume is equal to  $V_k - V_{k+1} +$  the volume of the added elements.

The purpose of  $AR_{max}$  is to prevent addition of so many elements in one iteration and therefore safeguarding the model's integrity. Usually, this value is set to be higher than 1% to keep the capability of adding new elements [22].

Convergence criterion can be investigated through equation 29:

$$error = \frac{\left| \sum_{i=1}^N C_{k-i+1} - \sum_{i=1}^N C_{k-N-i+1} \right|}{\sum_{i=1}^N C_{k-i+1}} \leq \tau \quad (29)$$

- $C$ : mean compliance
- $K$ : current iteration
- $\tau$ : allowable convergence tolerance
- $N$ : an integer which is usually set to be 5

Following these mathematical steps, the BESO algorithm can be created as follows:

1. Generating a finite element mesh and allocate proper initial values (0,1) to elements
2. Calculating the elemental sensitivity numbers based on equation set 25
3. Calculate the average sensitivity number by using the equation 26.

4. Determining the target volume for the next iteration by the equation shown in 27.
5. Add or delete elements based on the procedure introduced by Huang and Xie
6. Repeat the processes 2-5 until the constraint volume ( $V^*$ ) is obtained and the convergence criterion that is described in equation 29 is satisfied.

The BESO method enjoys a simple and flexible approach which makes it easily adoptable in commercial FEA programs. It has been employed to solve many linear and nonlinear problems, buckling, frequency optimization and etc [28]. Figure 3.14 illustrates the BESO algorithm which is similar to the condition-based algorithm that has been integrated in the Abaqus topology Optimization Module [22][28]. This configuration is presented in the Abaqus/CAE user's manual with the following explanation [29]:

*“Condition-based topology optimization uses a more efficient algorithm that uses the strain energy and the stresses at the nodes as input data and does not need to calculate the local stiffness of the design variables.”*

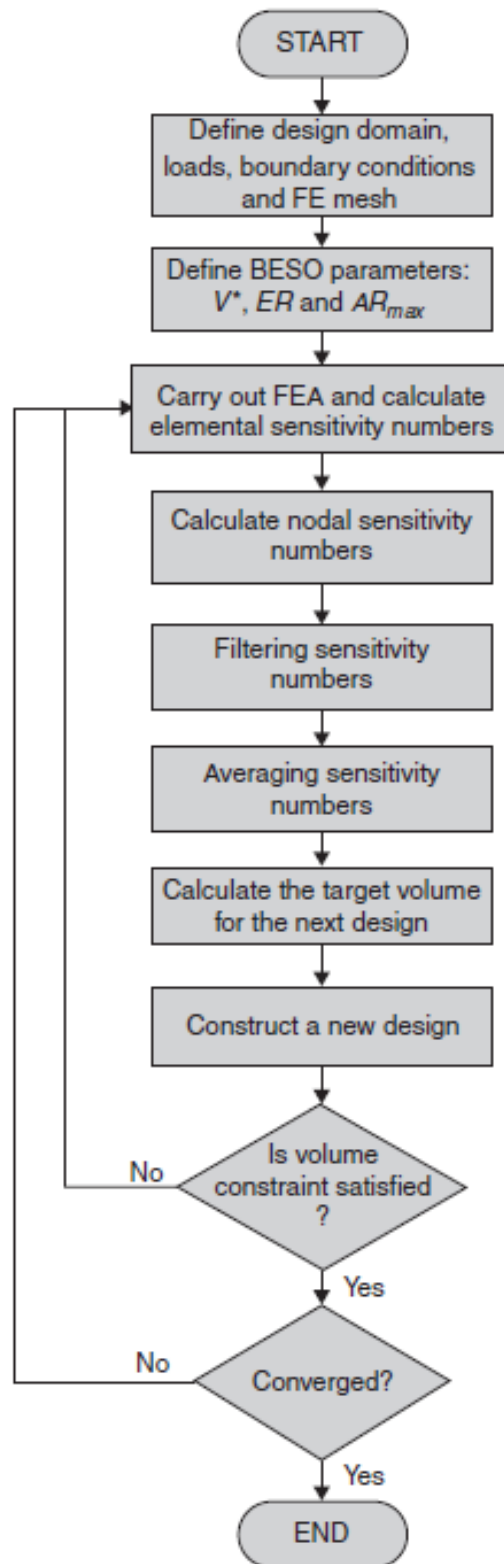


Figure 3.14 – Flowchart of the BESO algorithm[22].

### 3.3 Parametric modeling

Parametric modeling is a design process where codes and equations are used to produce and change the geometry of the model by modifying the input variables [30]. This is done through implementation of computer programming code that describes and connect the geometry of the model in a 3D draughting environment. The generated algorithms create an interlinked geometry which automatically reshapes when the input variables are altered [31]. Hence, making parametric modeling a highly efficient and flexible software tool in some cases compared to direct modeling, where geometry is modified within a 3D draughting program without any regard to programming and algorithms. The major advantage of parametric design is the flexibility to iteratively alter the model at any time during design [32]. As for direct 3D modeling using Computer Aided Design (CAD) software, everything needs to be redrawn repeatedly until the final design is achieved. This enables the designer to easily investigate multiple possibilities of geometry and potentially save a lot of time and shorten the design phase. Dynamo, Grasshopper 3D and Generative Components are some examples of such visual programming software.

#### 3.3.1 Rhinoceros 3D and Grasshopper 3D

Rhinoceros 3D is a 3D CAD software developed by Robert McNeel and Associates. The modeling software is based on NURBS (Non-Uniform Rational B-splines) geometry, explained in section 3.3.2. Inside Rhinoceros is an application called Grasshopper 3D (GH) implemented. This is a visual programming application, which enables the user to create and develop algorithms that generate very complicated geometries that can be baked back into Rhinoceros [33].

GH is a node-based plug-in. A node consists of coding, which compute an output based on input from the user, and can be viewed as the building bricks in GH. The GH environment is a 2D canvas where the nodes are visualized as rectangular "code-blocks" that are wired together, illustrated in Figure 3.15. This results in an interlinked geometry, where the wires connect both the input and output of the nodes together - creating a geometry which is displayed in Rhinoceros 3D. GH offers a large variety of nodes with different properties and outputs, making it possible to create complex models without knowing any coding. In addition, it is possible to create and customize new nodes by coding either in the programming language Python or C#. This makes GH a very versatile software and provides strong flexibility and design freedom [33].

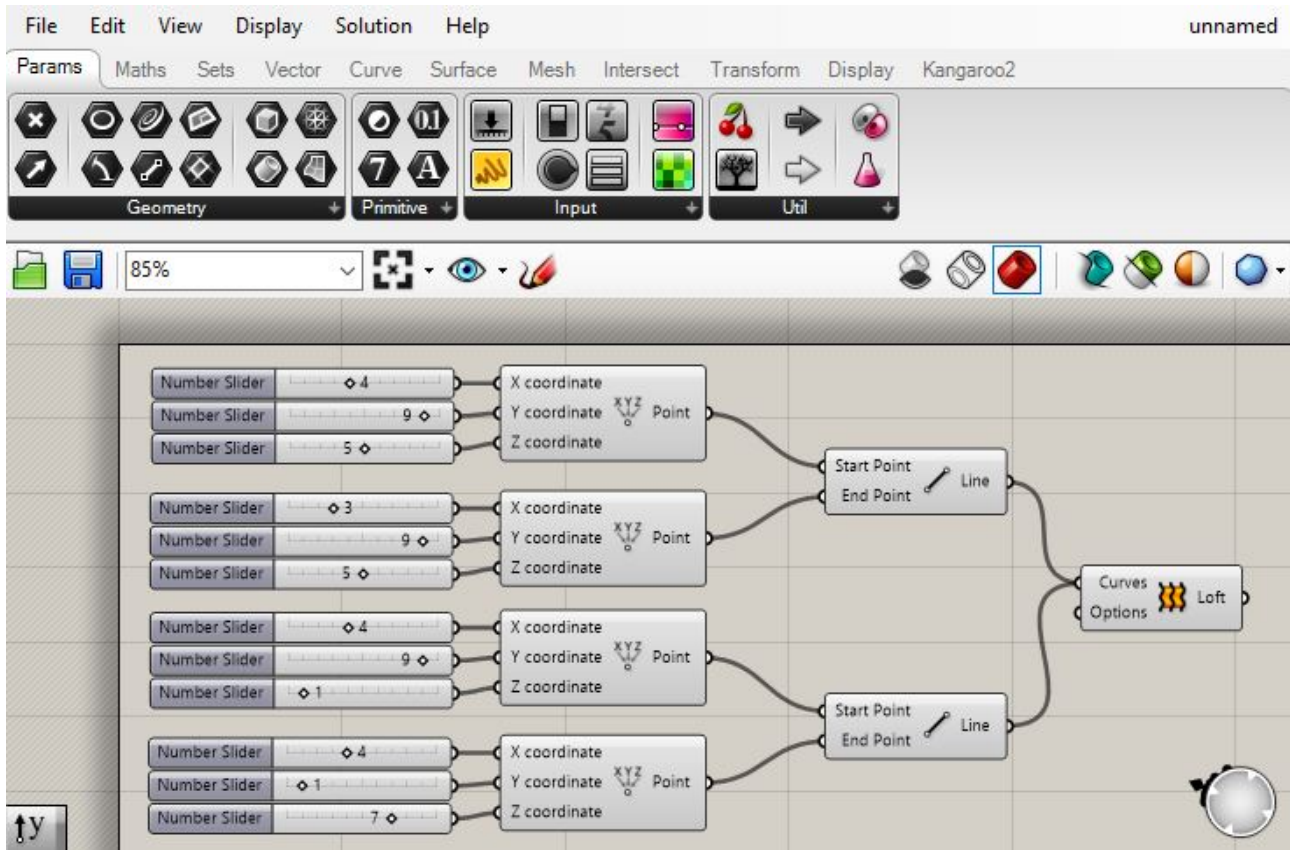


Figure 3.15 – Grasshopper 2D canvas [Appendix B].

### 3.3.2 B-splines and NURBS

The definition of NURBS are "Mathematical representations of 3D geometry that can accurately describe any shape from a simple 2D line, circle, arc, or curve to the most organic free-form surface or solid." [34]. A B-spline consist of several Bézier curves, where the ends of the curves are connected to each other. A Bézier curve is a parametric curve which describes and generates a smooth line by the use of control points [35]. The Bézier equation is stated below in equation 30, together with the Bernstein polynomial in equation 31.

$$C(t) = \sum_{i=0}^n b_{i,n}(t)P_i \tag{30}$$

$$b_{i,n}(t) = \binom{n}{i} t^i (1-t)^{n-i} \tag{31}$$

- $P_i$ : Control points of the curve, where  $i$  is the index.
- $n$ : Order/degree of the curve. The degree is determined by the number of control points, since  $n = i - 1$ .
- $b_{i,n}(t)$ : Bernstein polynomials, which is calculated by the use of binomial coefficients describing the weight of each individual control point for each value of the given parameter.

$B_{i,2}(t)$  in figure 3.16 illustrates the effect of each control point in a quadratic Bernstein polynomials. For a given value of  $t=0$ , only the black curve, which represents the first control point affects the Bézier curve.

This means that the curve will have the first control point as the start point. As the value for the parameter  $t$  increases, the impact from the first control point decreases. The impact from the other control points increases as the value of  $t$  increases in the range from 0-0.5 for this example. This effect is the same for higher degree polynomials, the only change being the presence of more control points effecting the shape of the curve. A higher order Bézier curve is able to produce a more complex line than a lower order Bézier curve [35][36]. The "R" in NURBS indicates that the B-spline curve have rational properties, meaning that the weight varies for each control point of the curve. Knowing this, the easiest way to alter the shape of a specific geometry part is to change the position of the control points which is closest to the given part [34]. Figure 3.17 illustrate the effect of both control point positioning and weighting.

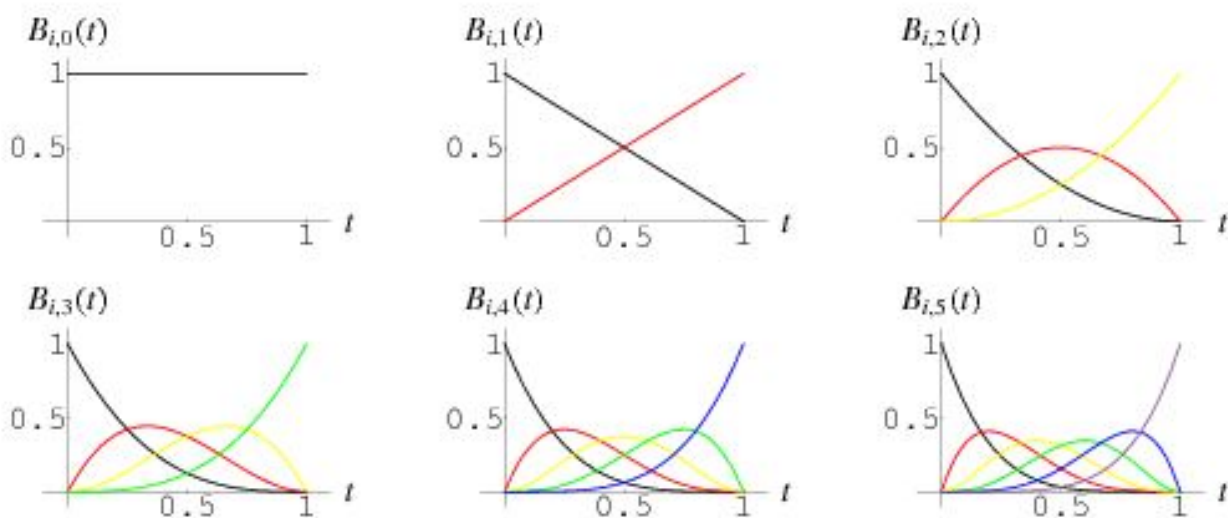


Figure 3.16 – Bernstein polynomials [37].

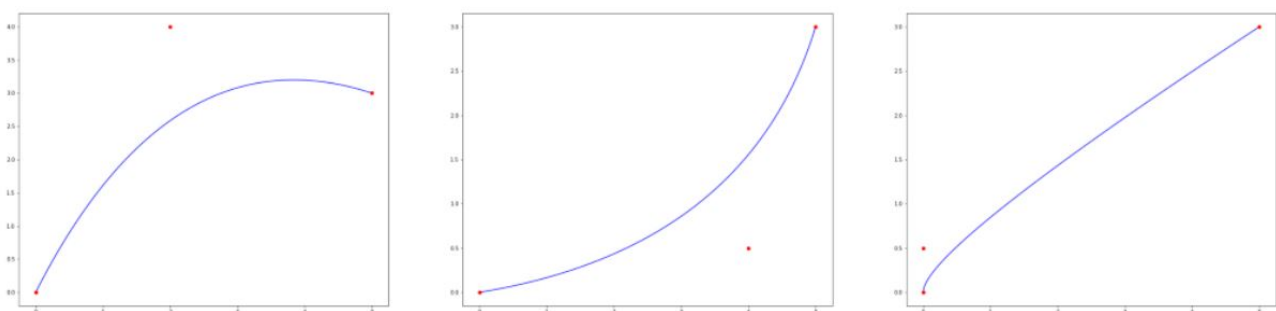


Figure 3.17 – Control points and weights with the resulting curve geometry [36].

A B-spline is as mentioned a special function which is defined as a piece-wise compilation of several Bézier curves where the ends are connected. The equation for the B-spline curve of the  $k$ th degree is stated in equation 32 and the Cox-de Boor recursion formula in equation 33 and 34 [38].

$$S(t) = \sum_{i=0}^n N_{i,k}(t)P_i \tag{32}$$

$$N_{i,0}(t) = \begin{cases} 1 & \text{if } t_i \leq t < t_{i+1} \\ 0 & \text{otherwise} \end{cases} \quad (33)$$

$$N_{i,j}(t) = \frac{t - t_i}{t_{i+j} - t_i} N_{i,j-1}(t) + \frac{t_{i+j+1} - t}{t_{i+j+1} - t_{i+1}} N_{i+1,j-1}(t) \quad (34)$$

- $P_i$ : Control points of the curve, where  $i$  is the index.
- $N_{i,j}$ : Cox-de Boor recursion formula which describes the basis functions for the given parameter  $t$ . The parameter  $t$  is determined in a so called knot vector, which is a vector of number values which describes the effect the control points have on the shape of the curve.

Unlike for the Bézier curve, the B-splines can have more control points than  $i = n + 1$ . By applying the Cox-de Boor formula, the impact of the control points are combined and the resulting shape is calculated. This is an explicit procedure, meaning that the calculations are based on information from the previous steps, starting from the basis function gained from equation 33. The usage of additional control points and higher order curves allow for a more complicated geometry output [38].

### 3.4 Abaqus

Abaqus/CAE is a multi-physics based simulation and modeling computer aided engineering (CAE) software [39]. CAE refers to software that can be used to perform virtual simulations and analysis tasks on CAD assemblies and designs [40]. This enables both designers and producers to perform virtual tests instead of having to perform them in real life - which can be very expensive and difficult to execute.

A CAE task can be divided into three stages; pre-processing, task solving and post-processing. In the pre-processing step the model design is developed and the relevant input parameters such as material properties and loading are added. Abaqus is a CAE software with a large selection of features. Some of the features that can be assigned to the CAE task are structural stress-, nonlinear-, optimization- and failure analysis. After the pre-processing stage, the task is computationally solved. This is a very demanding work and requires computers that are able to process a lot of data and perform complex calculation during a short amount of time. When the computing of the results is finished, the data can be post-processed and visualized with implemented tools in Abaqus [41].

Abaqus is composed of modules, where each module characterizes specific properties of the modeling process. The different modules are:

#### 3.4.1 Part

This module enables the user to create, edit and manipulate both new and imported geometry. All the different parts of the model must be added in this module. Abaqus is a very versatile software and collaborates very well with different kinds of CAD software - making it easy to import geometry from other software. The imported geometry for a 3D simulation is modeled as a solid, enabling the application of both material sections and materials. In addition, it is possible to partition the geometry into smaller parts. This is an important feature,

which enables the user to assign constraints to a specific selection of the imported geometry and to enable the use of structural hexahedron element type - explained below in the mesh module [42].

### 3.4.2 Property

This module enables the user to create materials, profiles, sections and composite layups. The large selection of material behaviors, shown in Figure 3.18, permits the user to modify realistic material properties. The profile and section options enable the user to compose and assign cross-sectional properties to the parts created [42].

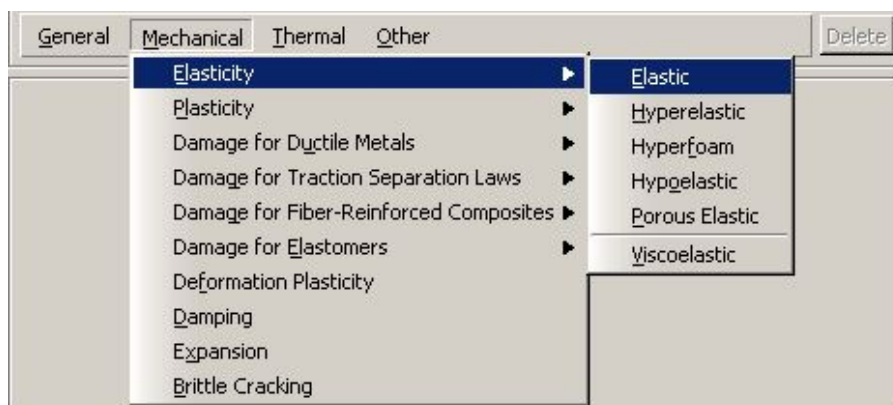


*Figure 3.18 – Material properties tab from Abaqus/CAE.*

### 3.4.3 Assembly

In the assembly module the user can create an assembly of the parts introduced in the part module, in other words, build the geometric model. The different parts are created separately in different coordinate systems, then imported into the assembly instance and assembled by introducing position constraints in a new mutual coordinate system [42].

### 3.4.4 Step

Enables the user to create analysis steps and specify output requests. Abaqus offer a large selection of analysis steps, each analysis step represents a particular procedure of how the analysis is to be performed. Among the alternatives are general static stress analysis - which is the recommended choice for analysis of concrete. This step is developed to perform simulations on linear and non-linear static and quasi static problems. It is possible to create multiple steps to the same model, making it possible to run several analyses at the same job. The environmental aspects like boundary conditions, loading and interactions are all step-dependent and it is important that they are assigned to the right step [42].

### 3.4.5 Load

In the load module the user can create and apply different load types, load combinations and boundary conditions (BC) to the model. The TO analysis is very sensitive to both BC and loading, meaning that minor changes could alter the whole geometry outcome. Due to this strong correlation between the resulting topology geometry and the BC's together with the loading, it is crucial that these are modeled as realistic as possible, concerning both direction and magnitude [42][43]. Figure 3.19 shows the application of load in Abaqus.



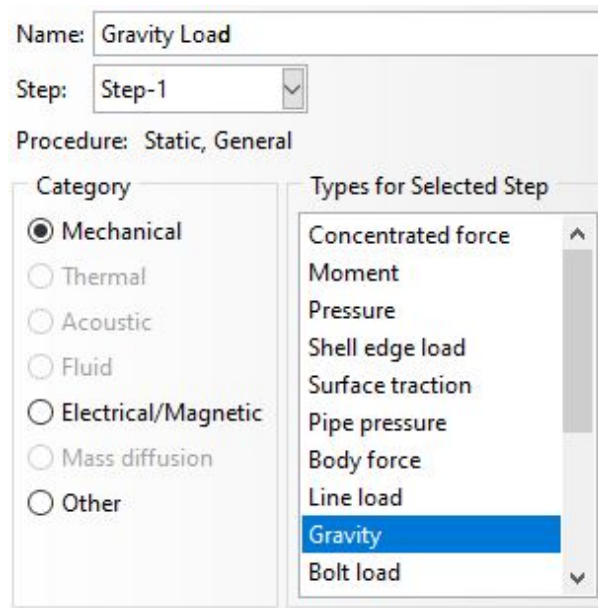


**Figure 3.19** – Application of load in Abaqus/CAE.

### 3.4.6 Mesh

Enables the user to mesh parts and assemblies. The module contains features as seeding, element types and different techniques for meshing. A mesh can vary in density, and is determined by the seeding value. Choosing the appropriate element type is also important to achieve a realistic and trustworthy result [42].

One can choose either tetrahedron or hexahedron element types. A study called “A Comparison of All Hexagonal and All Tetrahedron Finite Element Meshes for Elastic and Elasto-plastic Analysis”, by Steven Benzeley et al., found that hexahedron elements provide a more accurate solution compared to the linear tetrahedron elements. This was discovered due to the fact that linear hexahedron allows for deformation at a lower strain energy state. However, the tetrahedron elements are on the other hand more flexible and can be assigned to more complex designs, and are recommended for complicated topologies [42][44].

To increase the accuracy of the analysis, an option is to apply tetrahedron or hexahedron elements of quadratic order. The quadratic element types introduce an extra node in the middle of each edge, illustrated in figure 3.20, which provides a significantly more detailed analysis basis. Due to occurrence of stability issues in some complex non-typical geometries when applying hexahedron elements, it is recommended to use the quadratic tetrahedron element type CTETRA10 in Abaqus to obtain the numerical stability that is required to prevent errors. However, for regular shaped non-complex structures, the linear hexahedron element type C3D8 is recommended due to both computational time and sufficient accuracy. Higher order elements are more comprehensive to calculate due to the increased number of nodes, and requires a lot more computational power, but it is necessary in some cases to obtain realistic results [42][43].

Another option to improve the accuracy of the analysis is to increase the number of finite elements by adjusting the seeding value. A finer mesh will divide the geometry into smaller elements, resulting in a more precise output and consequently higher computational time. Furthermore, Abaqus have set a node restriction on 250 000

for the student version, which limits the possibilities and precision of both the FEA and TO simulations [42][43].

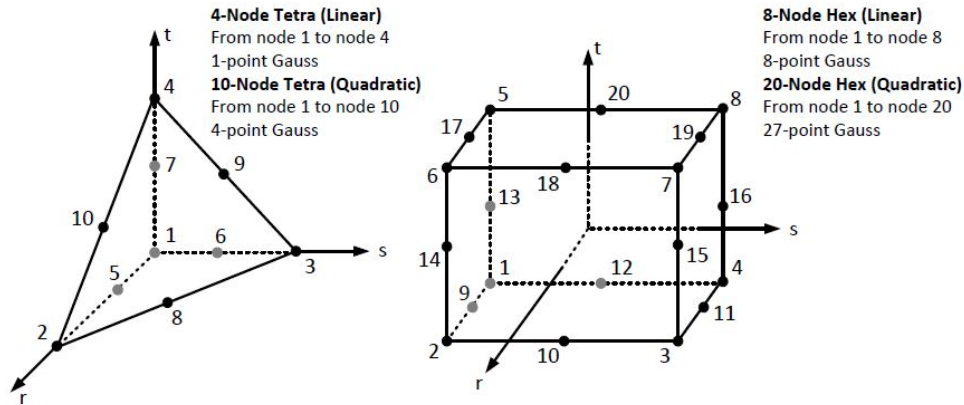


Figure 3.20 – Tetrahedron and hexahedron elements with both linear and quadratic geometric order [45].

### 3.4.7 Optimization

In the optimization module the TO task is created. Here the type of TO algorithm, design responses, objective functions and constraints are determined to define the type and objective of the TO [42].

Abaqus offer two types of topology optimization algorithms; sensitivity-based (SB) and condition-based (CB). As mentioned in section 3.2.5 and 3.2.6, the SB algorithm is based on SIMP and the CB algorithm is similar to BESO [42]. A design response is a singular scalar value, which are used to define both the objective function and the constraints. Abaqus provides a large selection of design responses. Some implemented design responses are volume, energy stiffness, strain energy and displacement [43][46]. Figure 3.21 visualize the steps in the optimization process.

To run a TO analysis, an objective function needs to be determined. Abaqus offers the choice of either maximizing or minimizing the design response values. Based on Equation 35 it shows that in order to maximize the stiffness of the design - Abaqus offers two possible objective functions [43]:

- Maximize the design response: stiffness
- Minimize the design response: strain energy

$$\text{Strain energy} = \frac{1}{\text{Stiffness}} \quad (35)$$

In addition, an optimization constraint needs to be determined. For TO analysis a volume constraint is normally applied, where the desirable volume fraction is chosen. This constraint, which is a performance constraint, together with the objective function represents the goal for the TO task. If the TO analysis is converging while attaining all the specified constraints, the task is deemed as a success [42][43].

Abaqus also includes some geometric constraints and restrictions [42]:

- **Frozen areas:** These are regions that are not to be altered during the optimization process, meaning that the density is locked to 1 throughout the simulation.
- **Cast conditions:** A very important feature in terms of actually being able to produce the instance. By introducing this constraint undercuts and internal voids are avoided, which is important to ensure a valid geometry that is possible to fabricate with the current production methods.

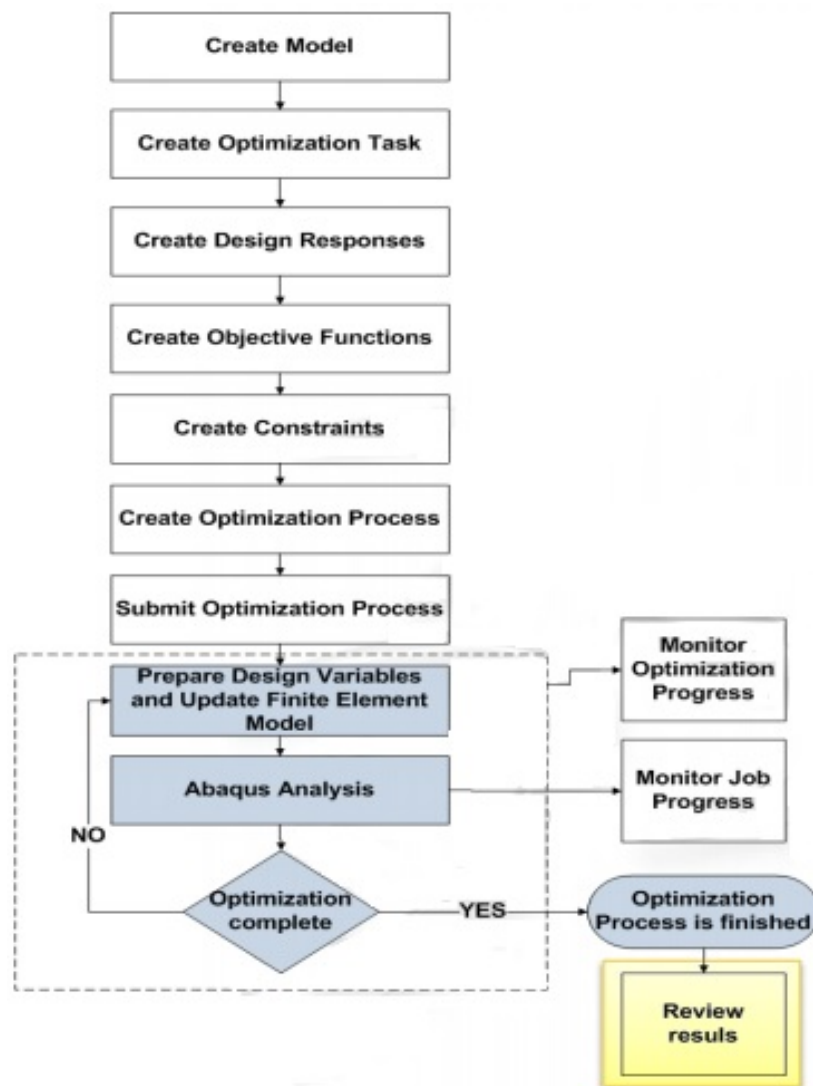


**Figure 3.21** – The Abaqus Topology Optimization Module work process [46].

### 3.5 Staircase

Staircases are one of the most ancient structural elements. The earliest human-made findings can be traced back to the prehistoric Tarxien Temple and Saflieni Hypogeum site in Malta, which are estimated to have been built between 3600-2500 BC [47]. Traditionally, staircases were built out of timber, stone or marble, with timber being the dominant material between the three. However, new nonflammable materials, such as steel

and reinforced concrete structures, became more convenient and attractive after 1945 due to the destruction that took place during the Second World War [48]. Despite their long history, the basic design of staircases did not change substantially. Yet, the developments in computer science and material technologies during the past two decades have enabled designers and engineers to imagine beyond these traditional concepts. Figures 3.22 - 3.25 demonstrate the evolution of staircases in the history.



**Figure 3.22** – Stone staircase at the Tarxien temple, Malta (3600–2500 BC) [47].



**Figure 3.23** – Northern staircase of the Louis XII wing, Blois, France (1501) [47].

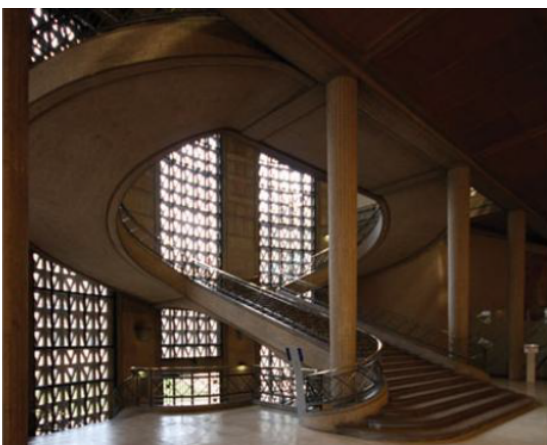


**Figure 3.24** – Palais d'Iena, the Conseil Economique et Social, Paris (1937-1943) [47].



**Figure 3.25** – Modular Pre-stressed UHPC Staircase (2009) [49].

A staircase's primary function is to transport people or objects between floors by dividing the differential height into smaller and more comfortable vertical trajectories referred to as steps. Staircases are constructed in different types, shapes, configurations and materials. While planning a building, a designer should look for so-

lutions to create an efficient, comfortable and reasonably safe staircase. One of the most critical decisions is the placement of the staircase inside the structure, due to the fact that the space it occupies have a huge influence on the overall design of the building. Other factors that greatly influence the staircase design are the space availability and accommodation, as well as the budget. Furthermore, the staircase should be designed to accommodate the expected flow of people in any kind of emergency situation, especially during fire [50]. Concrete staircases are either prefabricated or manufactured on site. Due to the increased control of the casting and curing conditions, prefabricated concrete stairs offers significant benefits compared to the conventional on-site manufacturing. Up until now, the use of traditional reinforced cages is the most common reinforcement method for constructing RC staircases. However, several studies and research projects have been conducted on possibility of using other reinforcement solutions, such as pre-stressed reinforcement and fiber reinforced UHPC [51][52].

### 3.5.1 Staircase components

Staircases are heavily space dependent structures, which often result in unique designs with specific needs for customization, creating a large variety of staircase designs. However, the main constitutive components of any staircase, illustrated in figure 3.26, are similar in all types of staircases and are discussed down below [53].

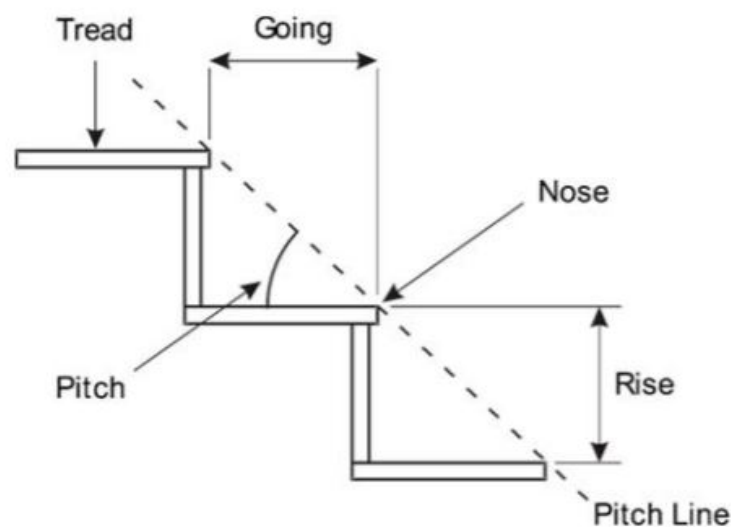


**Figure 3.26** – Components of staircase [53].

- **Step:** Part of the staircase that contributes to the purpose of any staircase and consists of a tread and riser is called a step. A staircase is comprised of a number of steps.
- **Tread:** The horizontal portion of a step which facilitates the stepping during the users' ascending or descending. All staircases are constructed with one fewer tread than the number of risers. The most commonly used tread dimensions are between 250-300mm [54].
- **Riser:** The vertical portion of a step, which acts as a support and connector for two consecutive treads, is called a riser. A staircase can be constructed with or without the use of a riser, depending on safety regulations and design. The height of the riser is an important parameter in the calculation phase to find

out the number of necessary steps in a given vertical distance. Nevertheless, the riser's height must be between 150mm - 220mm [54].

- **Landing:** The horizontal platform, that primarily serves the purpose of changing the orientation of the staircase and additionally grants an opportunity for the user to take a break. The minimum width of a landing should be at least three times larger than the width of a tread in the same staircase. It is recommended to include a landing platform after every 15 steps [54].
- **Flight:** The series of continues steps that are connected to each other without intervention of any break or landing is called a flight.
- **Pitch:** The angle between the horizontal and the diagonal line between the edge of two treads, is called the pitch of a staircase. Different codes have different recommendations for the pitch of staircases. For instance, according to British standard, pitch of a staircase can vary between 30-42 degrees [54]. It is noteworthy to mention that TEK17 does not provide any recommendation for the acceptable range of the pitch.

### 3.5.2 Staircase types

A wide range of staircase configurations are being constructed. Some of the most predominant types are shown in figure 3.27 and are briefly discussed below [55].

- **Straight staircase:** A linear staircase with all steps in one direction. This is one of the most predominant types, and are commonly used when the space availability for the staircase is narrow and long. Based on the height of the floor, straight staircases can be divided in two groups; with a landing in the middle when the height between the floors is relatively large, and without any landing when the height between the floors do not exceed a certain limit.
- **L-shaped staircase:** A L-shaped staircase is formed by bending a straight staircase 90 degrees at the transition point. This can be achieved by adding a landing platform, often located at in the middle of the staircase.
- **U-shaped staircase:** The combination of two parallel straight staircases joined together by a landing platform that creates a 180-degrees turn in the walking direction is called a U-shaped staircase. It can be constructed either with an intermediate landing or without a gap between the two flights. Additional support is sometimes required for the landing platform.
- **Spiral staircase:** A type of staircase which makes a complete turn without any interruption of landing platforms where wedge-shaped treads radiate around a central pole. They are compactly constructed and are the ideal solution for limited space. Spiral staircases are commonly employed as emergency exit in large buildings.
- **Curved staircase:** An arched staircase without landing, which similarly to the spiral staircase, has steps that follow a helical arc, whereas the radius tends to be larger to ease traversing for the users. Generally, they are provided at the rear of buildings to serve accessibility between various floors.

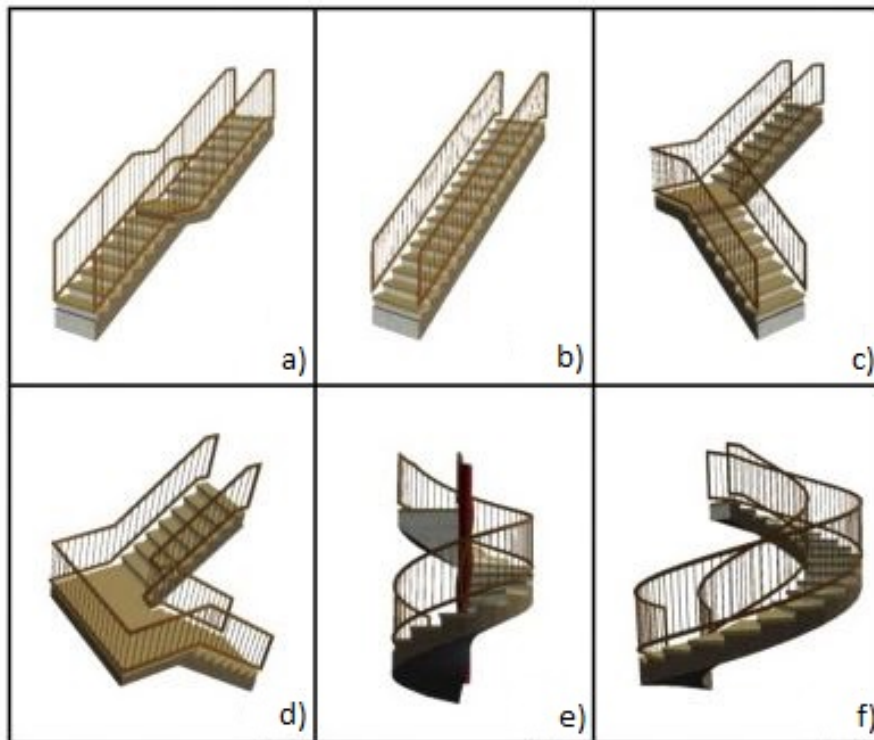


**Figure 3.27** – Different types of staircase. (a) and (b) Straight staircase (c) L-shaped staircase (d) U-shaped staircase (e) Spiral staircase (f) Curved staircase [55].

### 3.5.3 Regulations based on TEK17

The users' health, safety, welfare and comfortability, regardless of physical limitations, are the most important priorities when designing a staircase. Choosing proper height and width of steps play an important role to minimize the risk of falling over the steps [53]. Regulations on technical requirements for construction works (TEK17) is designed to serve to these purposes [50]. The regulation is intended to make sure that all the components of a project are planned, designed and implemented on the essence of good visual aesthetics and universal design. Dimensions of the steps, as well as other components of a staircase, shall be calculated for the expected flow of people to facilitate safe transport in all kinds of situations and for all sorts of users. The minimum requirements for staircases according to TEK17 are listed below [50]:

- The entire flight length of the staircase shall have a regular slope and the riser's height shall be held constant.
- Width of the treads shall be a minimum of 250mm. Additionally, the treads in straight staircases shall have an equal tread width, securing a predictable trajectory.
- Landings shall be large enough to stop and prevent the users from falling. Additionally, height differences that exceeds 3.3m requires a landing platform.
- Treads shall be constructed with a non-slip surface.
- The flight of a straight staircase shall have a minimum clearance width of 0.9m and minimum clearance height of 2.1m. Straight, internal flights of staircases in residential units shall have a minimum clearance

width of 0.8m and minimum clearance height of 2.0m.

- Flights that are not straight shall have a minimum clearance width that is at least 100mm wider than the requirement stated above.
- Treads in staircases with curved flights along the inside walking line shall have a minimum width of 150mm. In addition, the minimum tread width along the inside walking line in escape routes for large number of people shall be 200mm.
- The depth of landing from the edge of the top step to the opposite wall shall be at least 1.5m. It is noteworthy to mention that this recommendation is in contrast with the British regulation which recommends a minimum depth of three times larger than the width of a tread [54].

### 3.6 Basis for calculations

#### 3.6.1 Partial factors for materials

Engineering design should provide a safe structure, which is able to withstand the worst loading conditions. Deformation of the structure should not alter the appearance, durability or performance of the structure during its lifespan. These are the minimum requirements that every designer must fulfill despite the difficulties in evaluating the precise loading conditions and variations in the strength of the materials. To achieve the requirements described above, characteristic load is multiplied by some safety factors that are called partial factors for materials [56]. Generally, higher partial factors are employed for Ultimate Limit State design (ULS) compared to Serviceability Limit State design (SLS). The partial factors account for uncertainties such as inaccuracies and load deviations. In practice, this mean that a safety margin is implemented to avoid any material failure that leads to collapse of the construction due to errors and deficiencies of the designer. The partial factors for concrete in the ULS are given in section 2.4.2.4 in the Eurocode 2 [57] and are presented in table 3.1.

**Tabell 2.1N – Materialfaktorer for bruddgrensetilstander**

Dimensjonerende situasjoner	$\gamma_c$ for betong	$\gamma_s$ for armeringsstål	$\gamma_s$ for spennstål
Vedvarende og forbigående	1,5	1,15	1,15
Ulykkessituasjon	1,2	1,0	1,0

**Table 3.1 – Partial factor for concrete and steel [57].**

#### 3.6.2 Load and load factors

The total self-weight of a structure, both structural and non-structural, that acts throughout the design life is considered as dead load. In addition, permanent loads that are attached/added to the structure for the given reference period are also referred to as dead load. Section 4.1.2 in NS-EN 1990 is used to determine the characteristic values of self-weight, and of the densities and dimensions. NS-EN 1990 requires that the magnitude of the loads do not vary with time. Applied loads with variable actions that do not vary their magnitudes with time are classified as imposed loads. [58].



The combined effect of these structural loads and actions, together with belonging safety factors given in table 3.2, is termed the design load. By multiplying the characteristic loading with the associated safety factor, the design load is calculated according to equation 36 or 37 [57].

$$\text{Design Load} = 1.35 \times \text{Dead Load} + 1.05 \times \text{Imposed Load} \quad (36)$$

$$\text{Design Load} = 1.2 \times \text{Dead Load} + 1.5 \times \text{Imposed Load} \quad (37)$$

**Tabell NA.A1.2(B) – Dimensjonerende verdier for laster (STR/GEO) (Sett B)**

Vedvarende og forbigående dimensjonerende situasjoner	Permanente laster		Dominerende variabel last (*)	Øvrige variable laster (*)
	Ugunstig	Gunstig		
(Ligning 6.10a)	$\gamma_{G,sup} G_{k,sup}$	$\gamma_{G,inf} G_{k,inf}$	$\gamma_{Q,1} \psi_{0,1} Q_{k,1}$	$\gamma_{Q,i} \psi_{0,i} Q_{k,i}$
(Ligning 6.10b)	$\xi \gamma_{G,sup} G_{k,sup}$	$\gamma_{G,inf} G_{k,inf}$	$\gamma_{Q,1} Q_{k,1}$	$\gamma_{Q,i} \psi_{0,i} Q_{k,i}$

(\*) Variable laster er de som er oppført i tabell NA.A1.1

MERKNAD 1 Det brukes følgende sett med  $\gamma$ - og  $\xi$ -verdier ved bruk av uttrykk 6.10a og 6.10b:  
 $\gamma_{G,sup} = 1,35$ ;  
 $\gamma_{G,inf} = 1,00$ ;  
 $\gamma_{Q,1} = 1,50$  hvis ugunstig (0 hvis gunstig);  
 $\gamma_{Q,i} = 1,50$  hvis ugunstig (0 hvis gunstig);  
 $\xi = 0,89$ ;  
 (I Norge brukes 6.10a og 6.10b, slik at  $\xi \gamma_G = 0,89 \times 1,35 = 1,20$ ).

Se også NS-EN 1991 til NS-EN 1999 for  $\gamma$ -verdier som skal brukes for påførte deformasjoner.

MERKNAD 3 De karakteristiske verdiene for alle permanente laster fra ett opphav multipliseres med  $\gamma_{G,sup}$  hvis resultatet i form av den totale lastvirkningen er ugunstig, og med  $\gamma_{G,inf}$  hvis resultatet i form av den totale lastvirkningen er gunstig. F.eks. kan alle laster med opprinnelse i konstruksjonens egenvekt anses å komme fra én kilde; dette gjelder også om forskjellige materialer er brukt.

MERKNAD 4 For spesielle påvisninger kan verdiene for  $\gamma_Q$  og  $\psi_Q$  igjen deles inn i verdiene  $\gamma_Q$  og  $\psi_Q$  og modellens usikkerhetsfaktor  $\gamma_{\psi,Q}$ . En verdi for  $\gamma_{\psi,Q}$  som ligger mellom 1,05 til 1,15, kan brukes i de fleste vanlige tilfeller.

**Table 3.2 – Load factors for permanent and variable actions [57].**

### 3.6.3 Compressive strength

The compressive strength of the concrete indicates the quality of the concrete in the hardened state. This is a very important and useful mechanical property determined by multiplying the characteristic compressive strength ( $f_{ck}$ ) with the coefficient ( $\alpha_{cc}$ ) and dividing by the partial factor for concrete ( $\gamma_c$ ), as derived in equation 38.  $\alpha_{cc}$  takes two factors into consideration; the long term effects on the compressive strength and the unfavorable effect resulting from application of load. Due to the fact that the tensile strength of concrete

is about 12% of its compressive strength, concrete structures are rarely loaded in pure tension. Many concrete structures are also subjected to bending moment which might lead to a tensile failure. The compressive strength of different types of concrete qualities is given in Table 3.1 in the Eurocode 2. [57].

$$f_{cd} = \alpha_{cc} \times \frac{f_{ck}}{\gamma_c} \quad (38)$$

### 3.6.4 Modulus of elasticity

Modulus of elasticity is a measurement for the stiffness of concrete, and indicates the resistance to withstand deformations, when a load is applied to it. Due to the fact that concrete is a heterogeneous material, its elastic deformation is largely dependent on its composition and constituents. A concrete's modulus of elasticity is dependent on the properties and quantities of type of cement paste and aggregate used in the concrete mixture [59]. Higher modulus of elasticity means that concrete can withstand larger stresses, while a low modulus of elasticity is the indication that it will deform more easily under the same loading. However, the former also means that concrete starts to lose its ductility and become more brittle, which increase the possibility of appearing cracks. An empirical formula based on the compressive strength of concrete, given in equation 39, is used to determine modulus of elasticity of the concrete [57].

$$E_{cm} = 22 \times \left(\frac{f_{cm}}{10}\right)^{0.3} \quad (39)$$

- $E_{cm}$ : modulus of elasticity (MPa)
- $f_{cm}$ : cylinder compressive strength (MPa)

### 3.6.5 Durability

A structure that accommodates the requirements for serviceability, strength and stability throughout its design life, without significant loss of utility or excessive unforeseen maintenance, is classified as a durable structure [57]. Durability of concrete is dependent on physical and chemical properties of its constituent, exposed environment and time. Corrosion of steel reinforcement in the concrete structure has been an important issue which causes cracking, loss of strength and fragmenting of the concrete cover. The reinforcement in a structure should be covered enough to provide protection against carbonation, corrosion, fire and other kinds of unwanted deterioration factors. A concrete's cover makes the most significant contribution to the durability of a structure, due to the fact that it acts as the primary defense against physical and chemical attacks from the outside environment. Concrete strength, water/cement ratio, curing and minimum cement content are other important factors that can influence the durability of concrete [60].

### 3.6.6 Shear capacity

The shear capacity of concrete, ( $V_{Rd, c}$ ) is presented in equation 40 and it should be greater or equal to the minimum value obtained from equation 41. As long as the shear capacity is larger than the design shear force ( $V_{Ed}$ ), no risk of shear failure can be expected. However, if the occurring shear forces exceed the capacity of the structure, additional shear reinforcement must be added to prevent crack propagation and shear fractures. The load accountable for the shear failure relies on numerous factors such as shape, size, loading and structural

properties of structures.

The minimum amount of shear reinforcement should be added according to section 9.2.2 in the Eurocode 2, regardless of whether the occurring shear forces are lower than the minimum shear capacity or not. However, for structural members which do not provide any contribution to the structure's stability and/or the loading can be distributed transversely, shear reinforcement can be excluded [57]. The shear reinforcement design of structural members is based on a truss model, which is given in section 6.2.3 in Eurocode 2.

$$V_{Rd,c} = [C_{Rd,c} K (100 \rho_l f_{ck})^{1/3}] b_w d \quad (40)$$

with a minimum value of

$$V_{Rd,c} = v_{min} b_w d \quad (41)$$

- $C_{Rd,c} = \frac{k_2}{\gamma_c}$
- $k_2$  : 0.15 or 0.18, depending on the aggregate size,  $d_{max}$
- $\gamma_c = 1.5$
- $K = 1 + \sqrt{\frac{200}{d}} \leq 2.0$
- $\rho_l = \frac{A_s}{b \cdot d} \leq 0.02$
- $f_{ck}$  : Characteristic cylindrical strength in MPa.
- $V_{min} = 0.035 \cdot K^{\frac{3}{2}} \cdot \sqrt{f_{ck}} \cdot b_w \cdot d$
- $b_w$  : Width of the cross-section.
- $d$  : Effective depth of the cross-section.

### 3.6.7 Moment capacity

Similarly to shear capacity, moment capacity of a concrete element provides the maximum allowable bending moment at any section of the structure. If the design moment exceeds the moment capacity, the structure will fail due to bending. As described in section 3.6.3, concrete is very weak in tension compared to compression. Therefore, most of the concrete structures are reinforced with either steel bars, pre-stressed steel tendons or different types of fibers to increase their moment capacity. Steel rebar is a ductile material which maintains its structural properties even after it deforms to a certain extent. Equation 42 is derived in "Concrete Structures by S. I. Sørensen, based on section 6.2.6 in Eurocode 2 [61].

$$M_{Rd} = 0.275 f_{cd} b d^2 \quad (42)$$

- $M_{Rd}$  : Moment capacity
- $f_{cd}$  : Design cylindrical strength of concrete.
- $b$  : Width of the cross-section.
- $d$  : Effective depth of the cross-section.

### 3.6.8 Deflection

Deflection is calculated with regards to the shrinkage, characteristic dead loads and live loads. The serviceability of a concrete structure throughout its design lifespan is heavily dependent on its short- and long-term deflections. These two types of deflections can be caused by creep and shrinkage due to the loads that are applied to the structure. These loads can be categorized as dead loads, such as self-weight and pre-stressing (if applied), or live loads, such as wind and snow. Additionally, temperature changes can cause contraction and expansion of materials, which generate internal forces that cause problems related to deflection [62]. Apart from serious safety risks due to deflection, structures become also visually undesirable, when the total deflection exceeds  $\text{span}/250$  below the horizontal level. According to section 7.4.2 in Eurocode 2, span/effective depth ( $\frac{l}{d}$ ) ratio which is presented in table 3.3, will be adequate for avoiding deflection problems in normal circumstances, meaning that it is not necessary to calculate the deflection precisely. However, more accurate deflection checks are necessary for the structures with larger span/effective depth ratio [57].

**Table 7.4N: Basic ratios of span/effective depth for reinforced concrete members without axial compression**

Structural System	$K$	Concrete highly stressed $\rho = 1,5\%$	Concrete lightly stressed $\rho = 0,5\%$
Simply supported beam, one- or two-way spanning simply supported slab	1,0	14	20
End span of continuous beam or one-way continuous slab or two-way spanning slab continuous over one long side	1,3	18	26
Interior span of beam or one-way or two-way spanning slab	1,5	20	30
Slab supported on columns without beams (flat slab) (based on longer span)	1,2	17	24
Cantilever	0,4	6	8

**Note 1:** The values given have been chosen to be generally conservative and calculation may frequently show that thinner members are possible.  
**Note 2:** For 2-way spanning slabs, the check should be carried out on the basis of the shorter span. For flat slabs the longer span should be taken.  
**Note 3:** The limits given for flat slabs correspond to a less severe limitation than a mid-span deflection of  $\text{span}/250$  relative to the columns. Experience has shown this to be satisfactory.

**Table 3.3 – Span/effective depth ratio [57].**

### 3.7 3D printing

The construction industry is constantly developing, and is slowly becoming more and more digitized. As a result of this, the traditional way of working with 2D drawings are substituted with advanced 3D CAD software. This new technology grants both architectures and engineers with a vast amount of freedom in design, and grants the possibility of discovering unwanted and unforeseen failures at an early stage. TO concrete is a relatively uncharted area, which is mostly due to the combination of complicated topologies and lack of suitable fabri-

cation methods for such designs. The traditional timber formwork in combination with Computer Numerical Control (CNC) milling is one of the most applied fabrication methods, but is not flexible enough to produce the most complicated TO geometry. Therefore, in order to fabricate these complex organic geometries, a more advanced production method is required, such as 3D printing [52][63].

3D printing, also known as additive manufacturing, is a fabrication method for producing solid objects based on digital geometry files. The first study on 3D printed concrete formwork was presented by Volker Ruhl in 1997, where the traditional and conventional forming practice was first challenged with the use of 3D printing. In the recent years, methods like binder jetting, robotic hot-wire cutting, robotic abrasive-wire cutting and fused deposition modeling (FDM) 3D printing have been developed and used to fabricate formworks [9]. A study called "*Submillimeter Formwork 3D-Printed Plastic Formwork for Concrete Elements*", by Andrej Jipa, concludes that it is possible to obtain complex concrete geometries by the use of thin 3D printed FDM formwork shells [63].

As mentioned before, FDM is one among many 3D printing technologies that is suited for the printing of formwork. This technology introduces filament into a so-called hot-end, which melts the filament in the nozzle and places the melted filament onto the construction bed by extrusion. The material used is a Polyactic Acid (known as PLA), which is a thermoplastic polymer that melts with temperatures close to 200°C, depending on the type of PLA used. One of the massive advantages with FDM printing is the support function, which enable the user to create geometries with overhangs, such as cantilevers [63]. The extrusion process is illustrated in Figure 3.28.

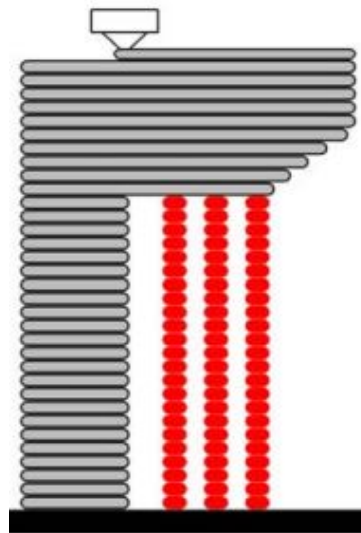


**Figure 3.28** – The fabrication process of a FDM 3D printer illustrating the extrusion of a cantilever geometry with the belonging support structure marked in red [63].

To create a solid, the digital part is divided into horizontal layers - creating a quantity of cross-sections. The layers are converted to coordinates and vectors, which is the input that is exported to the actual 3D printer. This data is the pathway for the 3D printer, which is first read, then processed and executed. The 3D printer can move the nozzle in x-, y- and z-direction and in addition control the elevation by lifting and lowering the construction bed. One by one the layers are printed, resulting in a gradually growing structure as the construction bed is lowered and/or the nozzle is lifted. This additive 3D printing method provides accuracy down to

0.2mm, making it possible to manufacture with very high precision. Such level of precision of the formwork requires a concrete mix with aggregate sizes below 0.2mm to prevent plugging and secure a proper flow of the concrete [52]. Figure 3.29 illustrates a Creality CR-6 SE 3D-Printer, which is the 3D printer used in this thesis - elaborated in Appendix C [52][63].

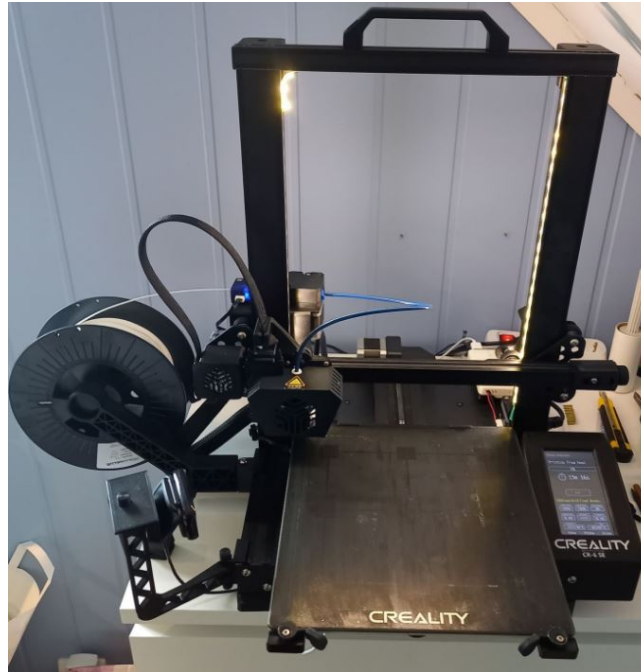


**Figure 3.29** – The 3D printer used in this thesis: Creality CR-6 SE 3D-Printer [Appendix C].

A critical factor concerning the use of thin 3D printed PLA shells is the limited strength of the formwork. Hydrostatic pressure, which is given by Formula 43, occurs when casting concrete into the formwork. Due to the low poor strength properties of thin PLA, the formwork needs to be strengthened. To obtain sufficient strength, it suggested to submerge the formwork in either sand or water, and if needed strengthen the outside of the formwork with resin or epoxy. By submerging the formwork into sand or water, the hydrostatic pressure is counteracted by the surrounding substance, canceling out the internal pressure in the formwork. To be able to cast monolithically, a timber framework most often needs to be introduced, in order to secure proper support and prevent unwanted deflections. In addition, it is possible to monitor the cast if a translucent PLA is chosen - enabling the user to secure a proper cast where all the voids are filled inside the formwork [63].

$$p = \varrho \times g \times d \quad (43)$$

- p: Hydrostatic pressure [N/m<sup>2</sup>]
- $\varrho$ : Concrete density [kg/m<sup>3</sup>]
- g: Gravity constant [m/s<sup>2</sup>]
- d: Height of the cast [m]

Other benefits with 3D printing are the lowering of building cost and labor work. According to Andrei Jipa's report "*Submillimeter Formwork 3D-Printed Plastic Formwork for Concrete Elements*" and David W. Johnston

*"Design and Construction of Concrete Formwork"*, the formwork cost of a free form concrete structure can be close to 60% of the total cost of the concrete structure. By introducing 3D printed formworks, it is possible to reduce costs due to the material reduction of formwork and lowering the labor demands. With that being said, the 3D printing technology adds new costs to the fabrication line in terms of digital formwork development and manufacturing - and it is unclear how beneficial it is in terms of cost savings. Jipa states that with a customized tool-path generation algorithm, it is possible to save up to 50% printing time compared to common commercial slicer tool algorithms. Therefore, with further development and research it shows a high potential for large economical savings - and despite of cost, it either way grants a huge degree of freedom in regards to design [63] [64].

### **3.8 Literature study**

A literature study is an analytical process of gathering and evaluating existing research to increase knowledge of what is already done on the current topic. The information gathered can be used to confirm or deny one's hypotheses, strengthen and support arguments and/or reveal important findings in new studies [65].

To perform conceptual feasibility study of a topologically optimized concrete staircase, the information gathered from the literature study is crucial. The current research done in this field is limited, due to TO being a new and relatively unexplored area in the concrete structures. Therefore, the researchers in this field are very open to sharing their findings - so that the development will go faster. Down below is a summary of the most important research papers used in this thesis.

#### **3.8.1 3D-Printed Formwork for Bespoke Concrete Stairs - Andrei Jipa et al.**

A study by Andrei Jipa et al., with a focus on the fabrication process of concrete stairs. Concrete has the ability to be cast into complicated geometries, making it a highly versatile material with a large potential for design freedom. The limitation is the current formwork production methods available in the industry, which is poorly applicable for casting complex geometries. This paper introduces the use of 3D-printed formwork, looking specifically on the appliance of Fused Deposition Modeling (FDM), presented in detail in section 3.7 [52].

Two cantilever step prototypes were developed, highlighted in figure 3.30 and 3.31. Prototype A was developed by the use of the BESO algorithm, explained in section 3.2.6. The TO process assumed concrete to be a homogeneous material, and later added post-tensioned reinforcement (4mm and 10mm tendons) to initiate the compressive properties of the concrete. FDM 3D-printing was used to create a 0.8mm thick formwork. Prototype A uses a self-compacting concrete with aggregate size limited to 0.14mm, enabling the concrete to fill all voids inside the formwork. Before casting, the reinforcement was placed and the formwork exterior was covered in sand to be able to withstand the hydrostatic pressure from the concrete. In addition, a blowhole was introduced to get rid of excess air inside the formwork, preventing unwanted air holes in the geometry [52].



**Figure 3.30** – Prototype A [52].



**Figure 3.31** – Prototype B [52].

Prototype B was developed by the use of NURBS geometries. A similar concrete mix was applied, the only difference being the addition of 10mm steel fibers - to counteract shrinkage cracks and increase the shear capacity. The formwork was printed accordingly to Prototype A, and is illustrated in figure 3.32, with integrated space for the reinforcement. Prototype B also investigated the possibility of connecting two steps using post-tensioned tendons of 10mm [52].

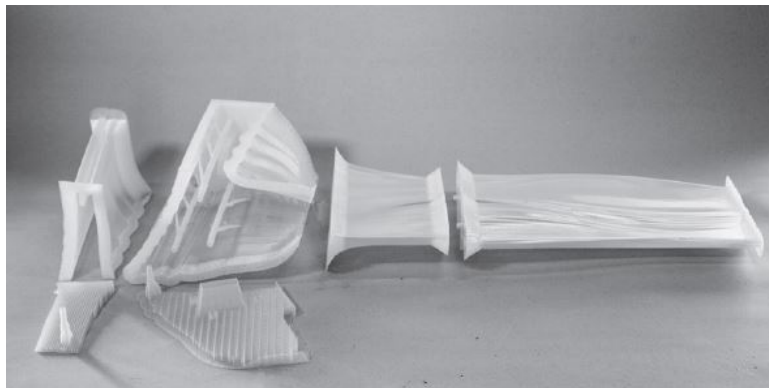


**Figure 3.32** – 3D printed formwork [52].

Findings from the paper [52]:

- Increased design freedom. The FDM printing technology opens up for more complicated designs that is not possible to produce with the existing production methods.
- Potential for huge material savings. Prototype A showed a material saving for concrete of more than 50%. In addition, the material used for the formwork where only 700g and 1400g for prototype A and B respectively.
- Precision of the production method can be improved. The shells are very thin, and was deflected in some places due to the hydro-static pressure from the concrete.
- FDM 3D-printing enable the integration of different functional features, such as duct channels and electrical conduits.



- There is a production challenge in regards of embedding the reinforcement into the concrete due to the high complexity of the design.
- Corrosion can be a problem due to insufficient concrete cover.
- Another factor is the large amount of time it requires to print the formwork. By the use of an FDM 3D-printer the different prototypes were printed in a time range from 24-48 hours.
- The size of the building volume is limited due to the maximum capacity of the 3D-printer.

### **3.8.2 Topology optimized reinforced concrete walls constructed with 3D printed formwork - Triveni Mudaliar et al.**

A research paper by T. Mudaliar, R. Lequesne and M. Fadden on a topologically optimized RC wall structure with the use of FDM 3D printing. The main objectives of the report were to examine the usability of 3D printed formworks, analyze the sensitivity of the TO models by altering the input parameters, study the correlation between stiffness and volume fraction, and lastly - examine how the stiffness, together with the correlating volume reduction is reacting to an increase of the concrete strength. To study these main objectives two different Abaqus models were developed [66].

One model was designed by implementation of steel reinforcement with the elasticity modules for steel and concrete, while the second model was designed without reinforcement by the use of a combined elasticity module based on rule of mixtures. The TO algorithm used for the analyzes was the SIMP method, explained in section 3.2.5. The objective function was set to "minimize the strain energy" and the volume-constraint was one of the chosen variables. Other variables that were investigated includes; mesh type and size, number of iterations cycles and compressive strength of the concrete/steel composite [66].

An FDM 3D-printer was used to produce a 0.125mm thick formwork. The formwork was then covered with epoxy to strengthen it and fasten the 3D-printed parts together. To secure a proper concrete cast, the mold were supported by both plywood and clamps - preventing it from yielding. By performing experiments in Abaqus, changing one parameter at the time and plotting the results for the different variables and parameters, the authors discovered some correlations and findings which are listed below [66]:

- By varying the mesh types and number of cycles it was proven that the same stiffness could be achieved with different types of elements.
- Based on the laboratory experiments, it is revealed that 3D-printed formwork has the ability to produce small-scale structures with good precision. In addition, it introduce promising properties that enable the producer to place the reinforcement properly inside the concrete.
- It is concluded that an effective way to counteract the resulting loss of strength from the reduction of stiffness is to increase the compressive strength of the material.
- The convergence rate is dependent on both element type and the volume constraint chosen. By introducing larger volume reduction constraints and/or assigning element types with few nodes (for example tetrahedron) the number of iterations is increasing. Mesh size on the other hand did not have an impact on the convergence rate of the analysis. With that being said, the mesh size reduction had a huge impact

on the computation time. It was showed that by reducing the mesh size from 1 inch to 0.125 inch, the time of computation was proven to be 17 times longer for this analysis!

- No proportional correlation was established between the volume reduction and stiffness, where the results were showing a lower stiffness increase than volume reduction. The authors propose that a reason for this is because that the removed material is being located near the center of the structure, resulting in a lower impact on the moment of inertia - than if the material were removed from the outer render of the structure.

### 3.8.3 An application of structural topology optimization to create staircase - Isabel Moreira et al.

A study by I. Moreira et al., with a focus on structural topology optimization of a staircase using Ultra High Performance Concrete (UHPC). The study looks into how to create the slenderest cross-section possible with the least amount of formwork. An iterative design process was conducted, where the results from the TO analysis was used as a basis to recreate a new and improved parametric design. The redesigned geometry was then applied the same loading and boundary conditions, and ran through the same TO analysis. Both the initial and optimized design results where then used as an analysis basis for comparison, to evaluate both the solid and void distribution. Based on this comparison a final parametric design was developed. To check for compliance with the building codes in regards to deflection, it was conducted static stress analyzes, which was then used to evaluate and redesign the geometry until the building requirements were fulfilled [51].

To perform the topology analysis, both the load and boundary condition regions were excluded from the optimization volume. The boundary conditions used was fixed translation in every direction at both the top and bottom landing. Material choice was UHPC, the TO goal was set to 50-80%, and the loads applied is stated in Table 3.4 [51].

Loading type	Value
Self-weight(program calculated)	volume *density
Service load	3000 N/m <sup>2</sup>
Finish load	1000 N/m <sup>2</sup>
Railing line load	740 N/m
Railing accidental vertical line load	2000 N/m
Railing accidental horizontal line load	8000 N/m

**Table 3.4** – Staircase loading according to Brazilian design code [51].

Another important factor assessed in this paper was the use of different mesh sizes. One of the findings of the paper is that with the use of finer mesh, one is able to produce a much more complex geometry, but it comes at the expense of higher computational time. By introducing finer mesh sizes to the geometry, it is shown that new topologies are created due to the increased load of information processed by the TO algorithm. Moreira concludes that mesh refinement has a positive effect up until a certain limit, where the geometry gets too complex and requires too much computational power [51].

The final design is presented in figure 3.33, illustrating a thicker cross-section along the inside of the staircase, which is due to higher stress levels compared to the outer layer of the staircase. Figure 3.34 illustrates a 3D-printed model of the final design with an integrated reinforcement duct [51].



**Figure 3.33** – Final staircase design [51].

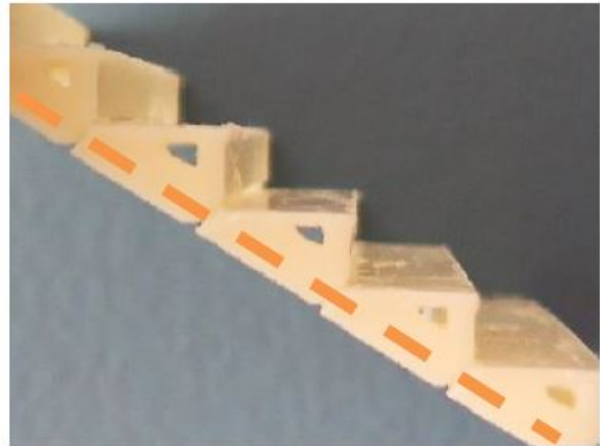


**Figure 3.34** – 3D-printed model [51].

### 3.8.4 Topology-optimized design, construction and experimental evaluation of concrete beams - Jackson L. Jewett et al.

In their research paper, Jewett et al. emphasized that there have been several research for employing topology optimization in reinforced concrete structures. Despite concrete's non-homogeneous behavior, the first studies considered composite RC structures as isotropic and linear elastic materials which provided simplified designs. Later on, several researchers applied an elasto-plastic truss algorithm to include non-linearity of reinforced concrete into the equation while others proposed fiber reinforced concrete for fabrication of concrete slabs. Although, there have been some empirical research into applying topology optimization in reinforced concrete, in many cases, no experimental testing has been performed and this poses some concerns about validity level of these papers. In light of this issue, Jewett et al. constructed three isotropic and linear elastic plain concrete design cases. In order to ensure an isotropic behavior for the experimental investigation, a minimum length scale equals to  $d_{min} = 5cm$  was introduced as a requirement in the designs [67]. These three design cases are listed below:

- Compliance design which aims to maximize the structural stiffness while constraining material use. There is no stress limit in this model.
- High Tension design where the goal is to minimize the structural volume (or mass) while respecting the constraints on compressive and tensile stresses within the structure. The limit on compressive stress is equal to compressive strength,  $f'_c = 34.5MPa$  and tensile stress limit is equal to  $11\%f'_c$ .
- Low Tension design with the same goal as the High Tension design and the same compressive stress limit, but the tensile stress limit sets at  $8\%f'_c$ .

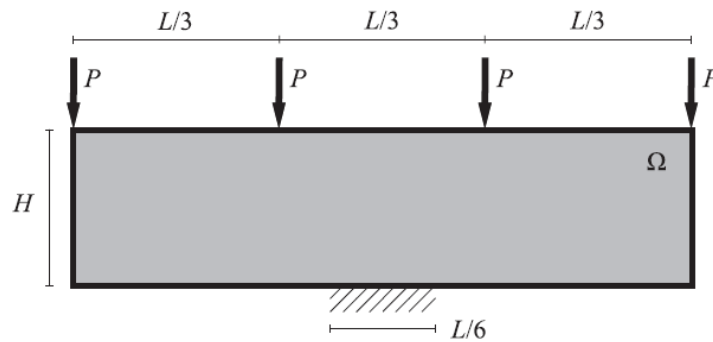


**Figure 3.35** – The case design [67].

The case study was a top beam of a 2D Hammerhead pier with a fixed support at the middle of the beam. Dimensions as shown in the figure 3.35 were  $L = 0.91m$ ,  $H = 0.23m$ ,  $t = 7.6mm$ , and four equal point loads,  $P = 2.2KN$ , were applied in four positions along the topside of the beam. Two topology optimization methods were applied for these three design cases; a density-based method has been employed for the Compliance design, and a stress-constrained topology optimization framework, which was proposed by Bruggi and Duysinx, was the basis of the method which was used in the High and Low Tension designs [67].

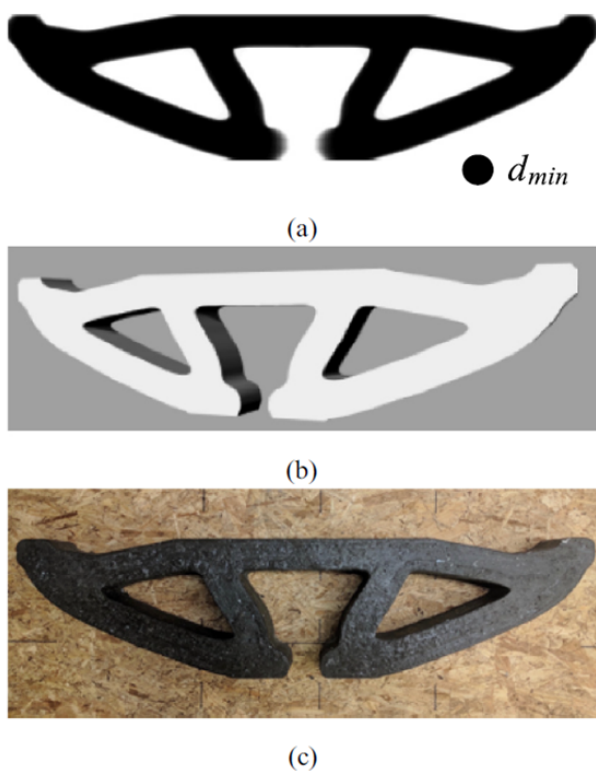


**Figure 3.36** – Compliance design:  
 (a) Unrounded design  
 (b) as-built design  
 (c) constructed specimen [67].

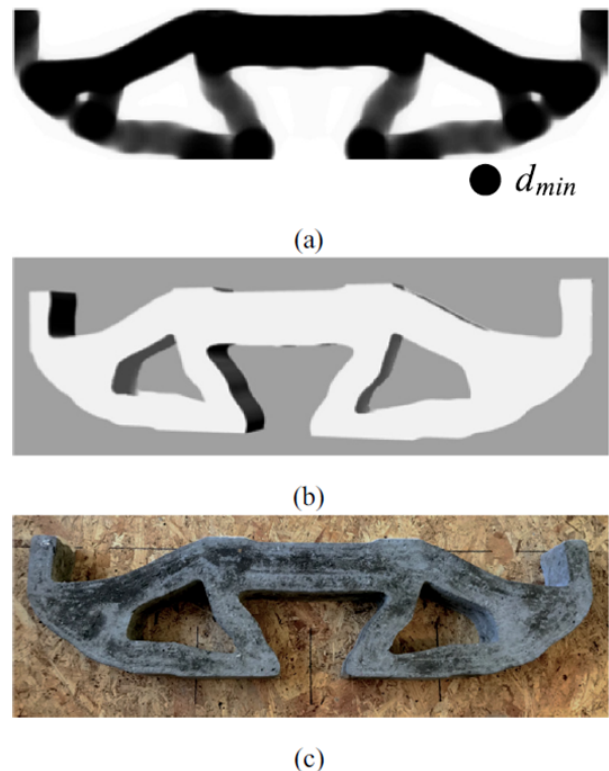


**Figure 3.37** – Low Tension design:  
 (a) Unrounded design  
 (b) as-built design  
 (c) constructed specimen [67].

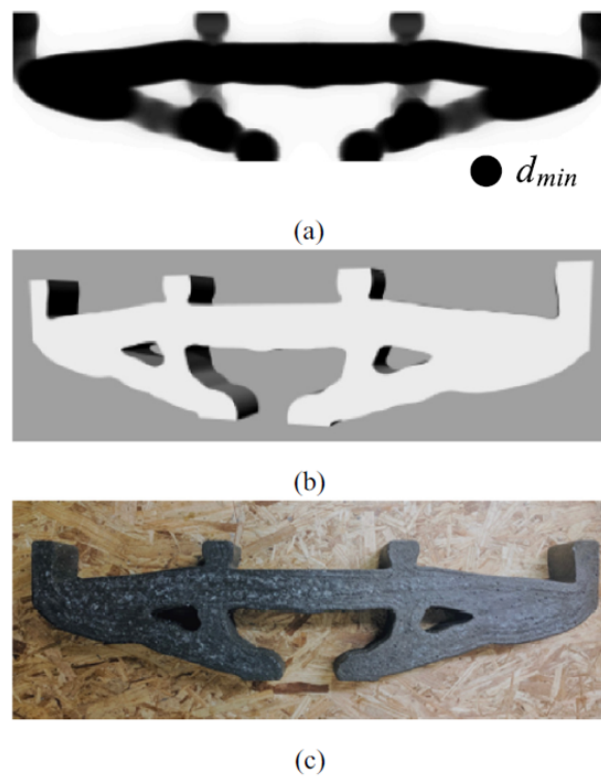


**Figure 3.38** – High Tension design: (a) Unrounded design (b) as-built design (c) constructed specimen [67].

Figures 3.36, 3.37 and 3.38 illustrate the constructed models for each design case. Material usage for the Compliance design has been reduced to 50% while for High and Low Tension designs, the material use is decreased to 49.3% and 52% respectively. Results from the force-displacement graph verify that for the design load, all experimental specimens behave elastically. Figure 3.39a displays the experimental compliance of the design cases plotted against the as-built volume. As expected, the Compliance design has a lower compliance and consequently higher structural stiffness. On the contrary, the High Tension design has a high compliance despite having relatively the same volume as the Compliance design. Variation of the compliance between the investigated test subjects is also higher in the High Tension design compared to the Compliance design which shows the increased robustness due to the higher structural stiffness in the latter design. Results from the Low Tension design show the similar stiffness and variation of the compliance as the Compliance design. This finding underlines the importance of the safety factors in the design process [67].

Results also show a relatively sizable difference between the unrounded compliance and as-built compliance in High and Low Tension designs compared to the Compliance design. This phenomenon was expected as more postprocessing was done in the rounded models of these two designs which considerably reduced the structural stiffnesses. Maximum load capacities were also obtained in the study. These capacities are plotted against as-built volume and are drawn in a graph which is shown in figure 3.39b. Based on this graph, the Compliance design has the highest load capacity in comparison to the two stress-constrained designs. It also has the highest averaged load capacity between the three designs. As expected, the Low Tension design has the higher load capacity than the High Tension design which is due to the fact that it is constructed with more material. It is noteworthy to mention that the large variation of load capacity in the Compliance design com-

pared to the two stress-based designs is interpreted as the fact that the Compliance design's specimens had negligible ductility [67].

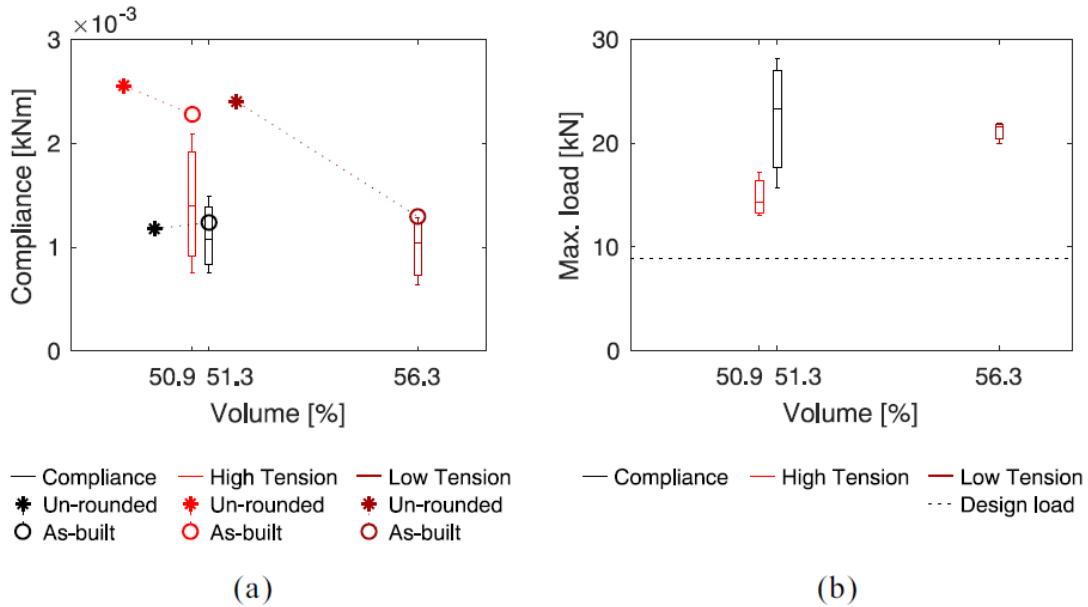


**Figure 3.39** – Results obtained from the experiments: a) compliance plotted against volume, b) maximum load capacity [67].

Maximum principal stress distributions from the unrounded and as-built models also obtained in the work. As shown in figure 3.40a-b, the results from the unrounded and as-built models of the Compliance design show that stress distributions are very similar. Figure 3.40e-f displays a great reduction in stress distributions after postprocessing. Nevertheless, the failure location was not affected by this stress distribution's reduction. On the other hand, the maximum stress location was greatly moved by postprocessing in the High Tension design as illustrated in figure 3.40c-d. This occurrence underlines that the structural stiffness of the High Tension design is very much dependent on the local composition of the concrete in different specimens [67].

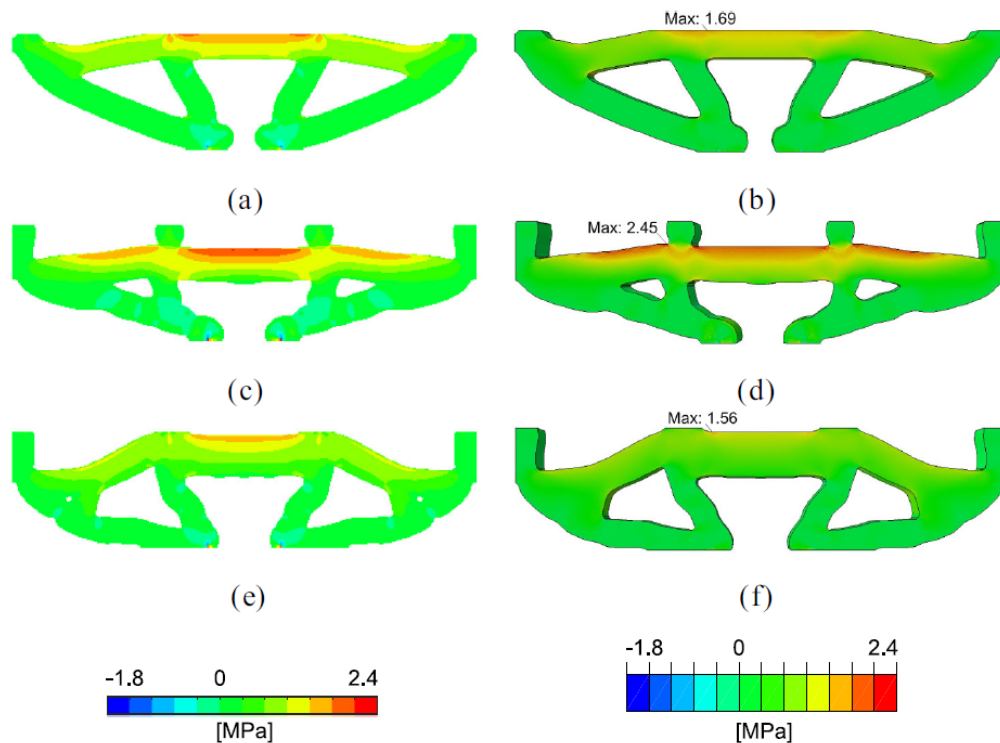


**Figure 3.40** – Maximum principal stress distributions: (a) unrounded Compliance design, (b) as-built Compliance design, (c) unrounded High Tension, (d) as-built High Tension, (e) unrounded Low Tension, and (f) as-built Low Tension [67].

The paper concludes the following points based on the results mentioned above [67]:

- The paper shows that topology optimization methods can be employed in anisotropic plain concrete structures where the constructed models verify their validity.
- The significance of the safety factors associated to the material properties was observed in the stress-based design framework.
- It was also observed that due to the extensive postprocessing the stress-constrained design framework was unable to attain 0-1 design which satisfy the minimum feature size requirement.
- Influence of the postprocessing on the behavior of the specimens was also demonstrated in the work which showcased the importance of better developed algorithms for obtaining better designs with less postprocessing requirement.
- The next research step is to introduce the reinforcement phase into the model and investigate the designs' behavior in a nonlinear analysis.

## 4 Research question

Reduction of material consumption has always been an important objective in design phase of any structure. Based on this criterion this study investigates the possibility of implementing topology optimization in manufacturing of a concrete staircase. The research question is formulated in corporation with the internal and external supervisor, and reads as follows:

How to develop and produce a topologically optimized concrete staircase?

- How can parametric modeling enhance the analysis process of the staircase?
- What impacts do sensitivity-based and condition-based algorithms with various mesh sizes and volume constraints have on stiffness and deflection of the staircase?
- What advantages and challenges are related to the use of fused deposition modeling manufactured formworks?

### 4.1 Limitations

To concretize the research question and limit the scope of the thesis, the following limitations were made:

- Placement of reinforcement and verification of the topologically optimized staircase according to Eurocode 2, is determined to be outside of the scope of the thesis, but are considered briefly in section 8.5 and 10.
- No other production methods than fused deposition modeling is investigated due to the magnitude of the report.
- Connections and joints are not considered in detail.
- Due to the node limitation in the Abaqus/CAE student version of 250.000 nodes, the mesh size is limited to 40mm for the reference model. To investigate the mesh dependency, a limited selection of two mesh sizes were chosen, 40 and 60mm. In addition, since the quadratic order elements drastically increase the number of nodes and the linear tetrahedron has proved to be less accurate than the linear hexahedron, only the latter element is selected [44].
- Cost of the topologically optimized staircase is not considered in detail.
- Due to complexities of non-linear analysis in combination with topology optimization and the node limitation in the student version of Abaqus, the reinforcement phase was excluded from the model and a linear analysis investigation was conducted instead.



## 5 Case and materials

In this section, the case of the report will be elaborated and necessary information regarding the modeling process, optimizing and analyzing of the staircase will be reviewed. The case is based on material from Rebartek AS and Contiga AS.

### 5.1 Background

The authors have been engaged through Rebartek to create a conceptual feasibility study and look into the potential of topology optimization in concrete, more specifically the development and manufacturing of a concrete staircase. As mentioned in section 2, application of TO in concrete structures is a relatively uncharted area in construction. The aforementioned, and the findings of successful application of topology optimization to inhomogeneous materials presented in section 3.8, together with the fact that TO has proven to be very successful with homogeneous building materials like steel and aluminum, established the foundation for the case.

Inspired by the literature study, the authors found it very interesting to look into the process of 3D printing to be able to create 3D models of the topology designs and formworks – together with increasing the knowledge and gain experience with the production method. This was done due to the recommendations from several papers which concluded that additive manufacturing (3D printing) is a viable option for printing formworks [10] [52]. In addition, it has a huge potential for further development combined with new technology. Due to the organic looking geometry from TO, it is necessary to be creative in ways of manufacturing, and 3D printing seems to be the most promising – as of now.

### 5.2 Conditions and drawing basis

The original design is a U-shaped staircase consisting of two separate concrete element parts, shown in figure 5.1 and 5.2. The lower part of the staircase presented in figure 5.3, was selected as the reference model in this study. An important condition was that the topologically optimized staircase design should accommodate the same functionality as the original design, other than that, there were given no other design restrictions. To retain the same functionality, it is important that the steps are flat and comfortable to use, as well as the staircase elements are easy to connect to surrounding concrete elements. Table 5.1 shows the dimension of the bottom staircase with riser height and tread width.

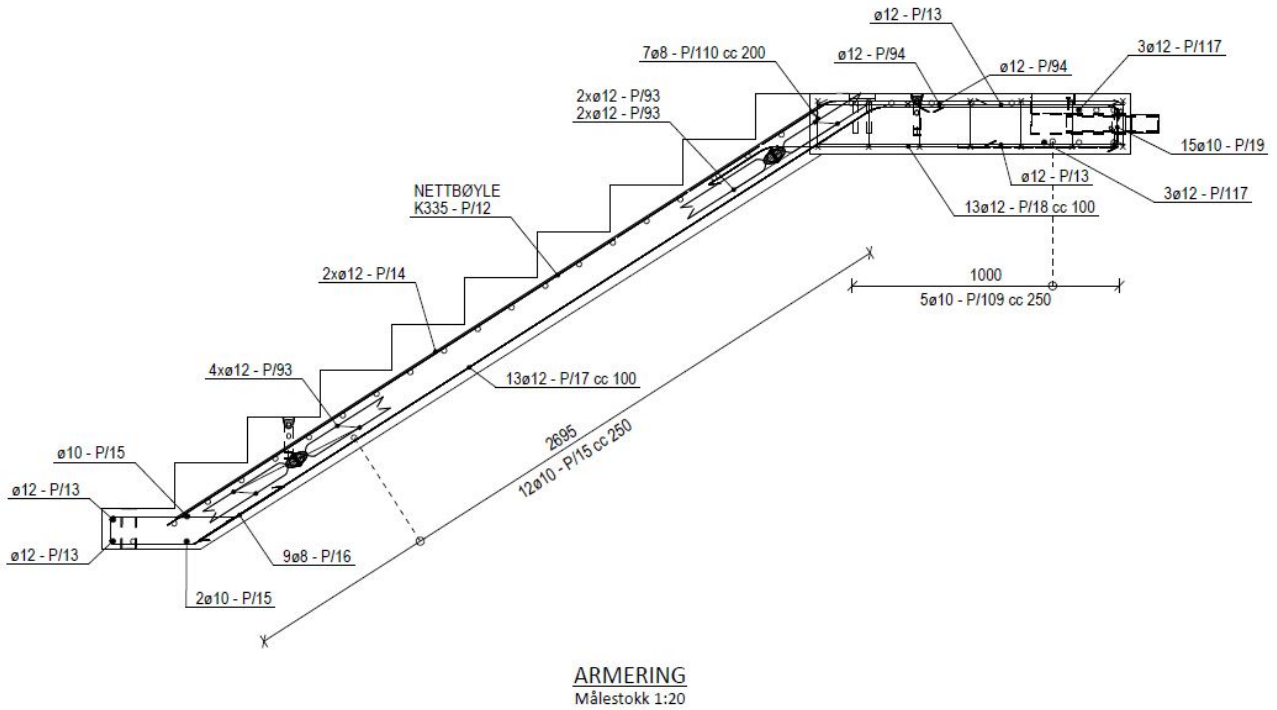


Figure 5.1 – Bottom staircase drawing from Contiga AS [Appendix A].

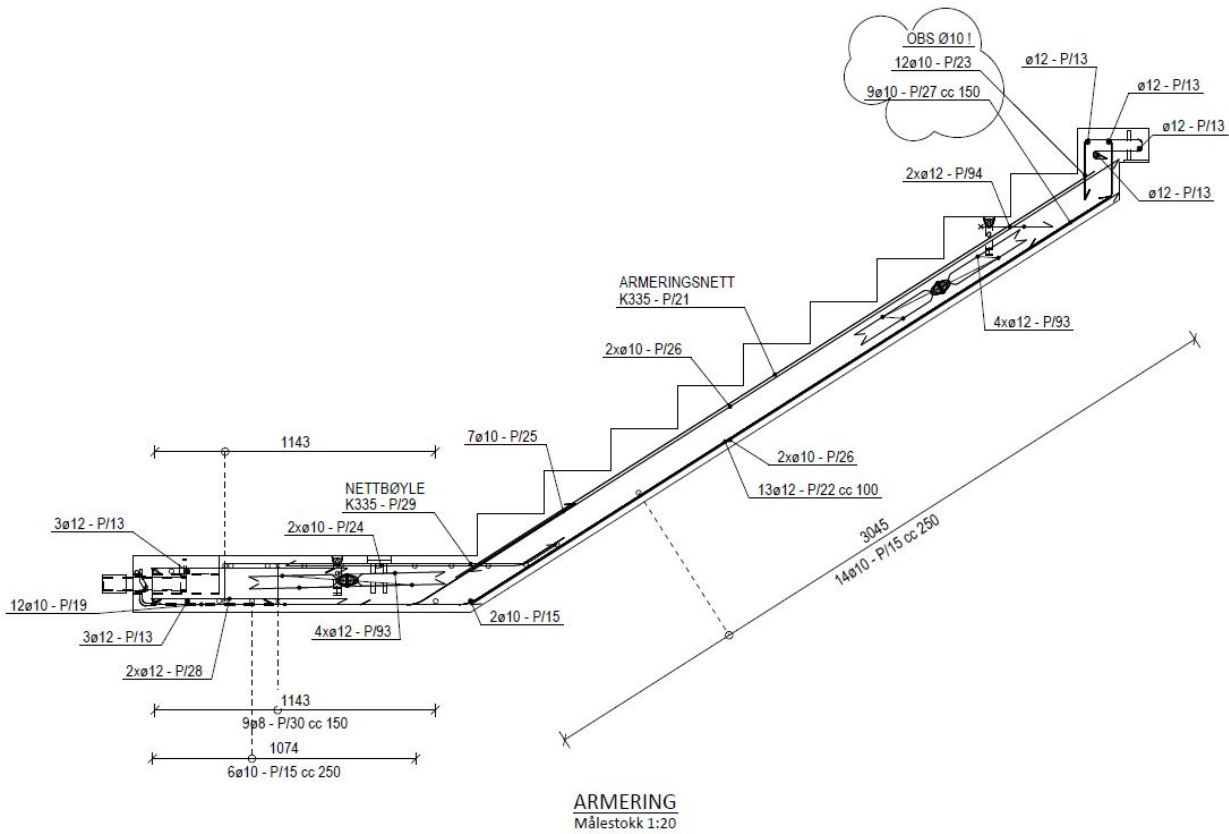


Figure 5.2 – Top staircase drawing from Contiga AS [Appendix A].



Elements	Measurement [mm]
Riser (R)	172.75
Tread (T)	272.00
Height of floor (H)	1554.75
Length of single flight	2448.00
Length of landing	1424.00
Width of flight	1200.00
Width of landing	1405.00

**Table 5.1** – Dimensions of bottom staircase [Appendix A].

### 5.3 Material

The staircase is constructed with the concrete quality B30. Material properties of the concrete is presented in table 5.2. Minimum concrete cover is set to 25mm.

Properties of concrete		
Concrete density	24.00	kN/m <sup>3</sup>
Concrete characteristic strength ( $f_{ck}$ )	30.00	N/mm <sup>2</sup>
Concrete design strength ( $f_{cd}$ )	17.01	N/mm <sup>2</sup>
Mean tensile strength ( $f_{ctm}$ )	2.90	N/mm <sup>2</sup>

**Table 5.2** – Properties of the B30 concrete [Appendix A].

### 5.4 Boundary condition

For simplicity, the staircase is assumed to be fixed for any axial movement at both ends. The bottom of the staircase is presumed to be rested on the floor/slab. Furthermore, the landing of the staircase is supported at two points by steel connectors which are embedded inside the wall. Ultimately, the staircase's flight and landing are treated as one unit.

### 5.5 Load condition

Calculated self-weight of the geometry, together with finishing load, are considered as dead load. Finishing load is taken as  $1 \text{ kN/m}^2$  [51]. The live load is taken from table 6.2 in Eurocode 1 [58]. Table 5.3 shows the applied loads to the staircase with their magnitude.

Loads	Flight [kN/m <sup>2</sup> ]	Landing [kN/m <sup>2</sup> ]
Selfweight	7.16	5.52
Imposed	3.00	3.00
Finishing	1.00	1.00
Design	15.78	13.57

**Table 5.3** – Type of loads applied to the staircase.

## 6 Method

### 6.1 Literature review

The goal of the literature review is to increase the level of knowledge and gain a solid theoretical foundation in the current field of research. This applies for both theoretical background, method and empirical data. In addition, it will contribute to form and change the objective for the thesis.

Most of the literature study is conducted with the use of academic search engines like Google Scholar, ScienceDirect and Oria. By the use of customized settings in the search engine the most relevant and latest information concerning TO of reinforced concrete is gathered. Due to the fact that TO of concrete is a relatively new and unexplored field of research, almost all research papers were published between 1980-2021, where the most relevant papers were published between 2015-2021. Academic books by the pioneers and experts of the fields are also employed to present the firsthand interpretation and description. The information gathered is then used as sources of information and basis for comparison and discussion of the results.

### 6.2 Parametric modeling with Grasshopper 3D

To develop the parametric model of the staircase, the plugin Grasshopper 3D in Rhinoceros 3D is used. The model is developed by the use of the following nodes in GH:

- Construct point
- Construct vector
- Unit vectors
- Number slider
- Negative
- Move
- Line
- End points
- Join curves
- Series
- Split list
- List item
- Boundary surfaces
- Extrude
- Rotate 3D
- Distance
- Subtraction
- Addition
- Multiplication
- Division

By the use of these nodes and drawings from Contiga AS, a 2D cross-sectional surface of a single staircase flight is first modeled. This cross-sectional area is then extruded into a solid, creating a solid staircase flight. The usage of number sliders implemented into the node-network provides the parametric function for the relevant variables, enabling changes to the geometry by simply changing the value of the number slider. To be able to recreate the U-shaped design model from Contiga AS, the bottom and top flight are given different customized parametric properties to enable specific adjustment in regards to both fastening and height of landing. In addition, an intermediate landing is created to be able to parametrically alter the width between the flights.

The FEM and TO analysis are performed on the GH model by the use of Abaqus CAE, elaborated in section 6.3. In order to speed up the analysis processes, the following properties are intentionally introduced to the GH model:

- The staircase is modeled as separate solids; bottom staircase, intermediate landing and top staircase.

This enables the user to export the model piece by piece, which is useful when it is not necessary to analyze the whole model.

- A concrete cover algorithm is implemented, which enables the user to easily assign "freeze region"-constraints and loads.

The development of the algorithm, together with the resulting GH model is given in detail in Appendix B.

## 6.3 Abaqus

### 6.3.1 Part module

As described in section 3.4.1, the solid geometry of the staircase is imported as a ACIS-file from Rhinoceros 3D, with a ".sat" format. The part is then divided into a number of smaller solids, by the use of the partitioning tool, to enable the option of choosing specific frozen regions and structured hexahedron elements. Figure 6.1 illustrates the partitioned part that was used for every simulation in this thesis.

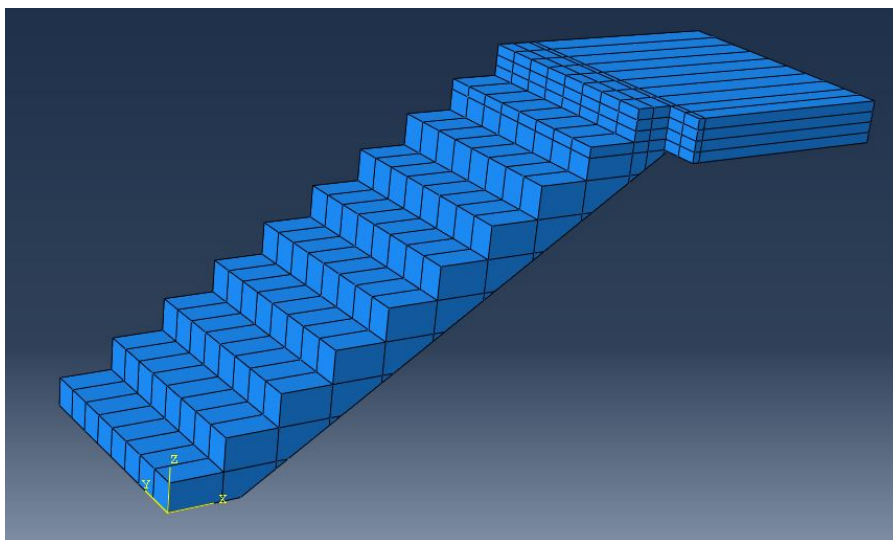


*Figure 6.1 – The imported and partitioned staircase geometry with the associated coordinate system.*

### 6.3.2 Property module

The material properties parameters for the concrete quality B30. Table 5.2 highlights the input parameters for concrete B30.

### 6.3.3 Assembly module

The staircase is oriented with the z-direction to be upward, y-direction representing the width of the steps and the x-direction representing the depth of the staircase, as illustrated in Figure 6.1.

### 6.3.4 Step module

An initial step is automatically added to provide the user with the option to modify and edit the model. In addition, a general static step is applied with the Nlgeom setting set to "off", creating a linear structural analysis

step. By ticking of boxes in the "Field output request manager", it is possible to choose which output variables will be retrieved in the simulation. The most relevant and typical output variables like strain energy, volume fraction, von Mises and deflection are selected.

### 6.3.5 Load module

The loads are calculated as separate pressure loads for the flight and the landing, where the live load is applied as a vertical pressure load and the dead-load as a gravity load with magnitudes accordingly to Table 5.3. Boundary conditions are applied at the supports as straight lines with U1, U2 and U3 set to zero displacement. Meaning zero displacement in both x (U1), y (U2) and z (U3) direction at the supports.

### 6.3.6 Mesh module

Hexahedron elements of the first order (linear) are the only element type used to mesh the model geometry. This is due to the combination of both the magnitude of the reference model and the node limitation in Abaqus, which prevent the use of elements of quadratic order. The assembly consists of one solid part as mentioned in section 3.4.6. To mesh the solid part, structured hexahedron elements of C3D8 type are assigned to the original design. Due to some application restrictions in Abaqus, it is needed to partition the geometry to divide the model into several regular shapes - which enables the use of the hexahedron element type. Figure 6.2 and 6.3 illustrate the meshed models with 40mm and 60mm mesh size, respectively.

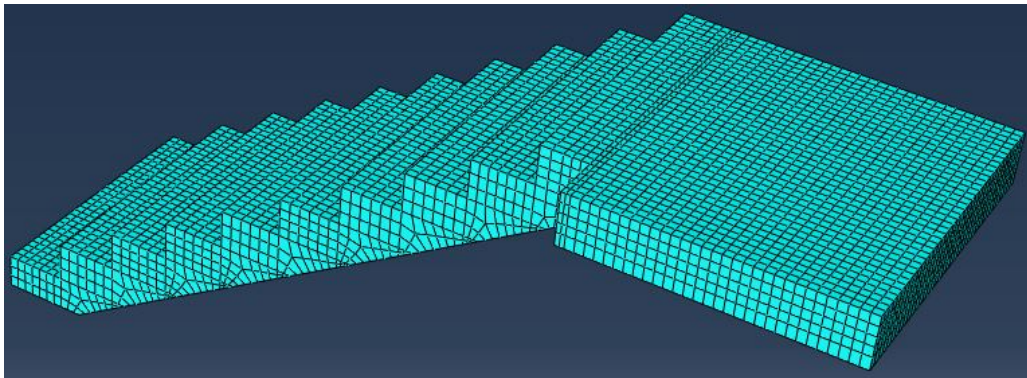


**Figure 6.2** – Mesh size set to 40mm.

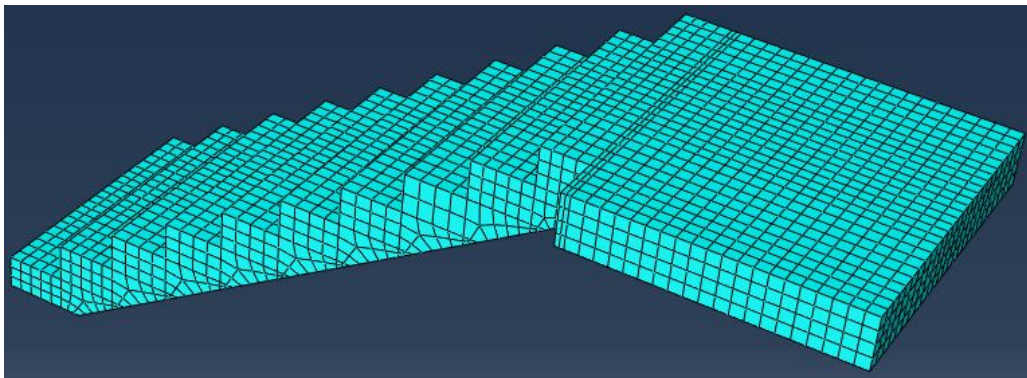


**Figure 6.3** – Mesh size set to 60mm.



### 6.3.7 Optimization module

The optimization tasks are conducted in accordance with the optimization manual from Abaqus [29] together with a written TO guide paper called "Structural Topology Optimization", written by Steffen Johnsen [43]. Design responses are chosen to be volume and strain energy. The objective function is set to minimize the strain energy, which at the same time maximizes the stiffness. In addition, several constraints are determined:

- Load and fastening areas are frozen.
- Demold control is not applied.
- The volume constraint is varied between 30-70% to investigate different TO possibilities and generate valuable data for comparison.

Figure 6.4 and 6.5 illustrates the Abaqus settings and input parameters.

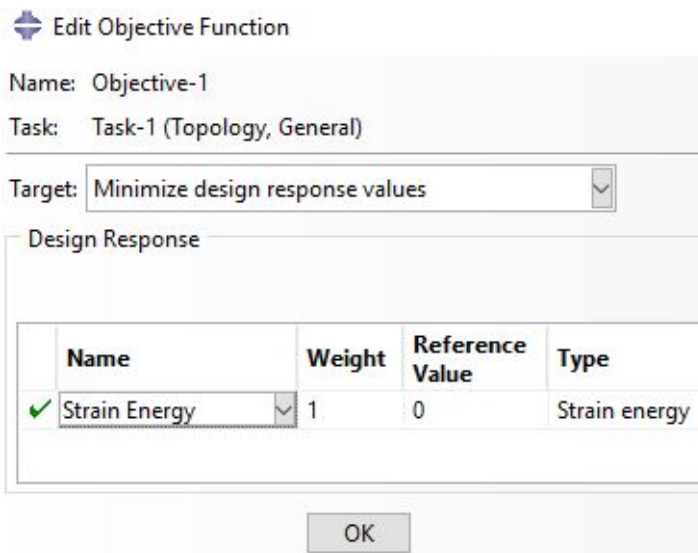


Figure 6.4 – Abaqus: Objective function.

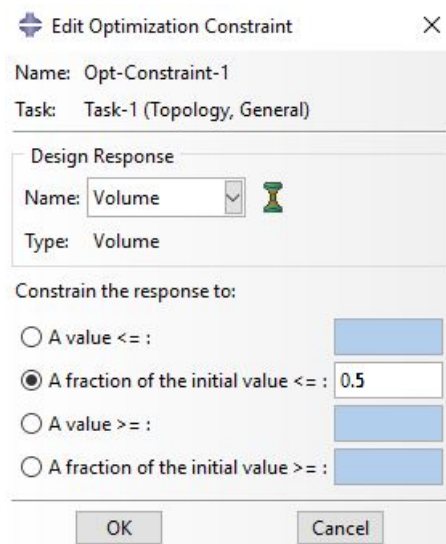


Figure 6.5 – Abaqus: Volume constraint.

## 6.4 3D printing

To be able to print the different designs and geometries, the output files from Abaqus are exported as ".stl"-files. ".stl"-files are mesh files, and it is therefore necessary to convert the Abaqus output files into a solid (".sat"-file format) by the use of a CAD software (Autodesk Fusion 360). The converted file format (.sat) was then imported to a 3D printing software called "Ultimaker Cura", which integrate very well with CAD software. This software is used to perform the 3D printing and has a huge range of possibilities, which can easily be applied through custom settings. The most relevant custom settings used for this thesis are stated in Appendix C.

It was decided to create a formwork of two steps inside of one formwork – to visualize the concept. Due to size limitations on today's 3D printers, it is not possible to print one single formwork for large scale structures and it was therefore also realistic to divide the staircase formwork into several small modular formworks. The formwork was therefore printed in 6 parts at a scale of 1:20, where each part was assigned with holes and/or

connection piers. This was done to be able to assemble the formwork pieces into one single formwork and illustrate the concept in a sufficient way.

The 3D printer used in this paper is a “Creality CR-6 SE 3D-Printer”, which is a Fused Deposition Modeling (FDM) technology printer, as described in section 3.7. It has a printing volume of 235x235x250mm and a print speed of 80-100 mm/s [68].

The whole procedure is given in detail in Appendix C.

## **6.5 Analysis of the reference staircase**

The U-shaped staircase presented in figure 5.3, was selected as the reference model in this study, and was provided by Contiga AS. Detailed calculations and design of the model are given in appendix A. To establish a basis for optimization, dimension and design properties of the reference model was checked and verified by the requirements in Eurocode 2 and technical requirements for construction works (TEK17). The thickness of the flight slab is verified according to table 7.4 in NS-EN 1992-1-1. Additionally, the risers and the treads were checked based on the presented regulations in TEK17.

### **6.5.1 Design load**

To determine the self-weight of the reference staircase, volume of concrete is calculated based on the reference drawing 5.3 and verified by the use of a FEM software. Self-weight of the staircase’s landing and flight is calculated separately with the help of density of concrete and calculated volume. Imposed load is taken from table 6.2 in Eurocode 1. Additionally, finishing load is considered 1 kN/m<sup>2</sup> [51]. Eventually, the design load is calculated according to equation 37 which gave the maximum value.

### **6.5.2 Shear capacity**

The maximum shear forces acting on the reference staircase are calculated according to section 9.2.2 in NS-EN 1992-1-2:2004+NA:2010 with regards to the current loading, and verified by the use of a FEM software. Shear resistance and minimum shear resistance of the reference staircase are calculated according to equation 40 and 41. Ultimately, the maximum shear forces are checked against the calculated shear resistances of each part in the reference model.

### **6.5.3 Moment capacity**

The moment capacity of the staircase is calculated according to section 6.2.6 in NS-EN 1992-1-2:2004+NA:2010 with equation 42. Maximum design moments due to the design load are calculated based on the assumed boundary condition and verified by the use of FEM software. Finally, the maximum design moments are compared with the respective moment capacities.

### **6.5.4 Deflection**

Maximum allowable and actual deflection of the reference staircase are calculated according to section 7.4.2 in NS-EN 1992-1-2:2004+NA:2010 with the use of table 3.3 . The deflections of the reference model and op-

timized staircases are obtained from Abaqus, and controlled against the allowable deflection according to the appearance and general utility of the structure, described in section 3.6.8. In order to provide a fair and realistic comparison, this study ignores local deflections and instead selects a point in mid span of the flight in each model as the reference point for maximum deflection. This designated point is located at the crossing point of the sixth tread and the corresponding riser.

## 6.6 Quality control and systematization

To ensure a valid and accurate work, performer of each task has first familiarized himself with the procedure and theory of that certain task. Particularly, in the design phase, the authors explored different credible guidelines and manuals to guarantee realistic models and reduce any human error. In order to eliminate any possible mistake in modeling phase, the performer runs two separate simulations. In case of any unexpected deviation in these two models, a third simulation in front of the whole team will be decisive.

All results are summarized in Excel sheets for further investigations. Each simulation case is labeled by the TO method that has been employed in that simulation, the date of operation, volume percentage of the original volume, number of iteration cycle limit, mesh size and the type of load condition that has been applied to the structure. This form of classification was later on proved to be very important and effective for data sorting. A similar systematization approach has been used for classification of different cases in this study. Some examples of this approach and their corresponding interpretations are shown below:

- SB\_40\_60 ⇔ A model based on sensitivity-based method with 40% volume percentage of the original volume and mesh size of 60mm.
- CB\_70\_40 ⇔ A simulation based on condition-based algorithm with 70% volume percentage of the original volume and mesh size of 40mm.

## 7 Results

This section presents the most important results and findings from the parametric modeling, topology optimization's simulations, calculations and 3D-printing methods described in section 6.

### 7.1 Parametric model

Figure 7.1 gives a visualization of the GH model's parametric properties. Each number slider represent a given feature of the staircase design that can be altered to change the geometry. The variables are:

- Height of the top landing
- Thicknesses of the top console
- Depth of the top landing
- Angle adjustment
- Depth of step
- Concrete cover
- Height of the bottom landing
- Number of steps
- Depth of the middle landing
- Width of the staircase flights
- Width of intermediate landing
- Depth of intermediate landing



**Figure 7.1** – The resulting parametric values, expressed by number sliders.

Figure 7.2 illustrates the final GH 2D canvas with the complete wired node-network. The node-network is categorized by the following:

- Green: Input parameters.
- Red: Bottom staircase flight.
- Blue: Top staircase flight.
- Orange: Intermediate landing.
- Yellow (small node to the right): Merged solids, whole model.

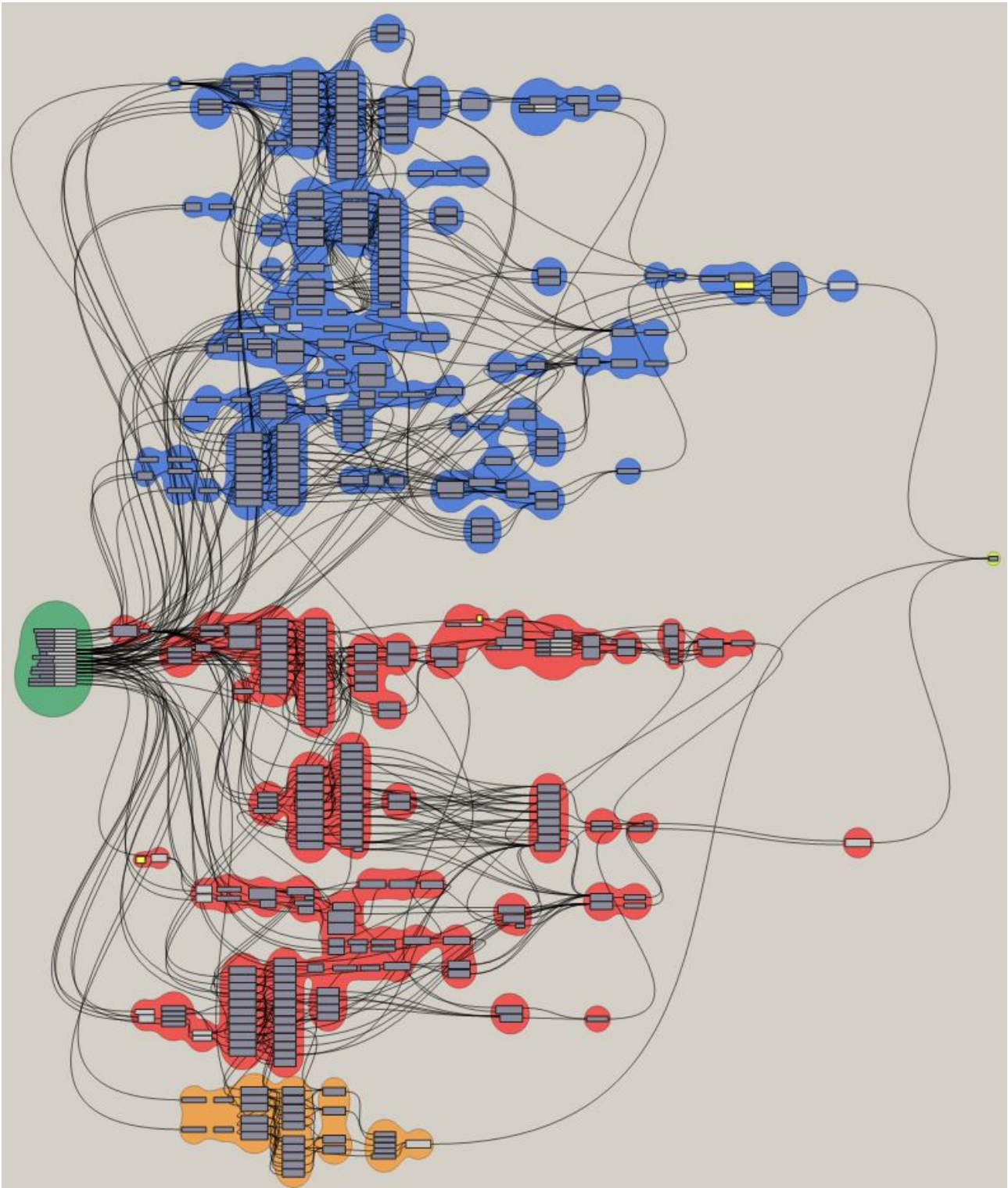


**Figure 7.2** – The resulting GH 2D canvas with the complete wired node-network.

By implementing the values from Contiga given in Table 5.1 and Appendix A into the GH model, the staircase design illustrated in Figure 7.3 were computed.

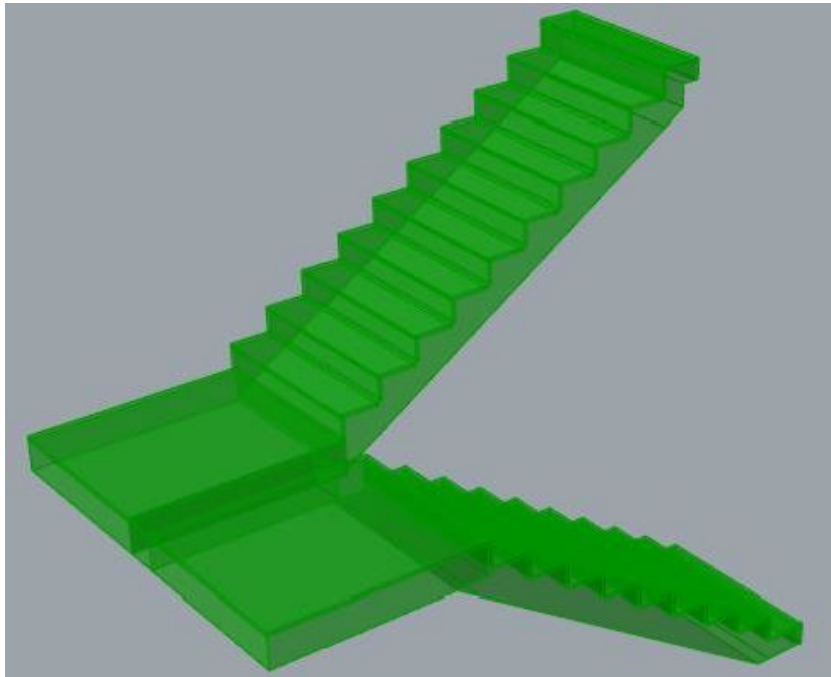


**Figure 7.3** – U-shaped staircase modeled in GH with the properties given from Contiga [Appendix A].

## 7.2 Structural analysis

The reference staircase is verified based on the dimension presented in the table 5.1 and the guidelines from Eurocode 2. Thicknesses of the staircase's flight and landing, based on calculation and the reference model are presented in table 7.1 The detailed calculation of verification of staircase is presented in Appendix D.

Element	Calculated [mm]	Reference [mm]
Flight slab	153.40	178.88
Landing slab	102.20	230.00

**Table 7.1** – Thickness of reference staircase slabs [Appendix D].

Design shear force and shear capacity are presented in table 7.2. Design moment and moment capacity are presented in table 7.3.

Shear	Capacity [kN]	Design [kN]	Moment	Capacity [kN-m]	Design [kN-m]
Flight	64.11	28.32	Flight	102.30	14.79
Landing	186.97	38.50	Landing	185.24	14.79

**Table 7.2** – Shear capacity and design shear of the reference staircase [Appendix D].

**Table 7.3** – Moment capacity and design moment of the reference staircase [Appendix D].

Deflection of the reference model is checked as described in section 6.5.4. Table 7.4 shows the maximum

allowable deflection of the reference model based on table 7.4N in Eurocode 2 and appearance and general utility. Effective span/effective depth is calculated regarding dimension of the reference drawing.

Element	L/d allowable	L/d actual	Span/250 [mm]
Flight	20.00	13.69	9.79
Landing	20.00	7.16	5.70

**Table 7.4** – Calculated deflection of the reference model [Appendix D].

### 7.3 Topology optimization

This part of the study will display the simulated models, and their corresponding deflection and strain energy. All simulations have been performed in Abaqus/CAE based on the method that has been described in 6.3. Subsequently, the obtained results will be shown in graphs for a better visualization.

#### 7.3.1 Reference model

Figure 7.4 displays the results of a finite element analysis of the original staircase from Contiga.

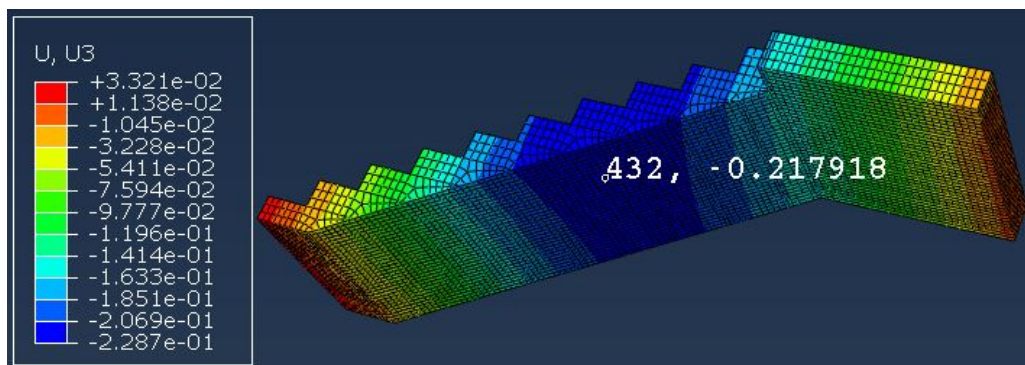


**Figure 7.4** – Reference model.

#### 7.3.2 Deflection

Figures 7.5 - 7.8 illustrate maximum deflection in different models. The results are presented from a-e, where a) is representing the volume constraint of 70% for all the figures. Note that as described in section 6.5.4, local deflections are overlooked and the deflection at node number 432 is assumed as the global maximum deflection.



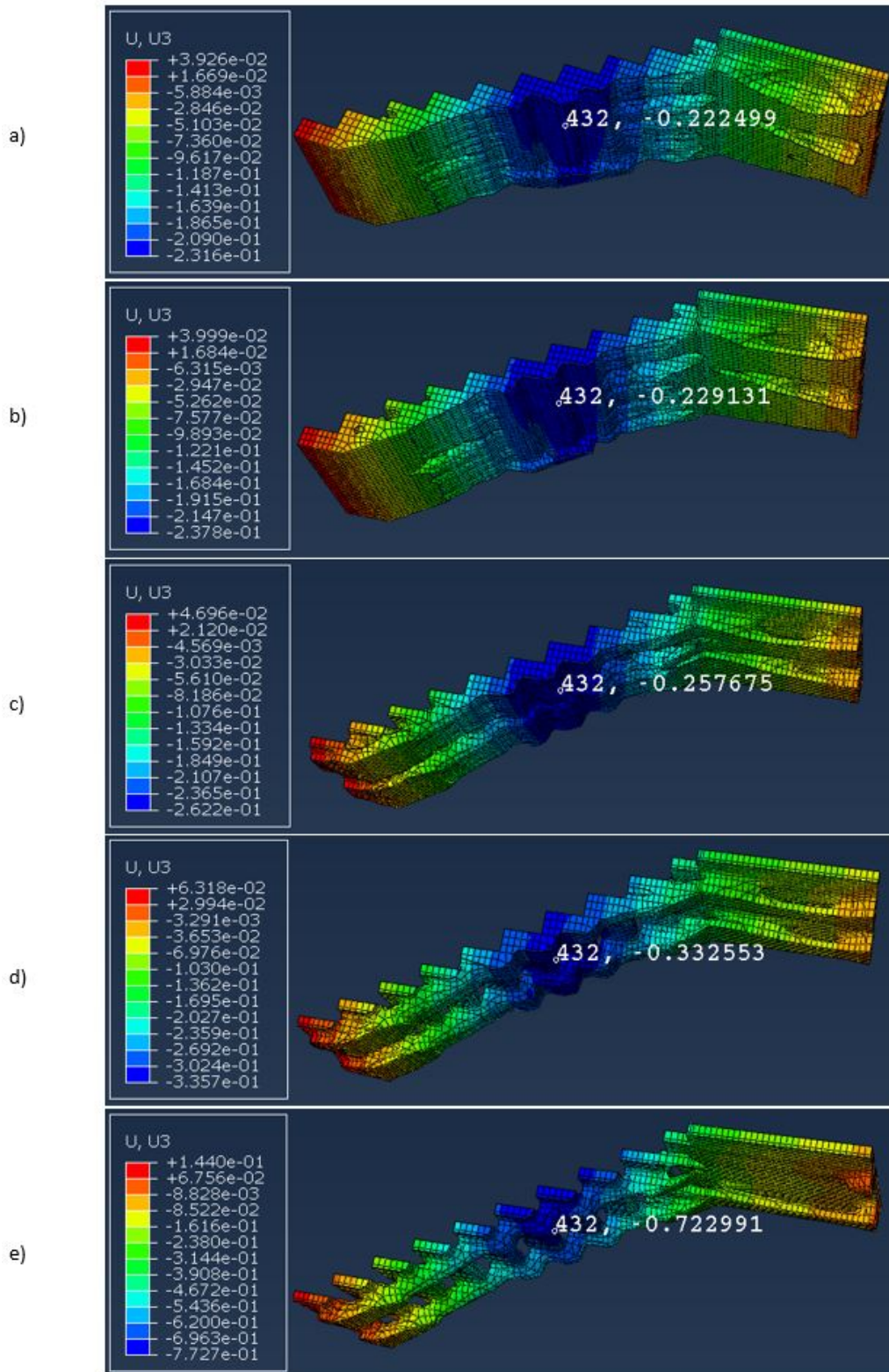


**Figure 7.5** – Deflection at reference point in sensitivity-based models with 40mm mesh size and a) 70%, b) 60%, c) 50%, d) 40% and e) 30% volume of the original volume.

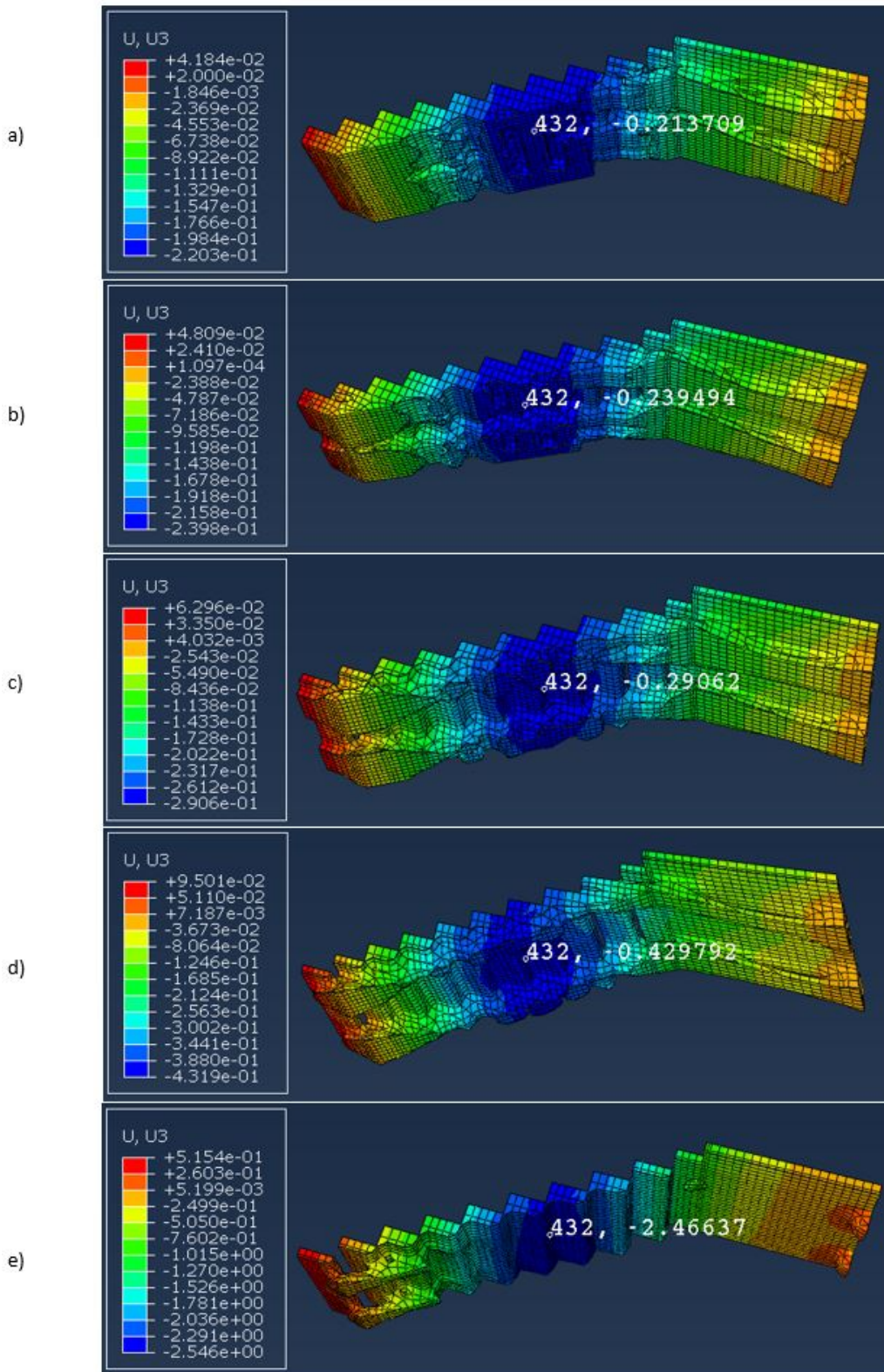


**Figure 7.6** – Deflection at reference point in sensitivity-based models with 60mm mesh size and a) 70%, b) 60%, c) 50%, d) 40% and e) 30% volume of the original volume.

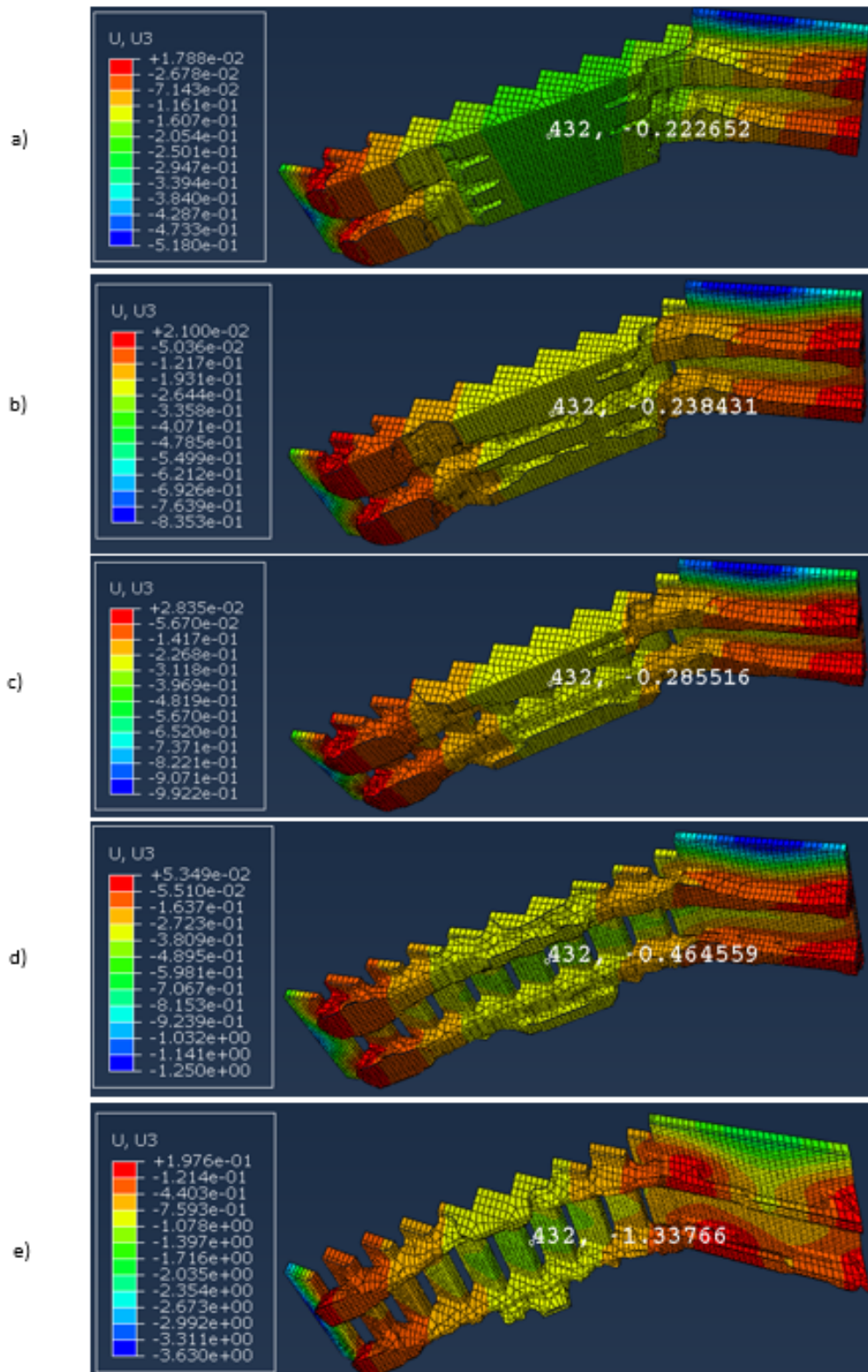


**Figure 7.7** – Deflection at reference point in condition-based models with 40mm mesh size and a) 70%, b) 60%, c) 50%, d) 40% and e) 30% volume of the original volume.

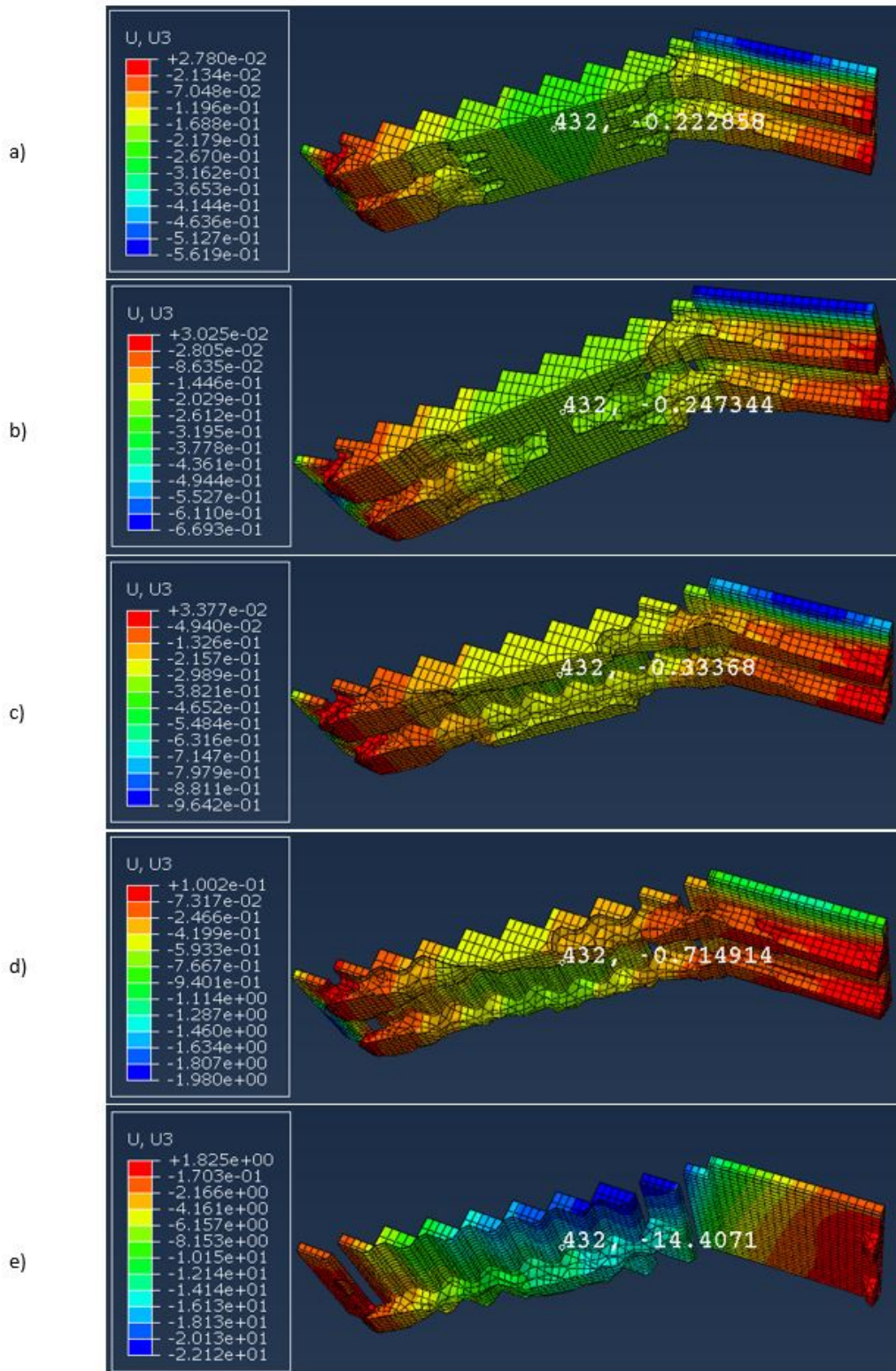


**Figure 7.8** – Deflection at reference point in condition-based models with 60mm mesh size and a) 70%, b) 60%, c) 50%, d) 40% and e) 30% volume of the original volume.

Furthermore, these results are plotted in a graph shown in figure 7.9. Additionally, for better visualization, the results of models with 30% of the original volume have been excluded and the remaining results are plotted in

figure 7.10. Corresponding results of the reference model from Contiga is plotted as a straight line in the latter.

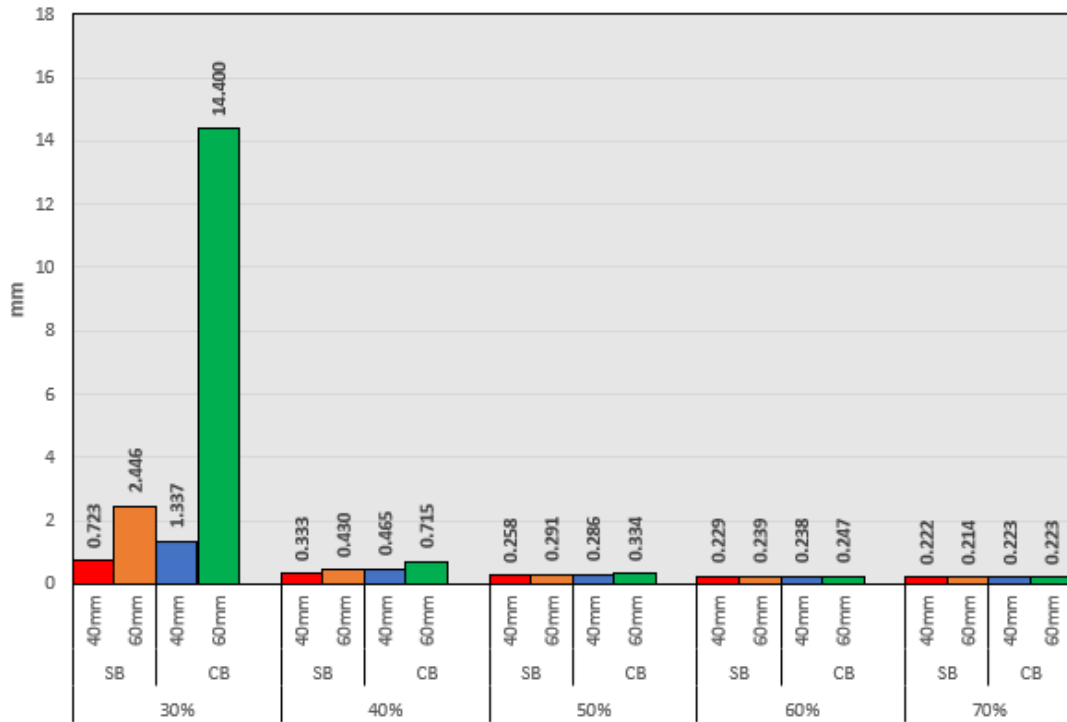


Figure 7.9 – Maximum deflection in all models.

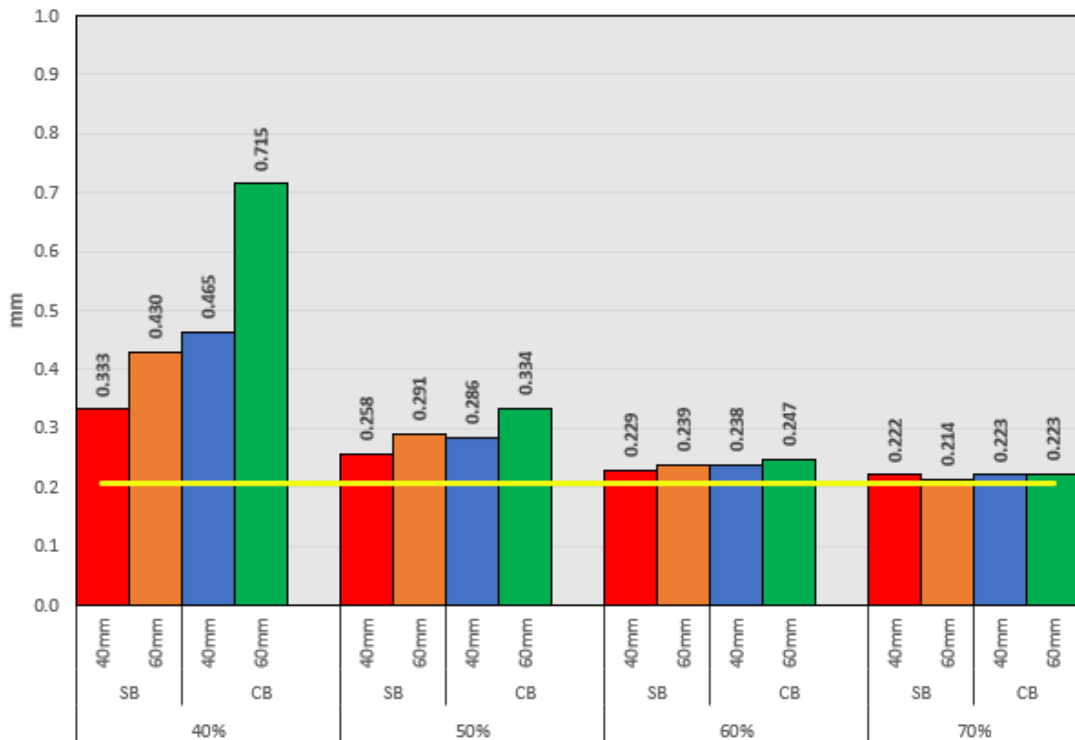
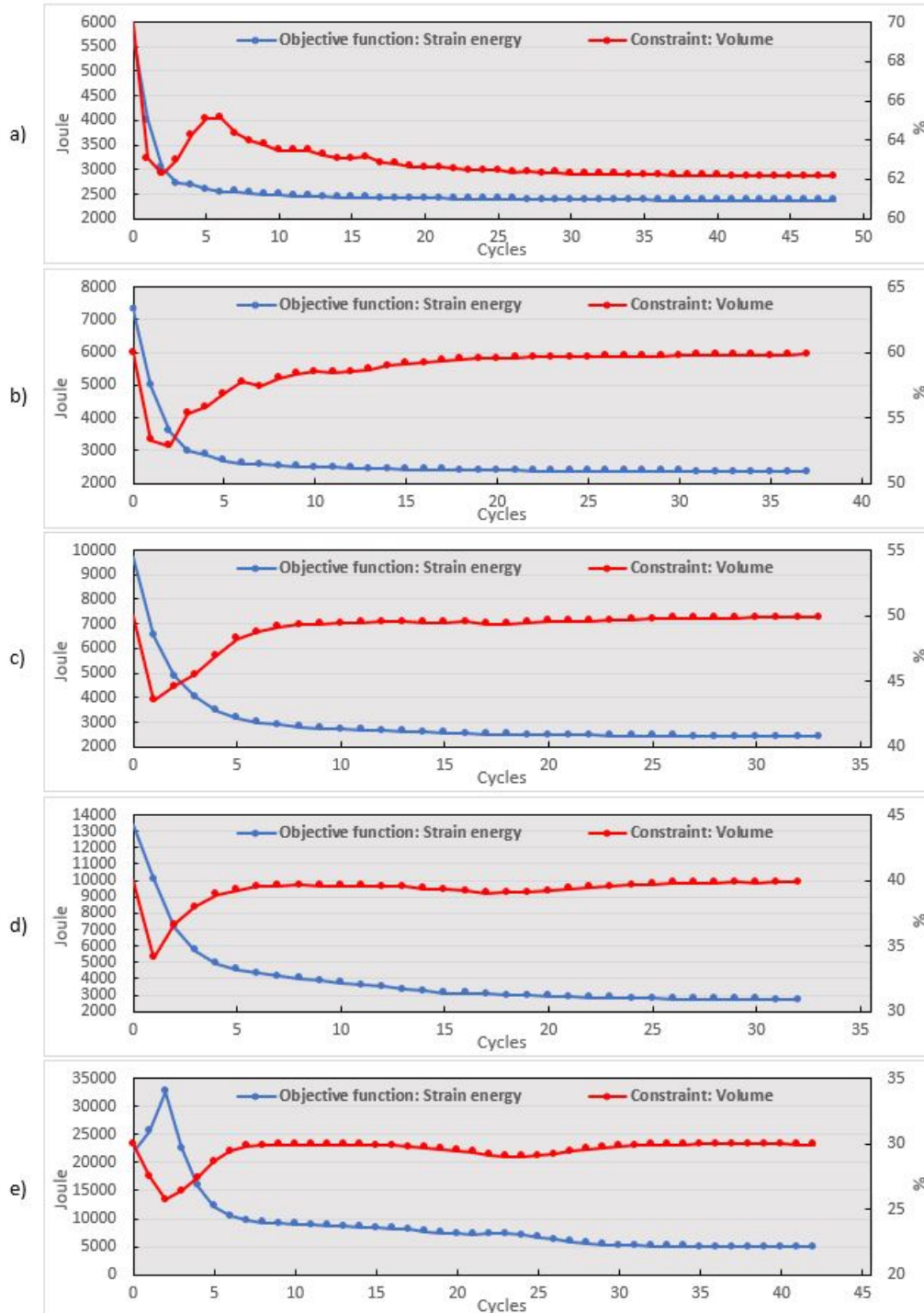


Figure 7.10 – Maximum deflection in all models except 30% against the deflection in the reference model.

### 7.3.3 Strain energy

Figures 7.11 - 7.14 illustrate the evolution of the strain energy with the associated volume fraction, ranging from 70-30%. The results are presented from a-e, where a) is representing the volume constraint of 70% for all the figures.



**Figure 7.11** – Evolution in strain energy of the sensitivity-based models with 40mm mesh size a) 70%, b) 60%, c) 50%, d) 40% and e) 30% volume of the original volume.

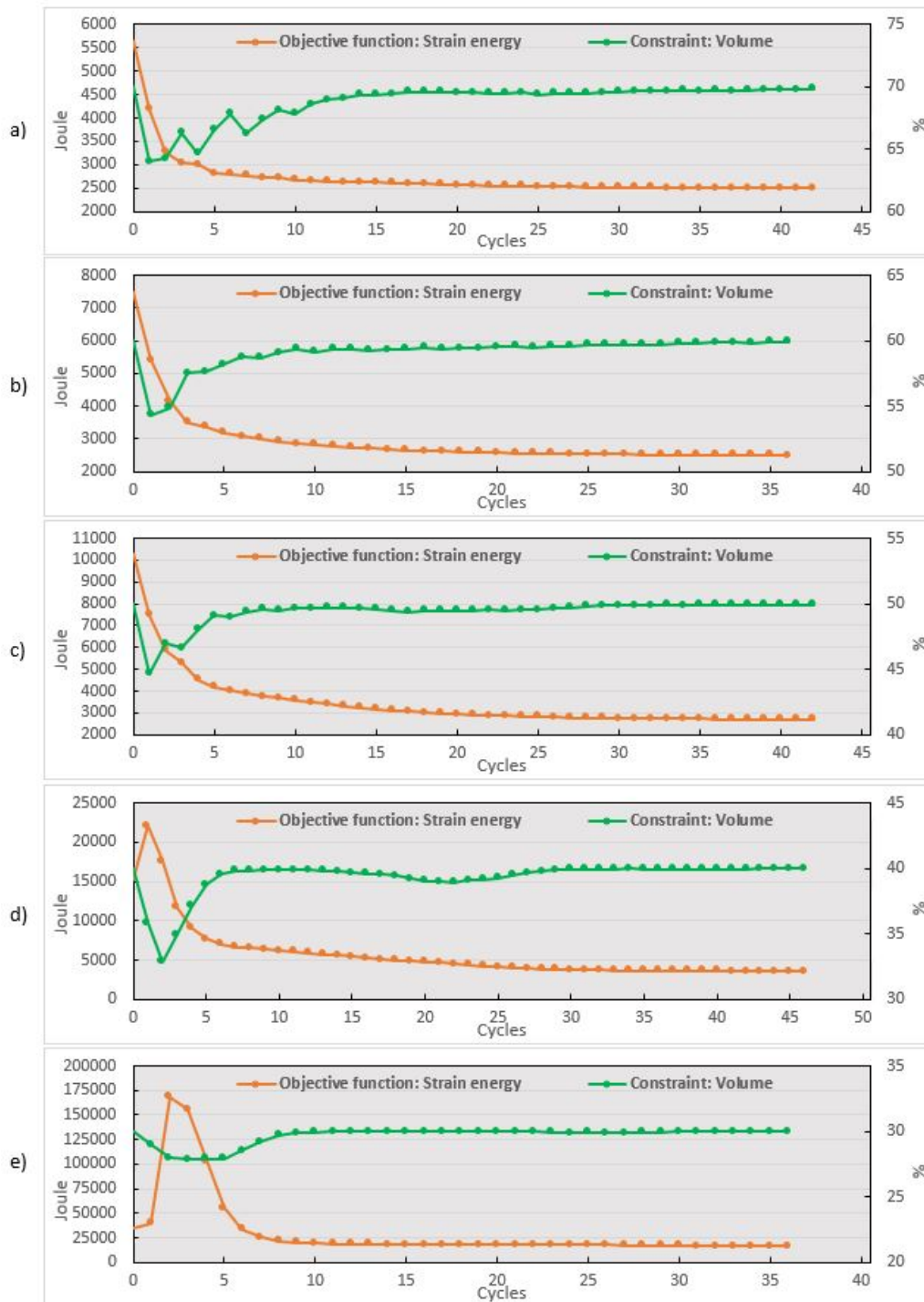


**Figure 7.12** – Evolution in strain energy of the sensitivity-based models with 60mm mesh size a) 70%, b) 60%, c) 50%, d) 40% and e) 30% volume of the original volume.

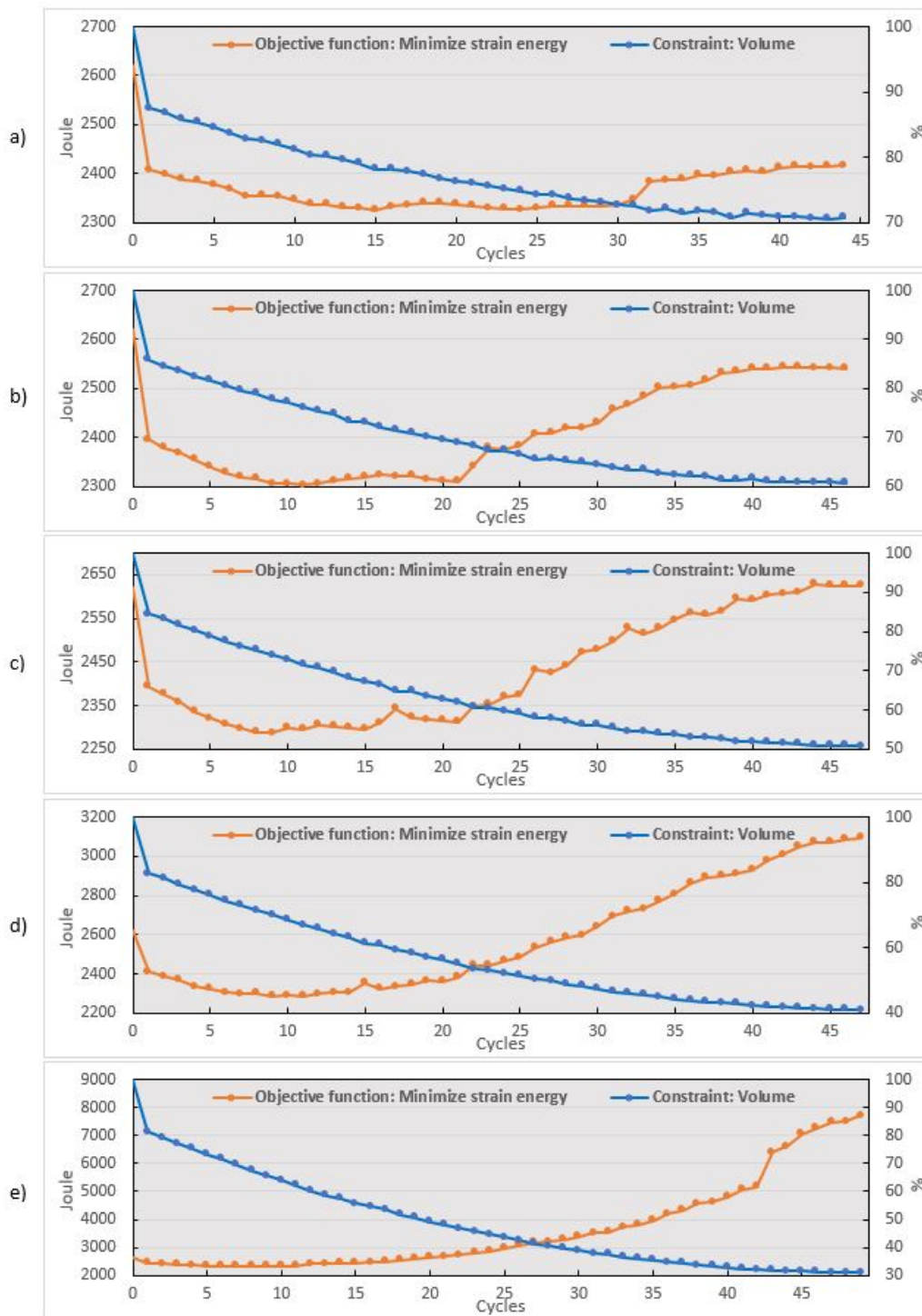


**Figure 7.13** – Evolution in strain energy of the condition-based models with 40mm mesh size a) 70%, b) 60%, c) 50%, d) 40% and e) 30% volume of the original volume.



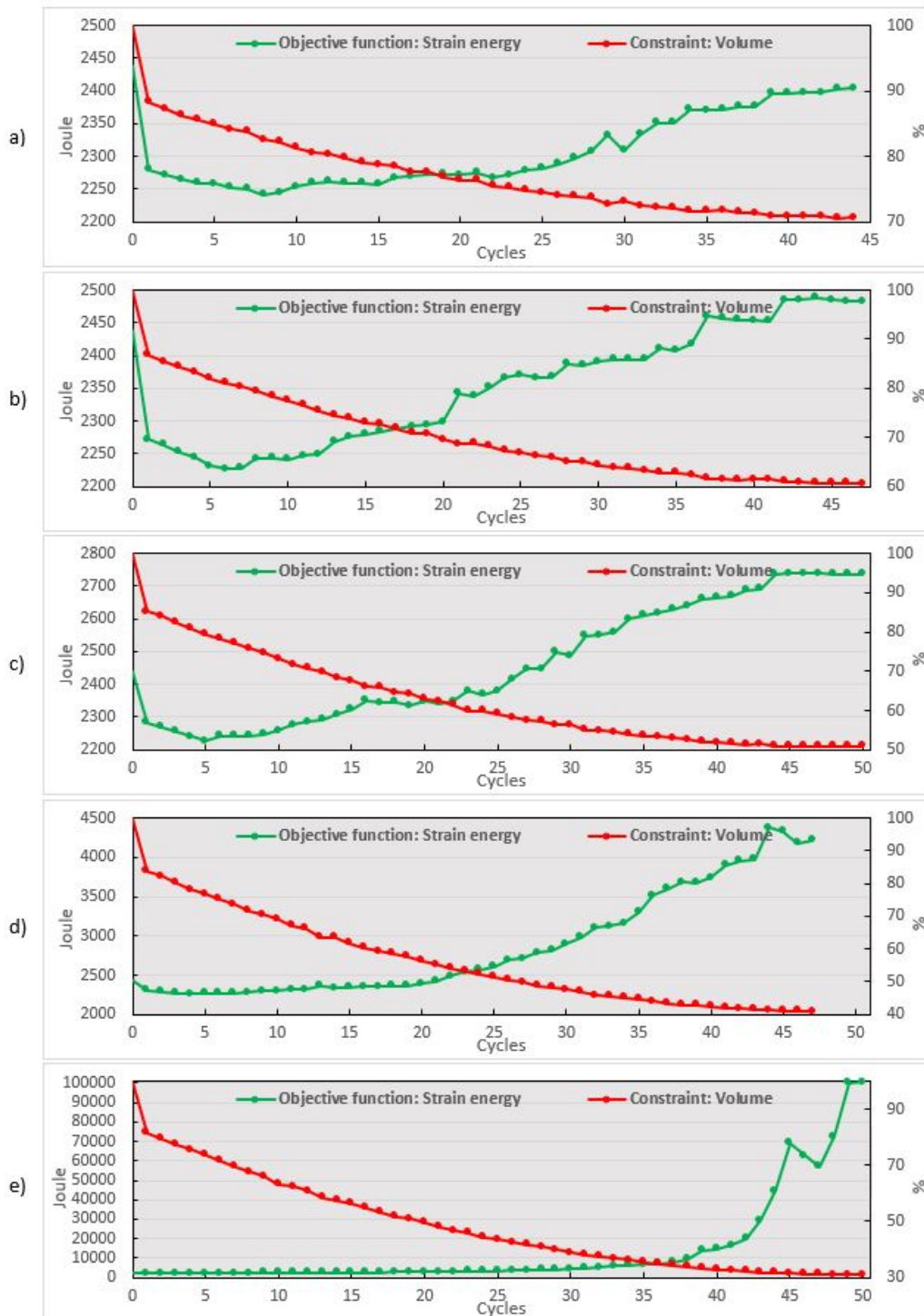


**Figure 7.14** – Evolution in strain energy of the condition-based models with 60mm mesh size a) 70%, b) 60%, c) 50%, d) 40% and e) 30% volume of the original volume.

Table 7.5 exhibits the attained strain energy and volume in each model at the final iteration.

Method	Mesh size [mm]	Volume constraint [%]	Cycle	Strain energy [J]	Achieved volume
Sensitivity-based	40	30	42	4915	29.95%
		40	32	2733	39.89%
		50	33	2416	49.90%
		60	37	2362	59.87%
		70	48	2368	62.16%
	60	30	36	16464	29.99%
		40	46	3560	39.98%
		50	42	2702	49.94%
		60	36	2506	59.92%
		70	42	2495	69.83%
Condition-based	40	30	49	7699	31.03%
		40	47	3095	40.95%
		50	47	2625	50.82%
		60	46	2542	60.78%
		70	44	2417	70.75%
	60	30	50	100448	31.04%
		40	47	4217	40.92%
		50	50	2737	50.94%
		60	47	2482	60.67%
		70	44	2404	70.69%

**Table 7.5** – Number of iterations, strain energy and achieved volume in each model.

Furthermore, these results are plotted in a graph shown in figure 7.15. Additionally, for better visualization, the results of models with 30% of the original volume have been excluded and the remaining results are plotted in figure 7.16. Corresponding results of the reference model from Contiga is plotted as a straight line in the latter.

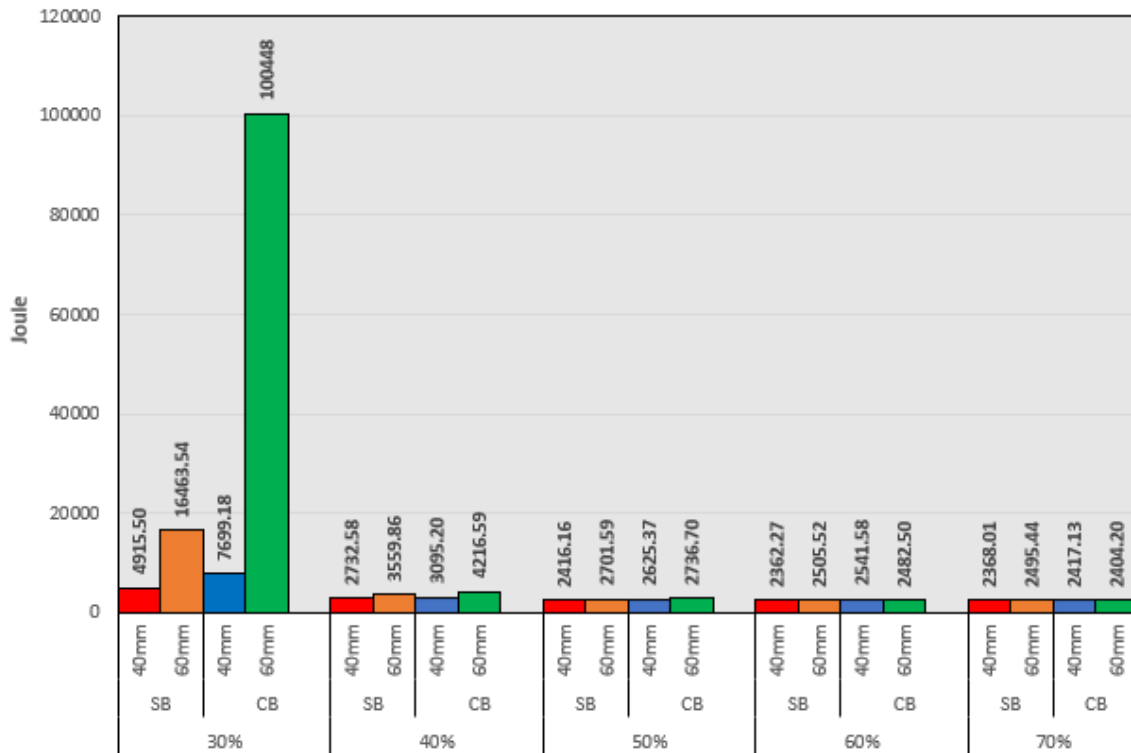


Figure 7.15 – Strain energy in all models.

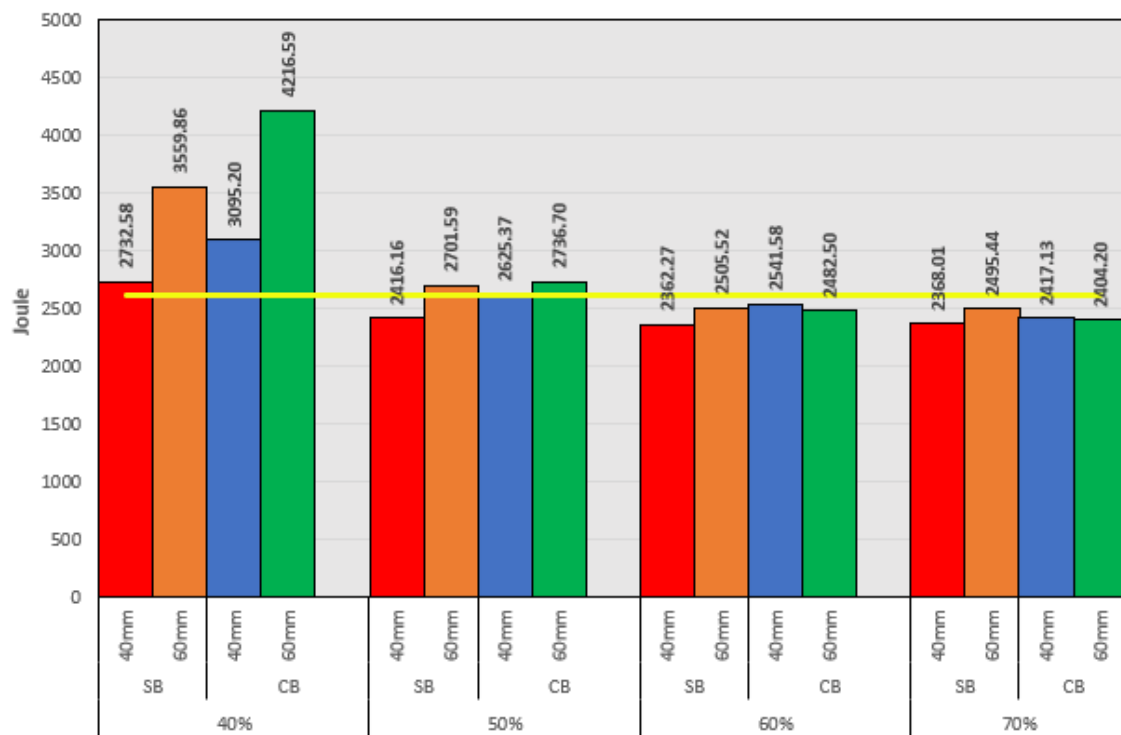
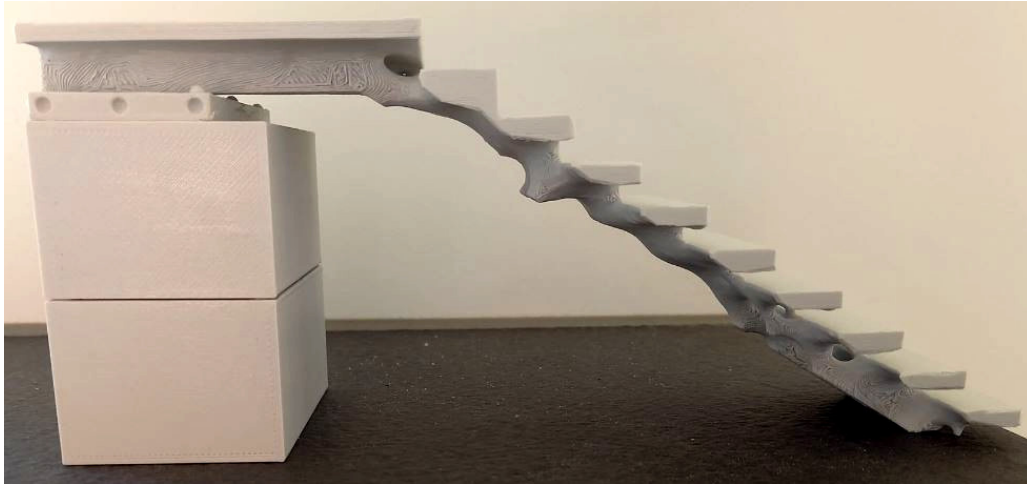


Figure 7.16 – Strain energy in all models except 30% against the initial strain energy in the reference model.

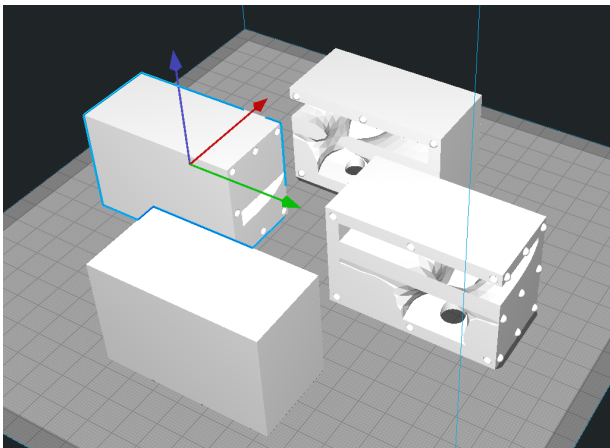
## 7.4 3D printing

Figure 7.17 illustrates a 3D printed TO design with 30% volume of the original volume in a 1:20 scale.



**Figure 7.17** – 3D printed topology optimized staircase with 30% volume of the original volume [Appendix C].

Figures 7.18 - 7.20 give a visualization of the formwork concept both assembled and disassembled. The illustrations are presented as results from the 3D printing program Ultimaker Cura.



**Figure 7.18** – Formwork parts [Appendix C].

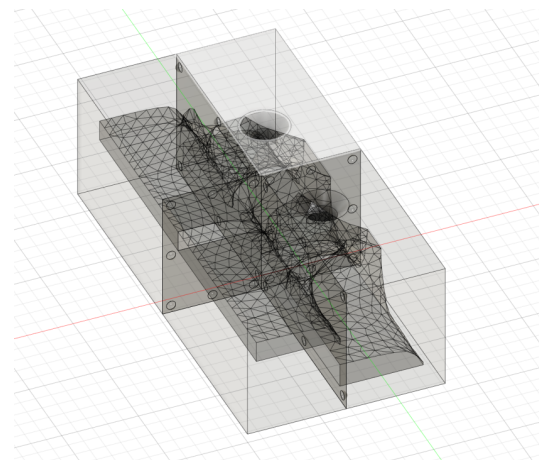


**Figure 7.19** – Assembled formwork [Appendix C].

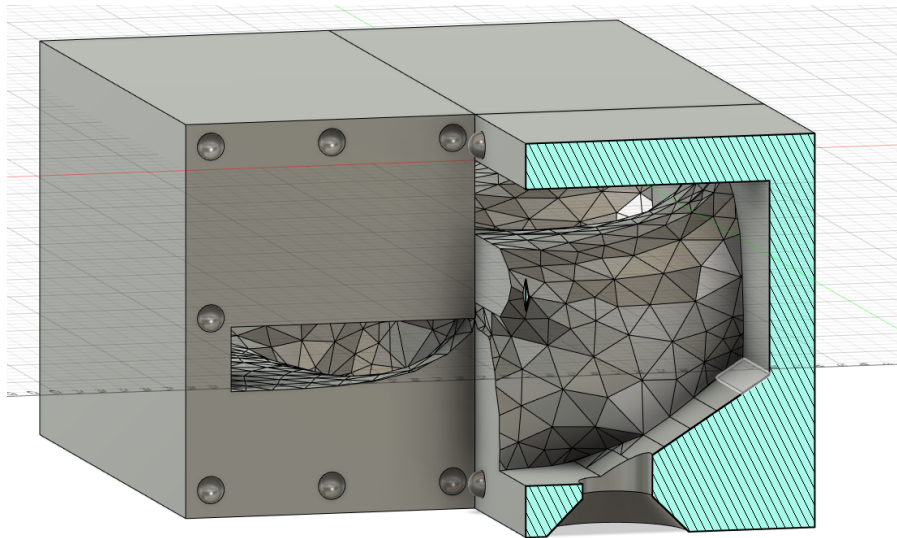


**Figure 7.20** – Visual presentation of a vertical cut of the formwork [Appendix C].

Figures 7.21 - 7.22 highlight the 3D printed formwork concept with two vertical cuts, printed in a 1:20 scale.



**Figure 7.21** – 3D printed formwork: Vertical cut [Appendix C].



**Figure 7.22** – 3D printed formwork: Vertical cut [Appendix C].

Table 7.6 exhibits the required printing time to manufacture the different formwork modules.

Model	Print time
Formwork 1	3h 2min
Formwork 2	3h 13min
Formwork 3	2h 55min
Formwork 4	2h 57min
Formwork 5	0h 20min
Formwork 6	0h 20min

**Table 7.6** – Print time [Appendix C].

## 8 Discussion

In this section the results obtained from section 7 will be discussed in light of the background theory and previous experience in the field.

### 8.1 Parametric modeling

Due to the scope of the thesis being a conceptual TO feasibility study, the authors wanted to create a parametric model that could be utilized not only for an explicit problem - but for any U-shaped staircase in general. Therefore, a parametric GH model was developed, presented in figure 7.2, with the resulting parametric values given in figure 7.1.

The parametric model increases both efficiency and flexibility in regards to simulation and computational time. By developing a parametric model, based on the drawings from Contiga, it was possible to redesign and easily make small adjustments with the use of the number sliders shown in figure 7.1. The number of variables enables the user to freely design a staircase geometry and customize it for specific project needs. A condition for the algorithm to work properly is that reasonable values have to be inputted, if not, the algorithm will fail to compute a legitimate geometry. For example, the only variable that can be set to zero without any problem is the concrete cover, if other variables are set to zero – the algorithm will fail to compute a geometry. Another example could be to increase the console thicknesses unrealistically high, resulting in a console height larger than the original step height. This is not considered a problem, but for a new user – it could take some time to get used to how the algorithm is built up and how to work it properly. Consequently, meaning that the parametric model is easy to use – once the understating and effect of the different input variables are understood and a realistic staircase is modeled.

Admittedly, the developed parametric model is not without drawbacks. The visual code is developed to suite a more or less traditional staircase, which puts restrictions on the architectural freedom in some areas. For instance, the back of the staircase must be modeled as a single solid, and cannot be divided into for example one or two diagonal beams. In addition, it is not possible to introduce cantilever steps or change each step individually. Therefore, the parametric model is mostly suited for prefabricated staircases similar to the one presented in section 5. If a more complex design than what the model can offer is desired, the visual code needs to be altered to enable the introduction of new variables. But the model is deemed more than sufficient for standard staircase designs, which have been the scope of this thesis, with the listed parametric properties in section 7.1. These parameters enable the user to customize the crucial connection points, such as both the top and bottom landing, with the surrounding structures and secure proper joint properties.

By tactically implementing a visual code for a concrete cover property it was possible to save a lot of time by facilitating the simulation process. As mentioned in section 6.3.1 the geometry output from GH is exported as a ".sat"-file into Abaqus, where it is partitioned into smaller volume fractions to enable the use of structural hexahedron mesh types. This proved to be an important feature to provide the option to divide the staircase into desired volume fractions to be able to assign the correct loading and apply the desired frozen regions. The aforementioned is of huge importance, since the TO task is very sensitive to the application of frozen regions. This is due to the fact that when frozen regions are introduced in a TO task, the frozen region are restricted from material extraction - meaning that material has to be removed from elsewhere. Often, this means that

material needs to be extracted from regions with higher stresses than what is present in the frozen regions. In other words, this leads in a less favorable TO geometry since the material extraction within the frozen regions could have introduced a more optimized solution. With that being said, it is completely necessary to introduce constraints, such as frozen regions, to the TO task to be able to obtain a fully functional staircase.

As stated in section 5, the only constraint from the supervisor was that the staircase should accommodate the same functionality as the original staircase. With this in mind, the steps and landing were frozen with a given concrete cover of 25 mm. In addition, the boundary conditions (BC) regions were set to frozen - securing a continuous design with proper fastening properties. Different types of support placement were tested, and it was obvious to see that the choices regarding BC had great impact on the TO result, which is consistent with theory. The BC were set to zero displacement in x-, y- and z-direction. Also, the BC were tactically placed to mimic the original staircase and to secure the same functionality in terms of fastening properties.

## 8.2 Structural analysis

The different slab thicknesses of the reference model are higher than the calculated thicknesses as presented in table 7.1. Additionally, the design moments due to the design loads are significantly lower than the moment capacity of the staircase. Calculation shows that the staircase's flight and landing are just approximately 15% and 8% utilized respectively when taking moment into consideration. Table 7.2 shows that shear resistance of the staircase is also considerably higher than the design shear forces. According to the results from table 7.2, the shear capacity utilization for the flight and the landing of the reference staircase are approximately 44% and 21% respectively. Similarly, allowable span/depth ratio is higher than the actual span/depth ratio. In this case, Eurocode 2 suggests that it is not necessary to calculate the deflection explicitly. This span/depth ratio check is sufficient for avoiding deflection problem under normal circumstances. Due to the fact that the reference model has a high slab thickness, low design shear, small design moment and minimal deflection, it can potentially be optimized. Reduction of the unnecessary concrete will result in a more economical staircase with lesser environmental impact.

## 8.3 Deflection

The deflection of the reference model at the reference point, obtained from Abaqus before optimization, is much lower than maximum allowable deflection, presented in table 7.4 with span/250. Larger deflections were observed in models ranging from 60% to 30% volume of the original volume with 60mm mesh size models than 40mm mesh size in both sensitivity-based and condition-based whereas in 70% volume of the original volume all the models have almost identical deflections. Maximum deflection of all models in 30% and 40% volume of the original volume, with the exception of SB\_40\_40, are in the range of 0.43mm and 14.4mm. These deflections are approximately between 2 to 66 times higher than maximum deflection in the reference model. Maximum deflections in other models are very close to maximum deflection of the reference model. It is worth noting that the CB models compute topologies with larger cantilever spans in the top landing and bottom step - creating larger local deflections at these locations. These local deflections in the models ranging from 70-40% are all below the maximum allowable deflection, as can be seen in figure 7.7 and 7.8.

Among all the TO models, CB\_30\_60 has a maximum deflection of 14.4mm, which is greater than the allowable deflection calculated based on serviceability limit of the reference model. Apart from this, maximum deflec-



tion of all models are well below the serviceability limit state. Comparing the results of deflection between condition-based model and sensitivity-based model, there is no significant difference between them, except for the condition-based and sensitivity-based models with 30% volume of the original volume. Keeping all the properties and constraints constant in SB\_30\_60 and CB\_30\_60, the deflection achieved by the condition-based algorithm is almost 6 times greater than the sensitivity-based algorithm. Similarly, different mesh sizes give almost the same deflection except the models with 30% and 40% volume of the original volume. It was observed in the results that as the original volume reduces from 70% to 30%, deflection of the optimized models increases with regards to the deflection of the reference model.

When the original volume is reduced in the process of optimization, weight of the staircase is reduced. The staircase becomes lighter in weight, which leads to lower self-weight and consequently lower dead load. Even though the staircase becomes lighter after TO while other applied loads and boundary condition are constant, it is not observed any remarkable variations in deflection and most of them are below the allowable limit except models with 30% volume of the original volume. It was seen from the results that deflection is not much dependent either on the mesh size or type of optimization up to 40% volume of the original volume. Deflection is increased drastically from 50% volume of the original volume to 40% volume of the original volume, especially in condition-based optimization with 60mm mesh size.

#### 8.4 Strain energy and stiffness

The results for strain energy are very insightful and promising. Apart from most of the models in 30% and 40% volume of the original volume, the amounts of strain energy in the remaining models are remarkably in range of strain energy of the original model. Notably, strain energy in all the 60% and 70% volume fraction models are lower than the strain energy of the original model which indicates that the objective function has successfully fulfilled. Meaning that, even by reducing 30-40% material, the created models are in fact stiffer than the original model. In the case of 50% of the original volume, it was observed that all models have produced almost alike strain energies. In this volume fraction, SB\_50\_40 has produced a model which reduced strain energy by 8%. The CB\_50\_40 model has a strain energy which is just above the original model while results from SB\_50\_60 and CB\_50\_60 show approximately 3-4% increase in strain energy. There are higher increments in 30% and 40% models. For instance, strain energies in the CB\_30\_60 and CB\_40\_60 models are respectively 3734% and 61% higher than the strain energy in the reference model. Nonetheless, it is noteworthy to mention that SB\_40\_40 has produced a topology with only 4% higher strain energy compared to the original model, which is remarkable considering that 60% of the material have been reduced in this model.

As is shown in table 7.5, all models, with the exception of two, converged before reaching the stopping condition. These two models were CB\_30\_60 and CB\_50\_60. Although figure 7.14 c) shows that CB\_50\_60 was almost on the verge of convergence. It is also demonstrated in the table 7.5 that while the achieved volume after 50 iterations for the CB\_50\_60 model is only 1% away from the goal volume, the final strain energy is close to the strain energy of the reference model. To the contrary, as it is apparent in figure 7.14 e), the CB\_30\_60 model is not even close to convergence. This is also evident in the table 7.5 that the obtained strain energy in the CB\_30\_60 model is extremely large for an achieved volume that is approximately 1% higher than the goal volume and the line is very unstable.

Generally, it was observed that the sensitivity-based algorithm with 40mm mesh size has always produced stiffer topologies than the other methods in each volume fraction. As discussed before for the 50-70% volume of the original volume, the sensitivity-based method with 40mm mesh size is the only algorithm that generated topologies that fulfilled the objective function, while the 40% volume of the original volume missed out with a small margin to achieve this goal. Strain energy of the SB\_30\_30 model is however 88% higher than the strain energy of the original model and therefore the objective function is not achieved. Furthermore, it was observed that the condition-based algorithm with 40mm mesh size produced the second best topologies with regards to stiffness for the models with 30-50% volume of the original volume, while the condition-based method with 60mm mesh size created models with lower strain energy in 60% and 70% of the original volume than the condition-based algorithm with 40mm mesh size. Evidently, models in 30-50% volume of the original volume based on the condition-based method with 60mm mesh size have the highest strain energy and as noted before, two of these models did not converge after 50 iterations.

The results point out that the mesh size is also impactful in achieving various strain energies. This behavior was expected from the sensitivity-based algorithm due to its similarities to the SIMP method, which has a mesh dependent algorithm. However, the same issue is evident in condition-based algorithm, especially in 30-50% volume of the original volume, which is not consistent with the assertion about mesh independency of the BESO that is similar to the condition-based algorithm in Abaqus. Apart from the models in 70% and 60% volume of the original volume which provide almost identical strain energies, finer mesh creates models which have lower strain energy than the coarse mesh. This signifies the fact, presented by Moreira et al. in section 3.8.3, that increasing the fineness of mesh to a certain level leads to better and more realistic results in complex geometries. In spite of employing finer mesh, table 7.5 displays that the number of iteration cycles did not necessarily increase, which is consistent with the findings of the paper with Mudaliar et al., presented in section 3.8.2.

A closer look at the cycle of iterations in figures 7.11 - 7.14 for each method reveals an interesting phenomenon. At the start of the cycle, the sensitivity-based algorithm reduces the volume up to the constraint objective. Afterwards, the algorithm proceeds until it converges. For the condition-based algorithm, the iteration starts from the original volume and then continues until either convergence or the stopping condition is reached. Both of these phenomena are in contrast with the properties of SIMP and BESO which has been discussed in the theoretical background. SIMP algorithm evolves based on continuously reducing material until the end of the cycle while the BESO proceeds on the basis of adding and removing material simultaneously during the cycle. None of these features were observed in the cycles of iterations.

## 8.5 Manufacturing

The authors found the use of FDM 3D printing to be very instructive and educational. To be able to produce organic looking topologies, such as the one illustrated in Figure 7.17, the use of new technology is absolutely necessary - and 3D printing looks to be a promising alternative.

The resulting conceptual formwork was printed in six parts, presented in Figure 7.18 - 7.22, where each part was assigned with holes and/or connection piers. This was done to be able to assemble the formwork pieces into one single formwork and illustrate the concept. In reality, the connections would have to be locked in

a better way to secure proper fastening and prevent unwanted failure and/or deflections. This simplification was made due to the fact that this was a conceptual thesis, rather than an explicit suggested solution in combination with the time limitations and lack of 3D printing experience.

To illustrate the usability, the FDM 3D printed formworks were assembled, and two holes were introduced - which can be used both for casting and air outlet. This is an important feature when casting concrete in closed formworks, which together with vibration secures a good concrete cast that fills the whole formwork and prevents unwanted void spaces. There may still occur small air bubbles, but larger air pockets that have an effect on both strength and concrete cover will be prevented as long as the aggregate used is small enough. It is very important that the aggregate size is smaller than the formwork details, so that the concrete is able to fill all the voids inside the formwork and not create plugs. The more advanced the details are, the finer aggregates must be applied for manufacturing.

In reality, the 3D printed formwork would be a much thinner shell and would need support when casted. The 3D printed formwork is remarkably light and are easy to assemble and transport – but there is a drawback that needs to be assessed and that is the rigidity of the formwork. Concrete is a dense and compact material, and will cause large transversal forces from the hydrostatic pressure when casting. These forces will increase in magnitude as the casting volume increases, and can cause strength problems for the formworks. To be able to cast the whole staircase in a single cast, it is necessary to strengthen the 3D printed formwork with external timber formwork – which increases the cost and labor work. In addition, it would be necessary to cover the outside of the 3D printed formwork in sand to minimize local deflections and also strengthen the formwork by applying resin or epoxy on the exterior surfaces.

One way to reduce the risk of deflection is to cast the staircase structure in components and assemble them together afterwards with for example post-tension reinforcement. This way the hydrostatic pressure is drastically lowered when casting, which lowers the need for supporting formwork and reduces the risk of formwork failure and following deflections. Due to the magnitude of the hydrostatic pressure during a monolithic concrete cast, in combination with the thin formwork shell, this approach looks to be the most promising alternative to reduce the risk of deformations. In the case of this study, it was observed that most of the simulations generated two beam shapes at each side of the flight. These two beams can be produced based on the procedure mentioned above, and the treads, risers and the landing can be mounted on them afterwards.

Another critical factor is the placement of reinforcement inside such formworks. Due to the complicated TO geometries, placement of traditional reinforcement cages is practically very challenging to accomplish. To be able to realize TO structures, new technology and creative solutions needs to be implemented in the manufacturing line. One promising feature is the use of robotic prefabricated tailor-made reinforcement cages. Another auspicious approach is the introduction of ultra high performance fiber reinforced concrete in combination with post-tensioned reinforcement. The use of ultra high performance concrete will enhance the structural strength and the post-tensioned reinforcement will provide the option to create modular staircases as discussed by Andrej Jipa and Isabel Moreira in section 3.8.1 and 3.8.3. Additionally, the structure requires less concrete cover due to the increased durability properties, which generate new and slenderer possibilities in terms of design. Another way to facilitate the implementation of reinforcement and secure a sufficient concrete cover is by post processing the results from Abaqus, through reshaping the geometry and introducing

reinforcement ducts. A practical method for this approach was applied by Jewett et al. and is discussed in section 3.8.4

The manufacturing time of the formworks is another important aspect of this method. To be able to create a functioning formwork, it is necessary to develop a more delicate connection system to assemble and secure the positioning of the different formwork elements. From the authors' experience, this proved to be a time-consuming procedure which of course would be shortened with experience. In addition, the actual manufacturing (3D printing) is also very time consuming. The total time it took to print the six different formwork parts were 12 hours and 47 minutes in total, as shown in table 7.6. These printing times are based on a 1:20 scale conceptual formwork assembly of just two steps of a staircase. In reality, formworks are printed in a 1:1 ratio with a degree of detail specified by the user. Both complexity, detail, size and the ability to support its self-weight during 3D printing are important in regards to printing time. Based on current research in this field such as "*3D-printed formwork of bespoke concrete stairs*" by Jipa et al., it is found that the manufacturing time of a formwork for a single step is estimated up to 48 hours [52]. In other words, the current additive manufacturing process of formworks is a very time-consuming fabrication method. One way of reducing the manufacturing time is to implement customized tool-path generation algorithms, that has been proved by Andrej Jipa to reduce the printing time up to 50% compared to the commercial algorithm used by Ultimaker Cura which is used for this thesis.

## 9 Conclusion

By introducing a parametric staircase model the simulation and computational efficiency are drastically improved. The parametrization of the staircase provides the option to effortlessly alter and customize the geometry of the staircase to secure proper structural joint properties for explicit problems. In addition, the customized concrete cover feature simplifies and accelerates the simulation processes in Abaqus.

Deflection check of the reference model before TO shows that both the landing and flight satisfy span/depth ratio. While optimizing by two different methods, condition-based models are slightly more deflected downwards than sensitivity-based models in all the cases. When it comes to mesh size, finer meshed models deflect marginally lesser than the coarser ones up to 50% volume reduction. The deviations were more visible in the models with 30% and 40% volume of the original volume. Deflection in most of the optimized models are well below the deflection limit for serviceability limit state, with the exception of the condition-based model with 30% volume of the original volume. Sensitivity-based model with finer mesh can produce stiffer topology in regards to deflection. All things considered, it is evident that reducing the volume up to 50% will not alter the deflection by a large margin with respect to the reference model.

The study demonstrates the fact that both sensitivity-based and condition-based algorithms in Abaqus are powerful tools for the application of topology optimization. That being said, it was evident that for the same mesh size, the former tends to create stiffer topologies than the latter. It is also conspicuous that mesh size can influence the topologies and results. In most cases, the finer mesh in both methods creates topologies with higher stiffness, especially in 30-50% volume of the original volume. However, strain energy in all models in 50-70% volume of the original volume is either lower or slightly higher than strain energy of the reference model. Considering all these effects, it is perfectly possible to reduce the material usage up to 50% and still maintain the stiffness of the original staircase.

The authors find that the use of fused deposition modeling 3D printed formwork has a huge potential in terms of design freedom. By the use of additive manufacturing, the geometric limitations from traditional timber formwork can be overcome to fabricate more intricate and organic looking structures. Nevertheless, FDM printed formworks are somewhat fragile and is in need of supporting timber formwork to secure a proper concrete cast without risk of deflections. Other drawbacks are the time-consuming manufacturing phase and challenges with placing of traditional reinforcement.

## 10 Recommendations

Due to complexities of nonlinear analysis and number of node's limitations in Abaqus student version, this master thesis conducted a linear analysis investigation into a concrete staircase. Therefore, the reinforcement, illustrated in figure 10.1, was excluded from the modeling phase. For that reason, the next step can be to run a nonlinear analysis into the case and study the impact of reinforcement in the created topologies and their respective stiffnesses. Possibility of applying different reinforcement types and solutions into the optimized models, and whether they satisfy the requirements in the Eurocode 2 can also be an important step towards implementing topology optimization in manufacturing concrete staircases.

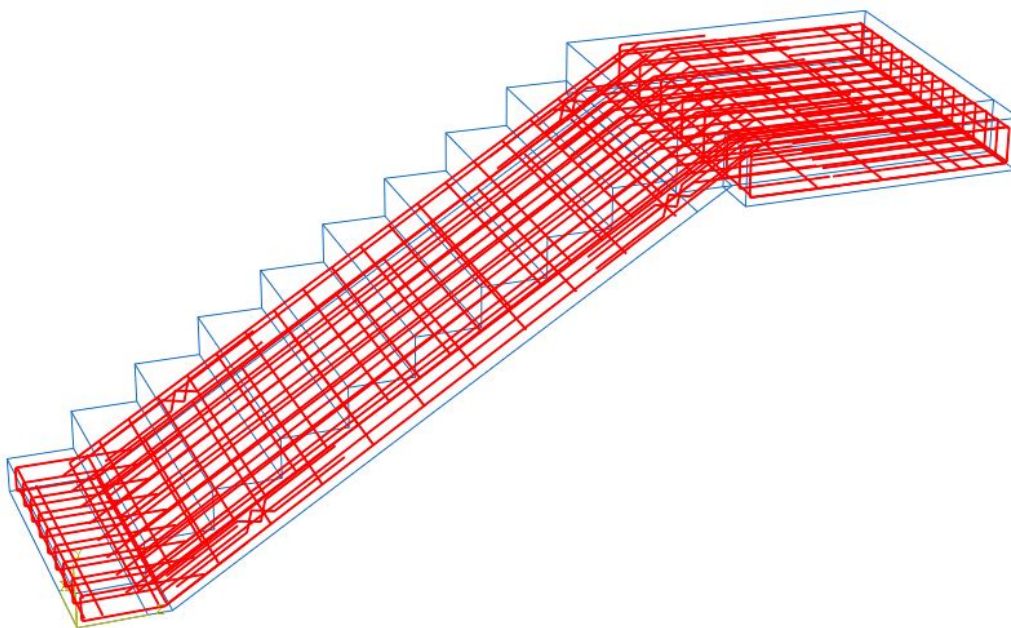


**Figure 10.1** – Modeled reinforcement for nonlinear analysis.

Throughout this work, many aspects of topology optimization were reviewed. Several models were introduced which showcased some of the potentials and challenges. Taking all this knowledge into consideration, the authors decided to present a conceptual design, which can be a good start to follow up this study. This staircase consists of two beams that are topologically optimized by the sensitivity-based algorithm in Abaqus. The volume constraint is set to 0.5 and the mesh size is 40mm. Both the treads and the landing are frozen regions, while the risers are entirely removed from the design. This recommended conceptual design is shown below in figure 10.2 and 10.3.

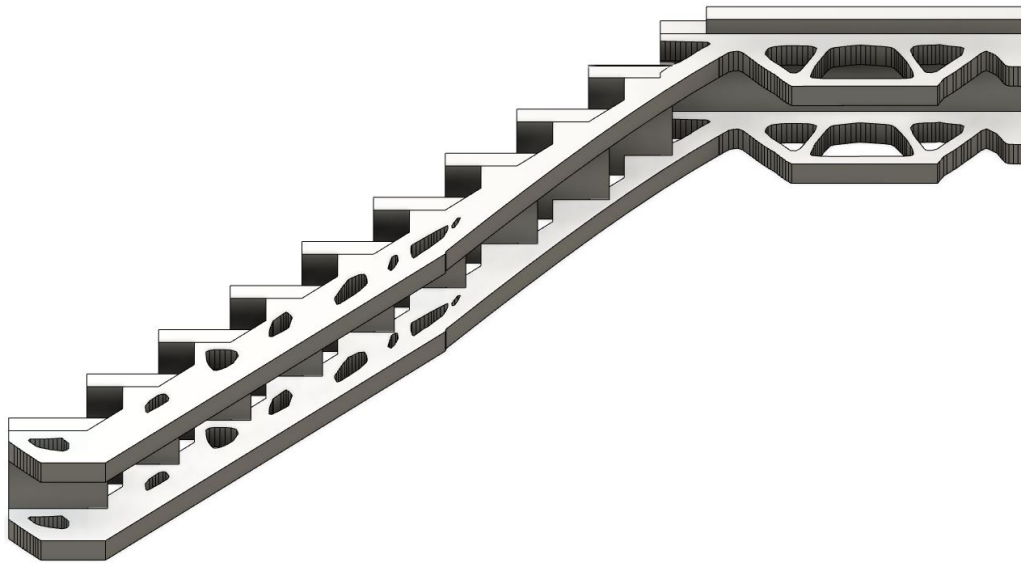


**Figure 10.2** – Topology optimized design.

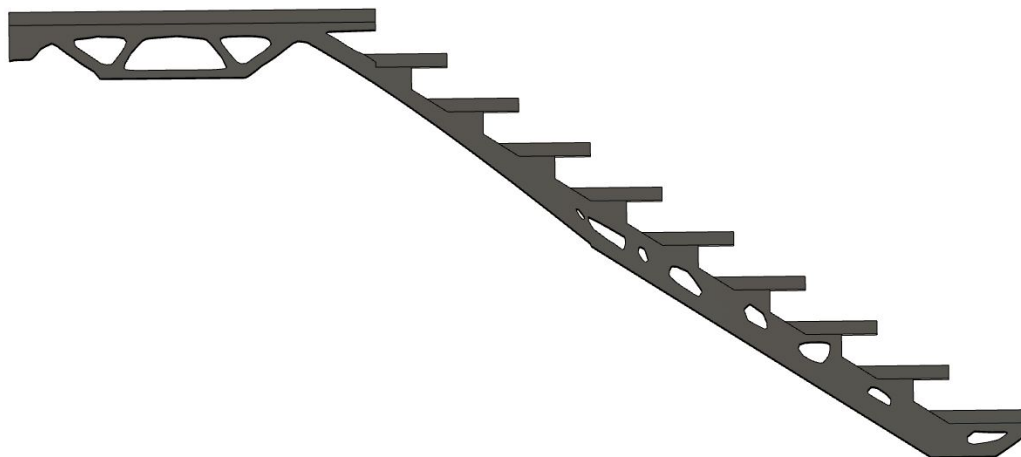


**Figure 10.3** – Topology optimized design.

## 11 References

- [1] Altair. *Altair and Airbus APWorks Team up to Make Additive Manufacturing a Reality for Customers*, 2016. URL: <https://www.altair.com/news/altair-and-airbus-apworks-team-up-to-make-additive-manufacturing-a-reality-for-customers> (visited on 04/23/2021).
- [2] M. Mitchell. *Parametric Concept Bridge*, MiketMitch.wordpress.com. URL: <https://miketmitch.wordpress.com/2015/05/18/parametric-concept-bridge/> (visited on 04/23/2021).
- [3] World Commission on Environment. *Report of the World Commission on Environment and Development: Our Common Future Towards Sustainable Development 2. Part II. Common Challenges Population and Human Resources 4*. Tech. rep. UN, 1990, pp. 16–17. URL: <https://sustainabledevelopment.un.org/content/documents/5987our-common-future.pdf>. Downloaded: 20/01/2021.
- [4] P. C. Aitcin and S. Mindess. “Introduction,” in: *Sustainability of Concrete*, 1st ed. New York, USA: Spon Press, 2011. Chap. 1, pp. 1–10.
- [5] The Explorer. *Read about the goals*, 2021. URL: [https://www.theexplorer.no/goals/?gclid=CjwKCAiAo5qABhBdEiwAOtGmbs3dIJj%5C%5CnewlineL%5C%7B%5C%5C\\_%5C%7DBwE](https://www.theexplorer.no/goals/?gclid=CjwKCAiAo5qABhBdEiwAOtGmbs3dIJj%5C%5CnewlineL%5C%7B%5C%5C_%5C%7DBwE) (visited on 01/21/2021).
- [6] L. Barcelo, J. Kline, and G. Walenta. “Cement and carbon emissions”. In: *Materials and Structures*, vol. 47, no. 6 (2014), pp. 1–15. DOI: <http://dx.doi.org/10.1617/s11527-013-0114-5>.
- [7] C. R. Gagg. “Engineering Failure Analysis”. In: *Cement and concrete as an engineering material: An historic appraisal and case study analysis*, vol. 40 (2014), pp. 114–140. DOI: 10.1016/j.engfailanal.2014.02.004.
- [8] A. Aguado, J.C. Galvez, and A.D.L. Fuente. “Sustainability evaluation of the concrete structures”. In: *International Conference on Concrete Sustainability ICCS16*, vol. 2 (2016), pp. 58–71. URL: <https://core.ac.uk/download/pdf/46111757.pdf>.
- [9] J. Feringa, A. Søndergaard, and D. Maier. “Robotic abrasive wire cutting of polymerized styrene formwork systems for cost-effective realization of topology-optimized concrete structures”. In: *Construction Robotics*, vol. 2 (2018), pp. 81–92. DOI: <https://doi.org/10.1007/s41693-018-0016-8>.
- [10] R. Giesecke, A. Jipa, and A. Meibodi. “3D-Printed Formwork for Prefabricated Concrete Slabs”. In: *1st International Conference on 3D Construction Printing*, vol. 1 (2018), pp. 1–9. DOI: <http://dx.doi.org/10.13140/RG.2.2.26722.89280>.
- [11] North East Reinforcement. *Steel fixing*, 2021. URL: [http://www.northeastreinforcement.co.uk/view\\_construction\\_services.php?cid=1](http://www.northeastreinforcement.co.uk/view_construction_services.php?cid=1) (visited on 01/20/2021).
- [12] Rebartek AS. *Automated reinforcement technology*, 2021. URL: <https://rebartek.com/> (visited on 01/20/2021).
- [13] O.C. Zienkiewicz, R.L. Taylor, and J.Z. Zhu. “The Standard Discrete System and Origins of the Finite Element Method,” in: *The Finite Element Method: Its Basis and Fundamentals*, 7th ed. California, USA: Elsevier Ltd., 2013. Chap. 1–12, pp. 1–530.
- [14] C. A. Felippa. “Finite Element Modeling: Mesh, Loads, BCs,” in: *Introduction to finite element methods*, 1st ed., Colorado, USA: Department of Aerospace Engineering Sciences and Center for Aerospace Structures University of Colorado, 2004. Chap. 1–25, pp. 1–675.



- [15] Learn 'n' Share Academy. *Simulation files for FEA of concrete beam in abaqus*, 2018. URL: <https://gumroad.com/1/aSWNS> (visited on 04/20/2021).
- [16] M. J. TURNER et al. "Stiffness and Deflection Analysis of Complex Structures". In: *Journal of the Aeronautical Sciences* 23.9 (1956), pp. 805–823. DOI: 10.2514/8.3664.
- [17] J. N. Reddy. "Mathematical preliminaries, integral formulations, and variational methods," in: *Introduction to the Finite Element Method*, 3rd ed., New York, USA: McGraw-Hill Education, 2019. Chap. 1–14, pp. 5–816.
- [18] G. P. Nikishkov. "Introduction to the finite element method". In: *University of Aizu Academia*, vol. 1 (2009), pp. 1–85. URL: <http://citeseerx.ist.psu.edu/viewdoc/download?doi=10.1.1.131.5563&rep=rep1&type=pdf>.
- [19] L.L. Howell. "Compliant Mechanisms". In: *McCarthy J. (eds) 21st Century Kinematics*, 1st ed., London, United-Kingdom: Springer, 2013. Chap. 7, pp. 189–216.
- [20] O. Querin, M. Victorica, and C. Alonso. "Size, shape, geometry and topology optimization," in: *Topology Design Methods for Structural Optimization*, 1st ed., Colorado, USA: Academic Press, 2017. Chap. 1-5, pp. 1–167.
- [21] M. P. Bendsøe and N. Kikuchi. "Generating optimal topologies in structural design using a homogenization method," in: *Computer Methods in Applied Mechanics and Engineering*, vol. 71, no.2 (1988), pp. 197–224. DOI: [https://doi.org/10.1016/0045-7825\(88\)90086-2](https://doi.org/10.1016/0045-7825(88)90086-2).
- [22] X. Huang and Y.M. Xie. "Evolutionary Structural Optimization Method," in: *Evolutionary Topology Optimization of Continuum Structures: Methods and Applications*, 1st ed., West Sussex, United Kingdom: John Wiley and Sons Ltd., 2010. Chap. 1-7, pp. 1–150.
- [23] C. Domb. *James Clerk Maxwell - Biography and Facts*, Britannica.com. URL: <https://www.britannica.com/biography/James-Clerk-Maxwell/Later-life> (visited on 02/12/2021).
- [24] G.I.N. Rozvany and T. Lewiński. "Structural Topology Optimization (STO) – Exact Analytical Solutions: Part I". In: *Topology Optimization in Structural and Continuum Mechanics*, 1st ed., London, United-Kingdom: Springer, 2014. Chap. 1, pp. 1–15.
- [25] T. M. Cherry. "Anthony George Maldon Michell, 1870-1959," in: *Biographical Memoirs of Fellows of the Royal Society*, vol. 8, no. 8 (1962), pp. 90–103. DOI: <https://doi.org/10.1098/rsbm.1962.0007>.
- [26] X. P. Li, L. Y. Zhao, and Z. Z. Liu. "Topological Optimization of Continuum Structure based on ANSYS". In: *MATEC Web of Conferences*, vol. 95, no. 07020 (2017), pp. 1–4. URL: <https://doi.org/10.1051/mateconf/20179507020>.
- [27] G. I.N Rozvany and T. Lewiński. "Aims, scope, methods, history and unified terminology of computer-aided topology optimization in structural mechanics". In: *Structural and Multidisciplinary Optimization*, vol. 21, no. 2 (2001), pp. 120–127. DOI: <https://doi.org/10.1007/s001580050174>.
- [28] L. Kelly. "Reducing design time: the impact of evolutionary structural optimisation on structural trade studies during preliminary design". In: *University of Southampton Academia*, vol. 1 (2015), pp. 1–204. URL: [https://www.researchgate.net/publication/299465734\\_Reducing\\_design\\_time\\_the\\_impact\\_of\\_evolutionary\\_structural\\_optimisation\\_on\\_structural\\_trade\\_studies\\_during\\_preliminary\\_design](https://www.researchgate.net/publication/299465734_Reducing_design_time_the_impact_of_evolutionary_structural_optimisation_on_structural_trade_studies_during_preliminary_design).

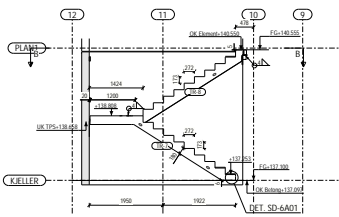
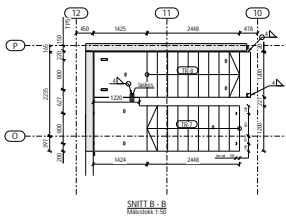
- [29] Abaqus documentation. *Creating Abaqus optimization models*, 2017. URL: <https://abaqus-docs.mit.edu/2017/English/SIMACAEANLRefMap/simaanl-c-optabaqus.htm> (visited on 03/23/2021).
- [30] M. Stavic and O. Marina. "Parametric modeling for advanced architecture Folding View project Architectural scale modelling in the digital age View project". In: *INTERNATIONAL JOURNAL OF APPLIED MATHEMATICS AND INFORMATICS*, vol. 5, no. 2 (2011), pp. 9–16. URL: <https://www.researchgate.net/publication/285467523>.
- [31] F. Fu. "Design and Analysis of Tensile Structures and Tensegrity Structures". In: *Design and Analysis of Tall and Complex Structures*, 1st ed., London, United-Kingdom: Butterworth-Heinemann, 2018. Chap. 7, pp. 213–249.
- [32] M. Alba. *What's the Difference Between Parametric and Direct Modeling?*, Engineering.com. URL: <https://www.engineering.com/story/whats-the-difference-between-parametric-and-direct-modeling> (visited on 02/22/2021).
- [33] R. Medina. *Introduction to parametric modeling*, Thinkparametric.com. URL: <https://thinkparametric.com/courses/grasshopper-101-introduction-to-parametric-modelling> (visited on 03/30/2021).
- [34] Rhinoceros. *What are NURBS?*, 2020. URL: <https://www.rhino3d.com/features/nurbs/> (visited on 02/22/2021).
- [35] K.H. Chang. "Geometric modeling". In: *e-Design: Computer-Aided Engineering Design*, 1st ed., Colorado, USA: Academic Press, 2015. Chap. 2, pp. 41–124.
- [36] O. Aflak. *Bézier Curve, Understand the mathematics of Bézier curves*, towardsdatascience.com. URL: <https://towardsdatascience.com/b%5C%C3%5C%A9zier-curve-bfffdadea212> (visited on 03/29/2021).
- [37] E. W. Weisstein. *Bernstein Polynomial*, MathWorld.com. URL: <https://mathworld.wolfram.com/BernsteinPolynomial.html> (visited on 03/29/2021).
- [38] Michigan Technology. *B-spline Basis Functions: Definition*, 2009. URL: <https://pages.mtu.edu/~shene/COURSES/cs3621/NOTES/spline/B-spline/bspline-basis.html> (visited on 03/29/2021).
- [39] J. Reiner and R. Vaziri. "Design and Analysis of Composite Structures". In: *Comprehensive Composite Materials II*, 2nd ed., California, USA: USA: Elsevier Ltd., 2018. Chap. 8, pp. 61–84.
- [40] Digital Engineering. *Computer-Aided Engineering (CAE)*, 2021. URL: <https://www.digitalengineering247.com/glossary/computer-aided-engineering-cae> (visited on 03/18/2021).
- [41] Dreambird. *Computer-aided engineering (CAE)*, 2021. URL: <https://www.dreambird.eu/useful/definitions/cae/> (visited on 03/18/2021).
- [42] Dassault Systèmes Simulia Corp. *Abaqus/CAE User's Manual*, 2011. URL: [http://130.149.89.49:2080/v6.11/pdf\\_books/CAE.pdf](http://130.149.89.49:2080/v6.11/pdf_books/CAE.pdf) (visited on 04/09/2021).
- [43] S. Steffen. "Structural Topology Optimization: Basic Theory, Methods and Applications". In: *NTNU Open*, vol. 1 (2013), pp. 1–197. URL: <https://ntnuopen.ntnu.no/ntnu-xmlui/handle/11250/241794>.

- [44] S. E. Benzley et al. "A Comparison of All Hexagonal and All Tetrahedral Finite Element Meshes for Elastic and Elasto-Plastic Analysis". In: *In Proceedings, 4th International Meshing Roundtable*, vol. 17, no. 4 (1995), pp. 1–13. URL: <https://www.researchgate.net/publication/267259986>.
- [45] J. C.R. Albino, L. A. Gonçalves Junior, and V. E. Beal. *On the convergence of solid meshes for the prediction of part distortions due to residual stresses*. 2019. DOI: <https://doi.org/10.1177/0954406219861405>.
- [46] Simulia. *Topology and Shape Optimization with Abaqus*, 2011. URL: <http://www.simulia.com/download/rum11/GL/Sandeep-Urankar-ATOM-SGL-RUM-2011.pdf> (visited on 03/19/2021).
- [47] J. W.P. Campbell and M. Tutton. "General theory of stair construction". In: *Staircases: History, Repair and Conservation*, 1st ed. London, United-Kingdom: Routledge Taylor and Francis Group, 2013. Chap. 1–5, pp. 3–68.
- [48] W. Mannes. "General theory of stair construction". In: *Techniques of Staircase Construction: Technical and Design Instructions for Stairs Made of Wood, Steel, Concrete, and Natural Stone*, 2nd ed. London, United-Kingdom: Springer Science and Business Media, 1986. Chap. 1, pp. 6–20.
- [49] B. Frettlöhr and M. Rippmann. *Modular stairs*, 2009. URL: [https://www.theexplorer.no/goals/?gclid=CjwKCAiAo5qABhBdEiwADtGmbs3dIJj%5C%5CnewlineL%5C%7B%5C%5C\\_%5C%7DBwE](https://www.theexplorer.no/goals/?gclid=CjwKCAiAo5qABhBdEiwADtGmbs3dIJj%5C%5CnewlineL%5C%7B%5C%5C_%5C%7DBwE) (visited on 05/17/2021).
- [50] *Regulations on technical requirements for construction works*, TEK17. 2017.
- [51] I. Moreira, R. Pauletti, and A. Lara. "An Application of Structural Topology Optimization to Creative Staircase Design". In: *Conference: IASS 2018 Creativity in Structural Design*, vol. 1 (2018), pp. 1–8. URL: [https://www.researchgate.net/publication/327552244\\_An\\_Application\\_of\\_Structural\\_Topology\\_Optimization\\_to\\_Creative\\_Staircase\\_Design](https://www.researchgate.net/publication/327552244_An_Application_of_Structural_Topology_Optimization_to_Creative_Staircase_Design).
- [52] A. Jipa et al. "3D-printed formwork for bespoke concrete stairs from computational design to digital fabrication". In: *Proceedings: SCF 2019 - ACM Symposium on Computational Fabrication*, vol. 1 (2019), pp. 1–12. DOI: <https://doi.org/10.1145/3328939.3329003>.
- [53] L. Vesela. "Staircase-dimensions of stair steps and their deviations of geometrical accuracy". In: *IOP Conference Series: Materials Science and Engineering*, vol. 1, no. 471 (2019), pp. 1–7. DOI: [10.1088/1757-899X/471/2/022012](https://doi.org/10.1088/1757-899X/471/2/022012).
- [54] *Building and buildings England and Wales - The building regulations*, 2010 No. 2214, 2010.
- [55] M. Afifi, B. Parke, and M. Al-Hussein. "Integrated approach for older adult friendly home staircase architectural design". In: *Automation in construction*, vol. 39 (2014), pp. 117–125. DOI: <https://doi.org/10.1016/j.autcon.2013.07.001>.
- [56] W. H. Mosley and J. H. Bungey. "Limit state design". In: *Reinforced Concrete Design*, 7th ed. London, United-Kingdom: Springer, 1982. Chap. 2, pp. 15–23.
- [57] *Prosjektering av betongkonstruksjoner Del 1-1: Almenne regler og regler for bygninger*, NS-EN 1992-1-1:2004+NA:2008, 2008.
- [58] *Laster på konstruksjoner - Del 2: Trafikklast på bruer*, NS-EN 1991-2:2003+NA:2010, 2010.
- [59] R. Dhir, G. Ghataora, and C. Lynn. "Concrete related applications". In: *Sustainable Construction Materials*, 1st ed. California, USA: Elsevier Ltd., 2017. Chap. 5, pp. 111–158.

- [60] D. W. S. Ho. "Durability of concrete". In: *The civil engineering handbook*, 2nd ed. Colorado, USA: CRC Press, 2003. Chap. 1–6, pp. 1–52.
- [61] S. I. Sørensen. "Dimensjonering og grensetilstander". In: *Betongkonstruksjoner: beregning og dimensjonering etter Eurocode 2*, 2nd ed. Bergen, Norge: Fagbokforlaget, 2010. Chap. 2-4, pp. 5–109.
- [62] R. I. Gilbert. "Shrinkage, cracking and deflection-the serviceability of concrete structures". In: *Electronic Journal of Structural Engineering*, vol. 1 (2001), pp. 2–14. URL: <https://citeseerx.ist.psu.edu/viewdoc/download?doi=10.1.1.493.1680&rep=rep1&type=pdf>.
- [63] Michigan Technology. *Submillimeter Formwork 3D-Printed Plastic Formwork for Concrete Elements*. 2018. DOI: <https://doi.org/10.3929/ethz-b-000237359>.
- [64] A. Alexander. *Design and Construction of Concrete Formwork*. URL: <https://www.engineersdaily.com/2014/06/manual-design-and-construction-of.html> (visited on 03/20/2021).
- [65] D. R. Thomas and I. D. Hodges. "Doing a literature review". In: *Designing and managing your research project: Core skills for social and health research*, 1st ed. New York, USA: Sage Publications, 2010. Chap. 7, pp. 150–174.
- [66] T. Mudaliar, R. Lequesne, and M. Fadden. "Topology optimized reinforced concrete walls constructed with 3D printed formwork". In: *Structural Engineering and Engineering Materials SL Report 20-1*, vol. 1 (2020), pp. 1–152. URL: <https://kuscholarworks.ku.edu/handle/1808/30279>.
- [67] J. L. Jewett and J. V. Carstensen. "Topology-optimized design, construction and experimental evaluation of concrete beams". In: *Automation in Construction*, vol. 102 (2019), pp. 59–67. DOI: 10.1016/j.autcon.2019.02.001.
- [68] Creality. *CR-6 SE 3D Printer*, 2020. URL: [https://www.theexplorer.no/goals/?gclid=CjwKCAiAo5qABhBdEiwA0tGmbs3dIJj%5C%5CnewlineL%5C%7B%5C%5C\\_%5C%7DBwE](https://www.theexplorer.no/goals/?gclid=CjwKCAiAo5qABhBdEiwA0tGmbs3dIJj%5C%5CnewlineL%5C%7B%5C%5C_%5C%7DBwE) (visited on 04/21/2021).

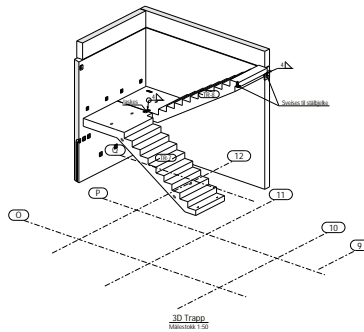
## **12 Appendix**

## **A Drawings from Contiga AS**



Elementer senket 20mm for flis på inntrinn og senket 5mm for teppellis på plan 1.

SNITT A-A  
Målestokk 1:20



TRAPPER		
Nummer	Vår	Årstid
TR 1	2008	1
TR 2	2008	1

REPOS		
Nummer	Vår	Årstid

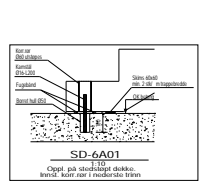
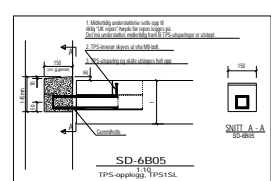
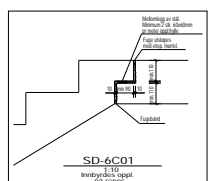
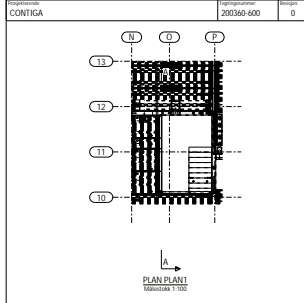
**REVISJONER**  
 Besøkt/utviklet: BOMBO  
 Teknisk/utviklet: BOMBO  
 Annet: BOMBO

**BESTEMMELSER**  
 Eksisterende konstruksjon: K1  
 Overbygning konstruksjon: 21.4-12 [int]  
 Tilsvarende overbygning konstruksjon: K1

**STYKKE**  
 Støtting utføres med NS-EN 1096-2:2008-A1:2011  
 Utviklingsmateriale: E12  
 Føringssystem: F2  
 Tappemateriale: Føringssystemer 2  
 Det skal henvises til de tekniske tegningene for detaljer og spesifikasjoner.  
 Kjøkkent med a-stil a=4 mm derom oppgjørst.

**TRAPP**  
 Støtting: God betong  
 Montasjepunkt: 80 mm, med en element 10 mm  
 Utviklingsmateriale: E12  
 Annet: F2  
 Føringssystem: F2  
 Oppgjørst: 21.4-12 [int]  
 Montasjepunkt: 80 mm  
 Montasjepunkt: 80 mm

**ANNET**  
 Alle tegninger er for stoffet 0/0/0.  
 Luftveisnett: Nordic Føringssystem Group  
 3.08 NE-D Universal Løst Løst  
 3.08 NE-D Universal Løst Løst



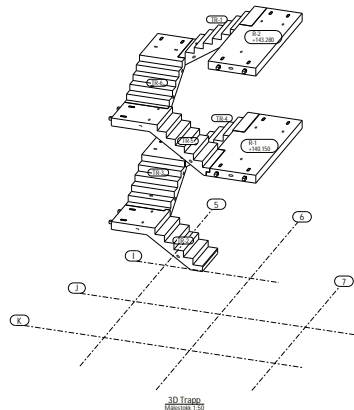
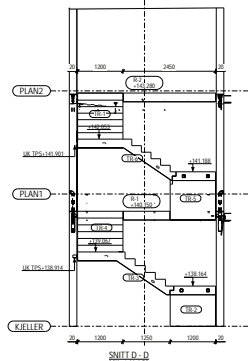
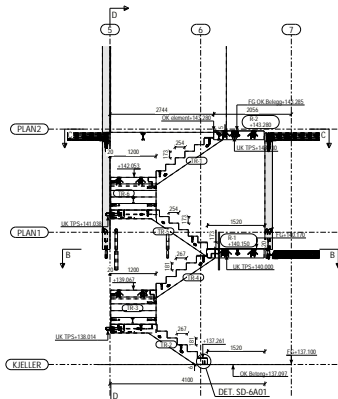
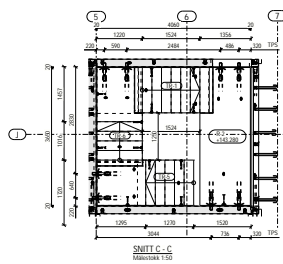
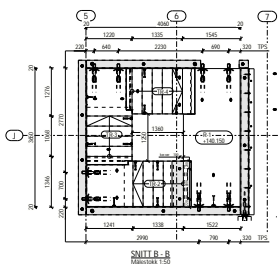
U	Revisjon	Dato	Utskrift
1	Revisjon	15.12.08	TE
2	Revisjon	15.12.08	TE

U	Revisjon	Dato	Utskrift
1	Revisjon	15.12.08	TE
2	Revisjon	15.12.08	TE

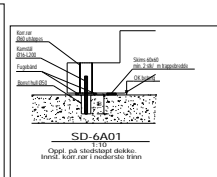
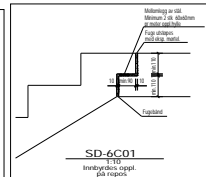
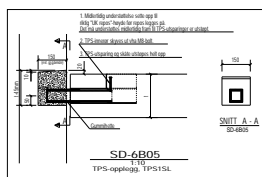
  

U	Revisjon	Dato	Utskrift
1	Revisjon	15.12.08	TE
2	Revisjon	15.12.08	TE



Elementer senket 20mm for flis på inntreinn  
Senket 20mm for flis på plan 1.  
Senket 5mm for teppeliss på plan 2.

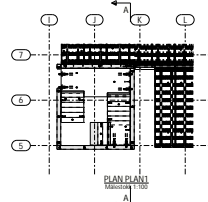
SNITT A  
Måttavla 1:50



TRAPPER		
Nummer	Etasj. #	Antall
TR.1	1.05	1
TR.2	1.05	1
TR.3	1.05	1
TR.4	1.05	1
TR.5	2.15	1
TR.6	1.05	1

REPOS		
Nummer	Etasj. #	Antall
RE1	2.05	1
RE2	2.05	1

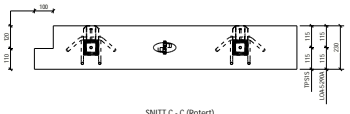
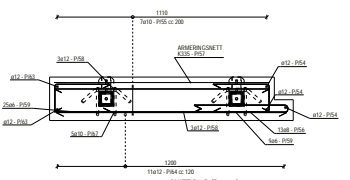
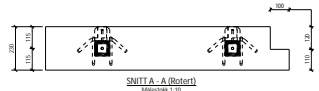
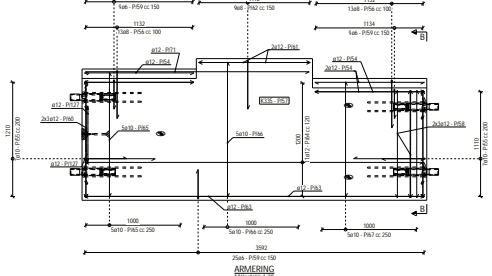
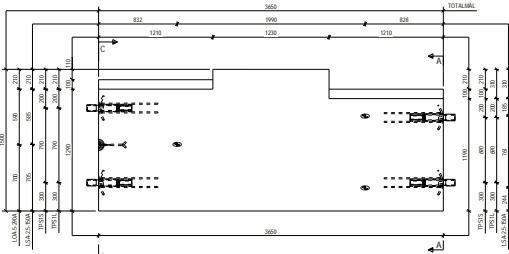
**REVISJONER**  
 BE1/2016: 0.30560  
 Saksnummer: 15051023  
 Annet: BGSNC  
**BESTEMMELSER**  
 1. Skapingspliktansvar: Ansvar for: 301  
 2. Skapingspliktansvar: Ansvar for: 301  
 3. Skapingspliktansvar: Ansvar for: 301  
 4. Skapingspliktansvar: Ansvar for: 301  
 5. Skapingspliktansvar: Ansvar for: 301  
 6. Skapingspliktansvar: Ansvar for: 301  
**FORSLAG**  
 1. Skapingspliktansvar: Ansvar for: 301  
 2. Skapingspliktansvar: Ansvar for: 301  
 3. Skapingspliktansvar: Ansvar for: 301  
 4. Skapingspliktansvar: Ansvar for: 301  
 5. Skapingspliktansvar: Ansvar for: 301  
 6. Skapingspliktansvar: Ansvar for: 301  
**ANMÆRKNING**  
 1. Skapingspliktansvar: Ansvar for: 301  
 2. Skapingspliktansvar: Ansvar for: 301  
 3. Skapingspliktansvar: Ansvar for: 301  
 4. Skapingspliktansvar: Ansvar for: 301  
 5. Skapingspliktansvar: Ansvar for: 301  
 6. Skapingspliktansvar: Ansvar for: 301



CONTIGA		200360-601		D	
0	Arbeidsdagning	144021	TE		
1	Arbeidsdagning	144021	TE		
2	Arbeidsdagning	144021	TE		
3	Arbeidsdagning	144021	TE		
4	Arbeidsdagning	144021	TE		
5	Arbeidsdagning	144021	TE		
6	Arbeidsdagning	144021	TE		
7	Arbeidsdagning	144021	TE		
8	Arbeidsdagning	144021	TE		
9	Arbeidsdagning	144021	TE		
10	Arbeidsdagning	144021	TE		
11	Arbeidsdagning	144021	TE		
12	Arbeidsdagning	144021	TE		
13	Arbeidsdagning	144021	TE		
14	Arbeidsdagning	144021	TE		
15	Arbeidsdagning	144021	TE		
16	Arbeidsdagning	144021	TE		
17	Arbeidsdagning	144021	TE		
18	Arbeidsdagning	144021	TE		
19	Arbeidsdagning	144021	TE		
20	Arbeidsdagning	144021	TE		
21	Arbeidsdagning	144021	TE		
22	Arbeidsdagning	144021	TE		
23	Arbeidsdagning	144021	TE		
24	Arbeidsdagning	144021	TE		
25	Arbeidsdagning	144021	TE		
26	Arbeidsdagning	144021	TE		
27	Arbeidsdagning	144021	TE		
28	Arbeidsdagning	144021	TE		
29	Arbeidsdagning	144021	TE		
30	Arbeidsdagning	144021	TE		
31	Arbeidsdagning	144021	TE		
32	Arbeidsdagning	144021	TE		
33	Arbeidsdagning	144021	TE		
34	Arbeidsdagning	144021	TE		
35	Arbeidsdagning	144021	TE		
36	Arbeidsdagning	144021	TE		
37	Arbeidsdagning	144021	TE		
38	Arbeidsdagning	144021	TE		
39	Arbeidsdagning	144021	TE		
40	Arbeidsdagning	144021	TE		
41	Arbeidsdagning	144021	TE		
42	Arbeidsdagning	144021	TE		
43	Arbeidsdagning	144021	TE		
44	Arbeidsdagning	144021	TE		
45	Arbeidsdagning	144021	TE		
46	Arbeidsdagning	144021	TE		
47	Arbeidsdagning	144021	TE		
48	Arbeidsdagning	144021	TE		
49	Arbeidsdagning	144021	TE		
50	Arbeidsdagning	144021	TE		
51	Arbeidsdagning	144021	TE		
52	Arbeidsdagning	144021	TE		
53	Arbeidsdagning	144021	TE		
54	Arbeidsdagning	144021	TE		
55	Arbeidsdagning	144021	TE		
56	Arbeidsdagning	144021	TE		
57	Arbeidsdagning	144021	TE		
58	Arbeidsdagning	144021	TE		
59	Arbeidsdagning	144021	TE		
60	Arbeidsdagning	144021	TE		
61	Arbeidsdagning	144021	TE		
62	Arbeidsdagning	144021	TE		
63	Arbeidsdagning	144021	TE		
64	Arbeidsdagning	144021	TE		
65	Arbeidsdagning	144021	TE		
66	Arbeidsdagning	144021	TE		
67	Arbeidsdagning	144021	TE		
68	Arbeidsdagning	144021	TE		
69	Arbeidsdagning	144021	TE		
70	Arbeidsdagning	144021	TE		
71	Arbeidsdagning	144021	TE		
72	Arbeidsdagning	144021	TE		
73	Arbeidsdagning	144021	TE		
74	Arbeidsdagning	144021	TE		
75	Arbeidsdagning	144021	TE		
76	Arbeidsdagning	144021	TE		
77	Arbeidsdagning	144021	TE		
78	Arbeidsdagning	144021	TE		
79	Arbeidsdagning	144021	TE		
80	Arbeidsdagning	144021	TE		
81	Arbeidsdagning	144021	TE		
82	Arbeidsdagning	144021	TE		
83	Arbeidsdagning	144021	TE		
84	Arbeidsdagning	144021	TE		
85	Arbeidsdagning	144021	TE		
86	Arbeidsdagning	144021	TE		
87	Arbeidsdagning	144021	TE		
88	Arbeidsdagning	144021	TE		
89	Arbeidsdagning	144021	TE		
90	Arbeidsdagning	144021	TE		
91	Arbeidsdagning	144021	TE		
92	Arbeidsdagning	144021	TE		
93	Arbeidsdagning	144021	TE		
94	Arbeidsdagning	144021	TE		
95	Arbeidsdagning	144021	TE		
96	Arbeidsdagning	144021	TE		
97	Arbeidsdagning	144021	TE		
98	Arbeidsdagning	144021	TE		
99	Arbeidsdagning	144021	TE		
100	Arbeidsdagning	144021	TE		

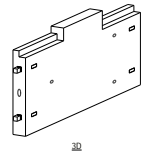


MONTAGEBRUK	Antal
01	1



RINNSTØPNINGSKODS			
Linj	Standard	Antal	Antall
1	UGA 2-200A	1	18
2	UGA 2.5-150A	3	83
3	1P525	4	82
4	1P525	4	82
Se eget tegning for alle standard		Totalt: 45 85 kg	

Pos. nr	Dim.	Kvalitet	Langs.	Tverrsnitt	Størrelse	Størrelse med standard lagtykkelse	Antall
P501	12	B500C	1205	0.8	11.4	11.4	14
P504	8	B500C	1015	0.4	10.4	10.4	28
P508	12	B500C	1140	1.0	6.1	11.4	6
P509	8	B500C	720	0.2	10	10	43
P510	12	B500C	1260	1.1	6.4	11.4	6
P511	12	B500C	1260	1.0	2.1	11.4	6
P513	8	B500C	1140	0.5	6.1	11.4	6
P517	12	B500C	2000	3.2	6.4	11.4	2
P518	12	B500C	2000	2.2	6.5	11.4	1
P519	10	B500C	1200	0.5	4.1	11.4	1
P516	10	B500C	1400	0.9	4.4	11.4	1
P517	10	B500C	1200	0.8	3.8	11.4	1
P511	12	B500C	2200	2.1	2.1	11.4	1
P127	12	B500C	845	0.4	1.2	11.4	2
P51	8/8	B500A	2000	19.7	19.7	11.4	1



Arbeidsnavn	1408121	TS
Rev	0	Sign.
Utskriftspakke	UGA BE 150A	
Informasjonskildene	DMG	Fachbereich
Informasjonskildene (for pros)	RECHNUNG	Bauabteilung
Basismaterial		Einzelteil
Druckbild metode	Druck	Din (A)
Overflate med form	Førings	1:14 pr
Overflate	25 mm	Overflate
Overflate (interne)	25 mm	Overflate
Fil (inkl. alle tegn og tegning)	10 mm	Antall skisser
Hauptversion 13		Dato
REPOS		Sign.
Engineering		15/12/20
KONTIGA		19/01/21
HEDLERING		200360
		R1
		0

ORIGINALFORMAT: A1 (504x411)

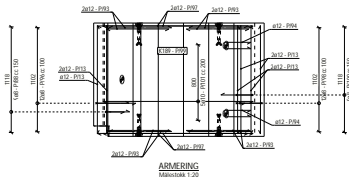
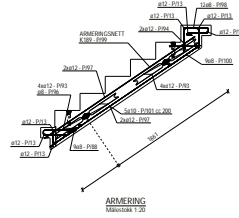
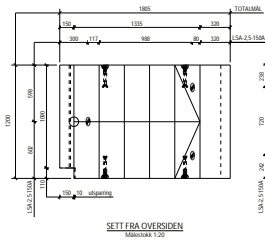
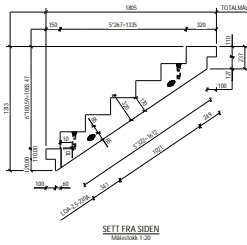




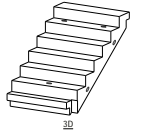




Utskik	Antal
01	1



Pro. Nr.	Dim.	Kvalitet	Langs.	Trans.	Stavelse	Stavelse med stivende lagplatt	Antal
P113	12	B500NC	150	0.8	7.1	150	7
P115	12	B500NC	150	0.7	7.6	150	11
P116	8	B500NC	400	0.2	2.2	150	6
P117	12	B500NC	840	0.7	4.0	150	8
P118	12	B500NC	405	0.8	1.1	150	5
P119	8	B500NC	840	0.3	4.0	150	12
P117	12	B500NC	100	1.7	0.8	150	8
P118	8	B500NC	840	0.3	4.0	150	12
P119	8	B500NC	96	0.4	3.5	150	9
P120	16	B500NC	100	1.2	5.9	150	1
P121	16	B500NC	100	1.7	4.7	150	1
Totalt i kasse							45.1 kg
Totalt nett.							6.7 kg



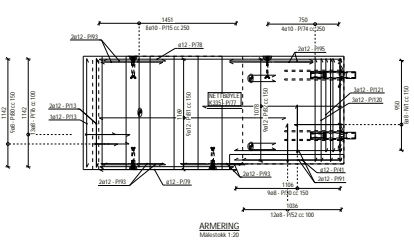
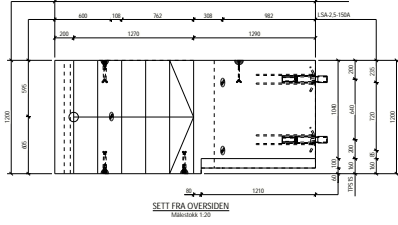
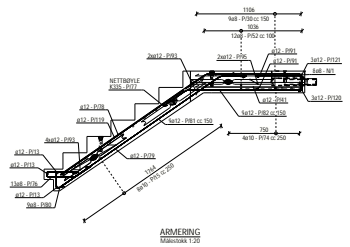
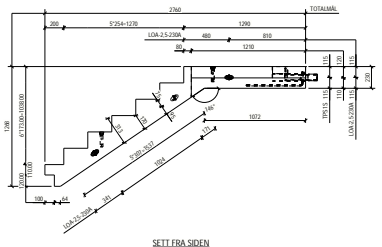
Etikettnummer: 22-4  
 Prosjektnummer: 20030  
 Prosjekt: Høyskolen 13

Utskik	Antal	Antal	Antal
1	1	4	6.7
2	1	3	6.1
Se tegnet for detaljer for ikke standard			
Totalt: 13.8 kg			

ORIGINALFORMAT: A1 (594x411)

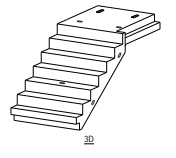
Arbeidsgrupp	1401121	TE
Rev	0	Sign
Utskik	0	Sign
Materialvalg	GS&E-TORR	
Informasjonskildene	DKK	Fachbetriebe
Informasjons kilde nr.1	1630004	Betonfertigbetone
Informasjons kilde nr.2	1630004	Betonfertigbetone
Informasjons kilde nr.3	1630004	Betonfertigbetone
Informasjons kilde nr.4	1630004	Betonfertigbetone
Informasjons kilde nr.5	1630004	Betonfertigbetone
Informasjons kilde nr.6	1630004	Betonfertigbetone
Informasjons kilde nr.7	1630004	Betonfertigbetone
Informasjons kilde nr.8	1630004	Betonfertigbetone
Informasjons kilde nr.9	1630004	Betonfertigbetone
Informasjons kilde nr.10	1630004	Betonfertigbetone
Informasjons kilde nr.11	1630004	Betonfertigbetone
Informasjons kilde nr.12	1630004	Betonfertigbetone
Informasjons kilde nr.13	1630004	Betonfertigbetone
Informasjons kilde nr.14	1630004	Betonfertigbetone
Informasjons kilde nr.15	1630004	Betonfertigbetone
Informasjons kilde nr.16	1630004	Betonfertigbetone
Informasjons kilde nr.17	1630004	Betonfertigbetone
Informasjons kilde nr.18	1630004	Betonfertigbetone
Informasjons kilde nr.19	1630004	Betonfertigbetone
Informasjons kilde nr.20	1630004	Betonfertigbetone
Informasjons kilde nr.21	1630004	Betonfertigbetone
Informasjons kilde nr.22	1630004	Betonfertigbetone
Informasjons kilde nr.23	1630004	Betonfertigbetone
Informasjons kilde nr.24	1630004	Betonfertigbetone
Informasjons kilde nr.25	1630004	Betonfertigbetone
Informasjons kilde nr.26	1630004	Betonfertigbetone
Informasjons kilde nr.27	1630004	Betonfertigbetone
Informasjons kilde nr.28	1630004	Betonfertigbetone
Informasjons kilde nr.29	1630004	Betonfertigbetone
Informasjons kilde nr.30	1630004	Betonfertigbetone
Informasjons kilde nr.31	1630004	Betonfertigbetone
Informasjons kilde nr.32	1630004	Betonfertigbetone
Informasjons kilde nr.33	1630004	Betonfertigbetone
Informasjons kilde nr.34	1630004	Betonfertigbetone
Informasjons kilde nr.35	1630004	Betonfertigbetone
Informasjons kilde nr.36	1630004	Betonfertigbetone
Informasjons kilde nr.37	1630004	Betonfertigbetone
Informasjons kilde nr.38	1630004	Betonfertigbetone
Informasjons kilde nr.39	1630004	Betonfertigbetone
Informasjons kilde nr.40	1630004	Betonfertigbetone
Informasjons kilde nr.41	1630004	Betonfertigbetone
Informasjons kilde nr.42	1630004	Betonfertigbetone
Informasjons kilde nr.43	1630004	Betonfertigbetone
Informasjons kilde nr.44	1630004	Betonfertigbetone
Informasjons kilde nr.45	1630004	Betonfertigbetone
Informasjons kilde nr.46	1630004	Betonfertigbetone
Informasjons kilde nr.47	1630004	Betonfertigbetone
Informasjons kilde nr.48	1630004	Betonfertigbetone
Informasjons kilde nr.49	1630004	Betonfertigbetone
Informasjons kilde nr.50	1630004	Betonfertigbetone
Informasjons kilde nr.51	1630004	Betonfertigbetone
Informasjons kilde nr.52	1630004	Betonfertigbetone
Informasjons kilde nr.53	1630004	Betonfertigbetone
Informasjons kilde nr.54	1630004	Betonfertigbetone
Informasjons kilde nr.55	1630004	Betonfertigbetone
Informasjons kilde nr.56	1630004	Betonfertigbetone
Informasjons kilde nr.57	1630004	Betonfertigbetone
Informasjons kilde nr.58	1630004	Betonfertigbetone
Informasjons kilde nr.59	1630004	Betonfertigbetone
Informasjons kilde nr.60	1630004	Betonfertigbetone
Informasjons kilde nr.61	1630004	Betonfertigbetone
Informasjons kilde nr.62	1630004	Betonfertigbetone
Informasjons kilde nr.63	1630004	Betonfertigbetone
Informasjons kilde nr.64	1630004	Betonfertigbetone
Informasjons kilde nr.65	1630004	Betonfertigbetone
Informasjons kilde nr.66	1630004	Betonfertigbetone
Informasjons kilde nr.67	1630004	Betonfertigbetone
Informasjons kilde nr.68	1630004	Betonfertigbetone
Informasjons kilde nr.69	1630004	Betonfertigbetone
Informasjons kilde nr.70	1630004	Betonfertigbetone
Informasjons kilde nr.71	1630004	Betonfertigbetone
Informasjons kilde nr.72	1630004	Betonfertigbetone
Informasjons kilde nr.73	1630004	Betonfertigbetone
Informasjons kilde nr.74	1630004	Betonfertigbetone
Informasjons kilde nr.75	1630004	Betonfertigbetone
Informasjons kilde nr.76	1630004	Betonfertigbetone
Informasjons kilde nr.77	1630004	Betonfertigbetone
Informasjons kilde nr.78	1630004	Betonfertigbetone
Informasjons kilde nr.79	1630004	Betonfertigbetone
Informasjons kilde nr.80	1630004	Betonfertigbetone
Informasjons kilde nr.81	1630004	Betonfertigbetone
Informasjons kilde nr.82	1630004	Betonfertigbetone
Informasjons kilde nr.83	1630004	Betonfertigbetone
Informasjons kilde nr.84	1630004	Betonfertigbetone
Informasjons kilde nr.85	1630004	Betonfertigbetone
Informasjons kilde nr.86	1630004	Betonfertigbetone
Informasjons kilde nr.87	1630004	Betonfertigbetone
Informasjons kilde nr.88	1630004	Betonfertigbetone
Informasjons kilde nr.89	1630004	Betonfertigbetone
Informasjons kilde nr.90	1630004	Betonfertigbetone
Informasjons kilde nr.91	1630004	Betonfertigbetone
Informasjons kilde nr.92	1630004	Betonfertigbetone
Informasjons kilde nr.93	1630004	Betonfertigbetone
Informasjons kilde nr.94	1630004	Betonfertigbetone
Informasjons kilde nr.95	1630004	Betonfertigbetone
Informasjons kilde nr.96	1630004	Betonfertigbetone
Informasjons kilde nr.97	1630004	Betonfertigbetone
Informasjons kilde nr.98	1630004	Betonfertigbetone
Informasjons kilde nr.99	1630004	Betonfertigbetone
Informasjons kilde nr.100	1630004	Betonfertigbetone

Montageblad	
Utskift	Antal
01	1



Pos. nr	Dim	Skalsid	Längd	Var. kg	Totalt	Skissa med styrvidg. lagomål	Antal
B11	8	BÖRNING	1125	0.4	3.6		9
B12	12	BÖRNING	1150	1.0	3.1		3
B13	10	BÖRNING	1150	0.7	5.1		8
B14	8	BÖRNING	1125	0.4	4.0		9
B15	12	BÖRNING	1050	0.9	0.9		1
B16	8	BÖRNING	850	0.3	3.9		12
B17	10	BÖRNING	1000	0.7	2.7		4
B18	8	BÖRNING	855	0.3	4.4		13
B19	12	BÖRNING	1095	2.4	2.4		1
B20	12	BÖRNING	1175	9.6	1.6		11
B21	8	BÖRNING	825	0.3	2.9		9
B22	12	BÖRNING	2300	2.1	10.3		5
B23	12	BÖRNING	1500	1.4	12.2		9
B24	12	BÖRNING	1135	1.0	2.0		2
B25	12	BÖRNING	840	0.7	4.5		6
B26	12	BÖRNING	625	0.6	1.3		2
B27	12	BÖRNING	825	0.8	1.4		2
B28	12	BÖRNING	1720	1.5	1.5		1
B29	12	BÖRNING	1000	1.0	2.9		3
B30	12	BÖRNING	960	0.9	2.4		3
B31	8	BÖRNING	1150	15.5	15.5		1

Totalt Längd: 82.5 kg  
Totalt var: 15.5 kg



Elvarvnummer: 20.6  
Påskrivningsnummer: 200360  
Projekt: Högskolan 13

Linje	Standard	Antal	Antal	Volym
1	LÖS 2.5-200A	4	87	
2	LÖS 2.5-150A	3	83	
3	1P525	2	62	
4	1P515	2	62	
Se signat lagring för alla standard		Totalt: 22.7 kg		

Arbetsgrupp	1401021	TE
Revisör	1401021	TE
Maskinprogramering	CGA BE-TONC	
Införskansningskälla	DKK	Fachbeton
Införskansnings (bet. nr)	1600000	Betonförhållande
Betonstyrka		C25/30
Betalningsmetod	Rekult	Dim. (A)
Överfl. med form	Förngat	Balansering
Överkl.ning	25 mm	Överkl.ning
Överkl.ning	25 mm	Överkl.ning
Överkl.ning	25 mm	Överkl.ning
Förskansnings (bet. nr)	1600000	Betonförhållande
Förskansnings (bet. nr)	1600000	Betonförhållande
Hauptverweis 13	1401021	TE
TRAPP	241300	TE
Projekt	200360	TR-5
Revisör		0

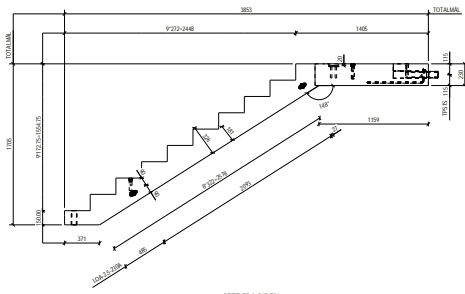
CONTIGA  
HOEGLERER-CONCRETE

ORIGINALFORMAT: A1 (044x41)

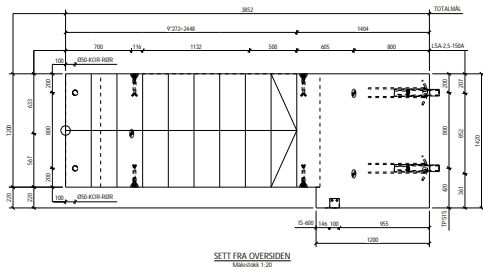




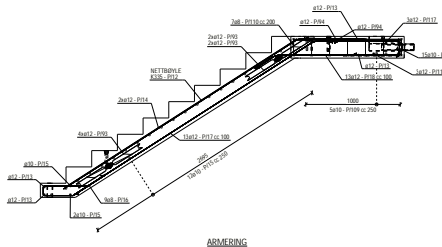
Montageplan	Ansik	Antal
01	1	



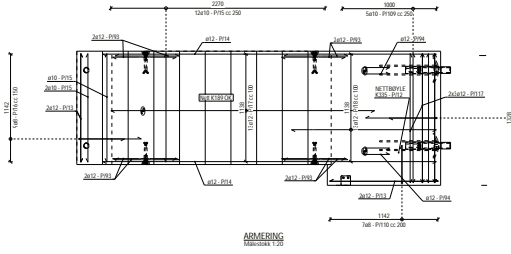
SETT FRA SIDEN  
Målestok 1:20



SETT FRA OVERSIDEN  
Målestok 1:20



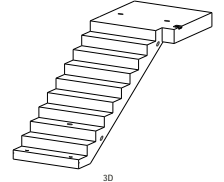
ARMERING  
Målestok 1:20



ARMERING  
Målestok 1:20

Pos. nr.	Dim.	Kvalitet	Langs.	Trans.	Stavelse	Stavelse med stredige lagtykkelse	Antal
P10	12	B500NC	1500	0.8	4.1	1100	4
P14	12	B500NC	3900	0.5	7.1	1100	7
P15	10	B500NC	1150	0.7	10.8	1100	15
P16	8	B500NC	1300	0.5	4.5	1100	4
P17	12	B500NC	3265	2.9	37.7	1100	13
P18	14	B500NC	1275	1.4	18.7	1100	13
P19	16	B500NC	1275	0.8	12.7	1100	15
P20	12	B500NC	840	0.7	6.0	1100	8
P21	12	B500NC	620	0.6	1.1	1100	2
P22	10	B500NC	1370	0.8	4.2	1100	5
P10	8	B500NC	900	0.4	2.6	1100	7
P11	12	B500NC	1370	1.2	7.3	1100	8
P12	8	B500NC	1150	2.1	21.3	1100	1

Totalt korrusert: 162.7 kg  
Totalt nett: 21.3 kg



Elevuttømmen: 20.7  
Rengjøringsmiddel: 2000g  
Prosjekt: Høyskolen i Gjøvik

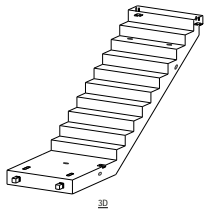
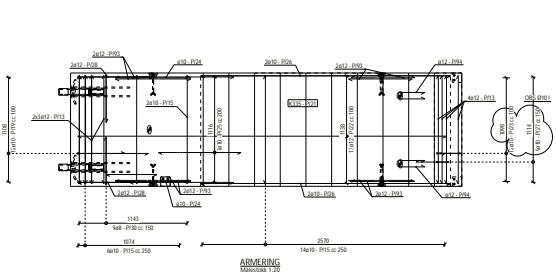
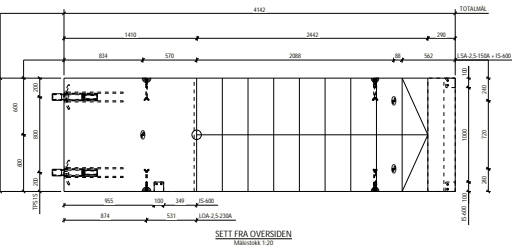
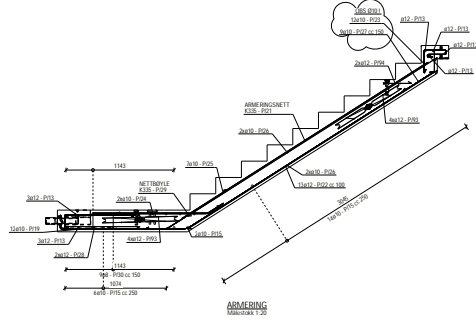
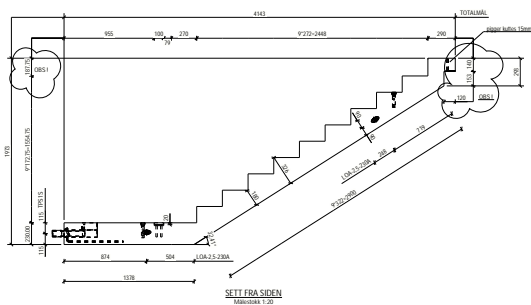
Utgangspunkt	Navn	Antall	Enheter
1	LS-400	1	1.2
2	LSA-2.5-200A	4	0.1
3	LSA-2.5-150A	3	0.1
4	PPS-L	2	0.2
5	TPS-S	2	0.2
6	SDS-K20-800L-1-102	2	0.0

Se også tegning for alle standarder. Totalt: 21.3 kg

ORIGINALFORMAT: A1 (504x411)

Arbeidsgruppe	1401021	TS
Rev. / Dato		Sign.
Materialvalg	GS&E-TING	
Informasjonskilder	DNK	Fachblätter
Materialkriterier (for valg)	RECHNUNG	Bearbeitungsblätter
Bestemmelse		Kostenblätter
Drifts- og vedlikehold	Reinlich	Dusj- og
Overflate med form	Formgitt	Betonggulv
Overflate	25 mm	Dekning
Opplysning om materialer	<= 10 mm	1200 kg
Fot. (for innlegg i rapport)	10 mm	Arbeidsblad
Hauptversion 13		Dato
TRAPP	Erstattet	241200
	Erstattet	040301
	Erstattet	200360
		Rev.
		0

MONTAGEBRUK	
Utskik	Ansik
01	1



Pos. #	Dim.	Kvalitet	Langs.	Trans.	Stavelse	Stavelse med skråning	Antall
PT11	12	B500NC	150	1.8	90.2	150	10
PT12	12	B500NC	150	0.7	95.6	150	27
PT13	10	B500NC	125	0.8	92.2	125	12
PT14	12	B500NC	490	1.9	50.7	490	13
PT15	10	B500NC	75	0.5	5.7	75	12
PT16	10	B500NC	120	0.7	1.4	120	7
PT17	10	B500NC	95	0.8	4.3	95	7
PT18	10	B500NC	325	1.9	7.7	325	4
PT19	10	B500NC	95	0.8	5.4	95	6
PT20	12	B500NC	80	0.7	2.8	80	4
PT21	8	B500NC	125	0.4	0.0	125	18
PT22	12	B500NC	80	0.7	4.0	80	8
PT23	12	B500NC	85	0.8	1.1	85	7
PT24	8	B500NC	150	0.3	0.3	150	1
PT25	8	B500NC	135	0.4	16.4	135	1

Arbeidsnummer	1481121	TS
Rev	0	Sign
Materialutførelse	GS4 BE-T09C	
Informasjonskildene	DNK	Fachbetriebe
Materialisering (for mat.)	RECHNOL	Besonderebetriebe
Besonderebetriebe		Kontaktservice
Bruttovekt (inkluderer)	Ståll	Dusj - G4
Overflate med lakk	Føringslag	Betonggulv
Overflate	25 mm	Overflate
Overflate (inkluderer)	<= 10 mm	Ståll
Fot (inkluderer)	10 mm	Arbeidsbetriebe
Hauptverweis 13		Dato
TRAPP	Engner	241220
	Erstatning	040217
	Prosjekt	200360
	TR-8	0

Elevnummer: 02.8			
Prosjektnummer: 00206			
Prosjekt: Trappvesen 13			
BANKSTYPERINGSGODES			
Linj	Standard	Antal	Pris
1	GS40	3	1.2
2	GS4-25-20A	4	0.7
3	GS4-25-150A	3	0.3
4	1P52	2	0.2
5	1P53	2	0.2
Se signet tegning for alle standard		Totalt	26.2 kg

ORIGINALFORMAT: A1 (GS4041)

## **B Development of parametric staircase by the use of Rhinoceros 3D and Grasshopper 3D**

# Development of parametric staircase by the use of Rhinoceros 3D and Grasshopper 3D

Due to limited knowledge of Grasshopper 3D, a parametric modelling camp at NTNU with Sverre Magnus Haakonsen and Marcin Luczkowski were attended. This camp was held in January 2021 and the objective of the camp is to introduce new users to Rhinoceros and Grasshopper 3D and teach both basics and comprehensive use of the software. The camp lasted for 4 days and can be found on this link: <https://www.youtube.com/c/CSDGNTNU/videos>

This parametric camp, together with previous knowledge of a similar software called Dynamo, we were able to develop our own model for the project. Parametric modelling grants a large degree of freedom in design. The design is based on the use of points, which is connected to produce lines and curves. These curves are then joined to create a single closed curve, which can then be patched into a surface and finally extruded into a solid.

The model was developed by the use of the nodes from Grasshopper listed below:

**Construct point.** Describe the origin of the staircase.

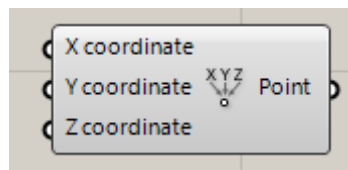


Figure 1 Construct point.

**Subtraction, addition, division and multiplication.** Nodes that perform calculations, which is necessary create an interlinked visual code, that are able to alter multiple geometries simultaneously.

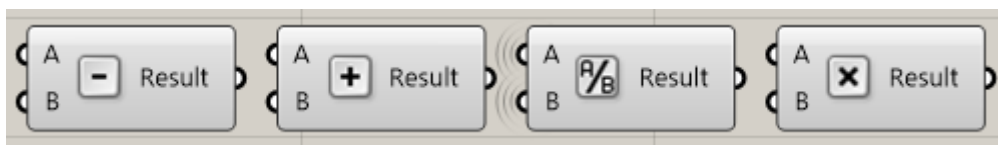


Figure 2 Subtraction, addition, division and multiplication.

**Unit vectors and vector.** Describes the movement and direction of the translation.

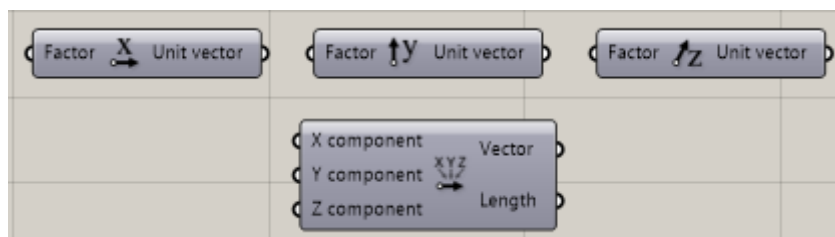


Figure 3 Unit vectors and and construct vector.

**Number slider.** Enables the user to change the input variable by sliding or simply inputting a number.

**Distance.** Measures the distance between two points.

**Negative.** Enables the use of negative numbers.

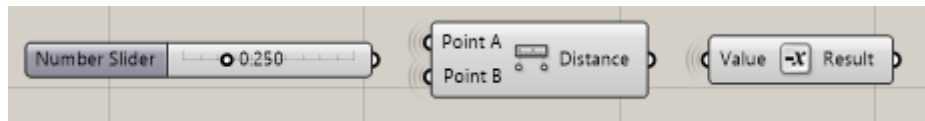


Figure 4 Number slider, distance and negative.

**Join curves, start-/end points, line.** Enables the user to creates lines and curves and connect them into a single curve.

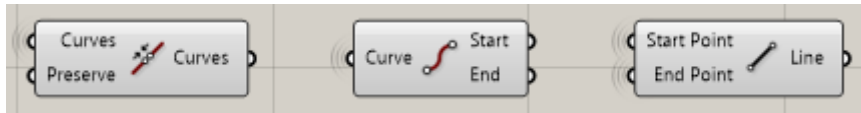


Figure 5 Join curves, star-/end points, line.

**Boundary surface and extrusion.** Enables the user to produce surface by patching and solids through extrusion.

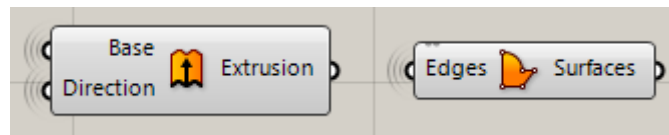


Figure 6 Boundary surface and extrusion.

**Move and rotate.** Enables the user to move and rotate a geometry by reading a translation vector and angle.

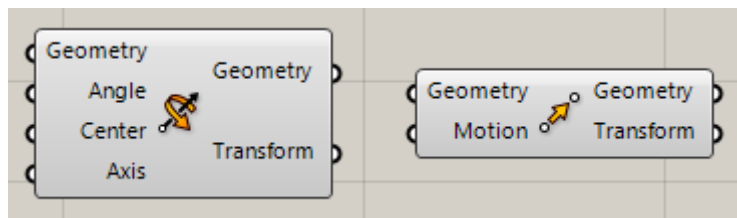


Figure 7 Geometry rotate and move.

**Series, list item and split list.** Enables the user to create and manage lists.

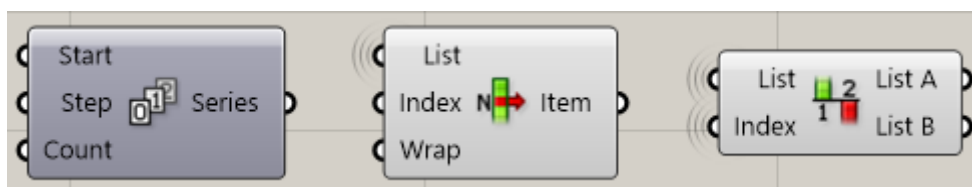


Figure 8 Series, split list and list item.

To construct the model similarly to the model from Contiga As the staircase was divided into three separate solids; the bottom, the intermediate and the top staircase. The model is built on the concept of coordinates in a 3D environment, where 1 single point is used as the origin of the model. Furthermore, the flight and landings are constructed by the use of vectors and moving operators – and made parametric by the use of number sliders.

The visual codes grouped in red are producing the steps of the staircase, as illustrated in Figure 11. To develop a parametric model a single starting point is used as the basis for the model. This point is then moved by the “move” node by inserting a “motion”, which is movement description given by the use of the “units vectors” and “construct vectors”. These vectors are given numbers in the form of “number sliders”, which is connected to a directional unit vector, either x-, y- or z-direction.

By introducing motions into the “move” operator, it is possible to parametrically construct new points as showed in Figure 9. These new points are connected with the “line” node, which connects to points into a single line, such lines are illustrated in green in Figure 11. After computing all the necessary curves, the node “join curves” are used to collect and compute a single combined series curve. The staircase design also including parametrically concrete cover, which enables the user to choose the wanted cover of the structure.

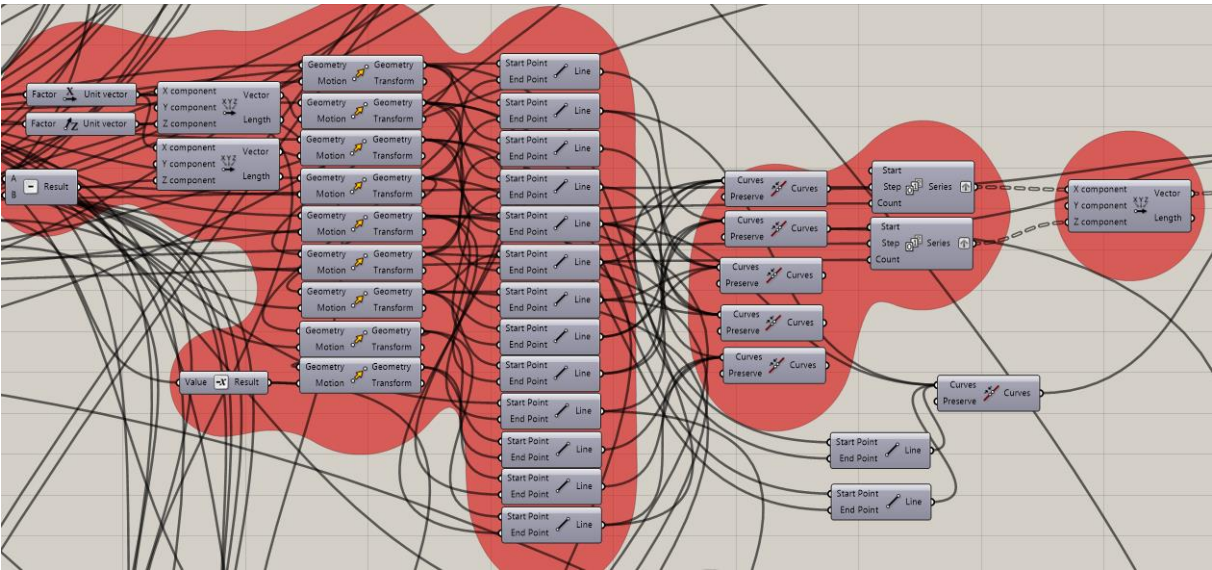


Figure 9 RED group: Visual code from Grasshopper 3D for modeling of the steps.

To be able to parametrically change the number of steps, a node called “series” is introduced, illustrated in Figure 10. This series takes in our case two parameters, “step” and “count” – resulting in an outputted list. These “series” are then inputted in an “construct vector”, which produces a number of translation vectors according to the number of steps inputted. These vectors are then connected to the initial step geometry and one translation is done for every vector – where each translation produce a new step at the top of the previous step.

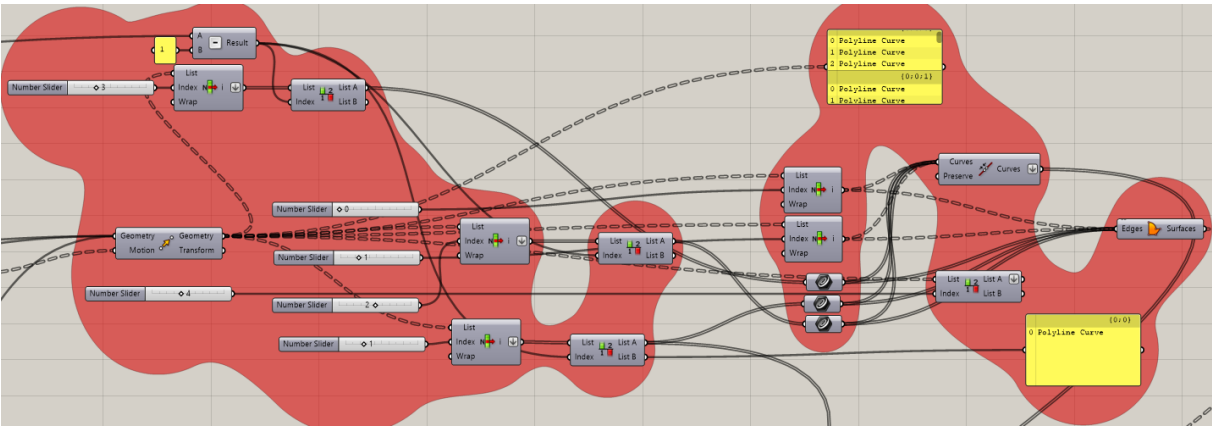


Figure 10 Visual code from Grasshopper 3D for modeling of the steps

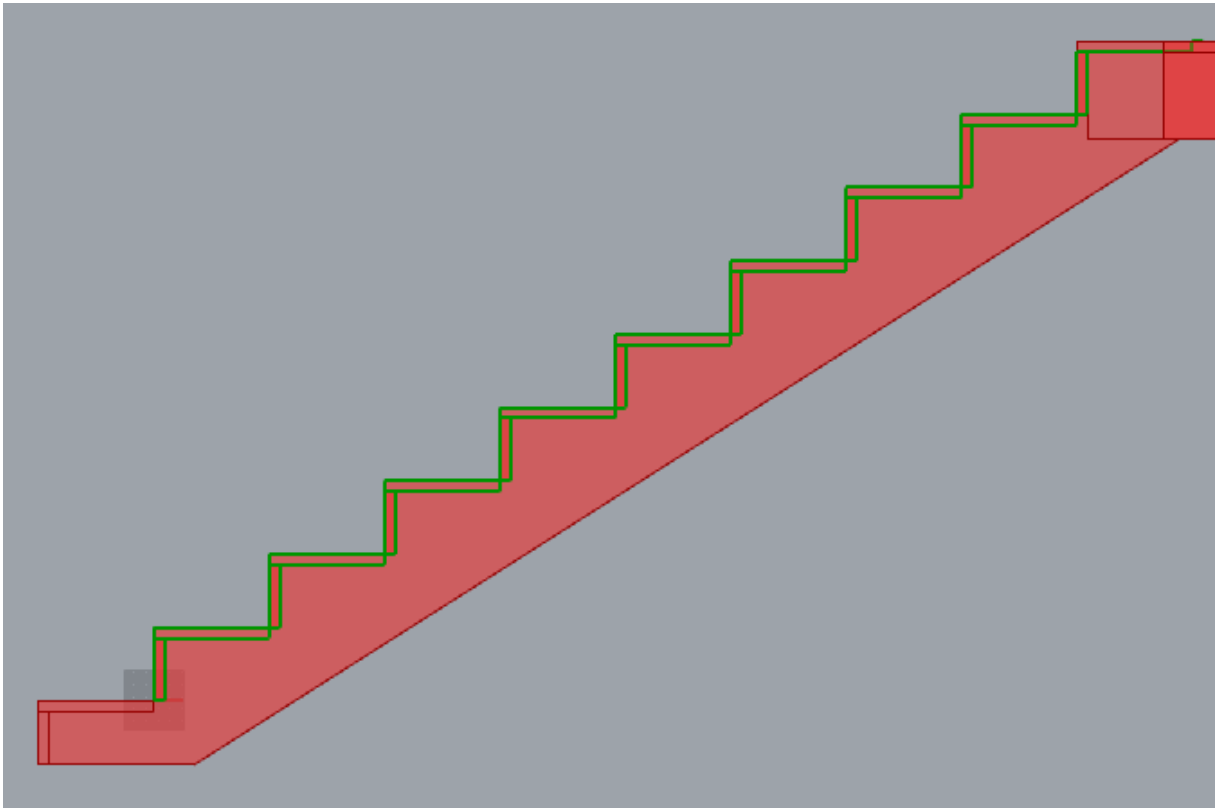


Figure 11 Output in Rhinoceros 3D from the RED group in Grasshopper 3D.

To be able to alter the bottom step of the flight, this step was coded separately. This way new variables were added to ensure a design that is independent of the middle steps. By doing this, it is possible to change and modify the connection between the staircase and slab element. The visual code is given in detail in Figure 12.

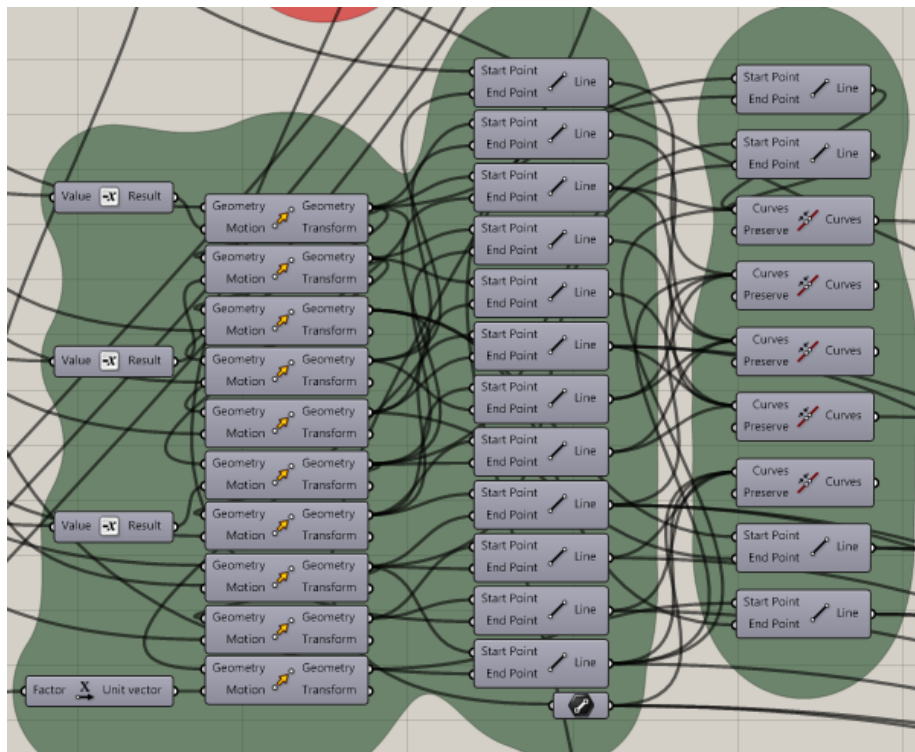


Figure 12 Visual code from Grasshopper 3D for modeling of the bottom step.

Figure 13 illustrates the output of the GREEN grouped coding from the Grasshopper 3D model.

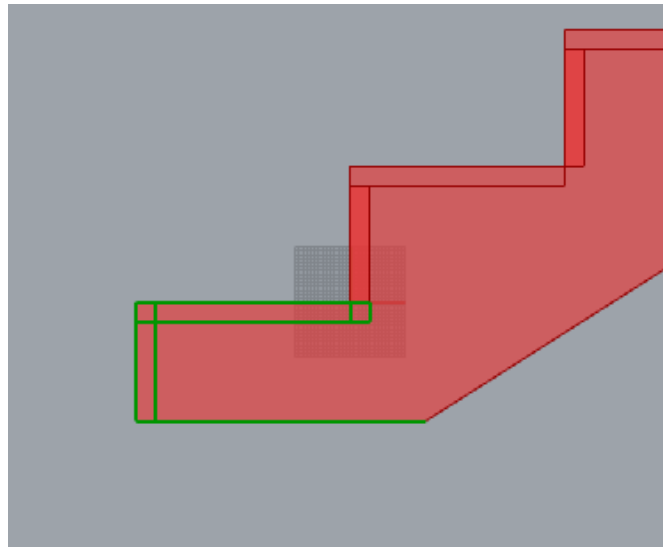


Figure 13 Output in Rhinoceros 3D from the GREEN group in Grasshopper 3D.

The back of the staircase flight is given in Figure 14 and 15. It is simply constructed by a single line made up of two points. To change the angle of the staircase, one has to alter the height of the riser and/or the depth of the step. This is implemented in the code by introducing the Pythagoras formula – where the point of the top landing is subjected to a motion based on the ratio between the riser and depth of the step. This way the angle of the back is adjusted and customized simultaneously as the riser height and step depth is changed – securing proper symmetry.

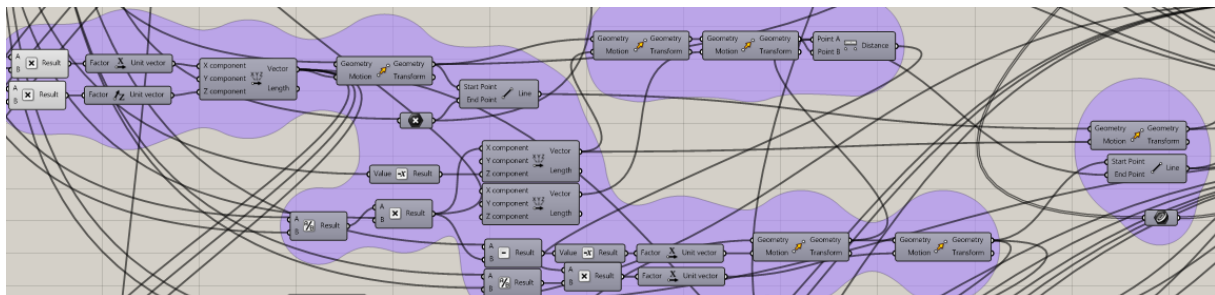


Figure 14 Visual code from Grasshopper 3D for modeling of the back of the staircase diagonal.

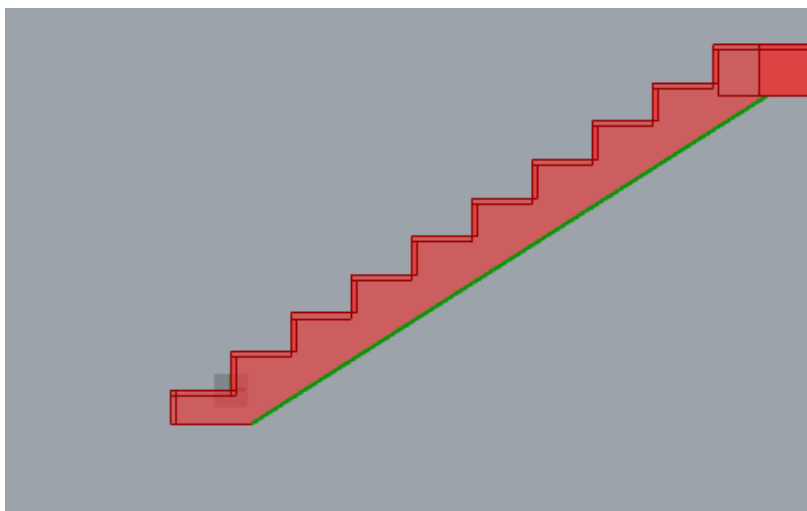


Figure 15 Output in Rhinoceros 3D from the PURPLE group in Grasshopper 3D.



The YELLOW group computes the top landing. It is developed the same way as the bottom step, just opposite and with different variables. This way it is possible to customize both the top and bottom landing without changing both at the same time. The visual code is illustrated in Figure 16 and the output to Rhinoceros 3D is shown in Figure 17.

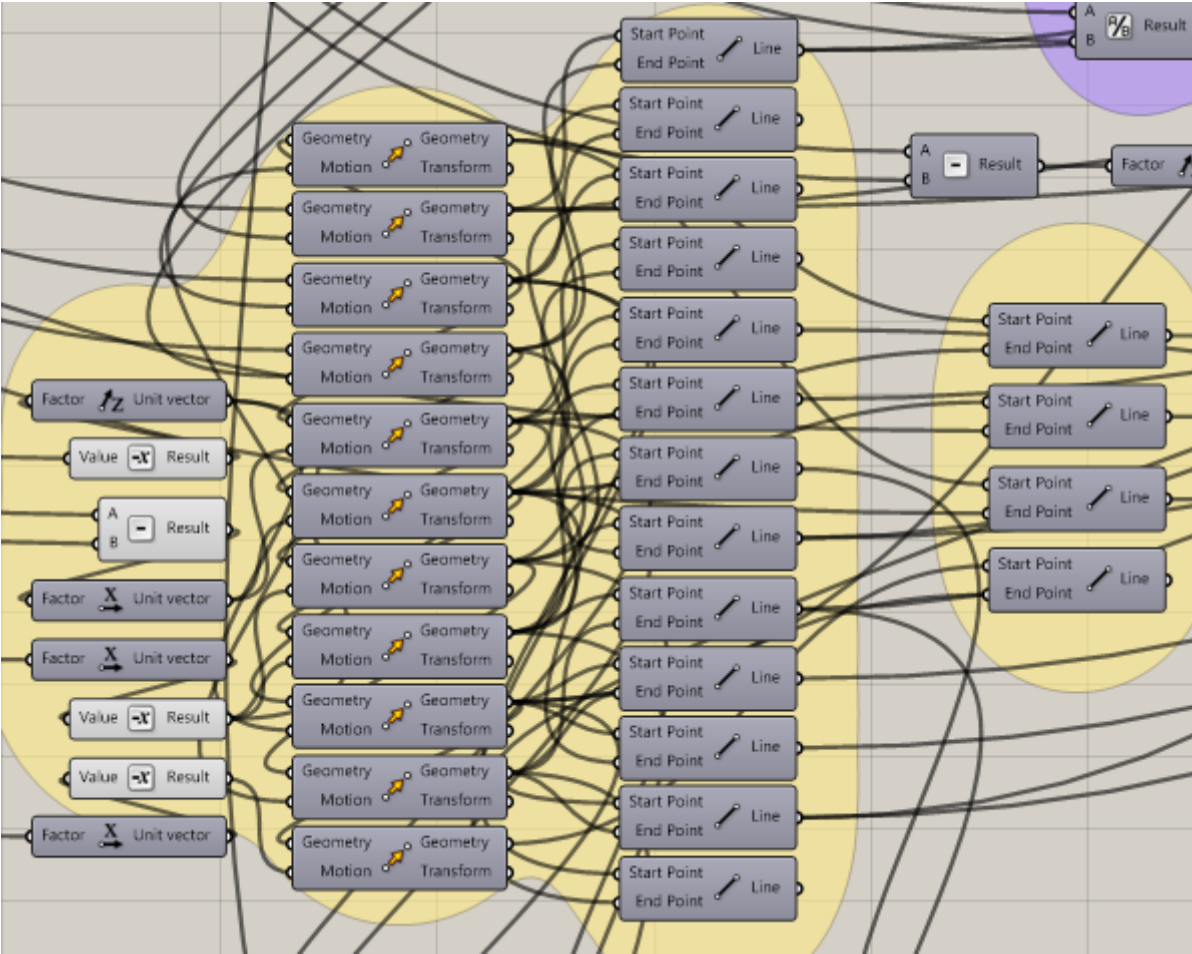


Figure 16 Figure 12 Visual code from Grasshopper 3D for modeling of the top step.

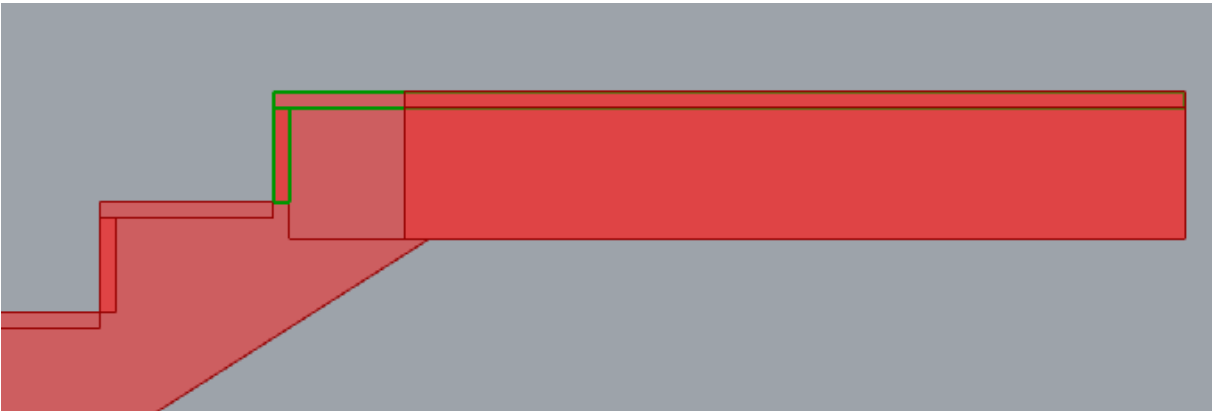


Figure 17 Output in Rhinoceros 3D from the YELLOW group in Grasshopper 3D.

Now that all the necessary points and lines are created, each separate surface of the cross-section can be created. This is done by joining the lines for each surface, illustrated in Figure 19, into a single curve for each surface by the use of the “join curves”-node. Afterwards, all the surfaces are collected into a “Brep”-node(boundary representation) and extruded with the “extrusion”-node. To perform the

extrusion a number slider is created and linked with a unit vector, resulting in a parametric extrusion in the unit vector's direction, as shown in Figure 18.

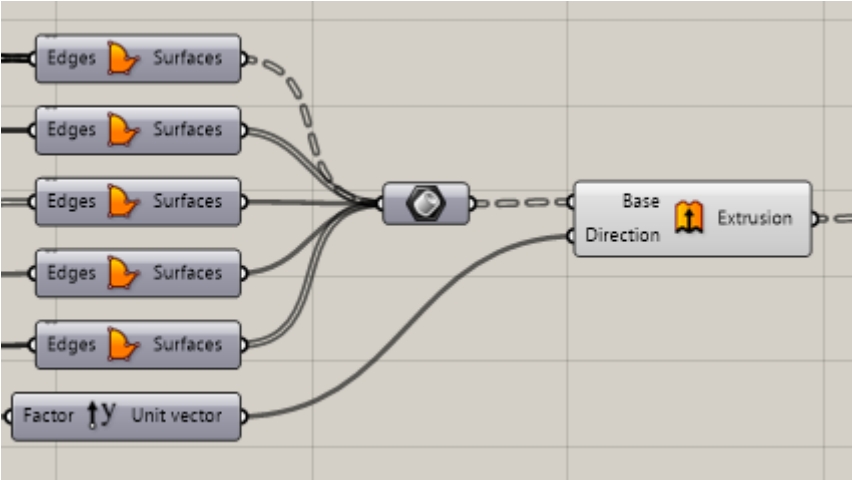


Figure 18 Collection and extrusion of the combined surfaces from ALL of the groups.

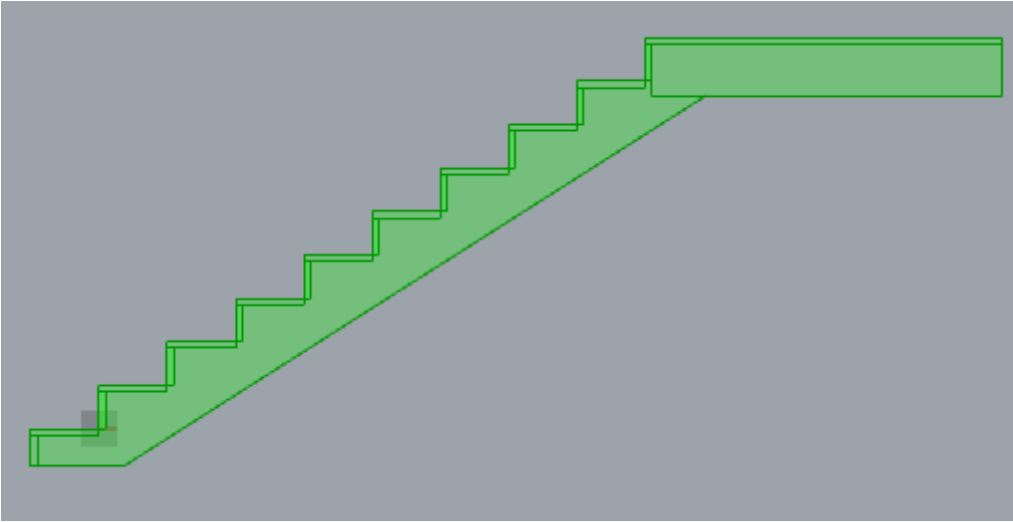


Figure 19 Cross-section of the bottom staircase which is extruded by a parametric width variable.

To model the intermediate landing a separate visual code was implemented, shown in Figure 20. The principles used are the same as for bottom staircase. An important change is the new starting point, which is moved to the end of the top landing. By introducing both a new depth and a new width variable, enables the user to customize the intermediate landing into the preferred geometry. This separate solid can be assigned both to the bottom and top landing, making it very versatile for computer analyzing. The output cross-section plotted in Rhinoceros 3D is shown in Figure 21.

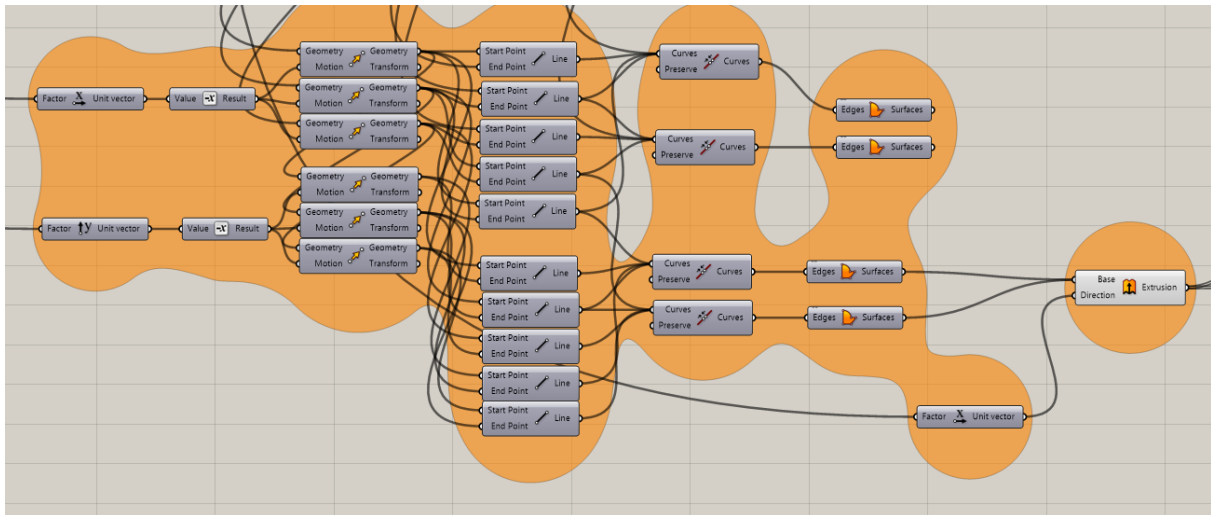


Figure 20 Visual code from Grasshopper 3D for modeling of the intermediate landing.

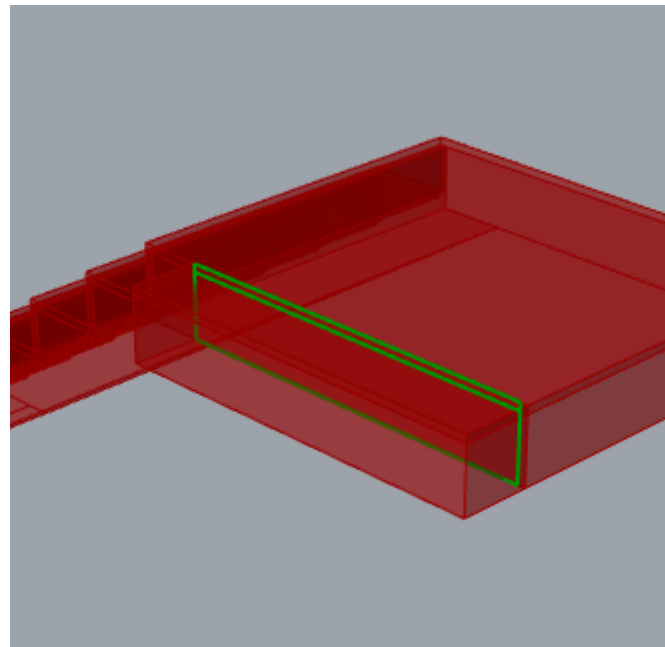


Figure 21 Output in Rhinoceros 3D from the ORANGE group in Grasshopper 3D.

Figure 22 represents the visual code of the top staircase. To compute the top staircase the same visual code was used as for the bottom staircase, with some alterations. First of all, the starting points was moved to the top of the bottom staircase. Secondly, the bottom and top landing were both given specific customization to provide the user the ability to design the joint connections between the landing and surrounding structures. This was an comprehensive job, as the developed algorithm were getting more and more advanced and interlinked. Meaning that a small alteration on one component could have a effect on another component – which was undesired. This was especially a challenge when modeling the top step and back of the staircase. By dividing these components into smaller components and using the ratio between the lengths and heights, it was possible to compute an algorithm were parametric changes could be done – without altering other geometry properties than the desired one.

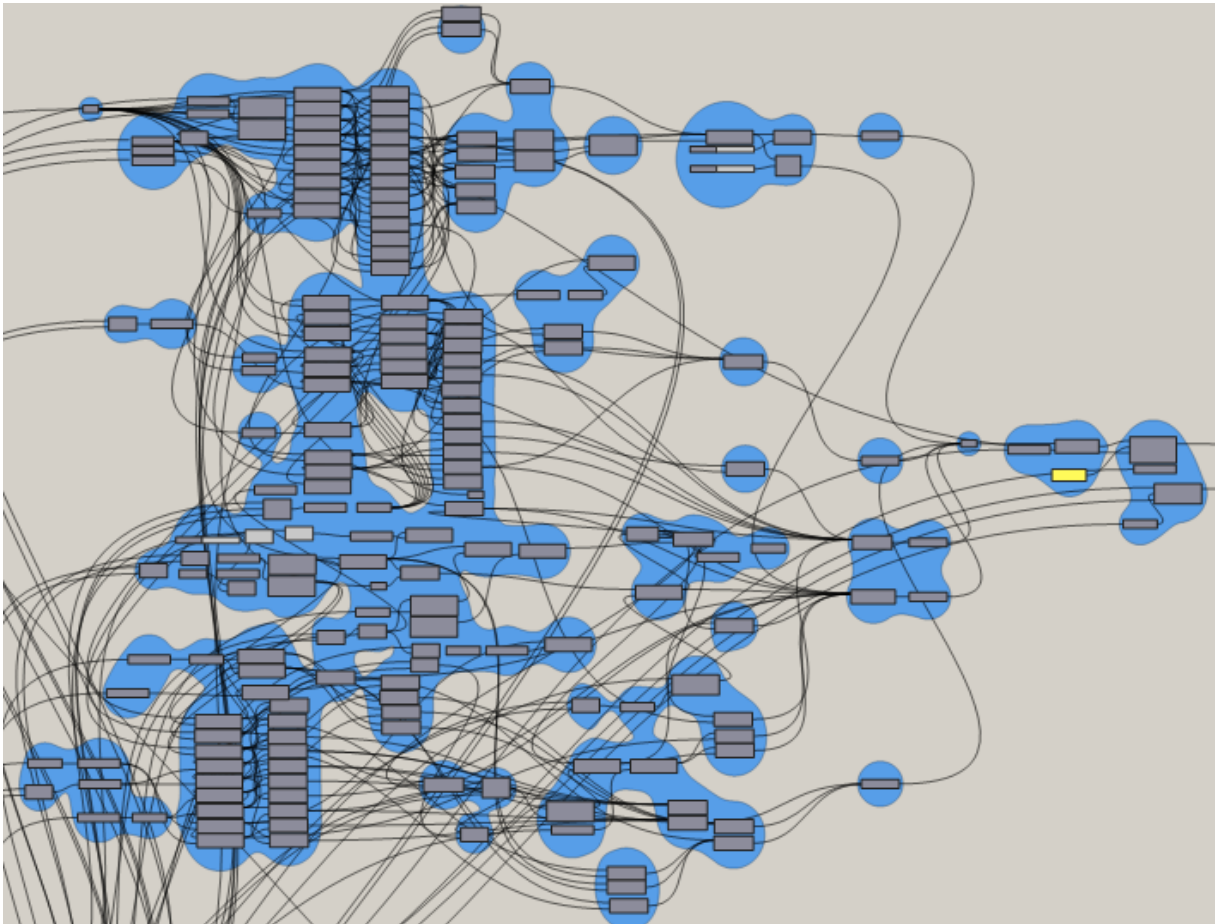


Figure 22 Visual code from Grasshopper 3D for modeling of the top staircase.

Figure 23 illustrates one the visual code for just the top step, highlighted in Figure 24.

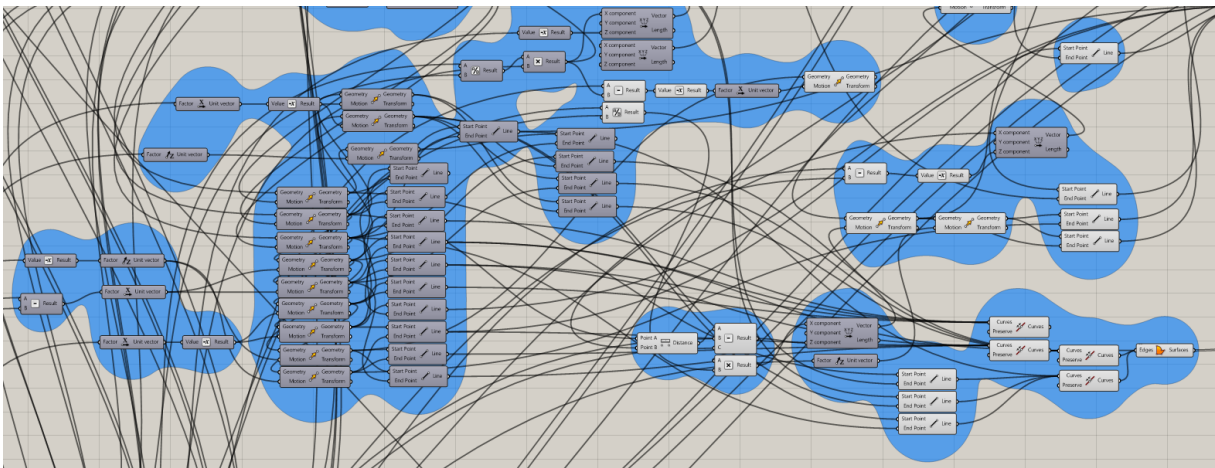


Figure 23 Detailed visual code for the customization of the top step of the top staircase.

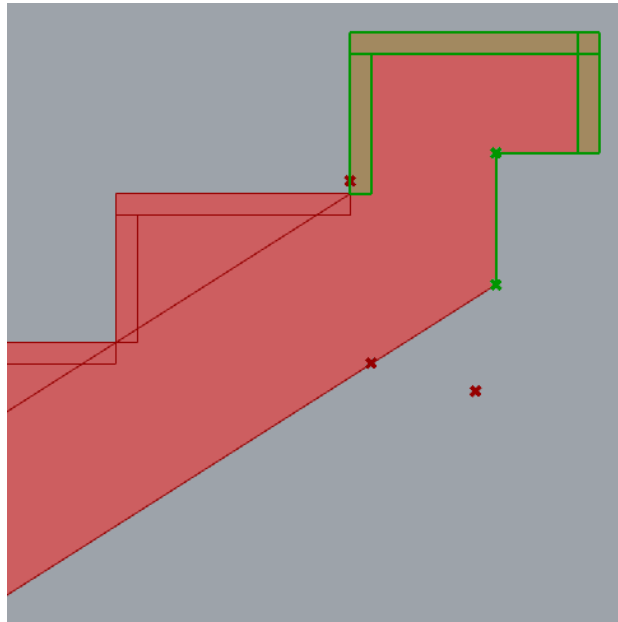


Figure 24 Output in Rhinoceros 3D from part of the BLUE group in Grasshopper 3D.

Finally, the top staircase geometry is rotated 180° by the use of “geometry rotate”-node and moved into place by the “move”-node, as shown in Figure 25. Attaching the bottom landing of the top staircase to the intermediate landing. The final resulting geometry used in our Abaqus analysis is shown in Figure 26.

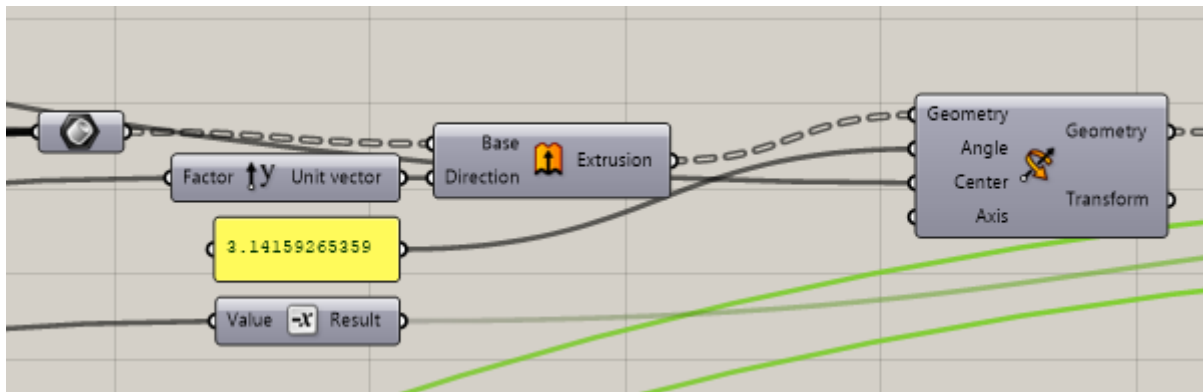


Figure 25 Visual code from Grasshopper 3D that moves and rotates the upper staircase.

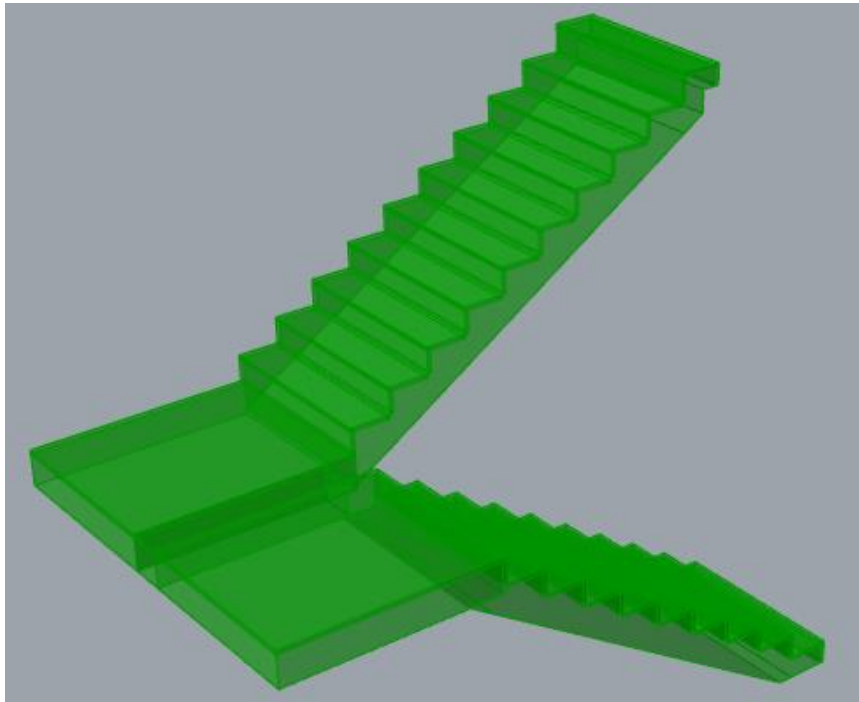


Figure 26 Output of the combined output from the bottom and top staircase, together with the intermediate landing.

In Figure 27 the resulting parametric variables are given. The number of variables enables the user to freely design a staircase geometry and customize it for specific project needs. A condition for the algorithm to work properly is that reasonable values have to be inputted, if not, the algorithm will fail to compute a legitimate geometry. For example, the only variable that can be set to zero without any problem is the concrete cover, if other variables are set to zero – the algorithm will fail to compute a geometry. Another example could be to increase the console thicknesses unrealistically high, resulting in a console height larger than the original step height. This is not considered a problem, but for a new user – it could take some time to get used to how the algorithm is built up and how to work it properly. To conclude, the parametric model is easy to use – once the understating and effect of the different input variables are understood and a realistic staircase is modeled.

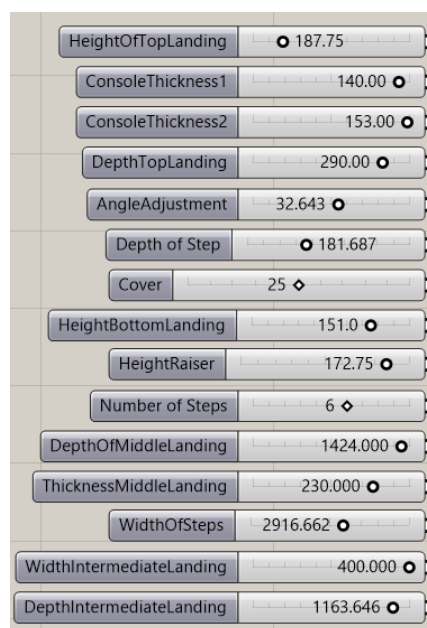


Figure 27 Parametric variables of the model

Figure 28-32 highlights some of the parametric properties of the developed model. The results are given as the output in the Rhinoceros 3D draughting environment.

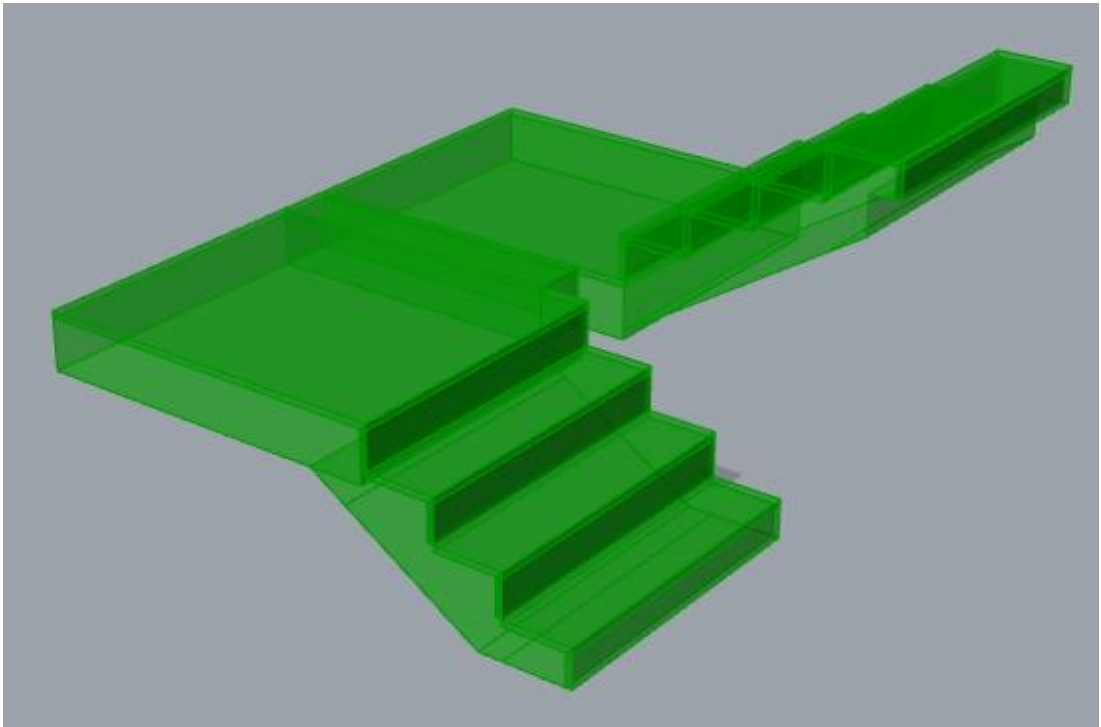


Figure 28 Fewer number of stairs.

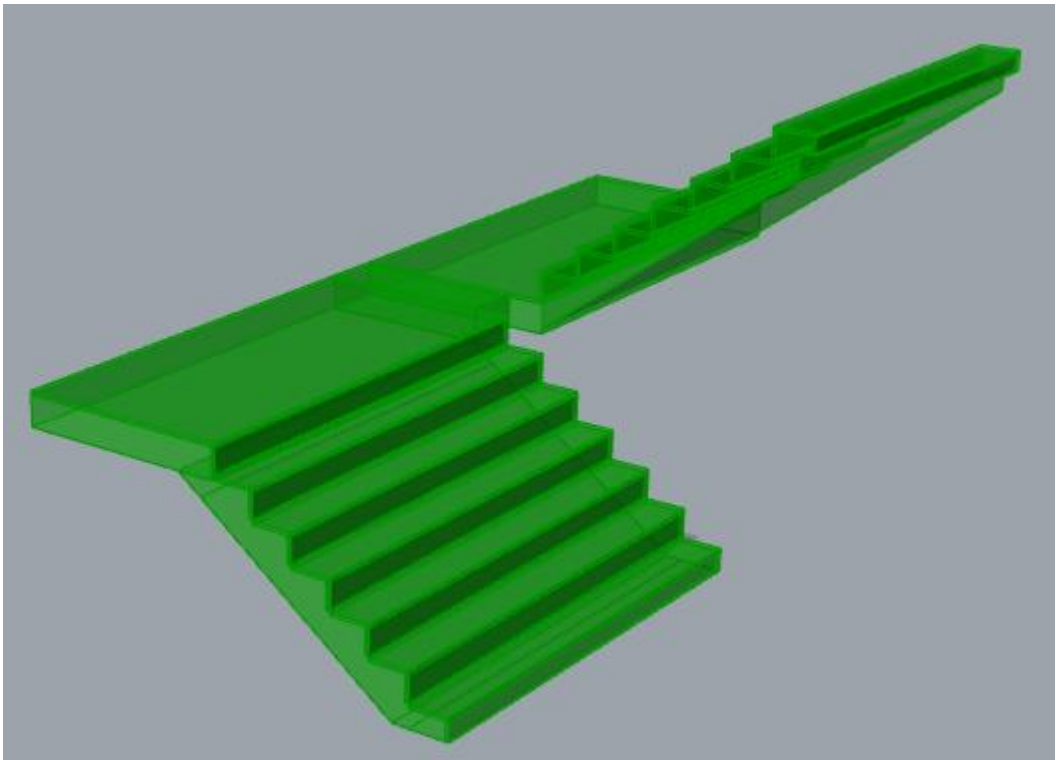
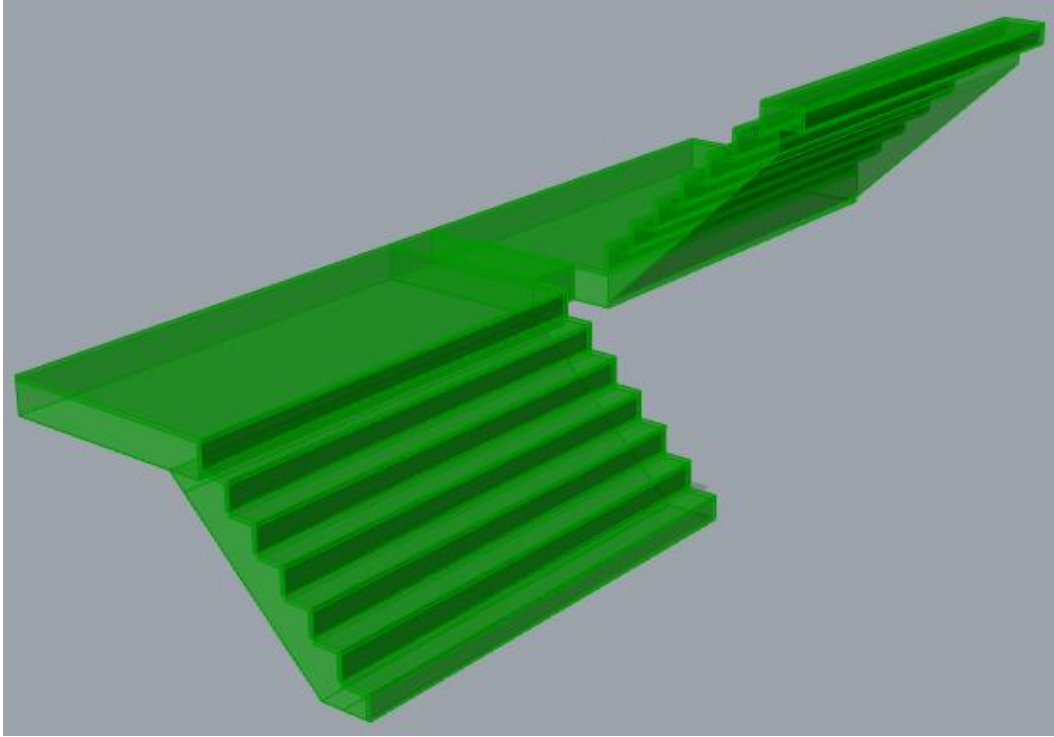
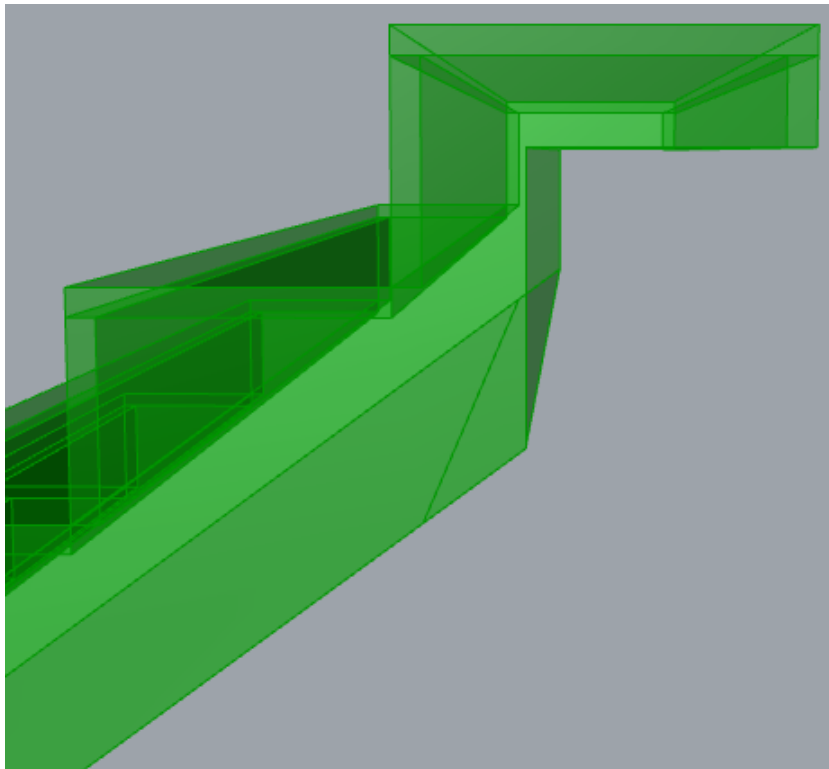


Figure 29 Increased step width and decreased number of stairs.



*Figure 30 Increased width and decreased step depth.*



*Figure 31 Altered top step.*



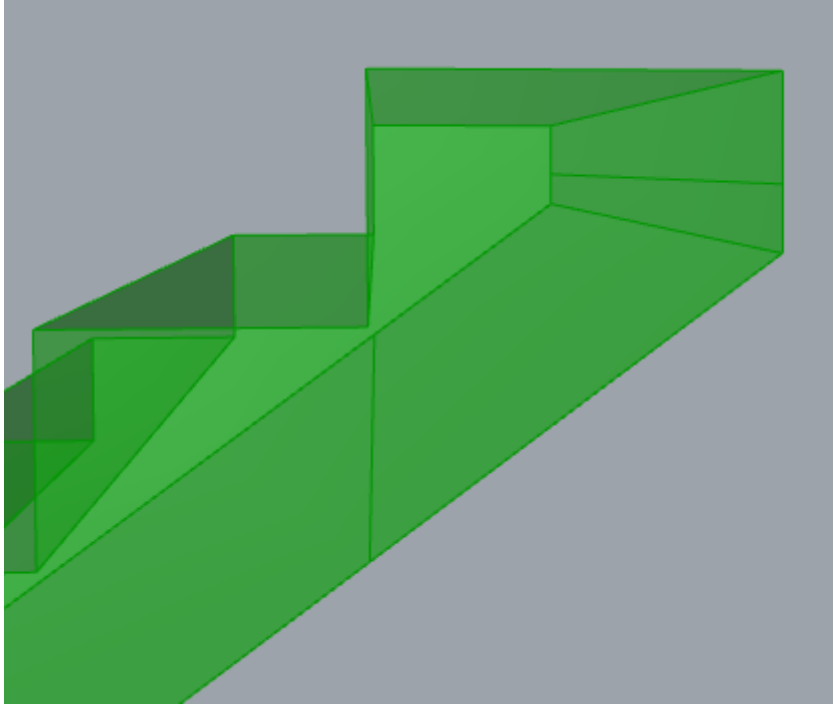


*Figure 32 Altered top step.*

## **C 3D printing of formwork and staircase models**

# 3D printing of formwork and staircase models

The authors found it very interesting to look into the process of 3D printing to be able to create 3D models of both the topology designs and formworks – together with increasing the knowledge and gain experience with the production method. This was done due to the recommendations from several papers which concluded that different types of additive manufacturing (3D printing) is a viable option for printing formworks. In addition, it has a huge potential for further development combined with new technology. Due to the organic geometry of TO, it is necessary to be creative in ways of manufacturing, and 3D printing seems to be the most promising – as of now.

The 3D printer used in this paper is a “Creality CR-6 SE 3D-Printer”, which is a Fused Filament Fabrication (FFF) technology printer, illustrated in Figure 1 and 2. This technology introduces filament into a so-called hot-end, which melts the filament in the nozzle and places by extrusion the melted filament onto the construction bed. The material used is a Polyactic Acid (known as PLA), which is a thermo plastic polymer that melts with temperatures close to 200°C, depending on type of PLA used. In regards of capacity, Creality CR-6 SE 3D-printer has a printing volume of 200x200x235mm.



Figure 1 Creality CR-6 SE 3D-Printer.

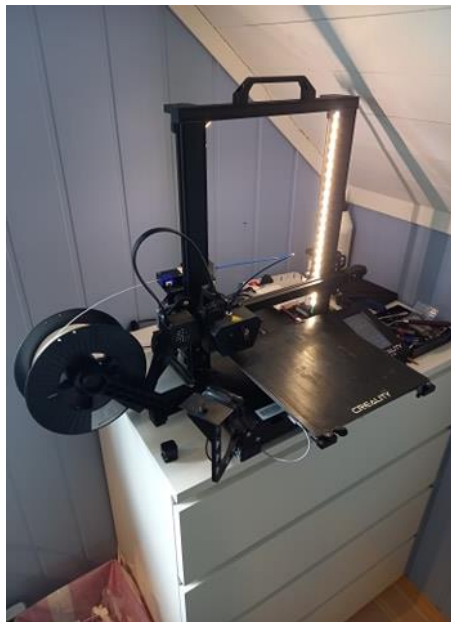


Figure 2 Creality CR-6 SE 3D-Printer.

To be able to print the different designs and geometries, the output files from Abaqus are exported as .STL files. STL-files are mesh files, and it is therefore necessary to convert the Abaqus output files into more a delicate file format that can be used for the 3D printing manufacturing. Due to the lack of export options in Abaqus, this proved to be more demanding than anticipated. But, by the use of Autodesk Fusion 360, it was possible to convert the mesh-file into a BRep (boundary representation), in other words a solid (ACIS filetype .sat) – which is exactly what is needed for the manufacturing process. The process is highlighted in Figure 3 and 4.

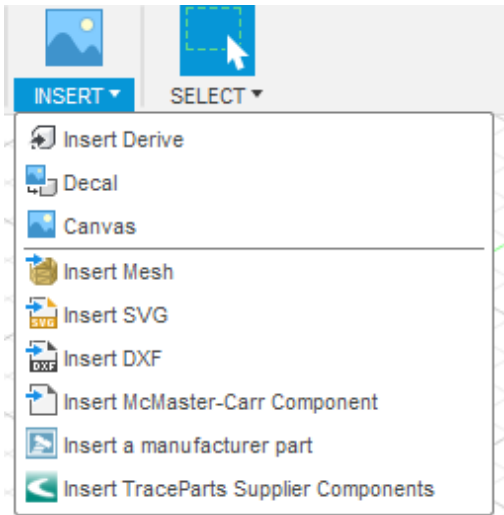


Figure 3 Fusion 360 mesh to BRep.

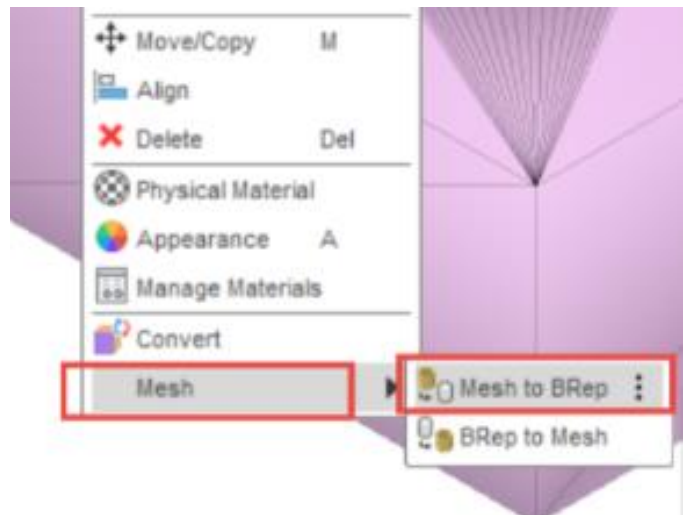


Figure 4 Fusion 360 mesh to BRep.

To begin with, the plan was to alter and do a little finish on the results from the Abaqus geometry, but this idea was skipped due to the magnitude of the files. Models up to 50MB proved to be inefficient and way to time consuming due to the heavy computation time. It was therefore decided to skip this redesign phase, and simply print the raw output from Abaqus due to time limitations.

The converted file format(.sat) was then imported to a 3D printing software called “Ultimaker Cura”, which integrate very well with CAD software. This software has a huge range of possibilities, which can easily be applied through custom settings. The custom settings used for this thesis are given below in Figure 5-9.



Figure 5 Print settings.



Figure 6 Print settings.

Quality		
Layer Height		0.2 mm
Initial Layer Height		0.2 mm
Line Width		0.4 mm
Wall Line Width		0.4 mm
Outer Wall Line Width		0.4 mm
Inner Wall(s) Line Width		0.4 mm
Top/Bottom Line Width		0.4 mm
Infill Line Width		0.4 mm
Initial Layer Line Width		100.0 %
Walls		
Wall Thickness		0.8 mm
Wall Line Count		3
Order Inner Walls By Inset		<input checked="" type="checkbox"/>
Horizontal Expansion		0.0 mm
Top/Bottom		
Top Thickness		0.8 mm
Top Layers		3
Bottom Thickness		0.8 mm
Bottom Layers		3
Infill		
Infill Density		20.0 %
Infill Line Distance		6.0 mm
Infill Pattern		Cubic
Infill Line Multiplier		1
Infill Overlap Percentage		10.0 %
Infill Layer Thickness		0.2 mm

Figure 7 Print settings.

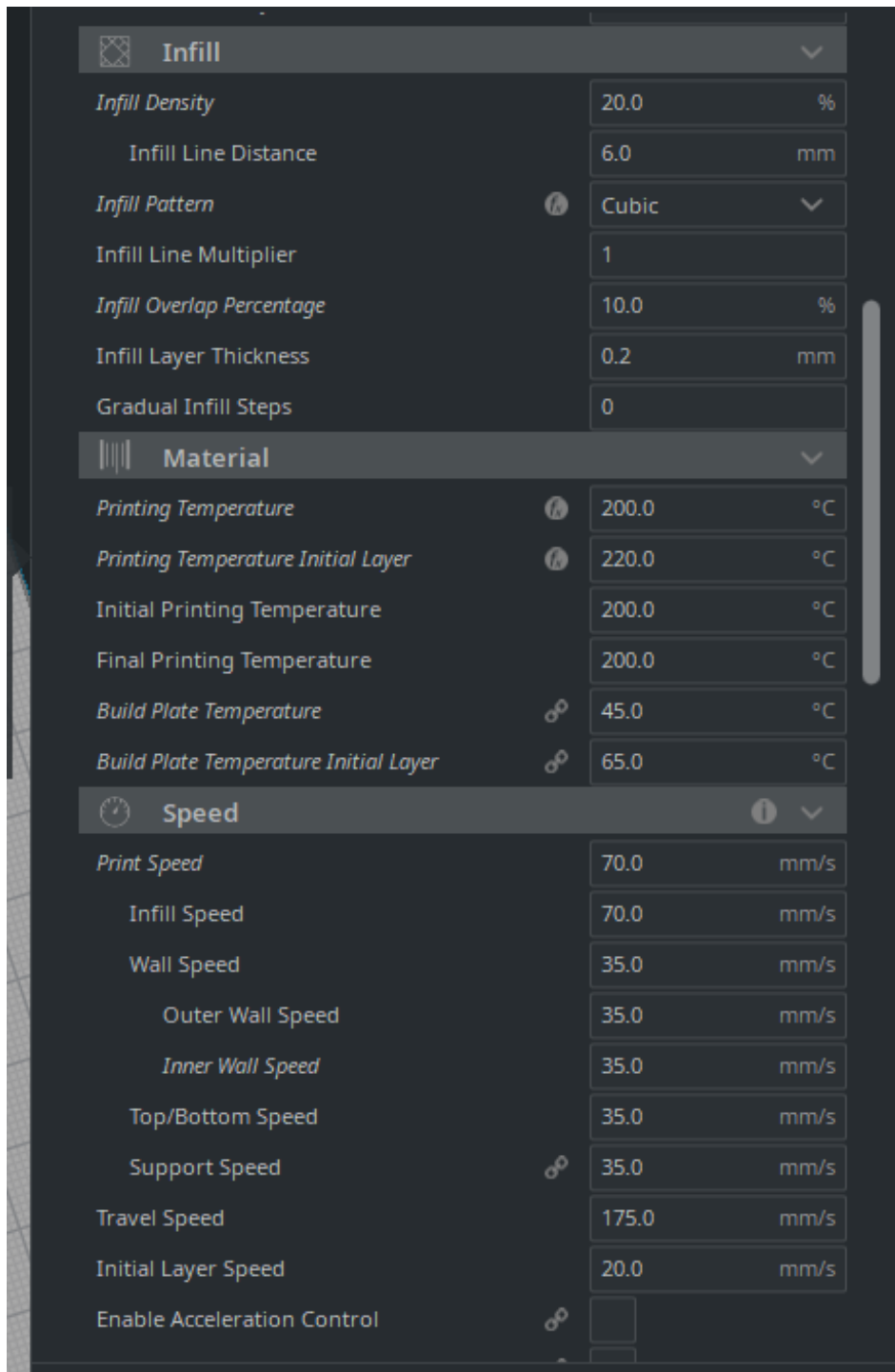


Figure 8 Print settings

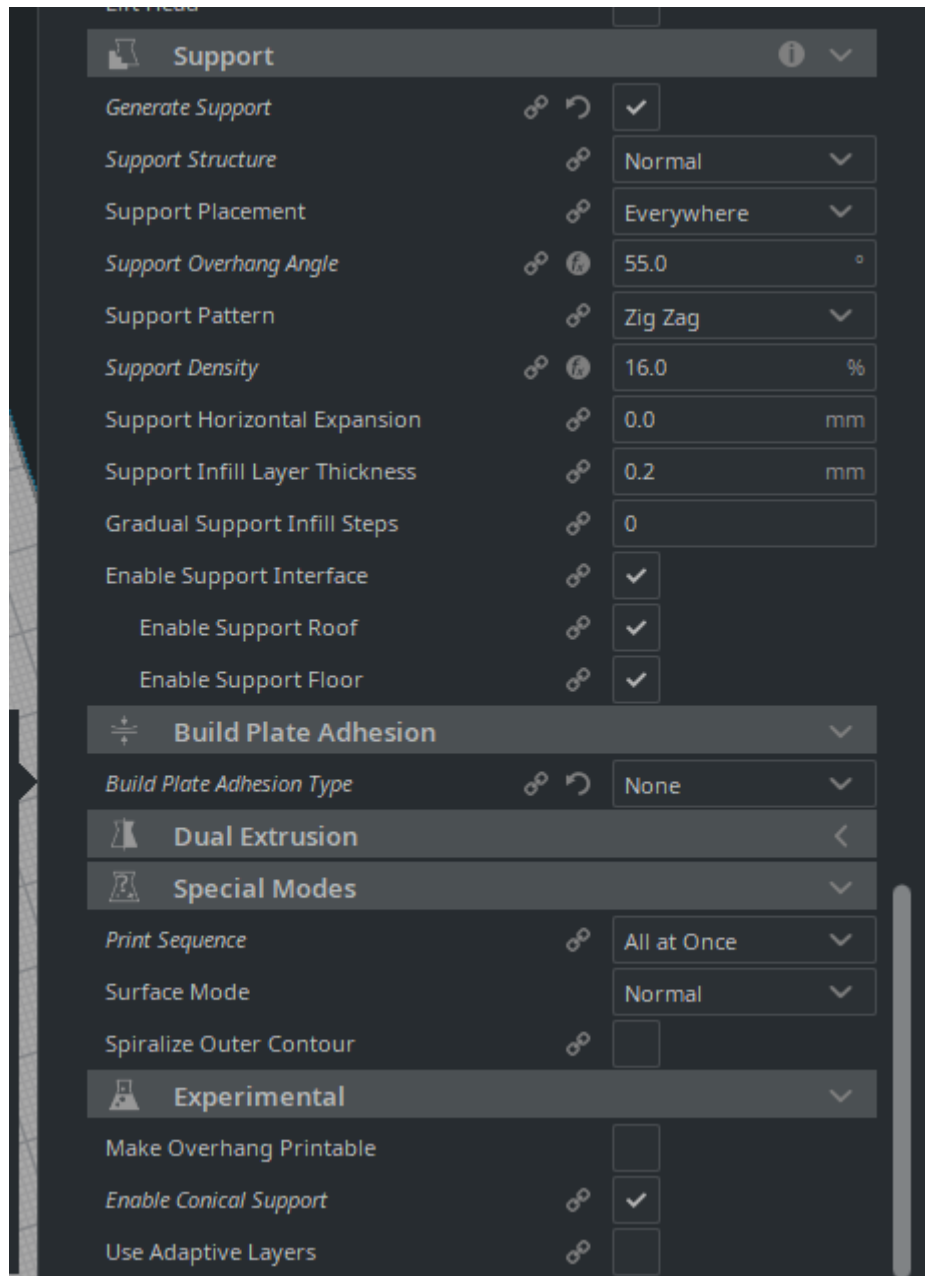


Figure 9 Print settings.

After the geometry is imported into Ultimaker Cura, the model can be sliced into horizontal layers based on the customized settings. The layers are then described by coordinates, which is the input that is exported to the actual 3D printer (“Creality CR-6 SE 3D-Printer”). This information is the pathway for the 3D printer, which is first read, then processed and executed. The 3D printer can move the nozzle in x- and y-direction and control the elevation by lifting and lowering the construction bed. One by one the layers are printed, resulting in a gradually growing structure as the construction bed is lowered.

First, two small 3D prints of a square shell and a round shell were executed to better be able to customize the settings in Cura. Figure 5 - 11 shows both the printing and settings used for the tests. As can be seen of the pictures, a feed rate and flow rate of 100% was used and an 0.16 offset in the z-direction – providing enough height for the 3D printer, so that the nozzle does not collide with the printed filament on the construction bed. In addition, the nozzle temperature was set to 200°C – which proved to be working well with the chosen light grey PLA.



Figure 10 Test print.

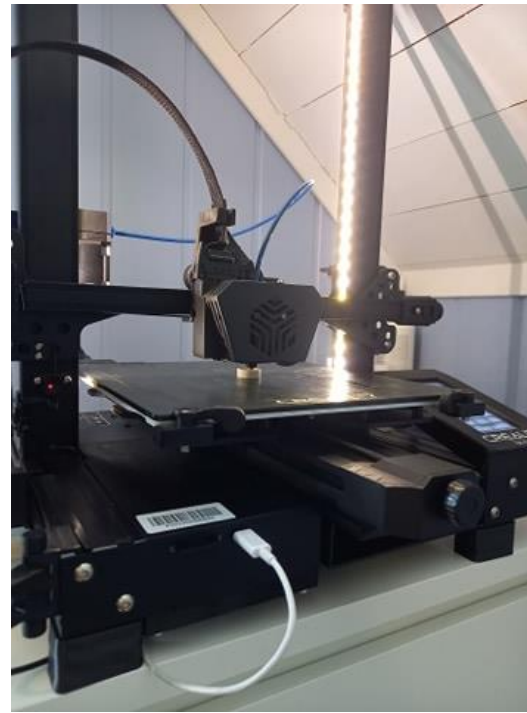


Figure 11 Test print.

To be able to print the staircase models and formworks, some support structure needed to be printed together with the design. Due to the fact that the 3D printer is printing PLA horizontally, it is limited to print angles less than  $45^\circ$ . Angles with a gentler slope will create a problem for the 3D printer, since it will be hard to provide enough support for the freshly printed and soft filament – resulting in inaccurate results and worst case a print error. To fix this problem, a setting called “generate support” was customized (as shown in Figure 9) and the result is shown in Figure 12 - 15. This way it is possible to print the models without problem, and easily remove the supporting structure after the print is finished.

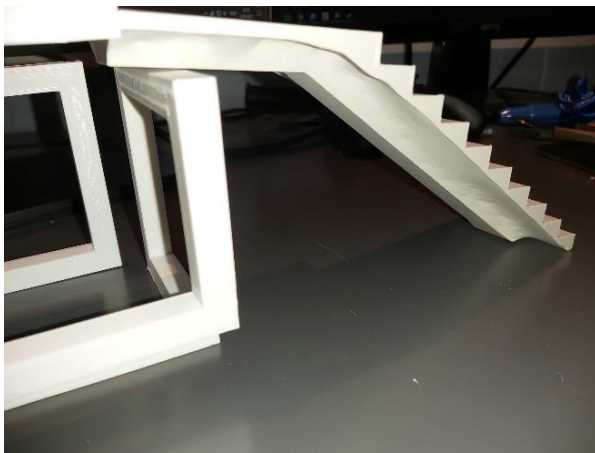


Figure 12 Staircase 1.

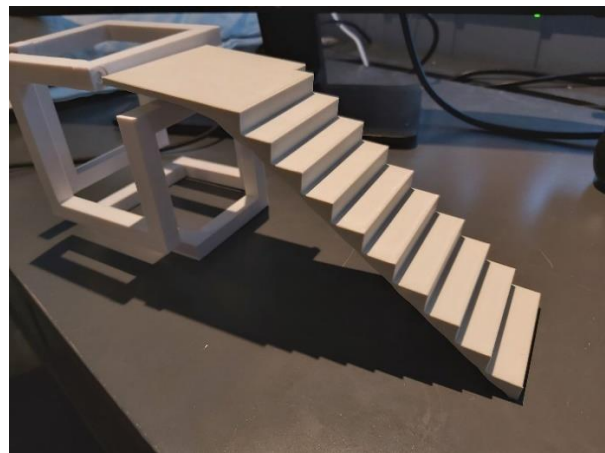


Figure 13 Staircase 1.





Figure 14 Staircase 1.

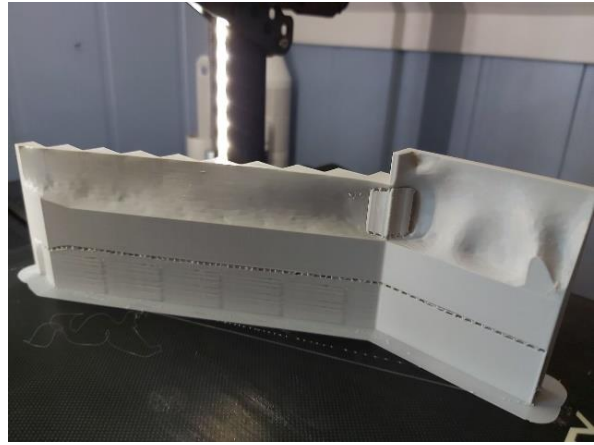


Figure 15 Staircase 1.

Another printing setting is the infill density and pattern. This setting enables the user to customize both density and pattern of the infill – which provides the rigidity of the 3D printed structure. The reason for doing this is to save material when printing. The infill chosen is not relevant for formwork production, since it is already so thin that it needs all the strength it can to sustain its shape and not deform when loaded. So in reality, the formwork will be printed without infill to ensure a higher stiffness. The infill was set to 20% of the original volume and is shown in Figure 16 – 17, and the finalized print is shown in Figure 18.



Figure 16 Staircase 1.

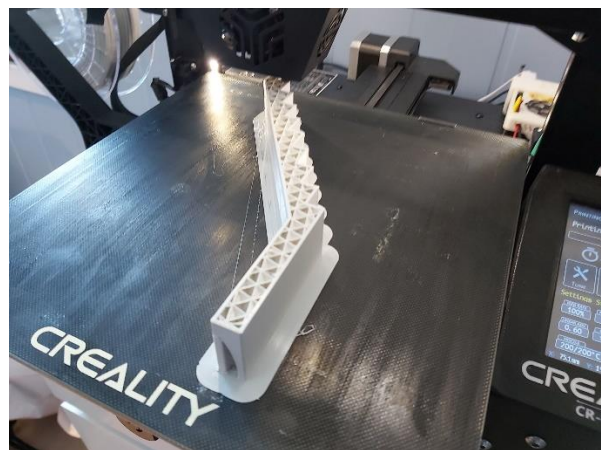


Figure 17 Staircase 1.

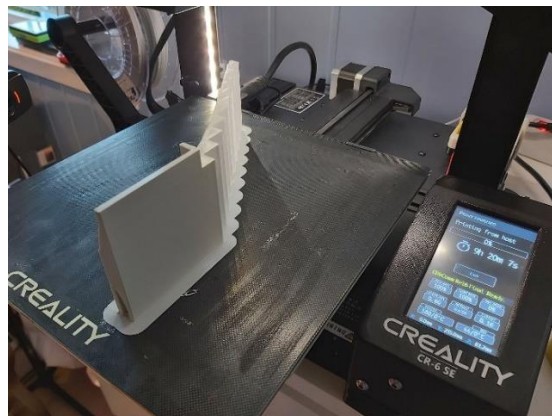


Figure 18 Staircase 1.

Another staircase design was also printed, highlighted in Figure 19 - 27. The same customized settings were used for this model as for staircase 1.



Figure 19 Staircase 2.

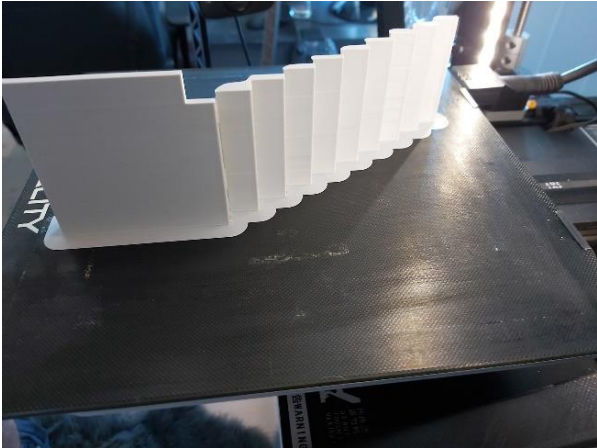


Figure 20 Staircase 2.

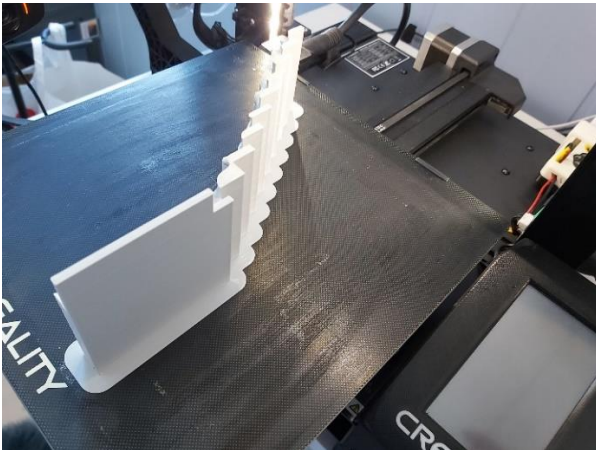


Figure 21 Staircase 2

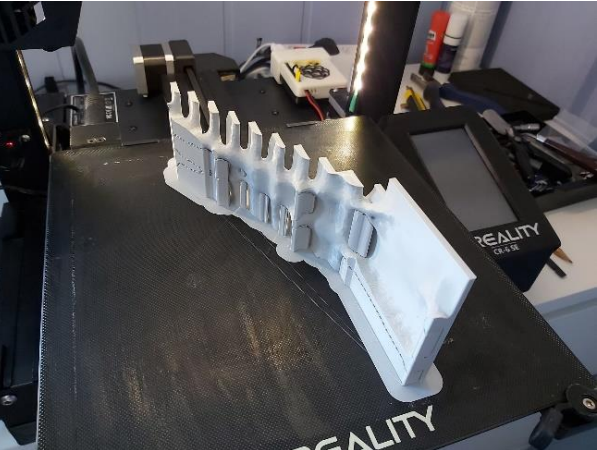


Figure 22 Staircase 2.

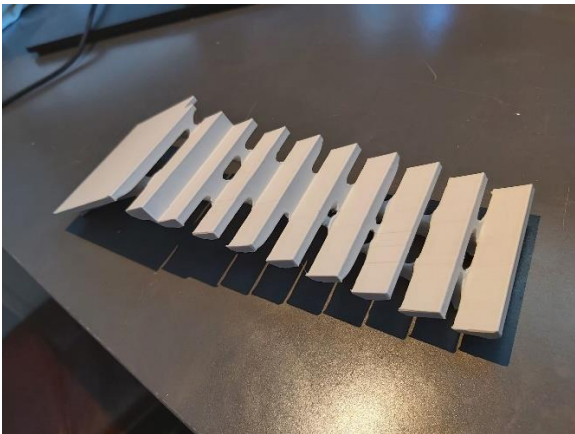


Figure 23 Staircase 2.

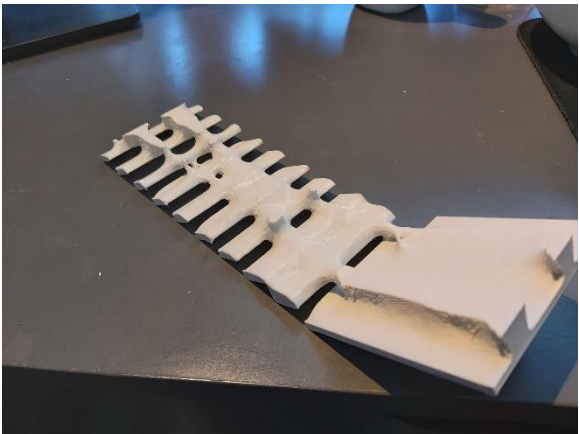
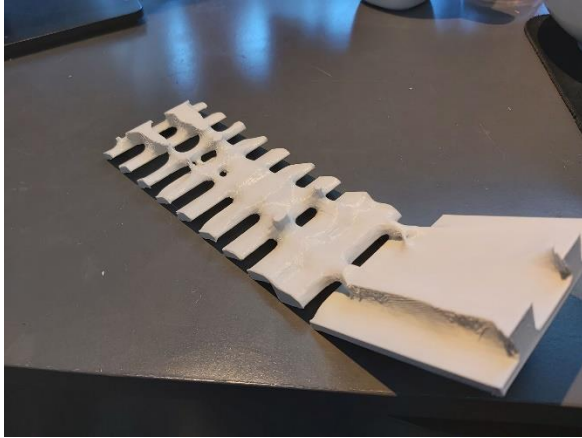
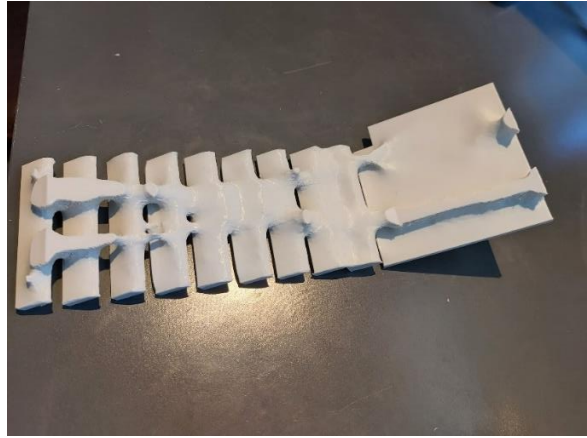


Figure 24 Staircase 2.



*Figure 25 Staircase 2.*



*Figure 26 Staircase 2.*

From the pictures it is clear to see that there are no holes in the both the landing and the steps. This, together with the flat ends – results in a fully functional staircase with no holes in the pathway. But the pictures clearly visualize the holes in the risers, which could be a slight safety problem – due to people getting their feet stuck together with the possibility of things dropping down in between the steps. This is something to evaluate, but due to little restrictions in design development, this was chosen to freely utilize the full potential of the TO algorithm – making the most organic shape.

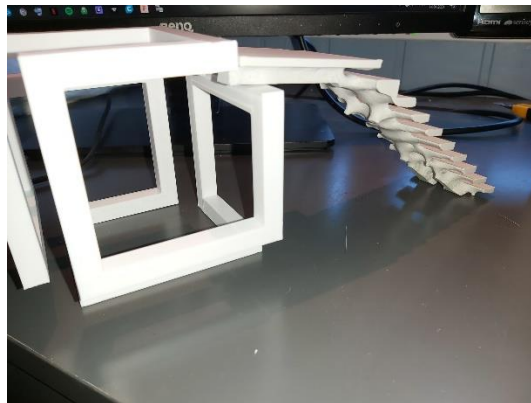


*Figure 27 Staircase 2.*

As mentioned, the authors really wanted to create a couple of formworks to increase the understanding and knowledge of the production method. There are many different approaches but due to time limitations the authors needed to choose one method and stick with it. It was decided to create a formwork of two steps inside of one formwork – to visualize the concept better. Due to size limitations on today's 3D printers, it is not possible to print one single formwork and it was therefore also realistic to divide the staircase formwork into several small formworks that is to be connected.

By the use of Fusion 360 the staircase was split into several smaller pieces, by the cutting tool. Furthermore, a rectangle solid was created and placed around the part to be molded. The staircase part was then used to cut the solid – resulting in a formwork as shown in Figure 28 – 31. This is a conservative way of creating a formwork, as it results in unnecessary thick formwork in some areas. This could also be done by the use of Cura's rendering function and which could result in material savings on the formwork print. But due to time limitations and lack of experience with 3D printing, it was decided to choose the first method – which illustrates the principle in a sufficient way.

The formwork was printed in 6 parts, where each part was assigned with holes and/or connection piers. This was done to be able to assemble the formwork pieces into one single formwork and illustrate the concept. In reality the connections would have to be locked in a better way to secure proper fastening and prevent unwanted failure and/or deflections.

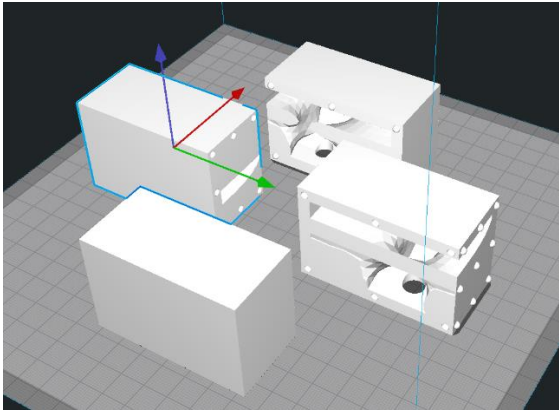


Figure 28 Formworks.

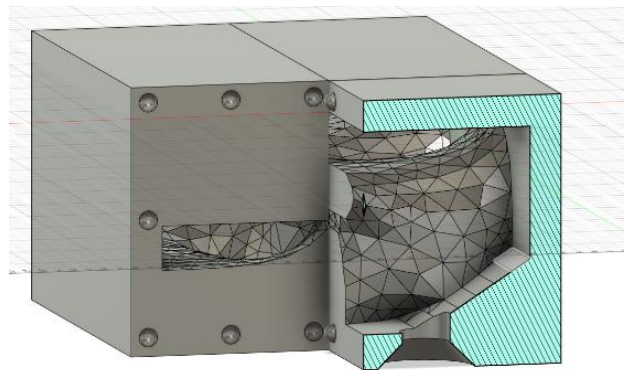


Figure 29 Formworks.

To illustrate the usability, the formworks were assembled and introduced two holes, which can be used both for casting and air outlet. This is an important feature when casting concrete in closed formworks, which together with vibration secures a good concrete cast that fills the whole formwork and prevents unwanted void spaces. There may still occur small air bubbles, but larger air pockets that have an effect on both strength and concrete cover will be prevented as long as the aggregate used is small enough. It is very important that the aggregate size is smaller than the formwork details, so that the concrete is able to fill all the voids inside the formwork and not create plugs. The more advanced the details are, the finer aggregates must be applied for manufacturing. In this case, a finer aggregate size is necessary for the casting of staircase 2, than for staircase 1.

In reality the 3D printed formwork would be a much thinner shell and would need support when casted. The 3D printed formwork is really light and are easy to assemble and transport – but there is a drawback that needs to be assessed and that is the rigidity of the formwork. Concrete is a dense and compact material with a density of  $2400 \text{ kg/m}^3$ , and will cause large transversal forces from the hydrostatic pressure when casting. These forces will increase in strength as the casting volume increases, and can cause strength problems for the formworks. To be able to cast the whole staircase in one go, it is necessary to strengthen the formwork with external scaffolding – which increases the cost and labor work. In addition, it could be necessary to cover the 3D printed formwork in sand to minimize local deflections. One way to reduce the risk of deflection is to cast the staircase structure in components and assemble together afterwards with for example post-tension reinforcement.

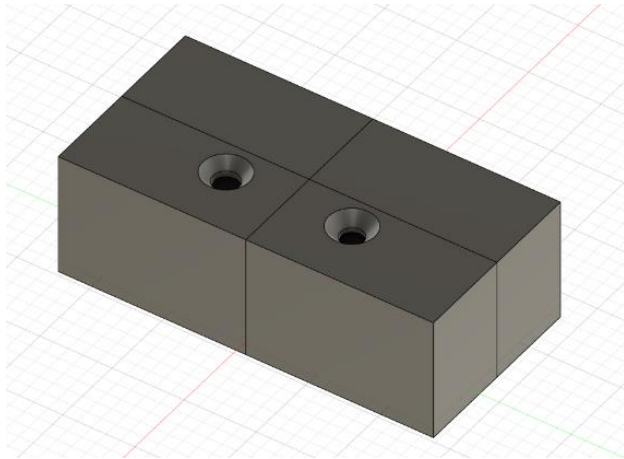


Figure 30 Formworks.

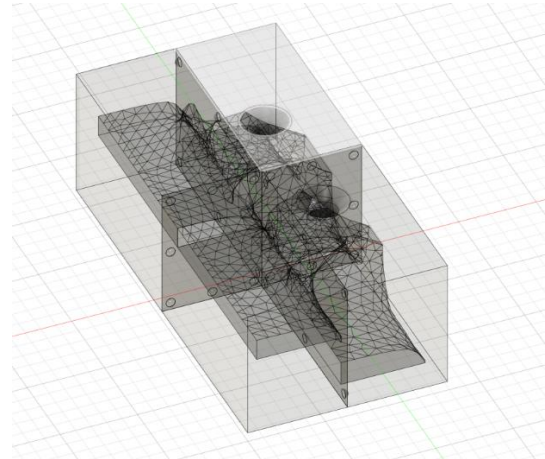


Figure 31 Formworks.

The manufacturing time of the formworks is another important aspect of this method. To be able to create a functioning formwork it is necessary to develop a more delicate connection system to assemble and secure the positioning of the different formwork elements. By the authors experience this seemed to be a time-consuming procedure (which of course would be shortened with experience). In addition, the actual manufacturing (3D printing) is also very demanding. The time it took to print the two different staircase models was between 9 – 10 hours, as shown in Table 1. These printing time results are for two small, non-realistic sized, staircase models. In reality, formworks are printed in a 1:1 ratio with a degree of detail specified by the user. Both complexity, detail, size and the ability to support its self-weight during 3D printing is important in regards to printing time. Based on current research in this field such as “3D-printed formwork of bespoke concrete stairs” by Jipa. et. al., it is found that the manufacturing time for a formwork for a single step is estimated up to 48 hours.

Model	Print time
Staircase 1	9h 20min
Staircase 2	9h 48min

Table 1 Printing time.

3D printing has a huge potential, and enables huge flexibility and freedom in design. But it needs further development to increase the usability and both lower the manufacturing time and cost.

## **D Calculations of staircase according to Eurocode 2**

# Design verification of the reference staircase based on Eurocode and different regulations.

The reference staircase obtained from the Contiga AS is remodelled by Rhinoceros 3D and Grasshopper 3D. The staircase dimensions presented in *Table 2* are compared and verified according to the regulations presented in the *Table 1.*, which are extracted from TEK17 and from British standard, named as Building regulation 2010 (regulations2010building).

*Table 1: Regulations for design of staircase.*

Different regulations for design of staircase		
Description	Value	Unit
Straight flight of stairs shall have minimum clearance width	1200	mm
Straight flight of stairs shall have minimum clearance height	2100	mm
Maximum height difference for landing requirement	3300	mm
Maximum pitch of private stairs	42	deg
Maximum clearance width (staircase width)	1800	mm
Maximum number of risers allowed in a straight line	36	nos
Minimum riser height	150	mm
Maximum riser height	220	mm
Treads/going in a walking line shall be minimum	250	mm
2*rise + going	550-700	mm
All landings should be level		
Top and bottom landing should be provided		

Table 2: Dimension of reference staircase.

Dimension of staircase from drawing			
Riser (R)	172.75	mm	
Tread (T)	272.00	mm	
Height of floor (H)	1554.75	mm	
Length of single flight	2448.00	mm	
Width of landing	1405.00	mm	
Width of flight	1200.00	mm	
Length of landing	1424.00	mm	
2*Riser + Tread = 550-700mm	617.50	mm	within limit
Number of risers on each flight	9.00	No.	n = H/(R)
Number of treads on each flight	8.00	No.	
Effective length of flight and landing ( $L_{eff}$ )	2448.00	mm	

Design working life of the staircase is taken as 100 years according to table 2.1 in Eurocode 0. Corrosion induced by carbonation / Concrete inside building with low air humidity is assumed as environmental exposure of the staircase, so from table 4-1 in Eurocode 2, according to environmental condition XC1 is the exposure class.

Normal weight concrete of the characteristic strength 30 N/mm<sup>2</sup> (B30) is taken as the concrete grade. Density, design compressive- and tensile-strength are taken from the Eurocode 2 and presented in the Table 3

Table 3: Properties and assumptions for analysis

Properties and assumptions according to Euro-codes				
Description	Limit	Unit	Remark	Code
Imposed Load	2.0-4.0	kN/m <sup>2</sup>	Domestic and residential activities	Eurocode 1 -Table 6.2
Design Working life	100	Years	Building structures and other common structures	Eurocode 0 -Table 2.1
Exposure class	XC1		Corrosion induced by carbonation / Concrete inside building with low air humidity	Eurocode 2 -Table 4-1
Reinforcement	1	kN/m <sup>2</sup>	Increase for normal percentage of reinforcing	Eurocode 1 -Table A1
Minimum cover	25	mm	Structural Building class S4	Eurocode 1 -Table 4.4N



<b>Load factor</b>				
Self weight	1.2; 1.35			
Imposed Load	1.05; 1.5			
<b>Concrete</b>				
Concrete density	24.00	kN/m <sup>3</sup>	Normal weight Concrete	NS-EN 1991-1-1 - Table A1
Concrete characteristic strength (f <sub>ck</sub> )	30.00	N/mm <sup>2</sup>	B30 Assumed	
Concrete design strength (f <sub>cd</sub> )	17.01	N/mm <sup>2</sup>		
Mean tensile strength (f <sub>ctm</sub> )	2.90	N/mm <sup>2</sup>		

Normal weight B30 concrete of the characteristic strength 30 N/mm<sup>2</sup> is taken as the concrete grade. Density, design compressive- and tensile-strength are taken from the Eurocode 2 and presented in the *Table 3*.

Thickness of the reference staircase's waist slab is compared with the effective length by effective depth ratio assuming simply supported staircase. The reference staircase has greater thickness than the minimum required thickness as shown in *Table 4* and this greater value is taken for the further calculations.

*Table 4: Effective depth of waist slab*

<b>Calculation of staircase's slab thickness</b>			
L <sub>eff</sub> /d	20.00		NS-EN 1992-1-1 Table 7.4
Effective thickness of waist (h)	122.40	mm	According to L/d
Thickness of waist (h)	153.40	mm	Calculated
Thickness of waist (h)	178.88	mm	Taken from drawing
Average thickness of flight (y)	211.91	mm	$y = h(\sqrt{T^2+R^2})/T$
Average thickness of staircase (t)	298.28	mm	$t = y + (R/2)$

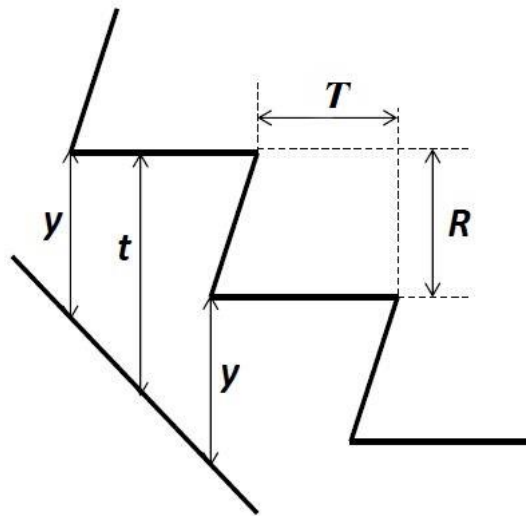


Figure 1: Average thickness calculation

Based on the geometry developed by parametric modelling of reference staircase, average thickness of staircase is calculated as shown in Figure 1 and volume of the landing and flight is calculated separately and multiplied by the concrete density to get the self-weight. Imposed load is taken from the Eurocode 1 and finishing load of  $1 \text{ kN/m}^2$  is assumed by the authors. Finish load and self-weight are taken as dead load. Design load as presented in Table 5 is calculated according to equations 6.10a and 6.10b in NS-EN 1990. The maximum value was obtained from equation 6.10b among two of them and used for the calculation of moment capacity and shear capacity of landing and flight which is presented in the.

Table 5: Design load calculation

Calculation of Loads			
<b>Landing</b>			
Effective thickness of landing slab	71.20	mm	According to $L/d$
Thickness of landing slab	102.20		Calculated
Thickness of landing slab	230.00	mm	Taken from drawing
waist slab self-weight	5.52	$\text{kN/m}^2$	Density * h
Imposed Load (p)	3.00	$\text{kN/m}^2$	Eurocode 1
Other load from finishing	1.00	$\text{kN/m}^2$	Assumed/Taken
Total dead load (g)	7.52	$\text{kN/m}^2$	
Design load (q)	13.35	$\text{kN/m}^2$	$1.35 * g + 1.05 * p$ (NS-EN 1990. 6.10a)
Design load (q)	13.57	$\text{kN/m}^2$	$1.2 * g + 1.5 * p$ (NS-EN 1990. 6.10b)
Design load (q)	13.57	$\text{kN/m}^2$	Maximum value

<b>Flight</b>			
Imposed Load (p)	3.00	kN/m <sup>2</sup>	
waist slab self-weight	7.16	kN/m <sup>2</sup>	Density * t
Steps self-weight	2.87	kN/m <sup>2</sup>	
Finishing load	1.00	kN/m <sup>2</sup>	
Total permanent load(g)	9.16	kN/m <sup>2</sup>	
Design load (q)	15.51	kN/m <sup>2</sup>	1.35 * g + 1.05 * p (NS-EN 1990. 6.10a)
Design load (q)	15.78	kN/m <sup>2</sup>	1.2 * g + 1.5 * p (NS-EN 1990. 6.10b)
Design load (q <sub>max</sub> )	15.78	kN/m <sup>2</sup>	Maximum value
Diameter of bar (ϕ)	12.00	mm	Assumed
Effective depth of Flight slab(d)	147.88	mm	h-ϕ/2-C
Effective depth of landing slab(d)	199.00	mm	h-ϕ/2-C

Moment capacity, shear capacity and allowable deflection of the reference staircase is calculated based on the Eurocode which is given in *Table 6*. Moment capacity and shear capacity are mostly related to concrete properties and size of the staircase. Design moment and design shear due to the design loads are given by the FEM analysis of the staircase. Additionally, both allowable and actual deflection are solely based on the geometry of the staircase which is presented in *Table 6*.

*Table 6: Analysis of reference staircase*

<b>Design verification of Flight</b>			
<b>Moment Calculation</b>			
Design Moment (M <sub>ed</sub> )	14.79	kN-m	From FEM
Moment capacity (M <sub>rd</sub> )	102.30	kN-m	0.275fcd*b*d <sup>2</sup>
<b>Shear Capacity Design</b>			Eurocode 2, 6.2.2(1)
k	2.00		
q	0.002		
Calculated shear resistance (V <sub>Rd,c</sub> )	64.49	kN	
Minimum shear resistance (V <sub>Rd,c</sub> )	80.18	kN	
Shear Capacity (V <sub>Rd,c</sub> )	80.18	kN	
Maximum Design shear force (V <sub>ed</sub> )	28.32	kN	safe
<b>Deflection Check</b>			Eurocode 2, 7.4.2
L / d allowable	20.00		Table 7.4N
L / d actual	13.69		

<b>Design verification of landing</b>			
<b>Reinforcement Calculation</b>			
Design Moment ( $M_{ed}$ )	14.79	kN-m	From FEM
Moment capacity ( $M_{rd}$ )	185.24	kN-m	$0.275f_{cd} \cdot b \cdot d^2$
<b>Shear Capacity Design</b>			
			Eurocode 2, 6.2.2(1)
k	2.00		
g	0.02		
Calculated shear resistance ( $V_{Rd,c}$ )	186.97	kN	
Minimum shear resistance ( $V_{Rd,c}$ )	151.60	kN	
Shear Capacity ( $V_{Rd,c}$ )	186.97	kN	
Maximum Design shear force ( $V_{ed}$ )	38.50	kN	safe
<b>Deflection Check</b>			
			Eurocode 2, 7.4.2
L /d allowable	20.00		Table 7.4N
L /d actual	7.16		